

**SYNTHESIS AND EMISSION STUDIES OF POLYPYRIDYL COMPLEXES  
OF PLATINUM(II)**

by

Jan-André Gertenbach B.Sc. (Hons), (Natal)

Submitted in partial fulfilment of the academic  
requirements for the degree of  
Doctor of Philosophy  
in the  
School of Chemical and Physical Sciences,  
University of Natal

Pietermaritzburg  
December 2002

*“Wer nichts als Chemie versteht, versteht auch die nicht recht.”*

Georg Christoph Lichtenberg, 1742 - 1799

## ABSTRACT

Chapter One serves as an introduction to the photophysical properties of square-planar 2,2':6',2''-terpyridyl and 6-phenyl-2,2'-bipyridyl ligand complexes of platinum(II). A brief description is provided of the absorption and emission spectra of each complex, the latter generally both in solution and the solid state. The assignments made to the absorption and emission bands are reported, together with the lifetimes of the emitting states where these have been measured. The relationship between the molecular and/or crystal structure of the complex and its photophysical properties is discussed. Given this background, the overall aims of the work in this dissertation are presented.

In Chapter Two the synthesis and characterisation of nine novel ligands are described. These are 4'-( $\beta$ -naphthyl)-2,2':6',2''-terpyridine (**4'- $\beta$ Np-terpy**), 4'-(*meta*-biphenyl)-2,2':6',2''-terpyridine (**4'-*m*Biph-terpy**), 4'-(*para*-biphenyl)-2,2':6',2''-terpyridine (**4'-*p*Biph-terpy**), 4-( $\beta$ -naphthyl)-6-phenyl-2,2'-bipyridine (**H4- $\beta$ Np-phbipy**), 4-(*para*-biphenyl)-6-phenyl-2,2'-bipyridine (**H4-*p*Biph-phbipy**), 4-phenyl-6-(2'-pyrazinyl)-2,2'-bipyridine (**4-Ph-pzbipy**), 4-(*ortho*-CH<sub>3</sub>-phenyl)-6-(2'-pyrazinyl)-2,2'-bipyridine (**4-*o*MePh-pzbipy**), 4-(*ortho*-CF<sub>3</sub>-phenyl)-6-pyrazinyl-2,2'-bipyridine (**4-*o*CF<sub>3</sub>Ph-pzbipy**) and 4-phenyl-2,6-bis(2'-pyrazinyl)-pyridine (**4-Ph-pybipz**).

In Chapter Three the synthesis, characterisation and photophysical properties of platinum(II) complexes of the ligands 4'- $\beta$ Np-terpy, 4'-*m*Biph-terpy and 4'-*p*Biph-terpy are described. The complexes are salts prepared of the following composition: [Pt(4'- $\beta$ Np-terpy)Cl]SbF<sub>6</sub> (**1**), [Pt(4'- $\beta$ Np-terpy)Cl]BF<sub>4</sub> (**2**), [Pt(4'- $\beta$ Np-terpy)Cl]CF<sub>3</sub>SO<sub>3</sub> (**3**), [Pt(4'-*m*Biph-terpy)Cl]SbF<sub>6</sub> (**4**), [Pt(4'-*m*Biph-terpy)Cl]BF<sub>4</sub> (**5**), [Pt(4'-*m*Biph-terpy)Cl]CF<sub>3</sub>SO<sub>3</sub> (**6**), [Pt(4'-*p*Biph-terpy)Cl]SbF<sub>6</sub> (**7**), [Pt(4'-*p*Biph-terpy)Cl]BF<sub>4</sub> (**8**) and [Pt(4'-*p*Biph-terpy)Cl]CF<sub>3</sub>SO<sub>3</sub> (**9**). Each ligand is characterised by a substituent in the 4'-position that has been designed to permit free rotation of that substituent about the interannular bond to the terpyridyl fragment. The rotational freedom allows the 4'-substituent to adopt an orientation nearly coplanar with that of the terpyridyl fragment. As a result of the extensive  $\pi$ -conjugation, there is a strong ligand-centred influence in their excited state emission spectra. Evidence is also presented for <sup>3</sup>MLCT (metal

to ligand charge transfer) character in the emitting state, in particular that the emission is quenched in coordinating solvents. In addition, an <sup>3</sup>ILCT (intraligand charge transfer) contribution has been proposed to account for the exceptionally long lifetimes measured in fluid solution for [Pt(4'-βNp-terpy)Cl]<sup>+</sup> (12 μs), [Pt(4'-pBiph-terpy)Cl]<sup>+</sup> (4 μs) and [Pt(4'-αNp-terpy)Cl]<sup>+</sup> (17 μs). We conclude that large easily ionisable substituents in the 4'-position of the terpyridyl moiety ensure long lifetimes in fluid solution for platinum(II) complexes of these ligands. The same assignments apply to the solid state spectra of the yellow or pale orange salts that exhibit monomeric emission in the solid state, these being: [Pt(4'-βNp-terpy)Cl]SbF<sub>6</sub> (**1**), [Pt(4'-βNp-terpy)Cl]BF<sub>4</sub> (**2**), [Pt(4'-βNp-terpy)Cl]CF<sub>3</sub>SO<sub>3</sub> (**3**), [Pt(4'-pBiph-terpy)Cl]SbF<sub>6</sub> (**7**) and [Pt(4'-pBiph-terpy)Cl]BF<sub>4</sub> (**8**). In the solid state two additional types of solid state emission have been identified in cases where intermolecular interactions are present. The first type is typical of red or dark orange salts *viz.*, [Pt(4'-mBiph-terpy)Cl]SbF<sub>6</sub> (**4**), [Pt(4'-pBiph-terpy)Cl]BF<sub>4</sub> (*red form*) (**8**) and [Pt(4'-pBiph-terpy)Cl]CF<sub>3</sub>SO<sub>3</sub> (**9**). All three salts exhibit MMLCT (metal-metal to ligand charge transfer) emission brought about by close intermolecular Pt...Pt interactions in the solid. Finally, the three orange compounds [Pt(4'-mBiph-terpy)Cl]SbF<sub>6</sub>.CH<sub>3</sub>CN (**4a**), [Pt(4'-mBiph-terpy)Cl]BF<sub>4</sub> (**5**) and [Pt(4'-pBiph-terpy)Cl]CF<sub>3</sub>SO<sub>3</sub> (**9**) exhibit simultaneous emission from IL (intraligand) and MMLCT states that are similar in energy. In the case of [Pt(4'-mBiph-terpy)Cl]SbF<sub>6</sub>.CH<sub>3</sub>CN (**4a**) the assignment of MMLCT emission is supported by a X-ray crystal structure determination that shows the cations interacting in dimeric pairs which have a platinum-platinum separation of 3.356(2) Å.

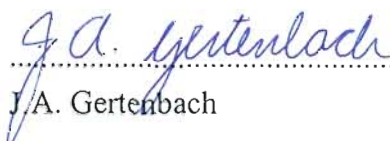
In Chapter Four the synthesis, characterisation and photophysical properties of the neutral complexes [Pt(4-βNp-phbipy)Cl] (**10**) and [Pt(4-pBiph-phbipy)Cl] (**11**) are described. The ligands, 4-βNp-phbipy and 4-pBiph-phbipy are closely related to 4'-βNp-terpy and 4'-pBiph-terpy, the only difference being that the terpyridyl fragment is replaced by a phenyl-bipyridyl moiety that binds to the platinum *via* a deprotonated carbon atom in the *ortho*-position of the phenyl ring. The stronger σ-donor strength of the anionic carbon atom is shown to result in: (i) a marked shift to the red in the MLCT absorption bands for the two complexes and (ii) a significant lowering of the energy of the emitting state, as compared to that observed for the cationic terpyridyl ligand derivatives. The assignment of the emission as <sup>3</sup>IL/<sup>3</sup>MLCT in origin remains the same, however, both in solution and in the solid state.

In Chapter Five we report the synthesis, characterisation and photophysical properties of a series of platinum(II) complexes of the ligands 4-Ph-pzbipy, 4-*o*MePh-pzbipy, 4-*o*CF<sub>3</sub>Ph-pzbipy and 4-Ph-pybipz *viz.*, [Pt(4-Ph-pzbipy)Cl]BF<sub>4</sub> (**12**), [Pt(4-*o*MePh-pzbipy)Cl]SbF<sub>6</sub> (**14**), [Pt(4-*o*MePh-pzbipy)Cl]BF<sub>4</sub> (**15**), [Pt(4-*o*MePh-pzbipy)Cl]CF<sub>3</sub>SO<sub>3</sub> (**16**), [Pt(4-*o*CF<sub>3</sub>Ph-pzbipy)Cl]SbF<sub>6</sub> (**17**), [Pt(4-*o*CF<sub>3</sub>Ph-pzbipy)Cl]BF<sub>4</sub> (**18**) and [Pt(4-*o*CF<sub>3</sub>Ph-pzbipy)Cl]CF<sub>3</sub>SO<sub>3</sub> (**19**). These ligands coordinate to platinum *via* a binding domain analogous to the terpyridyl fragment except that one (or both in the case of 4-Ph-pybipz) of the outer pyridine rings is replaced with a pyrazine ring. The ligands 4-*o*MePh-pzbipy and 4-*o*CF<sub>3</sub>Ph-pzbipy are distinguished from 4-Ph-pzbipy by the presence of bulky methyl and trifluoromethyl substituents, respectively, in the *ortho* position of the peripheral phenyl ring. Monomer emission measured in room temperature fluid solution in a 77 K rigid glass for the three luminophores *viz.* [Pt(4-Ph-pzbipy)Cl]<sup>+</sup>, [Pt(4-*o*MePh-pzbipy)Cl]<sup>+</sup> and [Pt(4-*o*CF<sub>3</sub>Ph-pzbipy)Cl]<sup>+</sup> derives from an excited state of <sup>3</sup>IL/<sup>3</sup>MLCT mixed orbital parentage. Their emission energies are stabilised compared to their terpyridyl analogues but emission lifetimes are essentially the same. Solid state emission spectra have been recorded for salts of the [Pt(4-*o*MePh-pzbipy)Cl]<sup>+</sup> and [Pt(4-*o*CF<sub>3</sub>Ph-pzbipy)Cl]<sup>+</sup> cations. In every case emission is derived from an excited state brought about by intermolecular interactions, either in the form of excimeric or of MMLCT emission. In general orange compounds {[Pt(4-*o*CF<sub>3</sub>Ph-pzbipy)Cl]SbF<sub>6</sub> (*orange form*) (**17**) and [Pt(4-*o*CF<sub>3</sub>Ph-pzbipy)Cl]BF<sub>4</sub> (**18**)} display excimeric emission and dark red compounds {[Pt(4-*o*MePh-pzbipy)Cl]SbF<sub>6</sub> (**14**), [Pt(4-*o*MePh-pzbipy)Cl]BF<sub>4</sub> (**15**), [Pt(4-*o*MePh-pzbipy)Cl]CF<sub>3</sub>SO<sub>3</sub> (**16**), [Pt(4-*o*CF<sub>3</sub>Ph-pzbipy)Cl]SbF<sub>6</sub> (*red form*) (**17**) and [Pt(4-*o*CF<sub>3</sub>Ph-pzbipy)Cl]CF<sub>3</sub>SO<sub>3</sub> (**19**)} display emission from a MMLCT excited state. The [Pt(4-*o*CF<sub>3</sub>Ph-pzbipy)Cl]SbF<sub>6</sub> (**17**) salt displays polymorphism, existing in two forms, one red and the other orange. In all cases the lower energy of the π-acceptor orbitals of the pyrazinyl-bipyridyl moiety causes emission to be at lower energies compared to that recorded for closely related terpyridyl analogues. Finally, attempts to coordinate the bis-pyrazinyl ligand, 4-Ph-pybipz, to platinum to form [Pt(4-Ph-pybipz)Cl]SbF<sub>6</sub> (**13**) were unsuccessful.

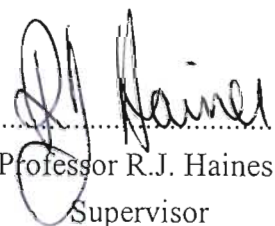
## PREFACE

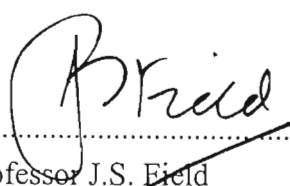
The experimental work described in this thesis was carried out in the School of Chemical and Physical Sciences, University of Natal, Pietermaritzburg, under the supervision of Professors Raymond J. Haines, John S. Field and Dr Orde Q. Munro.


These studies represent original work by the author and have not otherwise been submitted in any form for any degree or diploma to any University. Where use has been made of the work of others it is duly acknowledged in the text.

  
.....  
J.A. Gertenbach

We hereby certify that this statement is correct.

  
.....  
Professor R.J. Haines  
Supervisor

  
.....  
Professor J.S. Field  
Co-Supervisor

  
.....  
Dr O.Q. Munro  
Co-Supervisor

Pietermaritzburg  
December 2002

## TABLE OF CONTENTS

List of Figures	xiii
List of Schemes	xvi
List of Tables	xvii
Acknowledgements	xx
List of abbreviations and symbols	xxii

### CHAPTER 1

#### Photophysics of terpyridyl and phenyl-bipyridyl ligand complexes of platinum(II)

1.1 Background	1
1.1.1 The platinum terpyridyl complex	2
1.1.2 The platinum phenyl-bipyridyl complex	2
1.1.3 Applications of these compounds	3
1.2 Photophysical studies	3
1.2.1 Luminophores derived from the $[\text{Pt}\{4'\text{-R-terpy}\}]^{2+}$ unit	4
1.2.1.1 The $[\text{Pt}\{4'\text{-R-terpy}\}\text{Cl}]^+$ luminophore	4
1.2.1.2 The $[\text{Pt}\{(4'\text{-R})\text{-terpy}\}\text{CR}'^+]$ luminophore	33
1.2.1.2.1 The $[\text{Pt}\{(4'\text{-R})\text{-terpy}\}\text{CH}_3]^+$ luminophore	34
1.2.1.2.2 The $[\text{Pt}(\text{terpy})\text{CH}_2\text{R}]^+$ luminophore	36
1.2.1.2.3 The $[\text{Pt}\{4'\text{-R-terpy}\}\text{Ph}]^+$ luminophore (R = H or Ph)	37
1.2.1.3 The $[\text{Pt}(\text{terpy})\text{L}]^{n+}$ luminophore (L = anionic or neutral <u>N-donor</u> ligand; n = 1 or 2)	38
1.2.1.3.1 The $[\text{Pt}(\text{terpy})\text{L}]^+$ luminophore (L = anionic ligand)	38
1.2.1.3.2 The $[\text{Pt}(\text{terpy})\text{L}]^{2+}$ luminophore (L = neutral ligand)	38
1.2.1.4 The $[\text{Pt}(\text{terpy})\text{L}]^{n+}$ luminophore (L = anionic or neutral <u>O-donor</u> ligand; n = 1 or 2)	40
1.2.1.4.1 The $[\text{Pt}(\text{terpy})\text{OH}]^+$ luminophore	40
1.2.1.4.2 The $[\text{Pt}(\text{terpy})(\text{OMe})]^+$ luminophore	41
1.2.1.4.3 The $[\text{Pt}(\text{terpy})(\text{H}_2\text{O})]^{2+}$ luminophore	42

1.2.1.5 The [Pt(terpy)L] <sup>n+</sup> luminophore (L = anionic or neutral <u>S-donor</u> ligand; n = 1 or 2)	42
1.2.1.5.1 The [Pt(terpy)SR] <sup>n+</sup> luminophore (R = alkyl group)	43
1.2.1.5.2 The [Pt(terpy)SR] <sup>+</sup> luminophore (R = aryl group)	44
1.2.1.6 The [Pt(terpy)SCN] <sup>+</sup> luminophore	47
1.2.2 Luminophores derived from the [Pt(4-R-6-Ph-bipy)] <sup>2+</sup> unit	48
1.2.2.1 The [Pt(4-R-Ph-bipy)Cl] luminophore	48
1.2.2.2 The [Pt(Ph-bipy)NR] <sup>+</sup> luminophore	51
1.2.2.3 The [Pt(Ph-bipy)PR] <sup>+</sup> luminophore	52
1.3 Conclusions and Comments	54
1.4 Aims of this work	55

## CHAPTER 2

### Ligand Synthesis

2.1 Introduction	59
2.2 Synthesis and characterisation of the terpyridine ligands	64
2.2.1 Synthesis and characterisation of terpyridine derivatives with an extended $\pi$ -conjugated system in the 4'-position	64
2.2.1.1 4'-(R)-2,2':6',2''-terpyridines {R = $\beta$ -naphthyl (4'- $\beta$ Np-terpy), <i>m</i> -biphenyl (4'- <i>m</i> Biph-terpy), <i>p</i> -biphenyl (4'- <i>p</i> Biph-terpy)}	64
2.2.1.2 4-R-6-phenyl-2,2'-bipyridines {R = $\beta$ -naphthyl (H4- $\beta$ Np- phbipy), <i>p</i> -biphenyl (H4- <i>p</i> Biph-phbipy)}	66
2.2.2 Synthesis and characterisation of terpyridine analogues incorporating the pyrazine functionality	68
2.2.2.1 4-(2'''-R-phenyl)-6-(2''-pyrazinyl)-bipyridines {R = H (4-Ph- pzbipy), CH <sub>3</sub> (4- <i>o</i> MePh-pzbipy), CF <sub>3</sub> (4- <i>o</i> CF <sub>3</sub> Ph-pzbipy)}	68
2.2.2.2 4-phenyl-2,6-bis(2'-pyrazinyl)-pyridine (4-Ph-pybipz)	70
2.3 Experimental	73
2.3.1 4'-(R)-2,2':6',2''-terpyridines {R = $\beta$ -naphthyl (4'- $\beta$ Np-terpy), <i>m</i> - biphenyl (4'- <i>m</i> Biph-terpy), <i>p</i> -biphenyl (4'- <i>p</i> Biph-terpy)}	73
2.3.1.1 Synthesis of 1-(2''-pyridyl)-3-R-prop-2-en-1-one	73



2.3.1.2 Synthesis of 4'-(R)-2,2':6',2''-terpyridines {R = $\beta$ -naphthyl (4'- $\beta$ Np-terpy), <i>m</i> -biphenyl (4'- <i>m</i> Biph-terpy), <i>p</i> -biphenyl (4'- <i>p</i> Biph-terpy)}	74
2.3.2 4-R-6-phenyl-2,2'-bipyridine {R = $\beta$ -naphthyl (H4- $\beta$ Np-phbipy), <i>p</i> -biphenyl (H4- <i>p</i> Biph-phbipy)}	76
2.3.2.1 Synthesis of 1-(phenyl)-3-R-prop-2-en-1-one	76
2.3.2.2 Synthesis of 4-R-6-phenyl-2,2'-bipyridine {R = $\beta$ -naphthyl (H4- $\beta$ Np-phbipy), <i>p</i> -biphenyl (H4- <i>p</i> Biph-phbipy)}	77
2.3.3 4-(2'''-R-phenyl)-6-(2''-pyrazinyl)-bipyridines {R = H (4-Ph-pzbipy), CH <sub>3</sub> (4- <i>o</i> MePh-pzbipy), CF <sub>3</sub> (4- <i>o</i> CF <sub>3</sub> Ph-pzbipy)}	79
2.3.3.1 Synthesis of 1-(2'-pyridyl)-3-phenyl-prop-2-en-1-one	79
2.3.3.2 Synthesis of 1-(2'-pyridyl)-3-(2'''-R-phenyl)-prop-2-en-1-one (R = CH <sub>3</sub> , CF <sub>3</sub> )	79
2.3.3.3 Synthesis of <i>N</i> -{1-pyrazinyl-1-oxo-2-ethyl}pyridinium iodide (PZPI)	80
2.3.3.4 Synthesis of 4-(2'''-R-phenyl)-6-(2''-pyrazinyl)-2,2'-bipyridines {R = H (4-Ph-pzbipy), CH <sub>3</sub> (4- <i>o</i> MePh-pzbipy), CF <sub>3</sub> (4- <i>o</i> CF <sub>3</sub> Ph-pzbipy)}	80
2.3.4 Synthesis of 4-phenyl-2,6-bis(2'-pyrazinyl)-pyridine (4-Ph-pybipz)	82

## CHAPTER 3

### Synthesis and photophysical properties of terpyridyl ligand complexes of platinum(II)

3.1 Introduction	84
3.2 Results and discussion	86
3.2.1 [Pt(4'- $\beta$ Np-terpy)Cl]X [X <sup>-</sup> = SbF <sub>6</sub> <sup>-</sup> (1), BF <sub>4</sub> <sup>-</sup> (2), CF <sub>3</sub> SO <sub>3</sub> <sup>-</sup> (3)] {where 4'- $\beta$ Np-terpy = 4'-( $\beta$ -naphthyl)-2,2':6',2''-terpyridine}	86
3.2.1.1 Synthesis and characterisation	86
3.2.1.2 Photophysical properties	89
3.2.2 [Pt(4'- <i>m</i> Biph-terpy)Cl]X [X <sup>-</sup> = SbF <sub>6</sub> <sup>-</sup> (4), BF <sub>4</sub> <sup>-</sup> (5), CF <sub>3</sub> SO <sub>3</sub> <sup>-</sup> (6)] {where 4'- <i>m</i> Biph-terpy = 4'-( <i>meta</i> -biphenyl)-2,2':6',2''-terpyridine}	106
3.2.2.1 Synthesis and characterisation	106

3.2.2.2	Structural characterisation of [Pt(4'- <i>m</i> Biph-terpy)Cl]SbF <sub>6</sub> .CH <sub>3</sub> CN ( <b>4a</b> )	108
3.2.2.3	Photophysical properties	119
3.2.3	[Pt(4'- <i>p</i> Biph-terpy)Cl]X [X <sup>-</sup> = SbF <sub>6</sub> <sup>-</sup> ( <b>7</b> ), BF <sub>4</sub> <sup>-</sup> ( <b>8</b> ), CF <sub>3</sub> SO <sub>3</sub> <sup>-</sup> ( <b>9</b> )] {where 4'- <i>p</i> Biph-terpy = 4'-( <i>para</i> -biphenyl)-2,2':6',2''-terpyridine}	137
3.2.3.1	Synthesis and characterisation	137
3.2.3.2	Photophysical properties	140
3.3	Summary and Conclusions	161
3.4	Experimental	172
3.4.1	Synthetic procedures	172
3.4.1.1	[Pt(4'- <i>β</i> Np-terpy)Cl]X [X <sup>-</sup> = SbF <sub>6</sub> <sup>-</sup> ( <b>1</b> ), BF <sub>4</sub> <sup>-</sup> ( <b>2</b> ), CF <sub>3</sub> SO <sub>3</sub> <sup>-</sup> ( <b>3</b> )]	172
3.4.1.2	[Pt(4'- <i>m</i> Biph-terpy)Cl]X [X <sup>-</sup> = SbF <sub>6</sub> <sup>-</sup> ( <b>4</b> ), BF <sub>4</sub> <sup>-</sup> ( <b>5</b> ), CF <sub>3</sub> SO <sub>3</sub> <sup>-</sup> ( <b>6</b> )]	173
3.4.1.3	[Pt(4'- <i>p</i> Biph-terpy)Cl]X [X <sup>-</sup> = SbF <sub>6</sub> <sup>-</sup> ( <b>7</b> ), BF <sub>4</sub> <sup>-</sup> ( <b>8</b> ), CF <sub>3</sub> SO <sub>3</sub> <sup>-</sup> ( <b>9</b> )]	174
3.4.2	Crystal structure determination	183
3.4.2.1	Single crystal X-ray diffraction study on [Pt(4'- <i>m</i> Biph-terpy)Cl]SbF <sub>6</sub> .CH <sub>3</sub> CN	183

## CHAPTER 4

### Synthesis and photophysical properties of phenyl-bipyridyl ligand complexes of platinum(II)

4.1	Introduction	193
4.2	Results and discussion	194
4.2.1	[Pt(4- <i>β</i> Np-phbipy)Cl] ( <b>10</b> ) and [Pt(4- <i>p</i> Biph-phbipy)Cl] ( <b>11</b> ) {where 4- <i>β</i> Np-phbipy and 4- <i>p</i> Biph-phbipy are the anionic deprotonated form of the 4-( <i>β</i> -naphthyl)-6-phenyl-2,2'-bipyridyl (H4- <i>β</i> Np-phbipy) and 4-( <i>para</i> -biphenyl)-6-phenyl-2,2'-bipyridyl ligand (H4- <i>p</i> Biph-phbipy) ligands respectively}	194
4.2.1.1	Synthesis and characterisation	194
4.2.1.2	Photophysical properties	197
4.3	Summary and Conclusions	208

4.4	Experimental	213
4.4.1	Synthetic procedures	213
4.4.1.1	[Pt(4- $\beta$ Np-phbipy)Cl] ( <u>10</u> )	213
4.4.1.2	[Pt(4- <i>p</i> Biph-phbipy)Cl] ( <u>11</u> )	214
<b>CHAPTER 5</b>		
<b>Synthesis and photophysical properties of pyrazinyl-bipyridyl ligand complexes of platinum(II)</b>		
5.1	Introduction	218
5.2	Results and Discussion	220
5.2.1	[Pt(4-Ph-pzbipy)Cl]BF <sub>4</sub> ( <u>12</u> ) {where 4-Ph-pzbipy is 4-phenyl-6-(2''-pyrazinyl)-2,2'-bipyridine}	220
5.2.1.1	Synthesis and characterisation	220
5.2.1.2	Photophysical properties	222
5.2.2	[Pt(4-Ph-pybipz)Cl]SbF <sub>6</sub> ( <u>13</u> ) {where 4-Ph-pybipz is 4-phenyl-2,6-bis(2'-pyrazinyl)-pyridine}	229
5.2.2.1	Synthesis and characterisation	229
5.2.3	[Pt(4- <i>o</i> MePh-pzbipy)Cl]X [X <sup>-</sup> = SbF <sub>6</sub> <sup>-</sup> ( <u>14</u> ), BF <sub>4</sub> <sup>-</sup> ( <u>15</u> ), CF <sub>3</sub> SO <sub>3</sub> <sup>-</sup> ( <u>16</u> )] {where 4- <i>o</i> MePh-pzbipy is 4-( <i>o</i> -CH <sub>3</sub> -phenyl)-6-(2''-pyrazinyl)-2,2'-bipyridine}	230
5.2.3.1	Synthesis and characterisation	230
5.2.3.2	Photophysical properties	231
5.2.4	[Pt(4- <i>o</i> CF <sub>3</sub> Ph-pzbipy)Cl]X [X <sup>-</sup> = SbF <sub>6</sub> <sup>-</sup> ( <u>17</u> ), BF <sub>4</sub> <sup>-</sup> ( <u>18</u> ) CF <sub>3</sub> SO <sub>3</sub> <sup>-</sup> ( <u>19</u> )] {where 4- <i>o</i> CF <sub>3</sub> Ph-pzbipy is 4-( <i>o</i> -CF <sub>3</sub> -phenyl)-6-(2''-pyrazinyl)-2,2'-bipyridine}	239
5.2.4.1	Synthesis and characterisation	239
5.2.4.2	Photophysical properties	240
5.3	Summary and Conclusions	249
5.4	Experimental	259
5.4.1	Synthetic procedures	259

5.4.1.1 [Pt(4-Ph-pzbipy)Cl]X [X <sup>-</sup> = SbF <sub>6</sub> <sup>-</sup> (12), BF <sub>4</sub> <sup>-</sup> (13), CF <sub>3</sub> SO <sub>3</sub> <sup>-</sup> (14)]	259
5.4.1.2 [Pt(4- <i>o</i> MePh-pzbipy)Cl]X [X <sup>-</sup> = SbF <sub>6</sub> <sup>-</sup> (15), BF <sub>4</sub> <sup>-</sup> (16), CF <sub>3</sub> SO <sub>3</sub> <sup>-</sup> (17)]	260
5.4.1.3 [Pt(4- <i>o</i> CF <sub>3</sub> Ph-pzbipy)Cl]X [X <sup>-</sup> = SbF <sub>6</sub> <sup>-</sup> (18), BF <sub>4</sub> <sup>-</sup> (19), CF <sub>3</sub> SO <sub>3</sub> <sup>-</sup> (20)]	261

## APPENDIX A

### General experimental details

A.1 Experimental techniques	268
A.2 Instrumentation	268

## APPENDIX B

### Sources of Chemicals

B.1 Commercially available chemicals	270
B.2 Chemicals prepared by literature methods	271
References	272

## LIST OF FIGURES

		Page
Figure 1.1	The platinum terpyridyl fragment.	2
Figure 1.2	The platinum phenyl-bipyridyl fragment.	3
Figure 1.3	Molecular orbital diagram describing the effect on the molecular orbitals brought about by close intermolecular contact.	8
Figure 1.4	Perspective view of dimeric structure of [Pt(terpy)Cl]CF <sub>3</sub> SO <sub>3</sub>	10
Figure 1.5	Ligands synthesised in this work and their abbreviations.	56
Figure 2.1	<i>N</i> -{1-(2'-pyridyl)-1-oxo-2-ethyl}pyridinium iodide	62
Figure 2.2	Terpyridine moiety showing numbering scheme used.	65
Figure 2.3	Phenyl-bipyridine moiety showing numbering scheme used.	67
Figure 2.4	Pyrazinyl-bipyridine moiety showing numbering scheme used.	69
Figure 2.5	4-phenyl-2,6-bis(2'-pyrazinyl)-pyridine ( <b>4-Ph-pybipz</b> ) showing numbering scheme used.	71
Figure 3.1	Numbering and nomenclature of naphthyl rings.	84
Figure 3.2	Numbering and nomenclature of biphenyl rings in 4'-position of terpyridyl ligand.	85
Figure 3.3	Acetonitrile solution absorption spectra of the [Pt(4'-βNp-terpy)Cl] <sup>+</sup> and 4'-βNp-terpy chromophores recorded at 298 K.	90
Figure 3.3a	The acetonitrile solution absorption spectrum of the [Pt(4'-αNp-terpy)Cl] <sup>+</sup> chromophore recorded at 298 K.	92
Figure 3.4	Dichloromethane solution emission spectra of the [Pt(4'-R-terpy)Cl] <sup>+</sup> luminophores recorded at 298 K.	94
Figure 3.5	Solution emission spectra of [Pt(4'-βNp-terpy)Cl] <sup>+</sup> recorded in a rigid DME glass at 77 K.	97
Figure 3.6	Solution excitation spectra of [Pt(4'-βNp-terpy)Cl] <sup>+</sup> recorded in a rigid DME glass at 77 K.	100
Figure 3.7	Solid state absorption spectrum of [Pt(4'-βNp-terpy)Cl]CF <sub>3</sub> SO <sub>3</sub> recorded at 298 K.	102

Figure 3.8	Solid state emission spectra of [Pt(4'- $\beta$ Np-terpy)Cl]CF <sub>3</sub> SO <sub>3</sub> .	104
Figure 3.9	Solid state emission spectra of [Pt(4'- $\beta$ Np-terpy)Cl]CF <sub>3</sub> SO <sub>3</sub> .	105
Figure 3.10	Molecular geometry and numbering scheme used for the [Pt(4'- <i>m</i> Biph-terpy)Cl] <sup>+</sup> cation.	109
Figure 3.11	View of the [Pt(4'- <i>m</i> Biph-terpy)Cl] <sup>+</sup> cation with each of its four nearest neighbours in positions labelled A, B, C and D.	113
Figure 3.12	Overlap of a [Pt(4'- <i>m</i> Biph-terpy)Cl] <sup>+</sup> luminophore with its counterpart in position A.	114
Figure 3.13	Overlap of a [Pt(4'- <i>m</i> Biph-terpy)Cl] <sup>+</sup> luminophore with its counterpart in position B.	116
Figure 3.14	Overlap of a [Pt(4'- <i>m</i> Biph-terpy)Cl] <sup>+</sup> luminophore with its counterpart in position C.	117
Figure 3.15	Overlap of a [Pt(4'- <i>m</i> Biph-terpy)Cl] <sup>+</sup> luminophore with its counterpart in position D.	118
Figure 3.16	Acetonitrile solution absorption spectra of the [Pt(4'- <i>m</i> Biph-terpy)Cl] <sup>+</sup> and 4'- <i>m</i> Biph-terpy chromophores recorded at 298 K.	120
Figure 3.17	Solution emission spectra of [Pt(4'- <i>m</i> Biph-terpy)Cl] <sup>+</sup> recorded in a DME glass at 77 K.	124
Figure 3.18	Excitation spectra of [Pt(4'- <i>m</i> Biph-terpy)Cl] <sup>+</sup> recorded in a 30 $\mu$ M DME glass at 77 K.	126
Figure 3.19	Solid state emission spectra of [Pt(4'- <i>m</i> Biph-terpy)Cl]SbF <sub>6</sub> ( <b>4</b> ).	129
Figure 3.20	Solid state emission spectra of [Pt(4'- <i>m</i> Biph-terpy)Cl]SbF <sub>6</sub> .CH <sub>3</sub> CN	132
Figure 3.21	Solid state emission spectra of [Pt(4'- <i>m</i> Biph-terpy)Cl]BF <sub>4</sub> ( <b>5</b> ).	136
Figure 3.22	Solid state emission spectra of [Pt(4'- <i>m</i> Biph-terpy)Cl]CF <sub>3</sub> SO <sub>3</sub> ( <b>6</b> ).	138
Figure 3.23	Acetonitrile solution absorption spectra of the [Pt(4'- <i>p</i> Biph-terpy)Cl] <sup>+</sup> and 4'- <i>p</i> Biph-terpy chromophores recorded at 298 K.	141
Figure 3.24	Solution emission spectra of [Pt(4'- <i>p</i> Biph-terpy)Cl] <sup>+</sup> recorded in DME glass at 77 K.	146
Figure 3.25	Solid state emission spectra of [Pt(4'- <i>p</i> Biph-terpy)Cl]SbF <sub>6</sub> ( <b>7</b> ) { $\lambda_{\text{ex}}(\text{max}) = 400\text{nm}$ }.	149
Figure 3.26	Solid state emission spectra of [Pt(4'- <i>p</i> Biph-terpy)Cl]SbF <sub>6</sub> ( <b>7</b> ) { $\lambda_{\text{ex}}(\text{max}) = 450\text{nm}$ }.	150

Figure 3.27	Solid state emission spectra of [Pt(4'- <i>p</i> Biph-terpy)Cl]SbF <sub>6</sub> ( <b>7</b> ) { $\lambda_{\text{ex}}(\text{max}) = 450\text{nm}$ }.	152
Figure 3.28	Solid state emission spectra of the <u>yellow form</u> of [Pt(4'- <i>p</i> Biph-terpy)Cl]BF <sub>4</sub> ( <b>8</b> ).	154
Figure 3.29	Solid state emission spectra of the <u>red form</u> of [Pt(4'- <i>p</i> Biph-terpy)Cl]BF <sub>4</sub> ( <b>8</b> ).	156
Figure 3.30	Solid state emission spectra of [Pt(4'- <i>p</i> Biph-terpy)Cl]CF <sub>3</sub> SO <sub>3</sub> ( <b>9</b> ).	159
Figure 4.1	Acetonitrile solution absorption spectra of the [Pt(4- $\beta$ Np-phbipy)Cl] and 4- $\beta$ Np-phbipy chromophores recorded at 298 K.	198
Figure 4.2	Acetonitrile solution absorption spectra of the [Pt(4- <i>p</i> Biph-phbipy)Cl] and 4- <i>p</i> Biph-phbipy chromophores recorded at 298 K.	199
Figure 4.3	Dichloromethane solution emission spectra of [Pt(4- $\beta$ Np-phbipy)Cl] ( <b>10</b> ) and [Pt(4- <i>p</i> Biph-phbipy)Cl] ( <b>11</b> ) recorded at 298 K.	203
Figure 4.4	Solution emission spectra of [Pt(4- $\beta$ Np-phbipy)Cl] ( <b>10</b> ) and [Pt(4- <i>p</i> Biph-phbipy)Cl] ( <b>11</b> ) recorded in a DME glass at 77 K.	206
Figure 5.1	Acetonitrile solution absorption spectra of the [Pt(4-Ph-pzbipy)Cl] <sup>+</sup> and 4-Ph-pzbipy chromophores recorded at 298 K.	223
Figure 5.2	Dichloromethane solution emission spectra of the [Pt(4-R-pzbipy)Cl] <sup>+</sup> luminophores recorded at 298 K.	226
Figure 5.3	Solution emission spectra of the [Pt(4-R-pzbipy)Cl] <sup>+</sup> luminophores recorded in a 20 $\mu$ M DME rigid glass at 77 K.	228
Figure 5.4	Acetonitrile solution absorption spectra of the [Pt(4- <i>o</i> MePh-pzbipy)Cl] <sup>+</sup> and 4- <i>o</i> MePh-pzbipy chromophores recorded at 298 K.	232
Figure 5.5	Solid state emission spectra of [Pt(4- <i>o</i> MePh-pzbipy)Cl]SbF <sub>6</sub> .	238
Figure 5.6	Acetonitrile solution absorption spectra of the [Pt(4- <i>o</i> CF <sub>3</sub> Ph-pzbipy)Cl] <sup>+</sup> and 4- <i>o</i> CF <sub>3</sub> Ph-pzbipy chromophores recorded at 298 K.	241
Figure 5.7	Solid state emission spectra of the <u>red form</u> of [Pt(4- <i>o</i> CF <sub>3</sub> Ph-pzbipy)Cl]SbF <sub>6</sub> .	244
Figure 5.8	Solid state emission spectra of the <u>orange form</u> of [Pt(4- <i>o</i> CF <sub>3</sub> Ph-pzbipy)Cl]SbF <sub>6</sub> .	246

## LIST OF SCHEMES

		Page
Scheme 2.1	Generalised Kröhnke methodology.	60
Scheme 2.2	2:1 addition to give a pentane-1,5-dione	61
Scheme 2.3a	One possible method to synthesize 6-phenyl-2,2'-bipyridine	63
Scheme 2.3b	Second method to synthesize 6-phenyl-2,2'-bipyridine	63
Scheme 2.4	Synthetic route to pyrazinyl-bipyridine derivatives.	68



LIST OF TABLES

		Page
Table 2.1	<sup>1</sup> H NMR chemical shifts for the 2,2':6',2''-terpyridine moiety.	65
Table 2.2	<sup>1</sup> H NMR shifts for the 6-phenyl-2,2'-bipyridine moiety.	67
4'-βNp-terpy	Characterisation of 4'-βNp-terpy	74
4'- <i>m</i> Biph-terpy	Characterisation of 4'- <i>m</i> Biph-terpy	75
4'- <i>p</i> Biph-terpy	Characterisation of 4'- <i>p</i> Biph-terpy	76
H4-βNp-phbipy	Characterisation of H4-βNp-phbipy	78
H4- <i>p</i> Biph-phbipy	Characterisation of H4- <i>p</i> Biph-phbipy	78
4-Ph-pzbipy	Characterisation of 4-Ph-pzbipy	80
4- <i>o</i> MePh-pzbipy	Characterisation of 4- <i>o</i> MePh-pzbipy	81
4- <i>o</i> CF <sub>3</sub> Ph-pzbipy	Characterisation of 4- <i>o</i> CF <sub>3</sub> Ph-pzbipy	82
4-Ph-pybipz	Characterisation of 4-Ph-pybipz	83
Table 3.1	Emission from selected complexes in rigid glassy medium at 77 K.	99
Table 3.2	Bond distances at the binding domain of terpyridyl complexes of platinum(II).	110
Table 3.3	Angles between Pt-N bonds subtended at platinum centre.	111
Table 3.4	Summary of emission data recorded in dichloromethane solution at 298 K.	143 and 162
Table 3.5	Monomeric emission data recorded in a dilute glassy DME solution at 77 K.	165
Table 3.6	Summary of MMLCT emission data recorded in rigid glassy solution at 77 K.	166
Table 3.7	Solid state spectroscopic data of complexes in Group I.	167
Table 3.8	Solid state spectroscopic data of complexes in Group II.	168
Table 3.9	Solid state spectroscopic data of complexes in Group III.	170
Table 3.10	Infrared spectroscopic data.	175

Table 3.11	Solution absorption data.	176
Table 3.12	Solution absorption and emission spectroscopic data.	178
Table 3.13	Solid state absorption and emission spectroscopic data.	181
Table 3.14	Crystal data and structure refinement for [Pt(4'- <i>m</i> Biph-terpy)Cl]SbF <sub>6</sub> ·CH <sub>3</sub> CN.	184
Table 3.15	Atomic coordinates and equivalent isotropic displacement parameters for [Pt(4'- <i>m</i> Biph-terpy)Cl]SbF <sub>6</sub> ·CH <sub>3</sub> CN ( <b>4</b> ).	185
Table 3.16	Bond lengths for [Pt(4'- <i>m</i> Biph-terpy)Cl]SbF <sub>6</sub> ·CH <sub>3</sub> CN ( <b>4</b> ).	188
Table 3.17	Bond angles for [Pt(4'- <i>m</i> Biph-terpy)Cl]SbF <sub>6</sub> ·CH <sub>3</sub> CN ( <b>4</b> ).	189
Table 3.18	Anisotropic displacement parameters for [Pt(4'- <i>m</i> Biph-terpy)Cl]SbF <sub>6</sub> ·CH <sub>3</sub> CN.	191
Table 4.1	<sup>1</sup> H NMR chemical shifts for related phenyl-bipyridyl complexes.	197
Table 4.2	Comparison of low energy absorption bands for a selection of complexes.	201
Table 4.3	Comparison of room temperature fluid solution emission.	209
Table 4.4	Comparison of emission recorded in rigid glassy medium at 77 K.	211
Table 4.5	Infrared spectroscopic data.	215
Table 4.6	Solution absorption spectroscopic data.	216
Table 4.7	Solution absorption and emission spectroscopic data.	217
Table 5.1	Comparison of MLCT absorption energies for [Pt(4'-Ph-terpy)Cl] <sup>+</sup> and [Pt(4-Ph-pzbipy)Cl] <sup>+</sup> recorded in room temperature fluid solution.	224
Table 5.2	Comparison of MLCT absorption energies recorded in room temperature fluid solution.	233
Table 5.3	Summary of emission data recorded in dichloromethane solution at 298 K.	250
Table 5.4	Summary of emission data recorded in a rigid glass at 77 K.	251

Table 5.5	Emission comparison between [Pt(4-oMePh-pzbipy)Cl]SbF <sub>6</sub> and [Pt(4'-oMePh-terpy)Cl]SbF <sub>6</sub>	253
Table 5.6	Evaluation of emission stabilisation at 77 K due to the presence of pyrazine.	257
Table 5.7	Infrared spectroscopic data.	262
Table 5.8	Solution absorption data.	263
Table 5.9	Solution absorption and emission spectroscopic data.	265
Table 5.10	Solid state absorption and emission spectroscopic data.	266

## ACKNOWLEDGEMENTS

I wish to express my gratitude to Professors R.J. Haines and J.S. Field and to Dr O.Q Munro for their guidance and advice offered to me during the course of this research project.

I would like to thank Prof Dave “Our fearless leader” McMillin for his help at Purdue with collecting the photophysical data presented in this work. In particular his gentle guidance and friendly coaxing in extending my capabilities is especially appreciated, making my stay in under his leadership a pleasant one.

I would also like to acknowledge the efforts of:

Dr Grant Summerton for his tutelage and encouragement through my initial clumsy efforts in this field and for his infectious enthusiasm which imbued me with his aesthetic appreciation for luminescent complexes. Most importantly the humour brought to the every-day drudgery of lab work will not easily be forgotten.

Martin Watson for his tireless efforts at maintaining instrumentation and, in particular, to ensure a comprehensive exploitation of NMR spectroscopy.

James “Bob” Ryan for elemental analysis, highly skilled mechanical work and his ready assistance whenever required.

Leanne Cook of the Centre for Molecular Design at the University of the Witwatersrand for her able operation of the area detector diffractometer used for the X-ray crystal data collection.

André van Daele for his help in preparing samples “for export”. Your boundless enthusiasm, energy and sense of humour kept me going at trying times.

My sister, Ilze, whose exceptional effort at short notice and with little time at proofreading a thesis of which she understood very little was a work of intense determination.

The National Research Foundation and the De Beers Industrial Diamond Division for their generous financial assistance.

Members of the McMillin research group, Steph, Dugga, Keith “Winklepicker” Thomas and Miiista Wiiilson for your immediate acceptance among you and always ensuring a humorous working environment. Big Al, for putting me up when I was homeless, teaching me about gridiron, grilling out and what real American beef is.

Jeff and Jess. Your sincere welcome and hospitality was touching. Our friendship extends to more than friendly advice and support and is the lasting feature of my stay in the USA. Thank you for fantastic times together, I hope to see you in Africa.

Sadhna. I value your support and sense of what is real.

The Howick okes, mates second to none. All I can say is Faanks.

My friends and all the people who had to tolerate the unpleasant moods arising from frustrated research.

My exercise partners especially the Mirage Moffies and the Christmas Fairies, for keeping me sane at insane times, and ensuring that I stay well off the beaten track. Also Steffi, Jumbo and Rusty, truer friends I could not hope for as running partners.

Ilze and Edgar. Without your support and encouragement in the last year of this work, I would have been lost. Herzlichen dank liebe geschwister.

Finally, my parents deserve particular mention for their undying support and understanding. Don't worry Ma, your hints and concern did not go unnoticed. I hope the your tender nerves can abate little now.

## LIST OF ABBREVIATIONS AND SYMBOLS

abs	absorption
4'- $\alpha$ Np-terpy	4'-( $\alpha$ -naphthyl)-2,2':6',2''-terpyridine
bipy	2,2'-bipyridine
4'- $\beta$ Np-terpy	4'-( $\beta$ -naphthyl)-2,2':6',2''-terpyridine
4- $\beta$ Np-phbipy	anionic deprotonated form of the 4-( $\beta$ -naphthyl)-6-phenyl-2,2'-bipyridine (H4- $\beta$ Np-phbipy)
CH <sub>2</sub> Cl <sub>2</sub>	dichloromethane
1,5-COD	1,5-cyclooctadiene
CT	charge transfer
$\delta$	chemical shift in parts per million
DMF	N,N-Dimethylformamide
DMSO	dimethylsulfoxide
$\epsilon$	Molar absorbtivity (M <sup>-1</sup> .cm <sup>-1</sup> )
EHMO	extended Hückel molecular orbital (calculations)
em	emission
ether	diethyl ether
EtOH	ethanol
$\nu$	frequency
fwhm	full width at half maximum (peak height)
GC/MS	gas chromatography/mass spectrometry
HL	6-phenyl-2,2'-bipyridine, unless otherwise specified
HOMO	highest occupied molecular orbital
<i>i</i>	iso
I	intensity, unless otherwise specified
IL	intraligand
ILCT	intraligand charge transfer
IR	infrared
<i>J</i>	coupling constant

$\lambda$	wavelength
L	ligand, unless otherwise specified
LC	ligand centred
LF	ligand field
LLCT	ligand-to-ligand charge transfer
LUMO	lowest unoccupied molecular orbital
<i>m</i>	meta
M <sup>+</sup>	molecular ion
$\mu$	micro ( $\times 10^{-6}$ )
max	maximum
4'- <i>m</i> Biph-terpy	4'-( <i>meta</i> -biphenyl)-2,2':6',2''-terpyridine
MC	metal centred
MeCN	acetonitrile
MeOH	methanol
MLCT	metal to ligand charge transfer
mM	milli molar
$\mu$ M	micro molar
MMLCT	metal-metal to ligand charge transfer
m.p.	melting point
NMR	nuclear magnetic resonance
<i>o</i>	ortho
4- <i>o</i> CF <sub>3</sub> Ph-pzbipy	4-( <i>o</i> -CF <sub>3</sub> -phenyl)-6-(2''-pyrazinyl)-bipyridine
4'- <i>o</i> CF <sub>3</sub> Ph-terpy	4'-( <i>o</i> -CF <sub>3</sub> -phenyl)-2,2':6',2''-terpyridine
4- <i>o</i> MePh-pzbipy	4-( <i>o</i> -CH <sub>3</sub> -phenyl)-6-(2''-pyrazinyl)-bipyridine
4'- <i>o</i> MePh-terpy	4'-( <i>o</i> -CH <sub>3</sub> -phenyl)-2,2':6',2''-terpyridine
<i>p</i>	para
4- <i>p</i> Biph-phbipy	anionic deprotonated form of the 4-( <i>para</i> -biphenyl)-6-phenyl-2,2'-bipyridine (H4- <i>p</i> Biph-phbipy)
4'- <i>p</i> Biph-terpy	4'-( <i>para</i> -biphenyl)-2,2':6',2''-terpyridine

ph	phenyl
phbipy	6-phenyl-2,2'-bipyridine
Phe9	9-phenanthrolene
4-Ph-pybipz	4-phenyl-2,6-bis(2'-pyrazinyl)-pyridine
4-Ph-pzbipy	4-phenyl-6-(2''-pyrazinyl)-bipyridine
4'-Ph-terpy	4'-phenyl-2,2':6',2''-terpyridine
ppm	parts per million
Pyre1	1-pyrene
py	pyridine
pz	pyrazine
pzbipy	6-pyrazinyl-2,2'-bipyridine
PZPI	<i>N</i> -{1-pyrazinyl-1-oxo-2-ethyl}pyridinium iodide
sh	shoulder
<i>t</i> or <i>tert</i>	tertiary
terpy	2,2':6',2''-terpyridine
TFPB	tetrakis[3,5-(trifluoromethylphenyl)]borate
TMS	tetramethylsilane
UV	ultraviolet
vis	visible
X	counterion, unless otherwise specified



# Chapter One

**Photophysics of terpyridyl and phenyl-bipyridyl ligand complexes of platinum(II)**

**1.1 BACKGROUND**

The study of photophysical processes involving metal complexes is a relatively modern field of interest having only received wider attention following the definitive publication of “*The Photochemistry of Coordination Compounds*” by Balzani and Carassitti in 1971.<sup>1</sup> Prior to the 1970's only a handful of compounds had been studied. By photophysical processes we mean the ways in which atoms or molecules are brought to an electronic excited state from which the excited species returns to the ground state, leaving it indistinguishable from the atoms or molecules prior to excitation. Naturally the study includes the emission and non-radiative decay pathways by which the species is deactivated to the ground state.

The complexes under consideration in this study consist of oligopyridines coordinated to a metal centre. It is noteworthy that oligopyridines are capable of stabilising transition metals in either their lower or their higher oxidation states. First consider a transition metal in its low oxidation state. The metal is characterised by an excess of electron density and will thus be stabilised by a ligand that can accommodate or dissipate this electron density in a low lying, vacant orbital. Oligopyridines are well suited to this task having Lowest Unoccupied Molecular Orbitals (LUMO's) of suitable symmetry and energy for overlap with the filled metal d-orbitals. Vacant nonbonding or  $\pi$ -antibonding orbitals are capable of fulfilling this task. Transition metals in high oxidation states can in contrast be stabilised by strong  $\sigma$ - or  $\pi$ -donor ligands. Again, the Highest Occupied Molecular Orbital (HOMO) of the oligopyridine is well suited to this task in terms of both symmetry and energy. Therefore both high and low oxidation states of transition metal ions can be stabilised.<sup>2</sup>

The scope of the work in this study will encompass the photophysical studies of mononuclear complexes derived from terpyridyl and phenyl bipyridyl ligand complexes of platinum(II). Dinuclear ligand-bridged species are not included in this survey. A brief description of each complex moiety now follows.

### 1.1.1 The platinum terpyridyl complex

The prototype platinum(II) terpyridyl complexes are those involving 2,2':6',2''-terpyridine (terpy). In these complexes the terpy ligand functions as a tridentate ligand coordinating *via* the nitrogen donor atoms to three of the four coordination sites of square-planar platinum(II) as illustrated in Figure 1.1. Terpyridine has a well established predilection for adopting a planar geometry, which is preserved upon coordination to the planar platinum(II) to give a flat metal and ligand binding domain. The neutral ligand preserves the doubly positive charge which must be balanced by the charge of the substituent in the fourth site and by the use of a counterion.

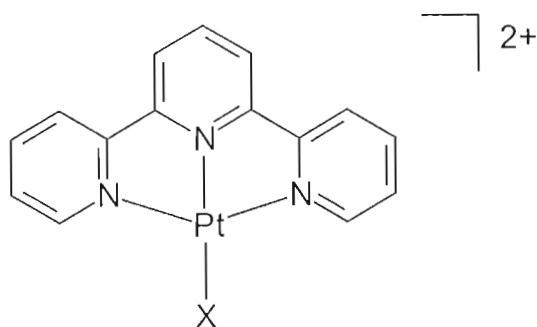


**Figure 1.1** *The platinum terpyridyl fragment*

### 1.1.2 The platinum phenyl-bipyridyl complex

The 6-phenyl-2,2'-bipyridyl ligand (phenyl-bipyridine or phbipy) is formally derived by replacing one of the outer pyridine rings of terpyridine with a phenyl group. In its phenyl C-deprotonated form the now anionic, tridentate ligand is able to provide a *C,N,N* planar donor set. The ligand orthometallates to the platinum(II) centre resulting in the complex substructure, illustrated in Figure 1.2. This substructure forms the basis for this second, related family of luminophores. As this is formally an anionic ligand only a single cationic charge needs to be neutralised. Charge balance is most often accomplished by the use of an anionic ligand in the fourth coordination site of platinum(II), thereby negating the need for a counterion. This has profound implications for packing arrangements in the solid state.

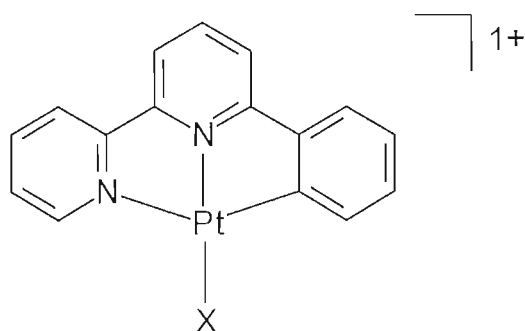


**Figure 1.2** *The platinum phenyl-bipyridyl fragment*

### 1.1.3 Applications of these compounds

Interest in polypyridyl complexes of platinum(II) has been fuelled by their potential utility in diverse fields. The terpyridine backbone is increasingly being utilised as a tridentate metal binding domain in metallosupramolecular systems and as a building block for metallodendrimers.<sup>3, 4</sup> These supramolecular metallodendrimers are designed to find application in solar energy conversion.<sup>5</sup> The ability of square-planar  $d^8$  metals to intercalate into DNA base pairs has been known for some time and this ability provides for a wide application of square planar platinum complexes in the biological domain.<sup>6</sup> Platinum terpyridines are also capable of acting as reagents for protein modification by binding to the histidine<sup>7-9</sup> and arginine<sup>10</sup> residues of proteins. Indeed the platinum terpyridine unit has been shown to be highly specific for histidine at pH 5.<sup>11</sup> Sensor technology<sup>12-14</sup> and information treatment<sup>15-19</sup> are fields in which applications for these complexes are expected. Our interest however lies in the luminescent properties of these compounds.

## 1.2 PHOTOPHYSICAL STUDIES

The luminescence properties of selected examples extracted from the literature will now be discussed in order to provide a foundation for our work. Emission assignments in the literature, discussed here, and also in our own work, are based on a localised molecular orbital approach. It has however been pointed out that this approach is inaccurate for  $d^8$  systems where metal-metal interactions are present.<sup>20</sup> (A valence bond model would be superior in this

case.) Miskowski and Houlding contend that the localised molecular orbital approach still provides a “reasonable description” of the lowest energy excited states.<sup>21</sup> Another premise often used in this field is that charge transfer (CT) processes comprise one electron centre-to-centre charge transfers although it has been suggested that this too could be an oversimplification.<sup>22, 23</sup>

Each subsection will be discussed according to the nature of the luminophore. Section 1.2.1 will deal with the photophysical studies of the platinum terpyridyl complex (described in section 1.1.1) which will be followed by a discussion of the luminescence studies of the platinum phenyl-bipyridyl complex (described in section 1.1.2). Dinuclear species in which two such luminophores are linked by a bridging ligand have been excluded from this discussion as they fall outside the scope of our study. Emission results from such species are however reported where they are relevant to the current discussion.

### **1.2.1 Luminophores derived from the [Pt{4'-R-terpy}]<sup>2+</sup> unit**

The compounds discussed in this section all have in common the [Pt{4'-R-terpy}]<sup>2+</sup> unit illustrated in Figure 1.1. The compounds only differ in the monodentate ligand bonded to platinum in the fourth coordination site and in the substituents on the terpyridyl ligand.

#### **1.2.1.1 The [Pt{4'-R-terpy}Cl]<sup>+</sup> luminophore**

This luminophore consists of terpyridine or a substituted terpyridine coordinated to platinum with a chloride ligand in the fourth coordination site of the platinum.

Interest in this luminophore goes as far back as 1976 when Lippard and coworkers showed that this moiety is capable of DNA intercalation.<sup>6</sup> The luminophore retained the curiosity of chemists working on its interactions with compounds of biological interest<sup>24, 25</sup>, with Kostić *et al.* showing the complex moiety to possess useful properties, in particular optical properties, which are of benefit for its use as a reagent for the covalent modification of proteins.<sup>26</sup> In this mode the chloride ligand is displaced, the luminophore described in this section being relegated to the role of a starting material for the biological interaction.

## *Absorption spectroscopy*

The solution absorption spectral properties of the  $[\text{Pt}(\text{terpy})\text{Cl}]^+$  luminophore in various media have been well documented<sup>6, 27 - 32</sup>, the results being in good agreement irrespective of the solvent or of the counterion. In all cases the absorbances adhere to Beer's Law in accordance with dissolution of the ionic salt into monomeric ions. Che *et al.* performed one of the early investigations of the optical and structural properties of  $[\text{Pt}(\text{terpy})\text{Cl}]^+$ , with an examination of the properties of  $[\text{Pt}(\text{terpy})\text{Cl}]\text{CF}_3\text{SO}_3$ .<sup>28</sup> Che and coworkers have interpreted the absorption spectrum of  $[\text{Pt}(\text{terpy})\text{Cl}]\text{CF}_3\text{SO}_3$  in acetonitrile in terms of two regions of absorptions, each with contrasting characteristics. The first set of absorbances in the 370 - 450 nm region shows a broad absorption band. In the second region absorptions occur between 300 and 350 nm as distinct, intense, vibronically structured bands. Vibrational spacings in this area range from 1270 to 1350  $\text{cm}^{-1}$ . The former set of absorbances are cautiously ascribed to metal-to-ligand charge transfer (MLCT) transitions  $[\text{Pt}(5d) - \text{terpy}(\pi^*)]$  by comparison with the absorption spectrum of  $[\text{Zn}(\text{terpy})_2]^{2+}$  which lacks peaks in this region. Evidence suggests that the absorbances in the second region arise due to  $^1(\pi - \pi^*)$  transitions of the terpyridyl ligand. Che and coworkers have found the band shape to be affected by the nature of the ligand in the fourth coordination site of platinum. In our context that means that the band profile depends on the nature of the luminophore. Here a halogen atom as the fourth ligand results in absorption bands reminiscent of intraligand  $\pi - \pi^*$  transitions. Che *et al.* propose that this phenomenon arises due to mixing between intraligand (IL) and MLCT excited states of the particular luminophore, the extent of the interaction being mediated by the ligand in the fourth coordination site of platinum. A similar coordination interaction has previously been described for  $d^6 \alpha$ -diimine complexes.<sup>33, 34</sup>

## *Emission spectroscopy*

The  $[\text{Pt}(\text{terpy})\text{Cl}]^+$  complex is essentially non-emissive in fluid solution at room temperature, with Che *et al.* reporting no emission from the luminophore under these conditions.<sup>27, 28</sup> But Crites, McMillin *et al.* have however been able to detect a very weak emission ( $\tau < 10$  ns) from a de-aerated dichloromethane ( $\text{CH}_2\text{Cl}_2$ ) solution at room temperature.<sup>30</sup> It is proposed that this lack of appreciable emission is due to the existence of low-lying d-d excited states which furnish convenient deactivation pathways *via* molecular distortions.<sup>27, 28, 30, 35, 36</sup>

The monomeric emission of [Pt(terpy)Cl]CF<sub>3</sub>SO<sub>3</sub> in a butyronitrile glass at 77 K is vibronically structured beginning at 470 nm and showing a spacing of *ca.* 1420 cm<sup>-1</sup> between the 0-0 and 0-1 transitions.<sup>28</sup> Emission spectra of the three related luminophores [Pt(terpy)X]<sup>+</sup> (X = Br, I, N<sub>3</sub>) recorded under the same conditions resemble that of [Pt(terpy)Cl]<sup>+</sup>. The Huang-Rhys factors (defined as I<sub>0,1</sub>/I<sub>0,0</sub>) are all *ca.* 0.6 and an <sup>3</sup>MLCT [Pt - terpy(π\*)] transition has been proposed as the emission origin in all four of these cases.<sup>28</sup>

A subsequent, more comprehensive study on the emission properties of [Pt(terpy)Cl]<sup>+</sup> was undertaken by Gray and coworkers.<sup>29</sup> The monomeric emission of the [Pt(terpy)Cl]<sup>+</sup> luminophore was investigated by the study of [Pt(terpy)Cl]PF<sub>6</sub> in 1:5:5 (v/v) DMF/EtOH/MeOH (DME) at 77 K. The results are directly comparable to those of Che *et al.*<sup>28</sup> as the difference in counterion is clearly not expected to affect the emission and any solvent effect arising from the dissimilarity in solvent matrix is foreseen to be negligible in the rigid matrix.<sup>37</sup> Gray *et al.* found multiple luminescence features, the dominant ones depending on the concentration of the solution or on the choice of excitation wavelength. The [Pt(terpy)Cl]<sup>+</sup> complex produces three independent transition types and each will now be discussed in turn.

In dilute (< 10 μM) glassy DME solution the emission measurements parallel those of Che and coworkers.<sup>28</sup> The emission produces a highly structured band with an origin at 470 nm. Peak progressions are sharply defined with a spacing of between 1100 and 1400 cm<sup>-1</sup> corresponding to the vibrational modes of terpyridine. The high energy feature of the dilute solution is shown to correspond to triplet absorptions in the emission-excitation spectrum (λ<sub>ex</sub> = 366 nm) of a dilute solution of [Pt(terpy)Cl]<sup>+</sup> and is assigned as the <sup>3</sup>(π-π\*) 0-0 line. Moreover the energy of the excitation bands were found to be unaffected by concentration changes, confirming the emission and excitation bands to be features of the monomer. The emission from isolated monomers is assigned to radiative decay from the terpy localized <sup>3</sup>(π-π\*) excited state by comparison with similar emission features displayed by platinum bipyridyl complexes.<sup>38, 39</sup> These measurements have been mirrored by Michalec, McMillin *et al.* with reports of [Pt(terpy)Cl]<sup>+</sup> recorded in a butyronitrile glass at 77 K.<sup>31, 32</sup>

The second emission occurs as a broad, weakly structured band at *ca.* 600 nm which is possibly composite in nature. This band is evident in the concentration range above 6 μM.

Gray *et al.* assign the band to “excimer-like” emission arising from  $\pi$ - $\pi$  interactions between partially stacked terpy ligands. The assignment is aided by the similarity of this emission with the crystalline emission of  $\{[\text{Pt}(\text{terpy})]_2(\mu\text{-pz})\}(\text{ClO}_4)_3 \cdot \text{CH}_3\text{CN}$  (pz = pyrazole) which has a long Pt...Pt distance of 3.432 Å.<sup>40</sup>

The third luminescence is characterised by a narrow unstructured band profile with an emission maximum at 720 nm. This luminescence is the only feature present when the solution is excited at 547 nm (which is *below* the onset of the dilute solution emission). The band profile and energy are typical of the emission one would expect from a dimeric system in which there is a metal-metal interaction.<sup>21, 28, 41</sup> In addition the feature is only apparent in solutions of concentration greater than 10  $\mu\text{M}$ . As the concentration is raised above this point, the energy of this third, low energy feature increases accordingly. Gray *et al.* propose that the emission is due to a metal-metal to ligand charge transfer (MMLCT)  $^3(\pi^* - d_{\sigma^*})$  transition based on the behaviour of the luminescence and by comparison with related binuclear species. This type of emission is an effect of oligomer formation which promotes intermolecular metal-metal interactions. The MMLCT transition can be explained in terms of a simple molecular orbital (MO) model reproduced in Figure 1.3. The  $d_{z^2}$ -orbital in the metal  $d^8$  electron configuration is full and by interaction with the equivalent  $d_{z^2}$ -orbital on the adjacent molecule splits into a bonding ( $d_{\sigma}$ ) and antibonding ( $d_{\sigma^*}$ ) combination. The  $d_{\sigma^*}$  orbital is sufficiently destabilised for it to become the HOMO in the ground state and hence the orbital to which electrons return upon relaxation by luminescence. The degree of  $d_{z^2}$  orbital splitting is a function of the extent of metal-metal interaction and consequently of dynamic intermolecular interactions in solution that promote the metal orbital interaction along the z-axis. Thus the MMLCT emission described in this case by Gray and coworkers is thought to involve an excitation from the  $d_{\sigma^*}$  metal-metal hybrid orbital to a  $\pi^*$  orbital localised mainly on the terpyridyl ligand. Clearly the effect of these intermolecular metal-metal interactions will be more pronounced in the solid state. These effects and their implications are discussed in greater detail later in this chapter when describing the solid state emission of the chloro(terpyridine chloro(terpyridine)platinum(II) luminophore (*vide infra*).



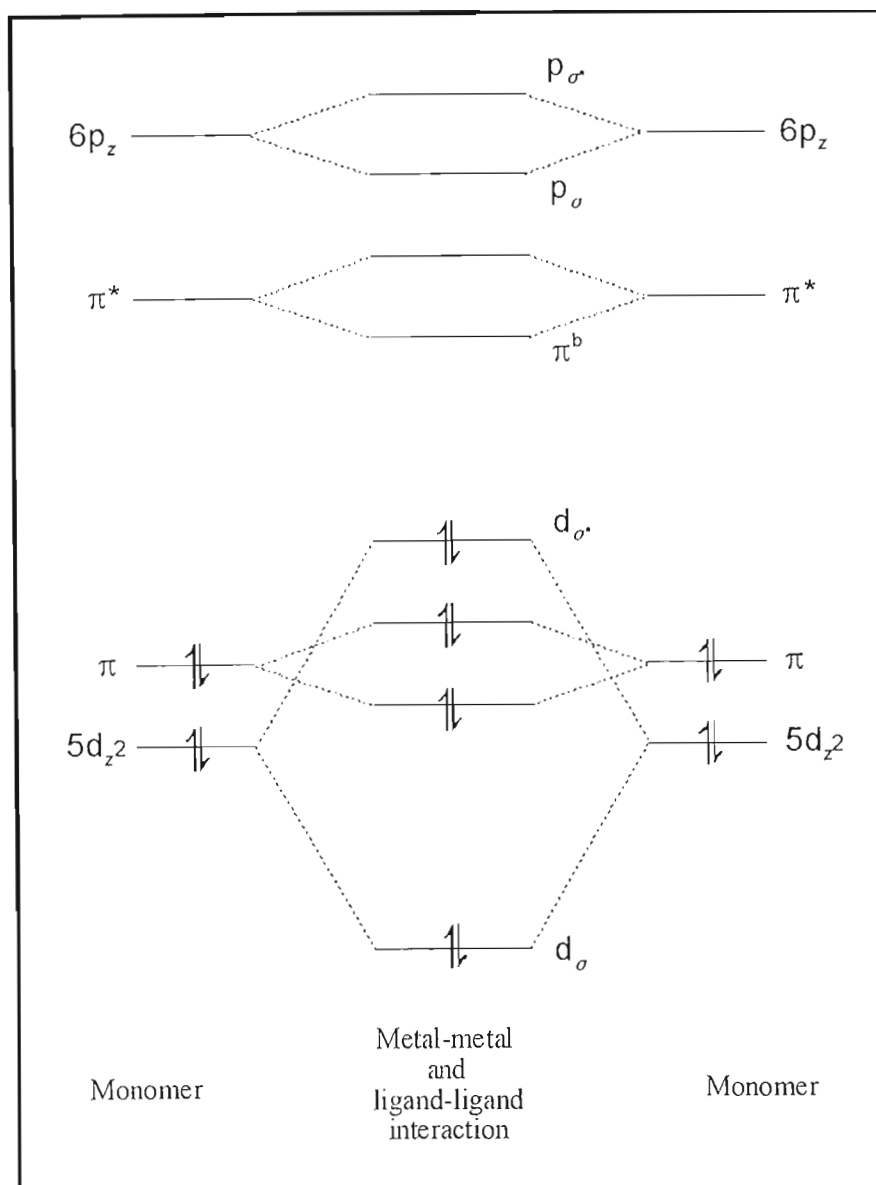


**Figure 1.3** Molecular orbital diagram proposed by Che *et al.* to describe the effect of close intermolecular contact on the molecular orbitals.<sup>28</sup>

In subsequent work by Campagna, Monsú Scolaro *et al.*<sup>42</sup> the compound [Pt(terpy)Cl]Cl was studied in a 4:1 (v/v) MeOH/EtOH glass at 77 K. The luminescence behaviour observed by Gray *et al.* was confirmed and, in addition, NMR experiments were performed that corroborate the aggregation of the complex in concentrated solutions as reported by Gray *et al.* Assignment of the excited state is in agreement with that of Gray *et al.*, although the group of Campagna *et al.* suggests a <sup>3</sup>MLCT contribution to the high energy emission (at 470 nm) from the monomer which Gray and coworkers describe as purely ligand centred. The metal contribution is proposed to account for the much shorter emission lifetime of 15  $\mu$ s, compared

to 300  $\mu\text{s}$  in the case of  $[\text{Pt}(\text{ppy})_2(\text{CH}_2\text{Cl})\text{Cl}]$  (where ppy is the *ortho*-C-deprotonated form of 2-phenylpyridine)<sup>43</sup>, and the lower energy emission origin, compared to that of a pure ligand-centred emitter such as  $[\text{Pt}(\text{ppy})_2(\text{CH}_2\text{Cl})\text{Cl}]$ .<sup>43</sup>

### *Solid-State emission spectroscopy*

Measurements have also been made of the emission spectrum of  $[\text{Pt}(\text{terpy})\text{Cl}]\text{CF}_3\text{SO}_3$  as a microcrystalline solid at both room temperature and at 77 K (in the first instance by Che and coworkers<sup>28</sup>; the salt was subsequently also studied by Gray *et al.*<sup>29</sup>). At both of these temperatures the band profile is structureless with the peak maximum occurring at a considerably lower energy compared to the monomeric emission in a butyronitrile glass. The room temperature spectrum achieves its maximum intensity at 600 nm  $\{\lambda_{\text{em}}(\text{max})\}$  and shows a shoulder at *ca.* 700 nm. Reducing the temperature to 77 K results in a red shift of the emission maximum from 600 to 625 nm and a reduction in the band width. Che *et al.* were also able to perform a X-ray crystal structure determination at room temperature<sup>28</sup> which shows the chloro(terpyridine)platinum(II) cations packing in face-to-face dimers, with each dimer having a Pt...Pt separation of 3.329 Å (see Figure 1.4). At such close contact a weak interaction between cations is anticipated in the solid state. The nature of these interactions and how they affect the solid state luminescence properties of the compound will now be discussed.

In explaining the solid state emission behaviour of  $[\text{Pt}(\text{terpy})\text{Cl}]\text{CF}_3\text{SO}_3$ , Che *et al.* noted that the close intermolecular contacts are probably influencing the emission properties of the compound, and referred to the work of Miskowski and Houlding who obtained similar emission characteristics for stacked Pt-diimine complexes and double salts such as  $[\text{Pt}(\text{bipy})_2][\text{PtCl}_4]$ .<sup>21, 41</sup> As described earlier in this chapter, an explanation based on the effect of close intermolecular approach in solution is utilised to account for spectral changes as the

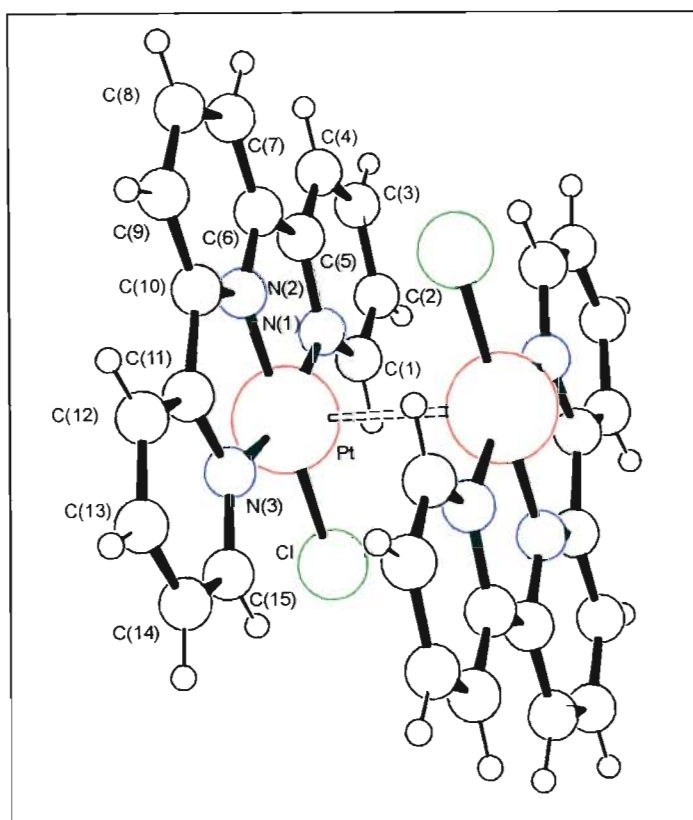


**Figure 1.4** Perspective view of dimeric structure of  $[Pt(terpy)Cl]CF_3SO_3$  (Plotted using coordinates taken from the structure of Che et al.<sup>28</sup>)

concentration of the luminophore in rigid glassy solution is increased. This approach was first adopted by Che and coworkers<sup>28</sup> who proposed the qualitative molecular orbitals representation reproduced in Figure 1.3. (The  $6p_z$ -orbitals which were not included in the original representation have been included here for the sake of completeness.) This molecular orbital diagram explains the difference in the arrangement of the molecular orbitals for the monomeric (*i.e.*, non interacting) state, recorded in dilute glassy medium, and that for the solid state where intermolecular interactions are present. Due to the interaction of  $z$ -directed orbitals, each splits into bonding (labelled  $d_\sigma$  and  $p_\sigma$ ) and antibonding combinations (labelled  $d_{\sigma^*}$  and  $p_{\sigma^*}$ ), the new set of molecular orbitals contributing to an overall stabilisation of the structure. This splitting is not only confined to the metal orbitals, as the interplanar spacing in the stack is often within the limit of ligand  $\pi$ - $\pi$  interactions. Thus it is proposed that the ligand- $\pi$  and  $-\pi^*$  orbitals are similarly stabilised. This produces the qualitative representation of the molecular orbitals shown in Figure 1.3.

The HOMO arising from this configuration of atom packing and hence electronic structure is the antibonding  $d_{\sigma^*}$ -orbital. This orbital is a metal-metal hybrid orbital localised near the two contributing platinum centres. The LUMO due to the bonding combination of adjacent  $\pi^*$ -orbitals is localised primarily on the ligand and has been labelled  $\pi^b$ , or more recently  $\sigma(\pi^*)$ .<sup>44</sup> The [ $d_{\sigma^*}$ - $\pi^b$ ] charge transfer excited state is thus produced by the promotion of an electron from a largely metal-metal hybrid orbital to a ligand-centred orbital. (It is for this reason that Gray *et al.* have subsequently adopted the appropriate notation “metal-metal to ligand charge transfer” (MMLCT) to refer to transitions of this type.<sup>29</sup>)

The important point in this discussion is that it is the intermolecular contact and overlap of platinum  $d_{z^2}$ -orbitals that is responsible for the distinctive emission behaviour. In particular Che *et al.* rationalise the difference in emission from the monomer (recorded in dilute butyronitrile glass at 77 K) compared to that in the solid state based on these intermolecular interactions and their molecular orbital scheme. The scheme accounts for the longer emission wavelength in the solid state by the smaller energy gap between the HOMO and LUMO in the case where orbital interaction is taking place. Significantly, in 1985 Gliemann and Yersin had shown that the red-shift in emission energy which occurs as the temperature of tetracyanoplatinate(II) compounds is reduced, could be attributed to metal-metal bond shortening as a consequence of thermal lattice contraction.<sup>45</sup> Indeed, Gray and coworkers have found a similar lattice contraction and enhanced metal-metal interaction for Pt-diimine complexes arranged in stacks in the solid state.<sup>46</sup> This finding is rationalised in terms of the MO diagram discussed here by noting that the reduced platinum-platinum separation will result in an enhanced orbital interaction. The magnified splitting will then produce a lower excitation at low temperatures and hence the emission is red-shifted. This chain of events is a direct consequence of the molecular arrangement in the solid state, whereby intermolecular contact allows for the overlap of  $d_{z^2}$ -orbitals on adjacent molecules. Hence the red emission of solid [Pt(terpy)Cl]CF<sub>3</sub>SO<sub>3</sub> is assigned to a ( $\pi^b - d_{\sigma^*}$ ) transition (see Figure 1.3).

Subsequent work has investigated the electronic spectroscopy of the luminophore in the solid state. Gray and coworkers undertook a study of the effect of intermolecular stacking interactions on the electronic spectroscopy of the [Pt(terpy)Cl]<sup>+</sup> luminophore by varying the nature of the counterion.<sup>29</sup> To this end the luminescent properties of [Pt(terpy)Cl]X [X<sup>-</sup> =

$\text{ClO}_4^-$  (red form precipitated from aqueous solution),  $\text{ClO}_4^-$  (orange-red form recrystallised from DMF/ether),  $\text{Cl}^-$ ,  $\text{CF}_3\text{SO}_3^-$ ,  $\text{PF}_6^-$ ] were investigated in the solid state. A crystal structure of the orange-red form of  $[\text{Pt}(\text{terpy})\text{Cl}]\text{ClO}_4$  revealed that the luminophores are packed in dimeric units [ $\text{Pt}\cdots\text{Pt} = 3.269(1) \text{ \AA}$ ] arranged along an infinite terpy- $\pi$  stack (spacing  $\sim 3.35 \text{ \AA}$ ). The energy of the luminescence band depends on the counterion ( $\text{PF}_6^-$ ,  $\text{ClO}_4^-$ ,  $\text{Cl}^-$ ,  $\text{CF}_3\text{SO}_3^-$ ) and on the method of crystallisation and is directly related to the colour of each salt. Differences therefore arise owing to the differing Pt-Pt and  $\pi$ - $\pi$  interactions in the lattice of each salt. The emission spectra of the salts recorded at ambient temperature are broad and structureless with maxima centred at 630 ( $\text{PF}_6^-$ ), 725 (red perchlorate salt), 645 (orange-red perchlorate salt), 650 ( $\text{Cl}^-$ ) and 640 nm ( $\text{CF}_3\text{SO}_3^-$ ) respectively. Reducing the temperature to 77 K has the effect of drastically narrowing each band (fwhm  $\approx 1000 - 2000 \text{ cm}^{-1}$ , where fwhm is the full width at half maximum) which at 77 K tails off to a lower energy suggesting unresolved vibronic structure in the terpy vibrational modes. Significantly the emission maxima are blue-shifted to 565 ( $\text{PF}_6^-$ ), 695 (red perchlorate salt), 640 (orange-red perchlorate salt), 640 ( $\text{Cl}^-$ ) and 625 nm in the case of the triflate salt. This is in contrast to the observations made by Che and coworkers that there is a red-shift in the emission maximum on cooling a solid sample of  $[\text{Pt}(\text{terpy})\text{Cl}]\text{CF}_3\text{SO}_3$ .<sup>28</sup> Gray and coworkers suggest that a red shift is only expected for linear chain compounds, *i.e.*, where there is a uniform Pt $\cdots$ Pt separation along the stack. This is certainly not the case for the orange-red perchlorate salt which, as mentioned above, packs in dimeric units in the solid state. Inevitably one must conclude that differences in sample preparation must account for the conflicting emission behaviour of salts made by the group of Che *et al.*<sup>28</sup> compared to the behaviour reported by Gray and coworkers.<sup>29</sup> The red shift observed by Che *et al.* has subsequently been reproduced by Field, McMillin *et al.*<sup>47</sup> (*vide infra*).

The emission for the 77 K spectra of the above salts have been assigned by Gray *et al.* to radiative decay from a  $^3[\text{d}_{\sigma^*}(\text{Pt}_2) - \pi^*(\text{terpy})]$  (MMLCT) excited state. However the excited state at ambient temperature was more difficult to assign. The suggestion is made that the room temperature emission bands originate from excimeric intraligand transitions resulting from  $\pi$ - $\pi$  interactions between adjacent luminophores. In their paper Gray and coworkers further allude to the question of whether the room temperature and low temperature emissions arise from two different excited states of the same luminophore or from two distinct sites in

the solid. However, despite a detailed study of the unusual temperature dependence of the emission by the  $\text{PF}_6^-$  salt in particular, no definite conclusion is reached.

Field, McMillin and coworkers have further contributed to the solid state spectroscopy of the chloro(terpyridine)platinum(II) moiety with the synthesis and study of its hexafluoroantimonate and triflate salts.<sup>47</sup> In contrast to the observations of Gray *et al.*<sup>29</sup> (*vide supra*) the orange triflate salt was found to show a distinct *red* shift in its emission maximum from 585 nm at ambient temperature to 613 nm at 100 K. This behaviour is in line with that reported by Che *et al.* for the same compound<sup>28</sup>, also in respect of an increase in intensity and narrowing of the width of the emission band on lowering the temperature. However, the temperature dependence of the emission by the yellow hexafluoroantimonate salt is different. In this case the wavelength of the emission maximum  $\{\lambda_{\text{em}}(\text{max})\}$  is essentially temperature independent, there being only an increase in intensity of the band as the temperature is reduced to 80 K. The fact that the emission maximum occurs at a much higher energy than that of the triflate salt and that this emission maximum is temperature independent has been linked to emission from monomeric (*i.e.*, non-interacting) platinum centres. The authors go further, relating the solid state emission by  $[\text{Pt}(\text{terpy})\text{Cl}]\text{SbF}_6$  to that recorded for  $[\text{Pt}(\text{terpy})\text{Cl}]\text{PF}_6$  by Gray *et al.*<sup>29</sup> Field, McMillin and coworkers propose that the 630 nm emission of the  $\text{PF}_6^-$  system which is absent below 100 K originates at a “trap site”.<sup>47</sup> The signal at 565 nm manifesting itself below 100 K parallels that of the  $\text{SbF}_6^-$  analogue. Similarly with the triflate salts, it is the emission at the lowest temperatures that show common features.<sup>27, 29</sup>

#### The effect of 4'-substitution

Clearly the presence of extended interactions in the solid state has a considerable effect on the optical and electronic properties of this luminophore in the solid state. The extended interactions can be manipulated by altering the counterion or the method by which the compound is crystallised. The effect of these two variables is somewhat unpredictable as evidenced by the variation in luminescence properties observed when different counterions and methods of crystallisation are used.<sup>28, 29, 47</sup> The next, perhaps more predictable, method for manipulating the emission of the chloro(terpyridine)platinum(II) luminophore was to add substituents to the terpyridine moiety. Although Che *et al.* were the first to describe the

synthesis and spectroscopic measurements of  $[\text{Pt}(4'\text{-R-terpy})\text{Cl}]^+$  (where  $\text{R} = \text{C}_6\text{H}_4\text{OMe-}p$ ,  $\text{C}_6\text{H}_4\text{Me-}p$ ,  $\text{C}_6\text{H}_4\text{Br-}p$ ,  $\text{C}_6\text{H}_4\text{CN-}p$ )<sup>28</sup>, the work of Crites, McMillin *et al.* in studying substituent effects in the 4'-position<sup>30</sup> will be discussed first. This description will be followed by a discussion of the luminescent properties of compounds which have aromatic substituents in the 4'-position, including those of Che and coworkers.<sup>28</sup>

In order to probe the effect of the substituent in the 4'-position, Crites, McMillin *et al.* synthesised the series of chloro(terpyridine)platinum(II) luminophores  $[\text{Pt}(4'\text{-A-terpy})\text{Cl}]\text{TFPB}$ , substituted with both electron withdrawing ( $\text{A} = \text{CN}$ ,  $\text{SO}_2\text{Me}$ ) and electron donating groups ( $\text{A} = \text{SMe}$ ,  $\text{NMe}_2$ ), and where TFPB is the non-coordinating counterion tetrakis[3,5-(trifluoromethyl)phenyl]borate.<sup>30</sup> The room temperature photophysics was studied in acetonitrile and dichloromethane solutions. As with the unsubstituted luminophore the compounds exhibit a series of intraligand  $\pi\text{-}\pi^*$  absorptions below 350 nm and charge transfer absorptions in the vicinity of 400 nm. The peak intensities of the CT absorptions are significantly enhanced in the substituted luminophores as compared to absorptions of the unsubstituted luminophore,  $[\text{Pt}(\text{terpy})\text{Cl}]^+$ , and the absorption maxima are shifted to lower energies.

The complexes are all luminescent in dichloromethane. In acetonitrile the  $\text{NMe}_2$  substituted luminophore is the only one to emit, the remainder likely experiencing solvent-induced exciplex quenching of the CT excited state. The emission spectra are all similar, showing well resolved vibrational maxima reported as 550, 590(sh) nm (CN), 542, 577 nm ( $\text{SO}_2\text{Me}$ ), 542, 575, 625(sh) nm (SMe) and 535, 570, 635(sh) nm ( $\text{NMe}_2$ ). Excitation measurements match the absorption spectra and emission decay is mono-exponential in all cases. Further, the substituents have the effect of significantly increasing the emission lifetime in dichloromethane relative to that of the unsubstituted  $[\text{Pt}(\text{terpy})\text{Cl}]^+$  luminophore at room temperature. The  $[\text{Pt}(\text{terpy})\text{Cl}]^+$  luminophore has an emission lifetime of less than 10 ns. In contrast the lifetimes of the 4'-substituted derivatives are 116 ns (CN), 21 ns ( $\text{SO}_2\text{Me}$ ), 142 ns (SMe) and 1920 ns ( $\text{NMe}_2$ ). The nature of the excited state is not conclusively assigned, although the emission results can be qualified by relaxation from a MLCT excited state as long as there exists another state influencing the decay. The difficulty lies in identifying this other state. If this state indeed exists, the structured band profile and enhanced emission lifetimes could be indicative of a further significant intraligand contribution to the excited state.

Solution emission studies of the 4'-substituted complexes (where A = CN, SMe and NMe<sub>2</sub>) have been supplemented by Crites Tears and McMillin in a subsequent study on quenching of the excited state by a range of Lewis bases.<sup>48</sup> The studies show the rate of exciplex quenching to increase as the donor number (an indicator of Lewis base strength<sup>49</sup>) of the solvent increases.

McMillin's work in this area has been extended by Cummings and coworkers with synthesis of the platinum(II)terpyridyl complex where a chlorine atom has been bonded in the 4'-position {viz. [Pt(4'-Cl-terpy)Cl]Cl}. This work forms part of an investigation into the effect of adding electron withdrawing substituents, in particular chlorine, to the terpy ligand.<sup>50</sup> In the same study a triply chloro-substituted complex, where the chlorine atoms are in the 4-, 4'- and 4''-positions, has also been made and its photophysical properties examined. This triply substituted complex will be discussed under a separate heading later in this section, *vide infra*.

A UV/vis absorption spectrum of the [Pt(4'-Cl-terpy)Cl]<sup>+</sup> luminophore was recorded in dilute acetonitrile (~ 10<sup>-5</sup> M) and shows no unexpected features. Bands in the 200 - 280 nm region are assigned to <sup>1</sup>π-π\* and a broad band at ~ 397 nm is attributed to a Pt(5d) → terpy(π\*) metal-to-ligand charge transfer transition. The assignments are based on the energy and relative intensities of the bands and by analogy with assignments made for other Pt(terpy)X<sup>-</sup> complexes.<sup>27,29</sup> Comparison is also made with similar spectra recorded for the uncoordinated ligand, corroborating the ligand-based assignment made for the bands at higher energy.

Emission has been recorded in an acetonitrile solution at 298 K and shows a broad band centred at *ca.* 600 nm which is quenched in the presence of oxygen. This quenching behaviour in conjunction with the energy, shape and intensity of the emission band lead the authors to a <sup>3</sup>MLCT assignment.

The authors make no attempt to reconcile this emission with (dissimilar) findings reported by Crites, McMillin and coworkers of closely related compounds where the 4'-position is also substituted with an electron withdrawing group (*vide supra*).<sup>30</sup> In particular, no results are reported of emission from dichloromethane solution as undertaken by McMillin *et al.*<sup>30</sup>



The emission of  $[\text{Pt}(4'\text{-Cl-terpy})\text{Cl}]^+$  in a 1:5:5 (v/v) DMF/EtOH/MeOH (DME) glass at 77 K was also studied. The luminescence at two concentrations has been reported. The first, essentially monomeric emission, recorded at  $\sim 10 \mu\text{M}$  shows a structured band with 0-0 transition at 480 nm and a vibronic spacing of  $\sim 1420 \text{ cm}^{-1}$ . This spacing corresponds to the frequency of ligand ring mode vibrations as measured in an IR spectrum, suggesting a strong ligand influence in the character of the excited state.

Cummings *et al.* also report the emission properties of the free ligand in DME glassy medium at 77 K. Both singlet and triplet emission is observed, with the analogous triplet  $\pi\text{-}\pi^*$  emission of the free ligand occurring at higher energy than that of the coordinated platinum complex. The authors regard this disparity in energy as evidence for metal character in the excited state of the platinum complexes. An assignment of the emission to relaxation from a  $^3(\pi\text{-}\pi^*)$  excited state is based in large part on the vibronic structure observed in the emission spectrum of  $[\text{Pt}(4'\text{-Cl-terpy})\text{Cl}]^+$  in dilute glassy solution at 77 K with the possibility of a MLCT contribution.

Emission spectra have also been recorded at concentrations higher than  $50 \mu\text{M}$  in the same glassy medium. At these concentrations a new, broad feature at lower energy becomes evident at 590 nm. This emission is similar to that previously observed for related platinum(II) terpyridyl complexes.<sup>29, 51, 52</sup> Cummings and coworkers regard diffusion from excited state species as unlikely and in analogy to Gray *et al.*<sup>29</sup> the feature is ascribed to “excimer-like” emission from weakly associated ground state aggregates. It is also noted that the 590 nm features are absent from spectra of room temperature fluid solutions of either the complexes or the free ligands.

No luminescence spectra of solid microcrystalline samples of the  $[\text{Pt}(4'\text{-Cl-terpy})\text{Cl}]\text{Cl}$  salt have been reported.

#### *Aromatic substitution in the 4'-position*

Studies in which the chloro(terpyridine)platinum(II) luminophore was substituted with an **aromatic** group in the 4'-position will now be discussed. This section will start with a

description of the photophysical properties of complexes where the 4'-position of the terpyridyl ligand has been substituted with a phenyl ring<sup>32, 42, 53</sup>, followed by a description of the photophysical properties of complexes where the phenyl ring in the 4'-position has been additionally substituted, first in the para-position<sup>28, 32</sup> and then in the ortho-position.<sup>54</sup> The final section dealing with chloro(terpyridine)platinum(II) complexes which have an aromatic substituent in the 4'-position, will describe the photophysical properties of luminophores where large fused-ring aromatic groups have been attached to this position.<sup>31, 32</sup>

### *Phenyl substitution in the 4'-position*

Campagna, Monsú Scolaro and coworkers undertook a comparative study in which terpyridine and 4'-phenyl-terpyridine (4'-Ph-terpy) were coordinated to platinum(II).<sup>42</sup> The fourth ligand comprised  $\text{Cl}^-$ ,  $\text{CH}_3^-$  or  $\text{Ph}^-$ . Thus the six complexes  $[\text{Pt}(\text{terpy})\text{Cl}]\text{Cl}$ ,  $[\text{Pt}(4'\text{-Ph-terpy})\text{Cl}]\text{Cl}$ ,  $[\text{Pt}(\text{terpy})\text{CH}_3]\text{Cl}$ ,  $[\text{Pt}(4'\text{-Ph-terpy})\text{CH}_3]\text{Cl}$ ,  $[\text{Pt}(\text{terpy})\text{Ph}]\text{Cl}$  and  $[\text{Pt}(4'\text{-Ph-terpy})\text{Ph}]\text{Cl}$  were synthesised and studied. In all cases the complexes were characterised, a detailed NMR study carried out and some photophysical properties measured. The absorption spectra in 4:1 (v/v) MeOH/EtOH fluid solution at ambient temperature and the luminescence in a 4:1 (v/v) MeOH/EtOH glass at 77 K were recorded. The results obtained for the latter four complexes will each be discussed in the relevant section of this chapter. The chloro(terpyridine)platinum(II) complex served merely as a reference point, confirming the results of Gray *et al.*<sup>29</sup> and Che *et al.*<sup>28</sup> for the same luminophore. Subsequent to the work of Campagna, Monsú Scolaro *et al.*<sup>42</sup>, Field, McMillin and coworkers investigated the photophysical properties of  $[\text{Pt}(4'\text{-Ph-terpy})\text{Cl}]^+$  in solution<sup>32, 53</sup>, but unlike the earlier study, an investigation of the solid state properties of  $[\text{Pt}(4'\text{-Ph-terpy})\text{Cl}]\text{A}$  ( $\text{A} = \text{SbF}_6^-$ ,  $\text{CF}_3\text{SO}_3^-$ ,  $\text{BF}_4^-$ ) was included. Where applicable these results will be discussed in conjunction with the findings of Campagna *et al.*<sup>42</sup>, as the luminophore is common to the work of both groups.

### *Absorption spectroscopy*

The absorption spectrum in acetonitrile solution of the  $[\text{Pt}(4'\text{-Ph-terpy})\text{Cl}]^+$  luminophore is unaffected by the nature of the counterion. As with the luminophore containing the unsubstituted ligand, the absorption spectrum at room temperature can be regarded in terms

of two regions separated at about 350 nm. The first region at higher energy consists of a relatively intense absorption at 283 nm ( $\epsilon$  31400 M<sup>-1</sup>.cm<sup>-1</sup>)<sup>53</sup> and an additional structured band between 300 and 350 nm. Campagna *et al.* in studying the same luminophore *viz.*, [Pt(4'-Ph-terpy)Cl]Cl.2H<sub>2</sub>O in 4:1 (v/v) MeOH/EtOH obtained essentially the same spectrum and noted that a more detailed assignment of the bands between 300 and 350 nm is prohibited by significant band overlap. What is noticeable is the practically identical absorbances at wavelengths shorter than 350 nm compared to the absorption spectrum of the unsubstituted species recorded under the same conditions.<sup>28, 29</sup> Both groups concur in assigning the absorption bands in this higher energy region to IL ( $\pi$ - $\pi^*$ ) transitions.<sup>32, 42, 53</sup>

In the second region, at wavelengths longer than 350 nm, there is a second absorption band of much weaker intensity ( $\epsilon$  7600 M<sup>-1</sup>.cm<sup>-1</sup>)<sup>42</sup> with  $\lambda_{\max}$  at 410 nm. This is at a slightly longer wavelength than that recorded for the analogous unsubstituted luminophore [Pt(terpy)Cl]<sup>+</sup>. Michalec, McMillin and coworkers have also recorded the absorption spectra in acetonitrile and in dichloromethane for the zinc-coordinated analogue. In contrast to the platinum-coordinated chromophore there is no reduction in absorption energy as the polarity of the solvent is increased by the use of acetonitrile rather than dichloromethane.<sup>32</sup> This absorption behaviour of the [Pt(4'-Ph-terpy)Cl]<sup>+</sup> luminophore is consistent with charge transfer transitions and both groups agree in assigning the bands to spin-allowed MLCT transitions<sup>32, 42, 53</sup>, based in part on studies made of related platinum-polypyridyl complexes, including those described earlier in this chapter.<sup>27-29, 44</sup>

### *Emission spectroscopy*

The emission of the [Pt(4'-Ph-terpy)Cl]<sup>+</sup> luminophore in fluid solution (both MeCN and CH<sub>2</sub>Cl<sub>2</sub>) is negligible.<sup>27, 32, 53</sup> This is reportedly due to the presence of accessible thermally populated, low-lying d-d excited states capable of promoting radiationless decay *via* molecular distortion<sup>27, 53</sup>, although Michalec, McMillin and coworkers make the point that dominant MLCT character of the excited state is likely to be susceptible to solvent induced exciplex quenching in donor solvents.<sup>32, 48</sup> Nevertheless, Michalec, McMillin *et al.* report the room temperature emission spectra of [Pt(4'-Ph-terpy)Cl]<sup>+</sup> in degassed butyronitrile and dichloromethane.<sup>32</sup> In deoxygenated dichloromethane the luminophore emits in a low

intensity, weakly structured band with 0-0 progression at 535 nm. This emission has a lifetime of 85 ns. No emission was detected from the butyronitrile solution at room temperature, with only the 77 K spectrum providing a detectable signal. The authors reconcile this behaviour with strong MLCT character in the nature of the excited state.

In order to avoid the thermal population of those excited states which allow for rapid non-radiative deactivation by molecular distortion, spectra are measured in a rigid matrix at 77 K. Campagna *et al.*, in their study of [Pt(4'-Ph-terpy)Cl]Cl in a 4:1 (v/v) MeOH/EtOH rigid matrix, identify three distinct emission origins<sup>42</sup>, each characterised by a different lifetime and emission energy analogous to the observations made by Gray *et al.* on the unsubstituted luminophore.<sup>29</sup> The intensity of each emission is found to be dependent on concentration and excitation wavelength. The first emission, dominant at the lowest concentration and due to luminescence from the isolated monomer, manifests itself in a vibrationally structured band (progressions  $\sim 1300\text{ cm}^{-1}$ ) with an origin at 515 nm. The emission is assigned to metal-perturbed <sup>3</sup>LC (ligand-centred) excited states based on the band profile and emission lifetime (15  $\mu\text{s}$ ) which, as the authors explain, is much shorter-lived than one would expect of a state having pure ligand character.<sup>43</sup> The second emission is detected as a broad, unstructured low intensity band at about 650 nm which is present in solutions with a concentration greater than 0.01 mM. The behaviour of the emission is consistent with aggregative phenomena and the emission is attributed to radiative decay from an excited state arising due to excimeric  $\pi$ - $\pi$  interactions between partially stacked ligands. This assignment is again based on similar conclusions drawn by Gray and coworkers for related complexes.<sup>29</sup> As the concentration is increased to 0.1 mM, a third emission with a narrow unstructured band profile is detected at 690 nm. Increasing the concentration further results in an increase in the intensity of this band at the expense of the monomeric emission at 515 nm. The position and intensity of the lowest energy emission band is highly dependent on the excitation wavelength. The excimeric emission at 650 nm obscures the low energy emission band at 690 nm when the excitation wavelength is below 480 nm. However, with an excitation wavelength greater than 500 nm, the luminescence at 690 nm is again dominant. The authors are confident in assigning this emission at 690 nm to a <sup>3</sup>MMLCT excited state based on the band shape, low energy of the emission maximum and on the concentration dependence which clearly indicates the presence of aggregation in solution.<sup>42,53</sup> Aggregation in solution is also confirmed by NMR experiments

in which certain resonances are shifted upfield as the concentration is increased or temperature reduced. Moreover, the emission behaviour displayed by the compound is a well established feature of luminescence from compounds in which metal-metal interactions are present.

The observations and conclusions drawn from the luminescence behaviour of  $[\text{Pt}(4'\text{-Ph-terpy})\text{Cl}]^+$  in a rigid matrix by Campagna, Monsú Scolaro *et al.* are endorsed by the subsequent work of Field, McMillin *et al.* on the same luminophore in a rigid butyronitrile glass recorded at 77 K.<sup>32,53</sup> By studying the solution photophysics of complexes with the 4'-phenyl-terpyridyl ligand coordinated to zinc(II) Michalec, McMillin *et al.* show that the ligand is not susceptible to ionisation and hence the excited state is unlikely to possess significant ILCT character.<sup>32</sup> The extended lifetime of the luminophore in fluid solution compared to the unsubstituted  $[\text{Pt}(\text{terpy})\text{Cl}]^+$  luminophore, allows conjecture for the participation of LC states as proposed by Campagna, Monsú Scolaro *et al.* but the possibility of an accessible <sup>3</sup>d-d excited state promoting radiationless deactivation is not completely discounted. Further, although the reduction potential of the  $[\text{Pt}(4'\text{-Ph-terpy})\text{Cl}]^+$  compound in solution is unaffected by substitution in the 4'-position, *i.e.* by the nature of the ligand, (which has been found to be the predominant influence of the ligand on the presence of a MLCT state<sup>55</sup>) the authors still consider the excited state of this luminophore to be dominated by MLCT character, in particular as a result of the marked solvent sensitivity experienced by the luminophore. Of interest are differences in the positions of the emission maxima as reported by the two groups. Field, McMillin and coworkers report the ligand-centred emission origin and MMLCT emission maxima at 505 and 726 nm respectively, compared to the values of 515 and 690 nm recorded by the group of Campagna and Monsú Scolaro. Clearly changing the matrix affects the position of the emission maxima. The central band due to excimeric interactions is reported at 622 nm by Field, McMillin and coworkers<sup>53</sup> and at 650 nm by Campagna, Monsú Scolaro and coworkers.<sup>42</sup> This discrepancy could, however, be a consequence of the broadness of the band and the inherent uncertainty that therefore arises in determining the exact position of the emission maximum. It is also interesting to consider the effect on the monomeric glass emission of introducing an aromatic moiety to the 4'-position of the chloro(terpyridine)-platinum(II) luminophore. Most noticeably, one observes that the lower energy of the <sup>3</sup>( $\pi$ - $\pi^*$ ) level for the phenyl substituted terpyridyl ligand is reflected in a longer emission wavelength (470 vs 515 nm).

The group of Field and McMillin go on to record the solid state emission of the yellow [Pt(4'-Ph-terpy)Cl]A (A<sup>-</sup> = SbF<sub>6</sub><sup>-</sup>, CF<sub>3</sub>SO<sub>3</sub><sup>-</sup>, BF<sub>4</sub><sup>-</sup>) salts.<sup>53</sup> The tetrafluoroborate and triflate salts also exist in red metastable crystalline forms. All the compounds show a strong temperature dependent emission in the solid state. The investigation is further aided by the crystal structure of the red metastable form of [Pt(4'-Ph-terpy)Cl]BF<sub>4</sub> determined at 153 K.

Although all the salts exist in the yellow form, the emission of the yellow tetrafluoroborate salt is discussed as representative of the other two. At 80 K the compound exhibits a structured emission (spacing ~1200 cm<sup>-1</sup>) with an origin at 518 nm. The band profile is very similar to the monomeric emission from the dilute butyronitrile glass recorded at 77 K, the position of each vibrational band being unaffected by temperature variations. This behaviour is consistent with emission from monomers showing no interactions in the crystal. The structured profile suggests a strong IL influence, but the shift to lower energy of the emission origin compared to the emission from the luminophore without a phenyl ring in the 4'-position (which has its highest energy band at 470 nm<sup>27, 29</sup>) is interpreted as being a consequence of metal influence on the excited state. The authors therefore assign the emission to an excited state that has both MLCT and IL  $\pi$ - $\pi^*$  character, described as (d, $\pi$ ) -  $\pi^*$ , based on the work of Crites, Cunningham and McMillin.<sup>30</sup> In this instance the state is thought to have triplet multiplicity based on an emission lifetime of 1  $\mu$ s at 80 K.

The red triflate salt is too unstable to allow emission measurements to be performed, rapidly regressing to the more stable yellow morph. A description of the solid state emission characteristics of the red chloro(phenyl-terpyridine)platinum(II) complex is therefore restricted to the solvated, red tetrafluoroborate salt, [Pt(4'-Ph-terpy)Cl]BF<sub>4</sub>.CH<sub>3</sub>CN, of which a crystal structure recorded at 153 K is reported. Interestingly the luminophores do not pack in a uniform stack, or even as dimers. Instead face-to-face packing takes place in sets of tetramers. Within a tetramer the Pt...Pt distance is approximately 3.3 Å whereas there is an inter-tetramer Pt...Pt separation of 4.680 Å which precludes d<sub>z<sup>2</sup></sub>...d<sub>z<sup>2</sup></sub> orbital interactions between tetramers. At room temperature, emission from the red salt is in a narrow asymmetric band with a peak intensity at 655 nm. A reduction in temperature to 80 K results in a further narrowing of the band and a red shift in the peak intensity to 730 nm. This behaviour in conjunction with a 1.1  $\mu$ s emission lifetime at 80 K is typical of the solid state luminescence one would expect for

infinite linear-chain structures in which there is a uniform Pt...Pt separation.<sup>21, 28, 41</sup> This is contrary to the picture presented by the X-ray diffraction experiments. The authors ascribe the emission to a <sup>3</sup>MMLCT excited state resulting from a [ $\pi^*(4'-\text{Ph-terpy}) \rightarrow d_{\sigma^*}$ ] relaxation. Triplet multiplicity is based on the emission lifetime.

#### Para-substitution of the aromatic 4'-phenyl moiety

In this section a description is provided of the photophysical measurements made by Che and coworkers on four platinum salts with the formulations  $[\text{Pt}(4'-p\text{RPh-terpy})\text{Cl}]\text{ClO}_4$  [R = OMe, Me, Br, CN], where 4'-pRPh is a *para*-substituted phenyl ring in the 4'-position of terpyridine.<sup>28</sup> More recently Michalec, McMillin *et al.* have also studied the complex where R = OMe, but used hexafluorophosphate as the anion.<sup>32</sup> Although the latter investigation is merely part of a larger study into the effect of large aromatic systems in the 4'-position, the photophysical properties have been investigated in far greater depth than in the original study by Che *et al.*<sup>28</sup> The absorption spectra of the set of complexes in Che and coworkers' study are all similar with intense high energy (29 - 330 nm) absorption bands resembling those of the free ligand and hence are assigned to intraligand transitions. In contrast to the absorptions shared with the free ligand, the complexes show an additional moderately intense band between 404 and 415 nm which Che *et al.* assign to spin-allowed MLCT transitions.<sup>28</sup> Michalec, McMillin *et al.* reach the same conclusions but in addition, their study includes a comparison of the absorption spectra of  $[\text{Pt}(4'-p\text{OMePh-terpy})\text{Cl}]\text{PF}_6$  recorded in dichloromethane with those measured in acetonitrile.<sup>32</sup> A shift to lower energy in the former solvent is seen as additional evidence for the MLCT nature of the bands at lower energy. Moreover, Michalec, McMillin *et al.* have also studied the zinc(II) complex in order to ascertain the extent to which MLCT character contributes to the nature of the excited state. No shift to lower energy is evident in the low energy absorption manifold of these zinc(II) complexes when a less polar solvent is used, providing further evidence for a MLCT assignment of these moderately intense absorption bands. This is useful in allowing the authors to discount the existence of low lying ILCT states evident in related complexes.<sup>32</sup>

These 4'-substituted complexes are significant in that they also display emission in degassed acetonitrile solution at 298 K. This is in contrast to the  $[\text{Pt}(\text{terpy})\text{L}]^{n+}$  (L = Cl, Br, I, N<sub>3</sub> and

$n = 1$ ;  $L = \text{NH}_3$  and  $n = 2$ ) species which are non-emissive under the same conditions.<sup>28</sup> {Note that Che *et al.* include the thiocyanate anion in their list of non-emissive complexes in degassed acetonitrile solution at room temperature<sup>26</sup>, but McMillin *et al.* have subsequently recorded emission from  $[\text{Pt}(\text{terpy})\text{SCN}]^{n+}$  in acetonitrile and in  $\text{CH}_2\text{Cl}_2$ .<sup>27</sup>} This is noteworthy, since, even the emission from the fluid solution of  $[\text{Pt}(4'\text{-Ph-terpy})\text{Cl}]^+$  is negligible (*vide supra*).

The emission of the  $[\text{Pt}(4'\text{-}p\text{OMePh-terpy})\text{Cl}]^+$  luminophore will now be discussed since it has been studied in greater detail by Michalec, McMillin and coworkers<sup>32</sup> than in the earlier study undertaken by Che.<sup>28</sup> In the latter study where emission is recorded in a room temperature degassed acetonitrile solution, Che *et al.* merely report the emission maximum at 582 nm with a lifetime of 8.5  $\mu\text{s}$ , and tentatively assign the luminescence to relaxation from a <sup>3</sup>MLCT state.<sup>28</sup>

Michalec, McMillin and coworkers record the luminescence of the  $[\text{Pt}(4'\text{-}p\text{OMePh-terpy})\text{Cl}]^+$  luminophore in BuCN and in dichloromethane.<sup>32</sup> The room temperature emission spectra show weakly structured bands with maxima at 555 and 560 nm respectively in each solvent. The emission lifetime in dichloromethane is 5.2  $\mu\text{s}$  and apparently somewhat shorter in butyronitrile, although no value is reported. Anomalous to the suggestion of Michalec, McMillin *et al.*, that participation of MLCT character would promote solvent induced deactivation of the emitting state in coordinating solvent,<sup>31,32</sup> the lifetime found by Che *et al.* is in fact longer than that found by Michalec, McMillin *et al.* in non-coordinating dichloromethane. Emission studies of the zinc(II) coordinated complex,  $[\text{Zn}(4'\text{-}p\text{OMePh-terpy})\text{Cl}_2]$ , show evidence for <sup>1</sup>ILCT fluorescence. This would mean that the *para*-OMe substituted phenyl ring is capable of undergoing ionization and that the platinum(II) coordinated complex is likely to have an ILCT contribution to its excited state. The authors regard the unexpectedly long emission lifetime at a relatively low emission energy (contrary to the predictions of the Energy Gap Law) as confirmation of an ILCT contribution to excited state. The fact that emission from  $[\text{Pt}(4'\text{-Ph-terpy})\text{Cl}]^+$ , which emits from a state that is thought to contain significant proportion of MLCT character, is completely quenched in a coordinating solvent while the *para*-substituted luminophore remains weakly emissive is regarded as a strong indication that ILCT processes are present in the excited state of  $[\text{Pt}(4'\text{-}p\text{OMePh-terpy})\text{Cl}]^+$ .<sup>32</sup>



Emission from the  $[\text{Pt}(4'\text{-}p\text{OMePh-terpy})\text{Cl}]^+$  luminophore in a rigid butyronitrile glass recorded at 77 K shows a structured band with its 0-0 transition at 526 nm. The emission assignment in this medium is no different to that made in room temperature fluid solution, and the radiative excited state is designated as  $^3\text{IL}^3\text{MLCT}$  in nature. In addition the excited state is thought to contain  $^3\text{ILCT}$  character based in large part on the emission behaviour of the ligand when coordinated to zinc(II) and also on the emission behaviour of  $[\text{Pt}(4'\text{-}p\text{OMePh-terpy})\text{Cl}]^+$  in dilute room temperature fluid solution, as discussed above.

#### Ortho-substitution of the 4'-phenyl moiety

Complexes in this subsection are distinguished by ligands which have an *ortho*-substituted phenyl ring in the 4'-position of the terpyridyl ligand. Two such ligands have been reported in the literature to date.<sup>54</sup>

Field, Summerton and coworkers report the synthesis and photophysical properties of the 4'-(*ortho*-methylphenyl)- and the 4'-(*ortho*-trifluoromethyl-phenyl)-substituted complexes.<sup>54</sup> These are  $[\text{Pt}(4'\text{-}o\text{MePh-terpy})\text{Cl}]^+$  and  $[\text{Pt}(4'\text{-}o\text{CF}_3\text{Ph-terpy})\text{Cl}]^+$  {where 4'-*o*MePh-terpy and 4'-*o*CF<sub>3</sub>Ph-terpy denote 4'-(*ortho*-methylphenyl)-2,2':6',2''-terpyridine and 4'-(*ortho*-trifluoromethylphenyl)-2,2':6',2''-terpyridine respectively}.<sup>54</sup>

Luminophores of this type have been intentionally made with the aim of producing non-planar luminophores which result from the interaction of the *ortho*-substituent with the protons of the central pyridine ring.<sup>54</sup> This non-planarity was expected to have interesting consequences in particular for the solid state packing arrangement and hence on the solid state emission properties of the solid.

#### Absorption spectroscopy

Absorption spectra for  $[\text{Pt}(4'\text{-}o\text{MePh-terpy})\text{Cl}]^+$  and  $[\text{Pt}(4'\text{-}o\text{CF}_3\text{Ph-terpy})\text{Cl}]^+$  have been recorded in an acetonitrile solution at 298 K.<sup>54</sup> The absorption profile for both chromophores in solution is very similar to those of the  $[\text{Pt}(\text{terpy})\text{Cl}]^+$  and  $[\text{Pt}(4'\text{-Ph-terpy})\text{Cl}]^+$  luminophores

which have been studied previously<sup>28, 53</sup> and hence band assignment is identical to that made in the earlier work. Vibrationally structured bands at wavelengths shorter than 350 nm are assigned to ligand centred  $^1(\pi-\pi^*)$  absorptions while the low intensity, poorly resolved peaks at wavelengths longer than 350 nm are assigned to Pt(5d)  $\rightarrow$  terpy( $\pi^*$ )  $^1$ MLCT transitions.<sup>54</sup>

### *Emission spectroscopy*

Emission measurements of [Pt(4'-oMePh-terpy)Cl]<sup>+</sup> and [Pt(4'-oCF<sub>3</sub>Ph-terpy)Cl]<sup>+</sup> in fluid solution at ambient temperatures was prevented by the poor solubility of both complexes in dichloromethane solution. No emission could be detected from an acetonitrile solution of either luminophore. Field, Summerton *et al.* ascribe this absence of emission to solvent induced exciplex quenching.<sup>54</sup>

Emission from [Pt(4'-oMePh-terpy)Cl]<sup>+</sup> could however be detected in a dilute DME glass at 77 K.<sup>54</sup> In this case the emission spectrum consists of a structured band which has its 0-0 transition at 477 nm. (No emission is reported for the related trifluoromethyl substituted luminophore under similar conditions.) The emission is assigned to a ligand centred  $^3(\pi-\pi)$  excited state<sup>54</sup> due to its similarity with emission observed for [Pt(terpy)Cl]CF<sub>3</sub>SO<sub>3</sub> in a dilute butyronitrile glass at 77 K.<sup>28</sup>

Most interesting is the solid state emission exhibited by each luminophore. Two complexes have been made from each luminophore by using either a hexafluoroantimonate or a tetrafluoroborate counterion, thus producing four complexes.<sup>54</sup> Of the four complexes, X-ray crystal structures exist for both [Pt(4'-oMePh-terpy)Cl]<sup>+</sup> salts and also for [Pt(4'-oCF<sub>3</sub>Ph-terpy)Cl]SbF<sub>6</sub>. Solid state emission assignments are made in conjunction with observations of the solid state structures.<sup>54</sup>

Emission from the four salts can be divided into two categories based on the nature of the emitting state. The first category is characterised by emission from the red [Pt(4'-oMePh-terpy)Cl]SbF<sub>6</sub> complex. In this case the solid state emission at room temperature is in a narrow (fwhm = 1635 cm<sup>-1</sup>), structureless and slightly asymmetric band with peak intensity at 616 nm. Reducing the temperature to 80 K results in a gradual shift in the emission maximum

to 673 nm, accompanied by an increase in intensity and a further reduction in band width (fwhm = 1119 cm<sup>-1</sup> at 80 K). The authors reconcile this behaviour with emission from an <sup>3</sup>MMLCT excited state brought about by close Pt...Pt interactions in the solid.<sup>54</sup> This assertion is confirmed by the solid state structure which shows head-to-tail stacking of luminophores in a linear chain resulting in a constant intermolecular Pt-Pt separation of 3.368(1) Å throughout the stack. Field, Summerton *et al.* associate such a short platinum-platinum spacing with a strong  $\sigma$ -interaction between overlapping d<sub>2z</sub>-orbitals and hence with the formation of the <sup>3</sup>MMLCT excited state.<sup>54</sup>

The second category contains both trifluoromethyl substituted complexes {[Pt(4'-oCF<sub>3</sub>Ph-terpy)Cl]SbF<sub>6</sub> and [Pt(4'-oCF<sub>3</sub>Ph-terpy)Cl]BF<sub>4</sub>} and the tetrafluoroborate salt of the [Pt(4'-oMePh-terpy)Cl]<sup>+</sup> luminophore. All three salts are yellow in colour, but more importantly display the same solid state emission behaviour.<sup>54</sup> Emission is characterised by a broad (fwhm > 2100 cm<sup>-1</sup>) structureless emission band which has an emission energy that is unaffected by alterations in temperature. The peak emission energy for all three salts occurs at wavelengths longer than 560 nm and is lower than that of the monomer emission measured in a dilute glass at 77 K. This emission is explained in terms of an excimeric excited state brought about by the inter-luminophore overlap of aromatic portions of the cations. Of the two solid state structures which exist for [Pt(4'-oMePh-terpy)Cl]BF<sub>4</sub> and [Pt(4'-oCF<sub>3</sub>Ph-terpy)Cl]SbF<sub>6</sub>, neither indicates the presence of close platinum-platinum overlap. However, an interplanar spacing of 3.42 and 3.46 Å respectively supports the assertion that inter-luminophore  $\pi$ - $\pi$  interactions are present in the solid state. In general the upper limit for effective  $\pi$ - $\pi$  interactions is regarded as 3.8 Å.<sup>56</sup> The emissive excited state of [Pt(4'-oCF<sub>3</sub>Ph-terpy)Cl]BF<sub>4</sub> is also identified as excimeric in nature due to the similarity of its emission behaviour to that of the two salts for which solid state structures exist which indicate an absence of close platinum-platinum interactions.<sup>54</sup>

All four complexes which are non-planar due to *ortho*-substitution of their phenyl ring show evidence for close intermolecular interactions in the solid state.<sup>54</sup> This observation has been associated with the non-planar luminophore whereby slippage is minimised and the close packing of luminophores results in a more energetically favourable packing arrangement where free space is minimised.

### *Fused-ring aromatic groups in the 4'-position*

In the last section dealing with aromatic substitution of the 4'-position, work is described where large *fused-ring* groups have been bonded to the chloro(platinum)terpyridyl luminophore. Michalec, McMillin *et al.* describe emission from complexes which have large fused ring aromatic groups in the 4'-position of the chloro(terpyridine)platinum(II) luminophore. Four ring systems were chosen. These are  $\beta$ -naphthyl (or 2-naphthyl)<sup>32</sup>,  $\alpha$ -naphthyl (or 1-naphthyl)<sup>32</sup>, 9-phenanthroline<sup>31,32</sup> and 1-pyrene<sup>31,32</sup>, which are abbreviated  $\beta$ Np,  $\alpha$ Np, Phe9 and Pyre1 respectively.

### *Absorption spectroscopy*

Solution absorption spectra have been recorded at ambient temperatures in acetonitrile and in dichloromethane. Intraligand  $^1(\pi-\pi^*)$  absorption bands dominate at wavelengths shorter than 350 nm.<sup>31,32</sup> The authors identify solvent sensitive MLCT absorption bands for the various luminophores at wavelengths between 400 and 500 nm. In general the absorption bands in a room temperature acetonitrile solution for [Pt(4'- $\beta$ Np-terpy)Cl]<sup>+</sup> {390 (shoulder), 411 nm}, [Pt(4'- $\alpha$ Np-terpy)Cl]<sup>+</sup> {393 (shoulder), 406 nm}, [Pt(4'-Phe9-terpy)Cl]<sup>+</sup> {388 (shoulder), 408 nm} occur at very similar energies. It is the MLCT absorption bands for the [Pt(4'-Pyre1-terpy)Cl]<sup>+</sup> chromophore which are distinguished by their exceptionally low energy; with maxima identified at 380(shoulder) and 432 nm in acetonitrile solution.<sup>31,32</sup>

The authors regard the stabilisation in absorption energy, as the size of the 4'-aryl group increases to 1-pyrene, as a feature which is inconsistent with absorption to a state that consists merely of a combination of IL and MLCT absorptions.<sup>31,32</sup> By studying the absorption spectra of each ligand coordinated to zinc(II) in order to exclude MLCT absorption bands, the authors identify ILCT (aryl to terpyridyl intraligand charge-transfer) bands at wavelengths longer than 350 nm for each of these four complexes which have an easily ionisable fused-ring group in the 4'-position of the terpyridyl ligand. Naturally these ILCT absorption bands are also present in the absorption spectra of the platinum(II) coordinated to each of the four ligands with large aromatic groups and contribute to the absorption intensity at wavelengths longer than 350 nm.

### *Emission spectroscopy*

Emission for four complexes with large fused-ring groups in the 4'-position *viz.*, [Pt(4'- $\beta$ Np-terpy)Cl]<sup>+</sup>, [Pt(4'- $\alpha$ Np-terpy)Cl]<sup>+</sup>, [Pt(4'-Phe9-terpy)Cl]<sup>+</sup> and [Pt(4'-Pyre1-terpy)Cl]<sup>+</sup> has been recorded in room temperature fluid solution and in a rigid glass at 77 K.<sup>32</sup> Emission at ambient temperatures will be discussed first, followed by a description of emission from these complexes in a rigid butyronitrile glass.

Unlike the phenyl substituted [Pt(4'-Ph-terpy)Cl]<sup>+</sup> luminophore, which emits only weakly ( $\tau$  = 85 ns) in a room temperature deoxygenated dichloromethane solution, the four complexes substituted with fused-ring aromatic groups all show a strong emission under these conditions, with emission maxima reported at 570, 588, 595 and 685 nm for [Pt(4'- $\beta$ Np-terpy)Cl]<sup>+</sup>, [Pt(4'- $\alpha$ Np-terpy)Cl]<sup>+</sup>, [Pt(4'-Phe9-terpy)Cl]<sup>+</sup> and [Pt(4'-Pyre1-terpy)Cl]<sup>+</sup> respectively. Emission profiles are either unstructured or weakly structured. The most striking feature, however, are the exceptionally long emission lifetimes which increase in length as the size of the aryl group increases in the series [Pt(4'- $\beta$ Np-terpy)Cl]<sup>+</sup> (12.1  $\mu$ s), [Pt(4'- $\alpha$ Np-terpy)Cl]<sup>+</sup> (16.6  $\mu$ s), [Pt(4'-Phe9-terpy)Cl]<sup>+</sup> (21.0  $\mu$ s) and culminating in the emission lifetime of [Pt(4'-Pyre1-terpy)Cl]<sup>+</sup> which is measured at a very long 64  $\mu$ s. Changing the solvent to more polar butyronitrile shifts the emission maxima to higher energies and reduces the emission lifetimes. This solvent sensitivity for the complexes was found to decrease as the size of the aryl group in the 4'-position increases to the extent that the emission lifetime of [Pt(4'-Pyre1-terpy)Cl]<sup>+</sup> in butyronitrile is still very long, and has been measured at 18  $\mu$ s.

(Note that differences in emission behaviour between the  $\alpha$ - and  $\beta$ -naphthyl substituted complexes are explained in terms of the differing degrees of rotational freedom of the two naphthyl rings relative to the terpyridyl ring system. The  $\alpha$ -naphthyl group is expected to have a lower rotational freedom due to the *peri*-interaction of the adjacent  $\alpha$ -protons on the naphthyl ring with the protons of the central pyridine ring. This effect is discussed in greater detail in Chapter 3.)

By analogy with similar platinum terpyridyl complexes the authors suggest that the excited state contains a measure of IL and MLCT character. What is clear is that the relative

contributions of states making up the emitting state is not consistent across the range of complexes discussed here. This is based on a violation of the Energy Gap Law<sup>57-59</sup> which predicts that for a series of complexes which have the same excited state makeup, those of lowest energy will have the highest non-radiative rate constants.<sup>57</sup> Thus the lowest energy states will be the longest lived, contrary to the trend seen here. This observation constitutes evidence that orbital parentage changes as the size of the aromatic group changes.

Studies of these ligands coordinated to zinc(II) provide evidence that an additional state influences the radiative decay, in particular, an ILCT state. The inclusion of ILCT character in the makeup of the excited state is based in large part on an investigation of the emission properties of each of the ligands coordinated to zinc(II).<sup>31,32</sup> Evidence for ILCT processes in the excited state is the presence of solvent dependent, structureless emission bands for the [Zn(4'-Aryl-terpy)Cl<sub>2</sub>] complexes with energies that reduce as the size of the aryl group is increased. A significant participation of ILCT character in the excited state is consistent with very long emission lifetimes in solution since MLCT processes are discouraged. A MLCT contribution to the excited state is susceptible to solvent induced exciplex quenching whereas the ILCT state has been found to suppress emission quenching of this kind. Thus the authors propose that ILCT processes become more dominant as the substituent in the 4'-position becomes more readily ionisable. In the case of the large fused-ring groups presented here this corresponds to an increase in the size of the fused-ring aromatic group.

The emission behaviour of the [Pt(4'-Pyre1-terpy)Cl]<sup>+</sup> luminophore deserves special mention. The small MLCT contribution to the excited state of the [Pt(4'-Pyre1-terpy)Cl]<sup>+</sup> luminophore allows observation of singlet fluorescence for the [Pt(4'-Pyre1-terpy)Cl]<sup>+</sup> luminophore. Metal participation facilitates rapid conversion from singlet to triplet excited states and hence it has been possible to observe radiative decay from an excited state of singlet multiplicity. This fluorescence is present as a broad structureless band with maximum at 640 nm with a lifetime of ~ 1 ns and is not as sensitive to quenching by oxygen as the triplet emission.

Emission was also recorded in a rigid butyronitrile glass at 77 K. The band profiles for each of the luminophores at 77 K exist as more explicitly structured bands compared to measurements made in a room temperature fluid solution and the maxima occur at slightly

higher energies. Maxima for the 0-0 transitions are reported as 542, 540, 538 and 648 nm for [Pt(4'- $\beta$ Np-terpy)Cl]<sup>+</sup>, [Pt(4'- $\alpha$ Np-terpy)Cl]<sup>+</sup>, [Pt(4'-Phe9-terpy)Cl]<sup>+</sup> and [Pt(4'-Pyre1-terpy)Cl]<sup>+</sup> respectively. In general the observations and assignments are no different to those made in a room temperature fluid solution.<sup>32</sup>

No solid state emission measurements have been made by Michalec *et al.* of luminophores with large fused-ring aromatic groups in the 4'-position.<sup>31, 32</sup>

### Triple substitution of the terpyridyl ligand

Two luminophores appear in the literature where the chloro(terpyridine)platinum(II) luminophore has been triply substituted in the 4, 4' and 4'' positions. In the first, Lai, Che and coworkers have bonded three tertiary-butyl (tBu) to each of these positions on the terpyridyl ligand<sup>52</sup> and in the second, Cummings *et al.* substituted these positions with chloride atoms.<sup>50</sup> The former luminophore will be discussed first.

Lai, Che *et al.* have synthesised a complex with the formulation [Pt(4,4',4''-tBu<sub>3</sub>-terpy)Cl]ClO<sub>4</sub> with the tBu-groups utilised to discourage aggregation in solution.<sup>52</sup> Another benefit of the tBu-groups is the improved solubility of the complex brought about by their use. UV/vis spectra obey Beer's law in the 0.5 mM - 10 mM concentration range and show the familiar pattern of <sup>1</sup>IL absorbances in a structured set centred at 328 nm and a broader <sup>1</sup>MLCT [(5d)Pt -  $\pi^*$ (tBu-terpy)] band in the 373 - 386 nm region. The authors speculate that the latter CT band may contain some <sup>1</sup>IL character based on UV/vis absorption spectra recorded for the isoelectronic gold(III) complex [Au(4,4',4''-tBu<sub>3</sub>-terpy)Cl](CF<sub>3</sub>SO<sub>3</sub>)<sub>2</sub> which was also synthesised as part of this study. The <sup>1</sup>IL bands of the gold(III) complex occur at higher energy than the analogous bands of the platinum(II) complex, hence the speculation to <sup>1</sup>IL mixing with the <sup>1</sup>MLCT state. Of particular interest is a very low intensity ( $\epsilon$  57 M<sup>-1</sup>.cm<sup>-1</sup>) shoulder barely observable at 465 nm. Similar bands have previously been assigned by Gray and coworkers<sup>29, 60</sup> to MMLCT transitions but this is regarded as unlikely in this case due in part to the bulky groups which are expected to discourage any form of oligomerisation. The feature at 465 nm is consistently present, even in the most dilute solution and its intensity has been shown to adhere to Beer's Law. This behaviour is inconsistent with what one would expect

of MMLCT behaviour and leads the authors to a <sup>3</sup>MLCT band assignment for this feature of the absorption spectrum.

The complex does not luminesce at room temperature in either the solid or solution states. Only at 77 K has emission been reported. Emission spectra have been recorded in a 1:1 (v/v) EtOH/MeOH mixture at 77 K in the 1  $\mu$ M - 1 mM concentration range. When the concentration is below 10  $\mu$ M, emission is in a vibronically structured band with the 0-0 progression at 467 nm and lower intensity peaks spaced at *ca.* 1400  $\text{cm}^{-1}$  to lower energy. Lai, Che and coworkers consider these features to be convincing evidence for the existence of an <sup>3</sup>IL ( $\pi\pi^*$ ) state as the emitting state, with reference to similar emission observed elsewhere.<sup>61</sup>

At concentrations greater than 100  $\mu$ M in the 1:1 (v/v) EtOH/MeOH mixture at 77 K a new dominant emission feature emerges as a broad unstructured band at *ca.* 620 nm  $\{\lambda(\text{em})_{\text{max}}\}$ . This emission is assigned to an “excimeric intraligand transition” in analogy to luminescence previously observed by Gray *et al.*<sup>29</sup> and brought about by  $\pi$ - $\pi$  interactions between the organic fragments of adjacent luminophores.

In the solid state [Pt(4,4',4''-*t*Bu<sub>3</sub>-terpy)Cl]ClO<sub>4</sub> is a yellow complex which does not luminesce at ambient temperatures. However, when the temperature is reduced to 77 K, emission is observable with peak intensity at 560 nm. This emission is tentatively ascribed to radiative decay from a <sup>3</sup>MLCT excited state. A solid state structure of the complex at room temperature has been determined from X-ray diffraction studies of a single crystal of the compound. These studies show the luminophores to pack head-to-tail with an interplanar spacing (between terpyridyl mean planes) of  $\sim 3.8$  Å and a Pt...Pt separation of 3.838(1) Å. This spacing is considered to be of sufficient magnitude to preclude the likelihood of significant interactions between adjacent luminophores. Other than this observation the authors enter into no explicit discussion relating the room temperature structure to the emission observed in the solid state.

The second luminophore of this type where the chloro(terpyridyl)platinum(II) moiety has been triply substituted (again in the 4, 4', and 4'' positions) was reported by Cummings and coworkers.<sup>50</sup> To this end, the hexafluorophosphate salt, *viz.* [Pt(4,4',4''-Cl<sub>3</sub>-terpy)Cl]PF<sub>6</sub>, and also the Magnus-type salt [Pt(4,4',4''-Cl<sub>3</sub>-terpy)Cl][Pt(dmsO)Cl<sub>3</sub>] have been synthesised (the



latter as an artifact of the synthetic route) and their emission properties studied. Of course the alteration of counterion had no significant effect on the solution emission studies since the  $[\text{Pt}(\text{dms})\text{Cl}_3]$  does not contribute to the observed emission, being merely present as a counterion. Since the solid state emission, where the counterion would no doubt play a significant role in the intermolecular dynamics determining the nature of the excited state, has not been reported, no further mention will be made of the latter species. In contrast to the strongly electron donating groups employed by Che *et al.*; Cummings chose instead to place electron withdrawing chloride atoms on the periphery of the terpyridyl ligand bound to platinum. Trends emerge that correspond well with the results obtained by Che *et al.*<sup>52</sup>

Molecular orbital calculations performed on the free ligand indicate that chloride substitution in the 4'-position substantially lowers the relative energies of the  $\pi^*$ -orbital associated with the aromatic terpyridyl ligand. The calculations indicate that successive substitution further lowers the energy of this orbital. The implication for any MLCT excited state (assuming a relatively constant metal-based HOMO) is a reduction in its energy. This prediction is borne out in the acetonitrile solution absorption spectra of the platinum-coordinated complexes that have been synthesised, with a reduction in energy (constituting a 2000  $\text{cm}^{-1}$  red shift) in the series  $[\text{Pt}(\text{terpy})\text{Cl}]^+$  (~ 390 nm),  $[\text{Pt}(4'\text{-Cl-terpy})\text{Cl}]^+$  (~ 397 nm) and  $[\text{Pt}(4,4',4''\text{-Cl}_3\text{-terpy})\text{Cl}]^+$  (421 nm). Moreover, Che's complex,  $[\text{Pt}(4,4',4''\text{-tBu}_3\text{-terpy})\text{Cl}]^+$ , which is triply substituted with electron donating tertiary-butyl groups<sup>52</sup> (*vide supra*) complies with this hypothesis by having a charge transfer band in the 373 - 386 nm region, suggesting that electron donation onto the terpyridyl ligand raises the energy of the  $\pi^*$ -LUMO and hence of the  $^1\text{MLCT}$  state.

Photoluminescence from acetonitrile solution at room temperature is a structureless band centred at 620 nm. The intensity of the emission is very sensitive to the presence of oxygen, being almost completely quenched in an air-saturated solution. By comparison with similar emission exhibited by related luminophores<sup>27, 28, 30, 52</sup> the authors conclude that the emission originates in an excited state which is  $^3\text{MLCT}$  in nature. Based on this deduction the bimolecular quenching rate constant is calculated to be  $3.1 \times 10^9 \text{ M}^{-1} \cdot \text{s}^{-1}$ . Interestingly, emission has an unusually long-lived lifetime of 1.9  $\mu\text{s}$ . This is noteworthy in light of the weak emission behaviour exhibited by the singly chloride-substituted derivative, (also described in this work by Cummings and discussed previously, *vide supra*)  $[\text{Pt}(4'\text{-Cl-terpy})\text{Cl}]^+$ , which is

practically non-emissive under these conditions. This suggests that the addition of chlorine substituents to the 4,4' and 4''-positions of the terpyridyl ligand lowers the energy of the MLCT excited state to a “modest” extent, yet sufficiently to make this state the more favourable deactivation pathway. Almost incredibly the  $[\text{Pt}(4,4',4''\text{-Cl}_3\text{-terpy})\text{Cl}]^+$  luminophore appears to be unperturbed by solvent induced exciplex quenching in acetonitrile and the comparative emission lifetime in a non-coordinating solvent, such as  $\text{CH}_2\text{Cl}_2$ , has not been reported.

Luminescence was recorded from a DME glass at 77 K and shows a structured band with strong vibronic progressions having a spacing of  $\sim 1290\text{ cm}^{-1}$ , the most intense band at highest energy. This most intense 0-0 band occurs at 483 nm. The vibronic spacing corresponds to intense bands observed in the IR spectrum of the complex and is ascribed to ring vibration modes of the aromatic ligand and is interpreted in the emission spectrum as evidence of a significant ligand contribution to the nature of the emissive state. Indeed, an assignment of the emission to radiative deactivation from a  $^3(\pi\text{-}\pi^*)$  state is made, based largely on the observed vibronic structure and with reference to similar emission observed by Gray and coworkers.<sup>29</sup> However, a MLCT contribution to the nature of the excited state is regarded as plausible. As before, emission energies are decreased according to the extent of chloro-substitution of the terpyridyl ligand,  $\lambda(\text{em})_{\text{max}}$  reducing in the order  $[\text{Pt}(\text{terpy})\text{Cl}]^+$  (474 nm),  $[\text{Pt}(4'\text{-Cl-terpy})\text{Cl}]^+$  (480 nm),  $[\text{Pt}(4,4',4''\text{-Cl}_3\text{-terpy})\text{Cl}]^+$  (483 nm), an effect again rationalised by successive chloride substitution bringing about a stepwise reduction in the nature of the excited state.

Unlike the  $[\text{Pt}(4'\text{-Cl-terpy})\text{Cl}]^+$  complex where the concentration dependence of the glass emission has been studied, no such concentration dependent study of the triply substituted derivative is reported. Neither have any solid state emission spectra been reported for either the  $\text{PF}_6^-$  or the  $[\text{Pt}(\text{dmsO})\text{Cl}_3]$  salts.

#### 1.2.1.2 The $[\text{Pt}(4'\text{-R-terpy})\text{CR}']^+$ luminophore

The framework for this luminophore consists of the platinum terpyridyl moiety with an anionic organic ligand bound in the fourth coordination site of platinum. Naturally this allows for different derivatives of not only the aromatic terpyridyl sub-fragment but also of the organic

ligand directly bound *via* the carbon atom to the platinum. This section is subdivided into three subsections of compounds fitting the classification, the subsections separated according to the nature of the organic ligand. The first subsection (1.2.1.2.1) describes the photophysics of compounds bearing a methyl group as the organic ligand. The following section (1.2.1.2.2) describes studies in which there is a methylene carbon bound to platinum, and the last subsection (1.2.1.2.3) incorporates the photophysics of compounds having aromatic carbon atoms coordinated to platinum.

#### 1.2.1.2.1 The $[\text{Pt}(4'\text{-R-terpy})\text{CH}_3]^+$ luminophore

The unsubstituted  $[\text{Pt}(\text{terpy})\text{CH}_3]^+$  luminophore was first synthesised by Romeo, Monsú Scolaro *et al.* with an investigation of the biological action of the complex in mind.<sup>51,62</sup> To this end five complexes have been synthesised consisting of the luminophore with a different counterion in each case. The following counterions were used:  $\text{Cl}^-$ ,  $\text{NO}_3^-$ ,  $\text{PF}_6^-$ ,  $\text{ClO}_4^-$  and  $\text{B}(\text{C}_6\text{H}_5)_4^-$ . Although UV/vis absorption measurements were made on each of these salts as part of the biological investigation<sup>51, 62</sup>, photophysical studies have subsequently been performed on only the chloride salt in alcoholic medium by Campagna, Monsú Scolaro *et al.*<sup>42</sup> in a paper specifically describing absorption and emission properties of the compounds. Absorption measurements at room temperature in a 4:1 (v/v) MeOH/EtOH solution and luminescence measurements at 77 K in the same medium (now a glass) were undertaken.<sup>42</sup>

The UV/vis absorption spectra show the familiar set of absorbances associated with platinum(II) polypyridyl complexes of this general type.<sup>27, 28, 44, 63, 64</sup> At high energy (between 250 and 400 nm) intense absorptions ( $\epsilon$  15900 - 10100  $\text{M}^{-1}\cdot\text{cm}^{-1}$ ) are assigned to transitions solely associated with the polypyridyl ligand by comparison with absorptions of similar complexes reported in the literature and by the similarity of these absorptions to those of the free ligand. Spin allowed MLCT ( $d\pi \rightarrow \pi^*$ ) absorptions appear as moderately intense bands in the visible region ( $\epsilon$  2000  $\text{M}^{-1}\cdot\text{cm}^{-1}$ ) peaking at 434 nm. The authors exclude possible metal-centred (d-d) transitions and ligand-to-metal charge transfer transitions on account of the high molar extinction coefficients. The fact that the ligand has no absorption bands at such a low energy prohibits a ligand centred assignment. Moreover the MLCT character is emphasised by comparing its absorption maximum of 434 nm with that of the related

chloro(terpyridine)platinum(II) luminophore which is at 404 nm. Campagna, Monsú Scolaro *et al.* argue that the donating effect of the methyl group onto the metal centre decreases the oxidation potential of the metal.<sup>42</sup> Hence the removal of an electron from the metal  $d\pi$  orbitals is easier and the MLCT bands occur at lower energy. At low concentrations ( $< 0.1$  mM) the absorption of the complex obeys Beer's Law with aggregation disrupting this linear relationship as the concentration is increased. Indeed Romeo, Monsú Scolaro *et al.* were able to fit the absorption data to a simple dimerisation model.<sup>51</sup> Aggregation in solution has been confirmed by Resonance Light Scattering (RLS) spectra as well as by NMR evidence, the effect being less pronounced in non-aqueous solvents.<sup>51</sup> The UV/vis absorption spectrum of the  $[\text{Pt}(4'\text{-Ph-terpy})\text{CH}_3]^+$  chromophore in 4:1 (v/v) MeOH/EtOH has also been recorded.<sup>42</sup> The spectral features parallel those of the parent complex.

The luminescence behaviour of methyl(terpyridine)platinum(II) in a 4:1 (v/v) MeOH/EtOH glass at 77 K is virtually the same as that of chloro(terpyridine)platinum(II) recorded under identical conditions by the same workers.<sup>42</sup> Both compounds show emission from excited states associated with the presence of three different species, although there are small differences in the position of the respective emission maxima. Each excited state produces a luminescence characterised by a distinctive emission wavelength and lifetime. Moreover, the three luminescence features have relative intensities dependent on both excitation wavelength as well as on the concentration of the complex in solution. These will now be described.

The highest energy emission is vibrationally structured with 0-0 band at 470 nm. Vibrational progressions of  $\sim 1300$   $\text{cm}^{-1}$  correspond to the dominant vibrational modes associated with the terpyridyl ligand. Accordingly, this luminescence feature is ascribed to a spin-forbidden metal perturbed  $^1\text{L}$  excited state. The excited state is linked to emission from monomers unaffected by interactions with adjacent luminophores. Campagna, Monsú Scolaro *et al.* propose the metal contribution to the excited state to account for the relatively short emission lifetimes compared to those recorded for pure intra-ligand emitters.<sup>42</sup> The second emission is intermediate in energy, occurring as a broad, unstructured and low intensity band centred at roughly 600 nm. Emission is from excimers arising from partial overlap of the aromatic ligands of adjacent complexes, in accord with the deductions made by Gray *et al.*<sup>29</sup> and Campagna *et al.*<sup>42</sup> from their studies of the corresponding emission of the closely related

[Pt(terpy)Cl]<sup>+</sup> luminophore. Lastly, there is a narrow unstructured emission band at 730 nm unambivalently ascribed to a <sup>3</sup>MMLCT excited state based on the spectral characteristics and concentration dependence of the band.

In the same article<sup>42</sup> the authors also report the luminescence properties of the [Pt(4'-Ph-terpy)CH<sub>3</sub>]<sup>+</sup> luminophore, distinguished from the previously described [Pt(terpy)CH<sub>3</sub>]<sup>+</sup> luminophore by the presence of a phenyl ring bound to the 4'-position of the terpyridyl ligand. Measurements were made under identical conditions, the phenyl substituted compound producing roughly the same luminescence behaviour and, in particular, displaying the same three emission origins as those observed for the parent compound. As found for luminophores with a chloride ligand coordinated directly to platinum (*vide supra*), the addition of the phenyl ring results in a red shift in the emission maximum of each luminescent feature. Of greater significance however, is the similarity in luminescence properties of the methyl(terpyridine)platinum(II) complexes to those of the chloro(terpyridine)platinum(II) complexes. In fact, replacing a Pt-Cl with a Pt-C bond has very little effect on the emission.

#### 1.2.1.2.2 The [Pt(terpy)CH<sub>2</sub>R]<sup>+</sup> luminophore

The only compound that falls into this category was unintentionally synthesised by Akiba and Sasaki in an attempt to exchange the hydroxyl ligand of [Pt(terpy)OH]<sup>+</sup> for pyridine derivatives in nitromethane solution.<sup>65</sup> Instead, a yellow compound was obtained of which single crystals were grown suitable for X-ray diffraction studies. The crystal structure of [Pt(terpy)CH<sub>2</sub>NO<sub>2</sub>]B(C<sub>6</sub>H<sub>5</sub>)<sub>4</sub> showed that the hydroxyl ligand had been replaced by a carbon-bonded nitromethyl group. There is an intermolecular Pt...Pt separation of 3.4039 Å which, according to the authors, would allow for only a weak Pt-Pt interaction, a hypothesis endorsed by the yellow colour of the compound. Two forms of the luminophore were synthesised, the other having a perchlorate counterion. In the communication the authors do not report any fluid spectroscopy measurements, merely contrasting the emission of the two complexes in the solid state at ambient temperature. The perchlorate salt exhibits a vibrationally structured band with vibrational progressions at 515 (the most intense), 555 and 595 nm. The emission of the tetraphenylborate salt has an unstructured, roughly symmetric band centred at 665 nm, the disparity being ascribed to an unequal intermolecular interaction in the respective salts. Akiba

and Sasaki make no attempt to investigate the origin of the excited state, but it is likely that the emission of the perchlorate salt arises due to IL transitions judging by the high energy origin, structured band profile and vibrational progressions (1200 - 1400  $\text{cm}^{-1}$ ) which correspond to the dominant stretching modes of the terpyridyl ligand. Given the available information the emission origin of the tetraphenylborate salt is less recognizable and without additional data an assignment is not possible.

#### 1.2.1.2.3 The $[\text{Pt}(4'\text{-R-terpy})\text{Ph}]^+$ luminophore (R = H or Ph)

Two compounds falling into this category were studied by Campagna, Monsú Scolaro *et al.*, as part of their study of the effect of ligand substitution in the fourth coordination site of platinum(II) on the photophysical properties of the luminophore.<sup>42</sup> The compounds of interest to this section are  $[\text{Pt}(4'\text{-R-terpy})\text{Ph}]\text{Cl}$  (R = H, Ph). Measurements were only made of the absorption spectra at room temperature and the glass emission at 77 K, both in a solution of 4:1 (v/v) MeOH/EtOH. The absorption spectra are similar to those of the related compounds in the series showing intense absorptions in the UV region (250 - 350 nm) and moderately intense absorptions in the high energy part of the visible spectrum at 424 and 426 nm for R = H and R = Ph respectively. Due to the similarity of the absorptions in the UV region to those of the free ligand, these bands were assigned to ligand-centred transitions. The band in the visible sector at  $\sim 425$  nm is ascribed to a spin allowed  $[(d,\pi) \rightarrow \pi^*]$  MLCT transition. Emission from glassy solution at 77 K comprises a single vibrationally structured band at high energy. There is an emission origin at 470 and 520 nm for  $[\text{Pt}(\text{terpy})\text{Ph}]^+$  and  $[\text{Pt}(4'\text{-Ph-terpy})\text{Ph}]^+$  respectively and these are also the most intense peaks in each case. Emission in both complexes is assigned to a metal perturbed intra-ligand transition based on the high energy of the bands and the vibrational structure. Metal character is suggested to account for the relatively short emission lifetimes. It is noticeable that the complexes that have a coordinated phenyl ligand lack the multiple luminescence features displayed by the related compounds described in the paper. The emission sources that are absent arise from excimeric and MMLCT excited states *i.e.*, states that arise from interacting luminophores in solution. It is proposed that the steric bulk of the coordinated phenyl ring accounts for the apparent absence of oligomerisation in solution. NMR spectroscopic experiments confirm the absence of intermolecular interactions, consistent with the assignment of the emission to monomers.

### 1.2.1.3 The [Pt(terpy)L]<sup>n+</sup> luminophore

(L = anionic or neutral N-donor ligand; n = 1 or 2)

This group of compounds consist of the platinum(II) terpyridyl substructure with a N-donor ligand in the fourth coordination site. The ligand may be anionic or neutral. The former group will be discussed first.

#### 1.2.1.3.1 The [Pt(terpy)L]<sup>+</sup> luminophore (L = anionic ligand)

Of the complexes falling into this category, there is only one for which the electronic properties have been studied. That is where L is N<sub>3</sub><sup>-</sup>, studied by Che *et al.*<sup>28</sup> At room temperature the absorption spectrum of [Pt(terpy)N<sub>3</sub>]<sup>+</sup> in acetonitrile solution consists of two obvious features. Intense vibrationally structured bands ranging from 314 to 348 nm are assigned to (π-π\*) transitions localized on the terpy ligand. The assignment is based on the energy of the band and the band profile. The second feature is a broad, low energy and weakly structured band with progressions at 374 and 385 nm. As these bands are absent from the absorption regime of both the free ligand and of [Zn(terpy)<sub>2</sub>]<sup>2+</sup>, they are associated with transitions involving the platinum centre. Hence the authors assign this low energy feature to a MLCT excited state.<sup>28</sup>

The complex does not luminesce in a room temperature fluid solution but shows a vibronically structured band (0-0/0-1 progression ≈ 1420 cm<sup>-1</sup>) in a butyronitrile glass at 77 K. The Huang-Rhys factor (defined as I<sub>0-1</sub>/I<sub>0-0</sub> where I<sub>0-1</sub> and I<sub>0-0</sub> are the intensities of the 0-1 and 0-0 transitions respectively) was found to be *ca.* 0.6. Emission in this matrix is tentatively ascribed to a <sup>3</sup>MLCT emissive state.<sup>28</sup> In the solid state the red [Pt(terpy)N<sub>3</sub>]<sup>+</sup> shows a strong emission with a lifetime of 0.2 μs.

#### 1.2.1.3.2 The [Pt(terpy)L]<sup>2+</sup> luminophore (L = neutral ligand)

A great variety of complexes of this type where the fourth coordination site is taken up by a neutral nitrogen donor ligand have been synthesised.<sup>66-73</sup> Interest is mainly in the biological application of these molecules<sup>8-10, 26, 74-78</sup>, but some work has also been undertaken on the

kinetics of the amine ligand substitution at the metal centre.<sup>79</sup> The doubly positive charge of the complex due to the two neutral ligands bound to the metal, results in a complex which has a greater DNA binding constant than that of  $[\text{Pt}(\text{terpy})\text{HET}]^+$  (HET = 2-hydroxyethanethiolate)<sup>74,75</sup>, which is arguably the most well known platinum terpyridyl DNA intercalator.<sup>6</sup> Luminescence studies of compounds where four nitrogen atoms are bound to the platinum atom are restricted to only a few examples.

The simplest ligand in this category is ammonia. The absorption spectrum of  $[\text{Pt}(\text{terpy})(\text{NH}_3)]^{2+}$  shows strong vibrationally structured absorptions at 328 and 343 nm which are assigned to ligand-centred  $\pi\text{-}\pi^*$  transitions.<sup>28</sup> Broad low intensity bands are evident at longer wavelengths (373, 391 nm), these being assigned to MLCT absorptions. The assignment is based in part on the absence of similar absorptions by the free terpyridyl ligand thereby clearly implicating metal character.

The compound does not luminesce in acetonitrile at ambient temperatures but emission does occur from a butyronitrile glass in a highly structured profile with its origin at 480 nm. Although the structured profile is reminiscent of emission from the free terpyridyl ligand, the luminescence is assigned to a MLCT excitation. However, Che *et al.* note that there is considerable ligand character in the excited state. In the solid state a microcrystalline sample is strongly luminescent with an emission lifetime of 0.5  $\mu\text{s}$ .<sup>28</sup>

Another example of this class of luminophore has acetonitrile as the fourth ligand coordinated to platinum. Some photophysical studies have been made on  $[\text{Pt}(\text{terpy})(\text{MeCN})]^{2+}$  by Field, McMillin and coworkers.<sup>47</sup> An emission spectrum at 77 K in a butyronitrile glass at a complex concentration of 150  $\mu\text{M}$  was recorded. The emission band is structured, with peaks ranging from 457 to 565 nm and showing the distinctive  $\pi\text{-}\pi^*$  vibrational progression characteristic of the C=N and C=C vibrations of terpyridine (1200 - 1500  $\text{cm}^{-1}$ ).

Emission in the solid state is more complex, even with the determination of the crystal structure of  $[\text{Pt}(\text{terpy})(\text{MeCN})](\text{SbF}_6)_2$  which shows each luminophore to be in a discrete monomeric environment.<sup>47</sup> The packing mode in the lattice excludes the possibility of metal-metal (all Pt...Pt distances > 4.9 Å) and  $\pi\text{-}\pi$  interactions in the solid. Emission spectra were



recorded in 40 K intervals between 80 and 240 K. Vibrational structure from  $^3\pi\text{-}\pi^*$  excited states is prevalent throughout this temperature range suggesting  $^3\text{IL}$  emission. At 240 K dominant emission maxima occur at 540 and 575 nm, with weaker bands at higher energies. As the temperature is reduced the relative intensities change with the high energy bands becoming the dominant features, showing a prominent 495 nm band at 80 K. Despite the apparent monomeric environment of each luminophore in the crystal, the dominant emission from a solid sample occurs at an unexpectedly lower energy compared to that of the butyronitrile glass, even at the lowest temperatures. Phase transitions to explain the luminescent behaviour are excluded since there is no abrupt change in the emission data. The authors point out that this behaviour is what one would expect if emission from defect sites in the crystal contribute to the observed emission. This effect is described as trap-site emission and arises when temperature dependent energy transfer in the bulk material to the defect sites allows for emission from lower energy trap sites. Since this energy distribution is temperature dependent, emission from the trap sites may no longer be feasible at the lowest temperatures and emission from a higher energy source appears. The implication is that the low temperature emission is most representative of the bulk material.<sup>47</sup>

#### 1.2.1.4 The $[\text{Pt}(\text{terpy})\text{L}]^{n+}$ luminophore

(L = anionic or neutral O-donor ligand; n = 1 or 2)

Luminophores with terpyridine and an oxygen donor ligand coordinated to square-planar platinum(II) are discussed in this section. The photophysics of compounds containing the anionic  $\text{OH}^-$  and  $\text{OMe}^-$  ligands bonded in the fourth coordination site will be described first and, finally, a case is mentioned in which a water molecule is coordinated to the metal centre.

##### 1.2.1.4.1 The $[\text{Pt}(\text{terpy})\text{OH}]^+$ luminophore

The  $[\text{Pt}(\text{terpy})\text{OH}]^+$  chromophore absorbs strongly in the 270 - 340 nm region producing a vibrationally structured band.<sup>27</sup> In this region the absorptions are ascribed to a ligand-centred origin. There is an additional set of three relatively intense bands ( $\epsilon$  1500 - 1600  $\text{M}^{-1}\cdot\text{cm}^{-1}$ ) between 385 and 460 nm due to transitions to a MLCT excited state. Assignment is deduced from the molar absorptivities and from the energy of the bands which are in the charge transfer region. All absorptions adhere to Beer's law at low concentrations.

Emission in acetonitrile solution at room temperature is characterised by a broad structureless band centred at 621 nm. The emission displays a slight solvent dependence, shifting to 610 nm in a dichloromethane solution.<sup>27</sup> (Wong and Lee found that the excited state is quenched by water and no emission is detected in this medium.<sup>80</sup>) The emission is assigned to a  $d(\text{Pt}) - \pi^*(\text{terpy})$  MLCT transition.<sup>27</sup> The absence of resolved vibrational structure in the emission band prohibits a ligand centred assignment, while the existence of an excimeric excited state as the source of the luminescence is unlikely as this would imply a concentration dependent emission band. Furthermore, the authors disregard the existence of a metal-centred (d-d) excited state as this would require the population of the antibonding  $d_{x^2-y^2}$  orbital. Interestingly, in an alcoholic frozen glass the compound does emit from a terpyridyl ligand-centred  $\pi-\pi^*$  excited state.<sup>27</sup>

Although the compound is non-emissive in aqueous solution, it does luminesce in the presence of particular DNA base pairs<sup>81</sup> and sodium dodecyl sulfate (SDS), provided the SDS concentration is greater than 6 mM.<sup>80</sup> This suggests the potential utility of the compound as a luminescent switch in biological systems.

#### 1.2.1.4.2 The $[\text{Pt}(\text{terpy})(\text{OMe})]^+$ luminophore

Absorption at ambient temperatures from this luminophore is similar to that from the previously described  $[\text{Pt}(\text{terpy})\text{OH}]^+$  luminophore with intense, structured absorption bands ranging from 270 to 340 nm being recorded in 9:1 (v/v) acetonitrile/methanol solution.<sup>27</sup> The low energy region between 370 and 480 nm also consists of three broad, weakly resolved maxima which are ascribed to MLCT transitions. Acetonitrile solutions of the methoxy coordinated  $[\text{Pt}(\text{terpy})(\text{OMe})]^+$  were found to convert to the hydroxy coordinated analogue and it is for this reason that the spectra were recorded in a 9:1 (v/v) acetonitrile/methanol mixture.

Emission from an acetonitrile solution produces a broad unstructured band with maximum intensity at 654 nm. Although non-emissive in dichloromethane, a methanol solution of the luminophore also emits at 654 nm at room temperature. As in the  $[\text{Pt}(\text{terpy})\text{OH}]^+$  case the luminescence is ascribed to a MLCT excitation. The assignment is made by the same reasoning as that proposed for the hydroxy(terpyridine)platinum(II) luminophore (*vide supra*).

The authors also report the solid state structure of  $[\text{Pt}(\text{terpy})(\text{OMe})](\text{BPh}_4)$  recorded at 298 K by X-ray diffraction experiments. No intermolecular contacts between cations are mentioned and presumably these are absent due to the very large anion. The solid state luminescence of the complex with which the solid state structure could have been correlated has not been reported.

#### 1.2.1.4.3 The $[\text{Pt}(\text{terpy})(\text{H}_2\text{O})]^{2+}$ luminophore

Finally, Wong and Lee briefly mention the photophysical properties of the di-cation  $[\text{Pt}\{4'-(p\text{-OMe})\text{-terpy}\}\text{H}_2\text{O}]^{2+}$  where a water molecule is coordinated to platinum.<sup>80</sup> The measurements formed part of an investigation of the interactions of this compound with sodium dodecyl sulfate (SDS). A detailed description of the luminescence of this platinum compound in the presence of SDS falls outside the scope of this investigation and will not be discussed here.

#### 1.2.1.5 The $[\text{Pt}(\text{terpy})\text{L}]^{n+}$ luminophore

(L = anionic or neutral S-donor ligand; n = 1 or 2)

Luminophores of this type have a thiolate ligand bonded to platinum(II) in the fourth coordination site, the other three sites being occupied by the tridentate terpyridyl ligand. Luminophores of this type can arguably be regarded as one of the most important classes of platinum(II)-terpyridyl complexes due to their significance in the biological setting. Compounds containing alkylthiolate ligands will be discussed first, followed by luminophores in which an aromatic ligand is coordinated *via* its sulfur atom to platinum.

##### 1.2.1.5.1 The $[\text{Pt}(\text{terpy})\text{SR}]^{n+}$ luminophore (R = alkyl group)

The simplest thioalkyl ligand *viz.* thiomethyl has been synthesised as part of a study of platinum assisted cyclisation of *S*-methyl 3-acyl-2-methyldithiocarbazates.<sup>82</sup> As such the photophysical properties of the platinum(II) terpyridyl complex, in the form of a UV/vis absorption spectrum, have been recorded merely as an additional characterisation.

Lippard and coworkers have synthesised a range of platinum(II) terpyridyl compounds incorporating a coordinated thioalkyl ligand.<sup>6,24,25,83</sup> The work was motivated by their interest in the biological action of these systems and as a result recording of the photophysical properties was not a priority. Subsequent work on an extensive range of compounds of this type (including ligands as elaborate as glutathione<sup>8, 71</sup>) have followed this trend.<sup>8, 70, 71, 78, 84 - 86</sup> The nature of the platinum(II)-sulfur bond in this environment has also been used by Shionoya and coworkers as the basis for the formation of cyclic metalloptides.<sup>87</sup>

Indeed, the significance of thioalkyl ligands to the biological setting can be gauged by efforts to model the structure of the  $[\text{Pt}(\text{terpy})\text{GS}]^+$  system (where GS represents glutathione), of which no X-ray crystal structure exists. An early attempt was made by the meticulous analysis of cross-relaxation effects in two-dimensional NMR nuclear Overhauser spectra<sup>88</sup> and subsequently by normal coordinate analysis in conjunction with vibrational spectroscopy.<sup>89</sup>

The work of Lippard does incorporate the absorption spectrum of  $[\text{Pt}(\text{terpy})\text{HET}]^+$  (where HET = 2-hydroxyethanethiolate) in aqueous solution.<sup>6, 83</sup> At concentrations below 15  $\mu\text{M}$  the concentration dependence of the absorption maxima follows Beer's law reflecting dissolution into monomeric ions. The absorption regime shows intense vibronically structured bands in the 240 - 350 nm region with an additional band at 475 nm. Although the authors do not attempt to assign the origin of the bands, the data are fitted to a dimerisation model for which an equilibrium constant for the dimerisation is calculated in the 0.1 - 10 mM concentration range. Aggregation in solution is confirmed by NMR studies and the crystal structure of  $[\text{Pt}(\text{terpy})\text{HET}]\text{NO}_3$  shows the luminophores packing face-to-face in dimeric pairs. The intermetallic Pt...Pt separation is 3.572 Å in each dimer but greater than 3.65 Å between each dimeric pair.<sup>6</sup>

Subsequent studies by Kostić *et al.* again focus on interactions of platinum(II) terpyridine with molecules of biological significance but includes measurements of UV/vis absorption spectra in 10  $\mu\text{M}$  aqueous solution.<sup>8</sup> The sulfur coordinated ligands in the fourth coordination site are HET and glutathione. The absorption spectra are not examined in substantial detail and assignment of the bands is based on their respective intensities and on their dependence on the choice of fourth ligand *i.e.*, their dependence on the nature of the luminophore. A generic

interpretation is made for all the complexes in the study and not surprisingly the bands between 300 and 350 nm are assigned to MLCT transitions while those below 300 nm are attributed to “transitions in the aromatic terpyridyl ligand”.<sup>8</sup> Cheng *et al.* report the copper mediated cleavage of two thiol ligands, *viz.*, glutathione and bis(aminoethyl)-aminoethanethiol (BAT) from the platinum(II) terpyridyl backbone and measure UV/vis absorption spectra of these complexes in deionized water.<sup>90</sup> Analysis of the absorption spectra is as superficial as that undertaken by Kostić *et al.*<sup>8</sup> for related luminophores.

#### 1.2.1.5.2 The [Pt(terpy)SR]<sup>+</sup> luminophore (R = aryl group)

Four reports have been published on complexes that comply with the criteria for inclusion in this section. The first merely comprises a NMR study of a range of thio-aryl substituted complexes.<sup>91</sup> A second (where S-phenyl is the aryl ligand)<sup>92</sup> reports the study of the DNA interactions of the complex and includes a dimerisation study of the complex monitored by UV/vis spectroscopy. Finally, Tzeng, Che and coworkers<sup>93</sup> and Yam, Wong and coworkers<sup>94</sup> incorporate photophysical studies of complexes falling into this category.

A series of *para*-substituted thiophenolato platinum-terpyridyl complexes have been synthesised by Brownlee and coworkers with the intention of studying the NMR properties and the effect on the <sup>13</sup>C and <sup>195</sup>Pt NMR resonances of substituting either electron withdrawing or donating groups on the thio-aryl portion of the complexes.<sup>91</sup> No photophysical measurements have been made.

The research group of Che has studied three compounds falling into this category where R is a thio-coordinated aryl ligand, the sulfur bonded ligands being pyridine-2-thiolate (S-py), pyrimidine-2-thiolate (S-pm) and quinolin-2-thiolate (S-quin).<sup>93</sup> X-ray diffraction analyses yielded crystal structures for the first two compounds, *viz.*, [Pt(terpy)S-py]ClO<sub>4</sub> and [Pt(terpy)S-pm]ClO<sub>4</sub>. The cations in the [Pt(terpy)S-py]ClO<sub>4</sub> salt pack as discrete dimers in the solid state with a metal-metal separation of 3.377 Å within each dimer. By contrast the [Pt(terpy)S-pm]<sup>+</sup> luminophores pack as monomers in the solid state having no close contacts with surrounding luminophores.

Absorption spectra were recorded in acetonitrile at room temperature with the concentration dependence of the absorbances conforming to Beer's law up to a concentration of 1 mM. At high energy in the UV region (310 - 350 nm) all three compounds show intense absorptions with vibronic structure which correspond to the vibrational modes of the terpyridyl ligand. Hence bands in this region are assigned to IL transitions. At lower energies the complexes absorb in broad structureless bands with maxima at 520, 482 and 510 nm for [Pt(terpy)S-py]<sup>+</sup>, [Pt(terpy)S-pm]<sup>+</sup> and [Pt(terpy)S-quin]<sup>+</sup> respectively. The low energy of these absorptions is conspicuous and compares well with the absorbance at 483 nm recorded for [Pt(terpy)}<sub>2</sub>(Gua)]<sup>3+</sup> (Gua = guanidine bridging anion).<sup>28, 95</sup> In the case of the bridged complex the absorption arises due to the existence of a MMLCT excited state which, in turn, is due to the metal-metal interaction. According to the authors it is unlikely that the low energy absorbances of the sulfur containing complexes have their origin in a MMLCT excited state since the available crystal structures show that there are no extended interactions even in the solid state. As a consequence Che *et al.* propose the existence of a  $\pi$ (thiolate) -  $\pi^*$ (terpy) ligand-to-ligand charge transfer (LLCT) excited state to account for the low energy of the absorbances. This proposal is strengthened by the solvent dependence of this long wavelength band, a pronounced blue shift being observed with increasing solvent polarity. In addition the authors show that the absorption energies correspond to the calculated energy transition from the thiolate  $\pi$ -orbital to the terpyridine  $\pi^*$ -orbital in each case. The  $\pi$ - and  $\pi^*$ -orbital energies were obtained from Hartree-Fock self-consistent field calculations.<sup>96-98</sup>

Emission spectra were recorded both in acetonitrile and in the solid state.<sup>93</sup> The compounds were all emissive with the exception of the [Pt(terpy)S-py]<sup>+</sup> which is non-emissive in acetonitrile solution. Solution luminescence maxima occur at 650 nm for [Pt(terpy)S-pm]<sup>+</sup> and at 708 nm for [Pt(terpy)S-quin]<sup>+</sup>. There is no appreciable difference in the position of emission maxima in the solid state, the [Pt(terpy)S-py]<sup>+</sup> luminophore emitting at 640 nm in this form. These maxima are comparable in energy to those arising from a MMLCT state. Not only do the available crystal structures exclude this possibility, but the emission maxima do not show the characteristic red shift associated with this emission origin upon lowering the temperature to 77 K. The intensities increase but peak energies remain essentially unchanged. Clearly intermolecular interactions are not responsible for the emitting state and the authors again propose a LLCT excited state to account for the emission properties of these compounds

by citing similar emission from related compounds.<sup>99-102</sup> Significantly these studies show that LLCT excited states possibly lie at lower energies than MMLCT excited states.

Yam, Wong *et al.* have prepared two platinum(II) terpyridyl complexes with an aromatic group coordinated *via* a sulfur atom to the fourth coordination berth on the metal atom.<sup>94</sup> The two thio-aryl ligands that were used are 4'-*S*-monobenzo-15-crown-5 and 3,4-dimethoxythiophenol, the former in order to study the metal ion binding of the pendant crown ether once coordinated to platinum(II) and the latter included for comparative purposes as a crown-free analogue unable to bind additional metal ions. A X-ray crystal structure of the complex incorporating the thio-coordinated crown ether ligand with a hexafluorophosphate anion in the outer coordination sphere is reported as part of this work. The cations stack to allow for a metal-metal displacement between nearest cations of 4.3908 Å. At such a significant separation in the solid state, the authors point out that the two platinum centres are unlikely to interact with one another.<sup>94</sup> However, electron spray ionisation (ESI) mass spectrometry experiments were carried out and in solutions of elevated concentration the presence of an ion cluster at  $m/z$  1599 is attributed to  $\{[Pt(terpy)(S\text{-benzo-15-crown-5})]_2(PF_6)\}^+$  and is therefore seen to constitute evidence for aggregation in solution at higher concentrations. The authors speculate that the aggregation is brought about by the weak metal-metal bonding and  $\pi$ - $\pi$  stacking interactions in the concentrated solutions.<sup>94</sup> Attempts to verify this phenomenon by UV/vis absorption measurements proved unsuccessful.

#### *Absorption of [Pt(terpy)(S-benzo-15-crown-5)](PF<sub>6</sub>)*

The absorption spectrum of  $[Pt(terpy)(S\text{-benzo-15-crown-5})](PF_6)$  in acetonitrile shows intense, vibronically structured absorption bands in the 300 - 350 nm wavelength range, typical of intraligand transitions localised to the aromatic terpyridine ligand.<sup>94</sup> At 572 nm, an energy regarded to be too low to allow an MLCT assignment, there is a broad absorption band. An assignment is therefore made of a LLCT,  $p_\pi(RS^-) \rightarrow \pi^*(terpy)$ , based on the electron donating strength of the thiolate group and in large part on assignments made by previous authors in similar cases.<sup>93, 102-104</sup> In particular the presence of the 520 nm absorption band observed by Tzeng, Che *et al.*<sup>93</sup> (*vide supra*) in the absorption regime of  $[Pt(terpy)S\text{-py}]^+$  (where S-py represents pyridine-2-thiolate) is invoked to endorse the LLCT assignment made by Yam,

Wong and coworkers. It is rationalised that the electron donating strength of the crown ether raises the energy of the  $p_{\pi}(\text{RS}^-)$  orbital by increasing electron density on the thiolate group. Hence the very low absorption energy of 570 nm compared to that of 520 nm for  $[\text{Pt}(\text{terpy})\text{S-py}]^+$ .  $[\text{Pt}(\text{terpy})(S\text{-benzo-15-crown-5})](\text{PF}_6)$  was found to be non-emissive both in solution and in the solid state.

The 3,4-dimethoxythiophenol coordinated compound was included as an analogue to allow for a comparison of the ion-binding capability of the crown ether coordinated complex with a complex unable to bind additional metal ions.<sup>94</sup> Hence no discussion of its photophysical behaviour of this luminophore is provided.

#### 1.2.1.6 The $[\text{Pt}(\text{terpy})\text{SCN}]^+$ luminophore

This luminophore is constructed from the platinum(II)-terpyridyl fragment with an anionic thiocyanate ligand coordinated as the fourth ligand.

The absorption spectrum of  $[\text{Pt}(\text{terpy})\text{SCN}]^+$  in acetonitrile follows Beer's law at low concentrations and shows the familiar high energy intense absorptions associated with the terpyridyl ligand.<sup>27, 28</sup> At longer wavelengths there is a broad, low intensity absorption with its most intense feature at 400 nm. With an intensity greater than metal-centred (d-d) absorptions and a frequency too low to fall in the  $\pi\text{-}\pi^*$  manifold, the low energy feature is assigned to a MLCT absorption.<sup>27, 28</sup> McMillin and coworkers<sup>27</sup> report  $[\text{Pt}(\text{terpy})\text{SCN}]^+$  to be emissive in both acetonitrile and dichloromethane at room temperature with emission maxima centred at 588 and 594 nm respectively. (This is in contrast to Che *et al.* who find the thiocyanate derivative to be non-emissive in degassed acetonitrile solution at room temperature.<sup>28</sup>) The band profile is broad and unstructured and the negligible solvent dependence of the emission maximum suggests that luminescence is not due to a LLCT excited state. These factors aid the authors in arriving at a MLCT assignment.

Solution emission studies of the thiocyanate coordinated luminophore has been supplemented by Crites Tears and McMillin in a study on quenching of the excited state by a range of Lewis bases.<sup>48</sup> The study clearly shows that the rate of exciplex quenching increases as the donor number (an indicator of Lewis base strength<sup>49</sup>) increases.



Che and coworkers have shown the [Pt(terpy)SCN]PF<sub>6</sub> salt to exhibit a strong luminescence in the solid state at room temperature and report the emission lifetime to be 0.4 μs.<sup>28</sup> The luminescence is assigned to a <sup>3</sup>MLCT excitation. Although McMillin and his group synthesised the tetrafluoroborate salt of the same luminophore, an investigation of the solid state luminescence did not form part of their study.<sup>27</sup>

### 1.2.2 Luminophores derived from the [Pt(4-R-phbipy)]<sup>2+</sup> unit

All the compounds in this section have in common the [Pt(4-R-phbipy)]<sup>2+</sup> unit illustrated in Figure 1.2. The compounds only differ in the monodentate ligand bonded to platinum in the fourth coordination site and in the substituents on the phenyl-bipyridyl ligand.

#### 1.2.2.1 The [Pt(4-R-phbipy)Cl] luminophore

The luminophore discussed in this section comprises the tridentate phenyl-bipyridyl ligand bonded to platinum(II) with a chloride ligand taking up the fourth coordination site of platinum. The phenyl-*ortho*-C-deprotonated aromatic ligand is anionic and in conjunction with the chloride ligand cancels the double positive charge on the metal. Thus no counterion is required and it is not possible to have the prominent counterion effect seen in the solid state luminescence of the chloro(terpyridine)platinum(II) luminophore (see section 1.2.1.1).

Constable and coworkers synthesised this luminophore in 1990 in a study of the coordination properties of the organic ligand with a variety of metal centres.<sup>105, 106</sup> A description of its photophysical properties followed in 1996 by Che *et al.*<sup>44</sup>

The absorption spectrum of [Pt(phbipy)Cl] was recorded in acetonitrile and obeys Beer's law in the 0.001 mM to 1 mM concentration range.<sup>44</sup> The absorption profile is reminiscent of that recorded for the closely related chloro(terpyridine)platinum(II) complex.<sup>28</sup> There are several intense absorptions at wavelengths between 250 and 370 nm which are assigned to intraligand transitions. At lower energies (400 - 450 nm) the spectrum shows broad, low intensity bands ( $\epsilon$  1550 - 1020 M<sup>-1</sup>.cm<sup>-1</sup>), the energy and intensity of which show a dramatic solvent dependence. These characteristics, in combination with similar behaviour of related

complexes<sup>28,41</sup>, allow the authors to assign the low energy absorption band to a Pt  $\rightarrow$   $\pi^*$ (ligand) <sup>1</sup>MLCT absorption. The authors rationalise this assignment by pointing out that the absorptions are too intense to be from metal-centred ligand field transitions and occur at too low an energy to have their origin in intraligand transitions. Che *et al.* further assign the absorption tail to MLCT transitions of triplet multiplicity.<sup>44</sup>

In contrast to the chloro(terpyridine)platinum(II) luminophore the chloro(6-phenylbipyridine)platinum(II) luminophore is highly emissive in fluid solution at ambient temperatures.<sup>44</sup> Even the [Pt(4'-Ph-terpy)Cl]<sup>+</sup> luminophore is only weakly emissive under these conditions.<sup>31, 32, 42, 53</sup> The emission maximum in acetonitrile is at 550 nm. The peak maximum is essentially unaffected by the solvent although, the emission lifetime and quantum yield decrease with an increase in the polarity of the solvent. The emission origin is assigned to a <sup>3</sup>MLCT excited state.

Interestingly the luminescence in a frozen glass at 77 K is highly solvent dependent. Luminescence measurements of the complex in a rigid matrix were made on dilute solutions (concentration  $\approx$  0.001 mM) in order to discourage the formation of excimers or interacting dimers. Under these conditions a vibrationally structured band with emission maxima ranging from 512 to 567 nm, depending on the solvent, is obtained. The emission is assigned to a <sup>3</sup>MLCT excited state based on the pronounced solvatochromism and the structured band profile.

A microcrystalline sample of [Pt(phbipy)Cl] luminesces at a significantly longer wavelength compared to the fluid and glass emission.<sup>44</sup> The room temperature emission profile is narrow, asymmetric and attains its peak intensity at 665 nm with a shoulder at 698 nm. A reduction in temperature is accompanied by a narrowing of this band and a red shift in the emission maximum to 700 nm. It is clear from the contrast in luminescence between the solution (monomeric) and solid state that the respective excited states have different electronic origins. This luminescence behaviour is typical for compounds in which there is a metal-metal interaction in the solid state. Thus the excited state from which luminescence occurs is believed to be <sup>3</sup>[(d<sub>σ\*</sub>) $\{\sigma(\pi^*)\}$ ], *i.e.*, <sup>3</sup>MMLCT in nature.<sup>44</sup> This assessment is supported by a crystal structure showing the luminophores packing in interacting dimeric units with a Pt...Pt separation of 3.345 Å.

The only other compound incorporating the chloro(phenyl-bipyridine)platinum(II) binding domain and on which photophysical studies have been carried out was synthesised and studied by Neve, Campagna *et al.*<sup>107</sup> In their quest for liquid crystals which incorporate a metal (metallomesogens), the compound  $[\text{Pt}(\text{L}_1)\text{Cl}]$ , where  $\text{HL}_1$  is the tridentate ligand 4'-(4-dodecyloxy)phenyl]-6'-phenyl-2,2'-bipyridine, was synthesised. Photophysical properties of the compound were studied and a X-ray diffraction analysis of the orange crystals yielded a crystal structure.

The absorption spectrum of  $[\text{Pt}(\text{L}_1)\text{Cl}]$  in dichloromethane at room temperature shows strong absorptions in the UV region ( $\lambda < 400$  nm) assigned to metal perturbed intraligand transitions. A weak shoulder at 365 nm is assigned to  $n \rightarrow \pi^*$  transitions involving the oxygen of the alkoxy group. At longer wavelengths in the visible region (at 420 nm) there is a moderately intense ( $\epsilon$  5400  $\text{M}^{-1}\cdot\text{cm}^{-1}$ ) absorption transition. This absorption band is displaced to higher energy when the same set of ligands are coordinated to palladium(II). A comparison with the absorption spectra of related terpyridyl<sup>27, 29</sup> and cyclometallated compounds of platinum(II) suggested an assignment of the band to a MLCT ( $d\pi \rightarrow \pi^*$ ) transition. The authors attribute the higher energy absorption of the palladium compound to the greater difficulty of oxidising palladium, thus confirming the assignment as a process involving oxidation or partial oxidation of the metal centre.

The emission spectrum of  $[\text{Pt}(\text{L}_1)\text{Cl}]$  in dichloromethane solution at room temperature exhibits an almost structureless band peaking at 590 nm, with a lifetime of 700 ns and is attributed to emission from  $^3\text{MLCT}$  energy levels. The assignment is based on the rate constant of the radiative transition which is correlated with values from the literature.<sup>108</sup> At 77 K in a butyronitrile glass the compound produces a structured emission band with its 0-0 transition at 545 nm. The band profile suggests emission from either a  $^3\text{MLCT}$  or  $^3\text{LC}$  excited state but the authors assign the band to a  $^3\text{MLCT}$  transition for the same reasons furnished for emission from the dichloromethane fluid solution.

The authors compare their solution emission findings with those of Che *et al.*<sup>44</sup> as described earlier in this section, noting that the emission maximum shows a red shift compared to the emission obtained by Che *et al.* for  $[\text{Pt}(\text{phbipy})\text{Cl}]$ . The red shift is attributed to the presence

of an additional phenyl ring in  $L_1$ . A greater emission lifetime and quantum yield is also shown by  $[\text{Pt}(L_1)\text{Cl}]$ . As the metal-centred d-d ( $^3\text{MC}$ ) state is known to facilitate radiationless decay, the authors rationalize the enhanced emission lifetime and quantum yield as being due to the greater difference in energy between the radiative excited state and the  $^3\text{MC}$  state.

In the solid state a weakly structured emission with a peak intensity at 590 nm is obtained from a microcrystalline sample of  $[\text{Pt}(L_1)\text{Cl}]$ .<sup>107</sup> The band is reminiscent of the solution luminescence and thus is apparently unaffected by intermolecular interactions in the solid state. This is confirmed by a crystal structure showing the luminophores packing head-to-tail in dimeric units with a Pt...Pt separation of 4.426 Å, a distance too large to support significant orbital interaction between the platinum centres. This is in contrast to the solid state emission of  $[\text{Pt}(\text{phbipy})\text{Cl}]$  where the platinum atoms lie much closer together, a disparity manifested in the emission of  $[\text{Pt}(\text{phbipy})\text{Cl}]$  which occurs at a much longer wavelength due to the metal-metal interaction. Neve, Campagna *et al.* do however identify possible sites where intermolecular  $\pi$ - $\pi$  interaction is possible although such interplay does not seem to have affected the emission properties of the compound.<sup>107</sup> Emission in the solid state is assigned to a  $^3\text{MLCT}$  excited state based on its similarity to the solution luminescence. The presence of a vibrational progression in the solid state emission is regarded as a particularly encouraging sign in support of the proposed excited state assignment.

#### 1.2.2.2 The $[\text{Pt}(\text{phbipy})\text{NR}]^+$ luminophore

Only one compound of this type has been reported in the literature,<sup>106</sup> this being  $[\text{Pt}(\text{phbipy})(\text{CH}_3\text{CN})]\text{PF}_6$  in which acetonitrile is bonded to platinum(II) in the fourth coordination site. Two forms of the compound are reported, a rapidly precipitated microcrystalline purple-blue form and an orange form grown from the diffusion of ether into a DMF solution of the complex. The orange crystals yielded a crystal structure with the luminophores packing in discrete dimeric pairs. The Pt-Pt separation is 3.28 Å within the dimer and 4.59 Å between dimers. Unfortunately no photophysical studies on this compound have been reported.

### 1.2.2.3 The [Pt(phbipy)PR]<sup>+</sup> luminophore

Members of this group of luminophores have 6-phenyl-2,2'-bipyridine and a neutral phosphine ligand coordinated to the square-planar platinum(II). Che and coworkers were the first to report the photophysical properties of compounds of this type starting with the [Pt(phbipy)(PPh<sub>3</sub>)]<sup>+</sup> luminophore in which triphenylphosphine is bonded to platinum(II) in the fourth coordination site.<sup>44</sup> The absorption regime in acetonitrile at room temperature resembles that of [Pt(phbipy)Cl] (see section 1.2.2.1) except that the charge transfer bands peaking at 405 - 460 nm are less intense, ( $\epsilon$  300 - 980 M<sup>-1</sup>.cm<sup>-1</sup>). These low energy bands are also assigned to MLCT transitions, although Che *et al.* do not specify to what extent, if any, the triphenylphosphine ligand influences the intensities of these transitions. The intensities comply with Beer's Law in the 0.001 - 1 mM concentration range.

Irradiation of the [Pt(phbipy)PPh<sub>3</sub>]<sup>+</sup> luminophore gives rise to emission both in solution and in the solid state. An acetonitrile solution of the luminophore emits in a broad band which peaks in intensity at 538 nm at room temperature. Reducing the temperature to 77 K introduces vibrational structure to the emission profile and shifts  $\lambda_{em}(max)$  to a higher energy (527 nm). This luminescence behaviour is similar to that observed for [Pt(phbipy)Cl] and the authors assign the solution emission to a <sup>3</sup>MLCT excited state by analogy.

The luminescence behaviour in the solid state is somewhat different. A broad and unstructured emission band centred at about 600 nm is observed, *i.e.*, the energy of the emission is significantly reduced as compared to that observed in fluid solution. Clearly interactions within the crystal affect the excited state as confirmed by a X-ray crystal structure determination of [Pt(phbipy)PPh<sub>3</sub>]ClO<sub>4</sub>. Due to the bulky PPh<sub>3</sub> ligands all Pt...Pt contacts exceed 4 Å and the possibility of metal-metal interactions can be excluded. However, the aromatic plane formed by the phenyl-bipyridyl ligand is 3.35 Å away from its closest counterpart on the adjacent cation, and is well within the threshold for overlap of  $\pi^*$ -orbitals. Consequently the emission is assigned to excimeric interaction of the phenyl-bipyridyl ligands.<sup>44</sup>

The next compound in this category is very similar to the one just discussed, the only differences being that the phenyl bipyridyl ligand has a *p*-tolyl group (abbreviated here as *p*MePh) substituted in the 4-position while the phosphine ligand is diphenylphosphinopropionic acid (Ppa).<sup>109</sup> In acetonitrile solution a MLCT Pt(5d) – ligand( $\pi^*$ ) absorbance is recorded at 430 nm as a broad, low intensity ( $1560 \text{ M}^{-1} \cdot \text{cm}^{-1}$ ) feature in the visible spectrum. The authors make this deduction by comparison with similar cyclometallated Pt(II) derivatives.<sup>41, 110</sup>

Emission spectra for  $[\text{Pt}(4\text{-}p\text{MePh-phbipyPpa})^+]$  were recorded in acetonitrile and in the solid state.<sup>109</sup> In acetonitrile at ambient temperatures the emission profile peaks at 542 nm and is assigned to a <sup>3</sup>MLCT transition. This maximum shifts to higher energy (528 nm) and shows vibrational structure (spacing  $1240 \text{ cm}^{-1}$ ) in a frozen solution, but the authors do not attempt to rationalise this behaviour. The emission spectrum recorded in the solid state exhibits a broad, weakly structured band peaking at 568 nm. The assignment of this band is based on the crystal structure of  $[\text{Pt}(4\text{-}p\text{MePh-phbipy})\text{Ppa}]\text{PF}_6$ . The phenyl ring in the 4-position of bipyridine appears to be essentially coplanar with the rest of the ligand. An interplanar spacing of  $3.68 \text{ \AA}$  allows  $\pi$ -stacking between the aromatic planes of the phenyl-bipyridyl portions of the ligands on neighbouring luminophores. On its opposite side the luminophore interacts by H-bonding between the carboxylic acids in adjacent molecules. The overall effect produces polymeric chains assembled by alternating hydrogen bonding and  $\pi$ - $\pi$  interactions. The authors conclude that the emission energy at 568 nm is too high to have its origin in a MMLCT excited state and a <sup>3</sup>MLCT excitation with partial excimeric character is proposed, based to a large extent on the solid state structure.

### 1.3 CONCLUSIONS AND COMMENTS

Although not exhaustive, the range of complexes surveyed here provide a sample of the wide variety of species that are based on a terpyridyl or phenyl-bipyridyl moiety bonded to platinum(II). What is immediately noticeable is the variety of ways in which researchers have been able to make simple alterations to the ligand structure and thereby bring about significant changes in the excited state properties of these compounds. For example, the addition of a substituent in the 4'-position has been shown to render the otherwise non-emissive  $[\text{Pt}(\text{terpy})\text{Cl}]^+$  luminophore luminescent in fluid solution. Extending on this idea, if the 4'-substituent is chosen to be an easily ionisable group the emission lifetime can be extended to as long as  $64 \mu\text{s}$  as in the case of  $[\text{Pt}(4'\text{-Pyre1-terpy})\text{Cl}]^+$ .<sup>32</sup> Another simple variation is to alter the nature of the fourth ligand bonded to platinum. As shown by the rich selection of groups that have been used as the fourth ligand, the synthetic procedures exist to facilitate the formation of a wide variety of complexes. Another variable is the choice of counterion, in particular its size, when the complex is ionic. Changing the counterion can have a dramatic effect on the crystal structure of the salt, affecting inter-luminophore interactions, and hence the solid state luminescence properties of the salt.<sup>29,47,54</sup> Taken together the various structural modifications allow the researcher a wide range of permutations in order to produce a complex with desirable photophysical properties. However, as the preceding survey shows, this class of compounds possesses a wide range of accessible excited states, each one of which is a potential emitter. Moreover, there are often small differences in the energies of the excited states and, for this reason, it becomes difficult to predict the nature of the emitting state. Indeed, a common theme in the results presented in Chapter 3, 4 and 5 is that emission is from a configurationally mixed state *i.e.*, one with contributions from different emission origins.

In addition to the possibility of tuning excited states *via* structural modifications, terpyridyl ligand complexes of platinum(II) have been studied for the following reasons<sup>27,44</sup>:

i) The terpyridyl ligand is a rigid, planar and a tridentate *N*-donor ligand that always imposes the same geometrical constraints at a metal atom centre.<sup>2</sup> The ligand's planarity is important as it negates  $D_{2d}$  distortions which promote radiationless decay of the excited state.<sup>36</sup>

ii) The complexes have an established history of low lying charge transfer states due to the extended  $\pi$ -system of the terpyridyl ligand. These states could have useful photochemical and photophysical properties.<sup>6, 26, 42</sup>

iii) It has been established that binding interactions between platinum(II) terpyridines and biological molecules such as DNA are possible.<sup>24, 25</sup> The complexes have also been employed as protein modification reagents<sup>11, 26</sup>, demonstrating additional potential in this growing field involving the study of the biological activity of coordination compounds.

iv) Square-planar platinum(II) complexes often stack one above the other in the solid state, forming linear chains. These linear chains have the potential of possessing interesting photophysical properties.<sup>21, 41, 45, 46, 53, 111</sup>

v) Certain polypyridyl ligand complexes of platinum(II) exhibit solvatochromism. The solvatochromism appears to have its origins in the presence of  $d_{z^2}(\text{Pt})$ - $d_{z^2}(\text{Pt})$  interactions, either in concentrated solutions due to aggregation<sup>112</sup>, or in the solid state due to parallel stacking of the chromophores.<sup>113</sup> The development of chemical sensors based on their emission properties is a current and topical area of research.<sup>114</sup>

Clearly the study of the photophysical properties of platinum(II) complexes of terpyridyl and related ligands is a fertile area of research, both at the fundamental and applied levels.

#### 1.4 AIMS OF THIS WORK

It is against this background that the photophysical properties of the new compounds synthesised in this work have been studied. A range of terpyridyl or terpyridyl-like ligands have been used, these being illustrated in Figure 1.5 with their abbreviations. The complexes studied contain one of these ligands with, in each case, a chloride ligand bonded to platinum(II) in the fourth coordination site. Thus the compounds studied can be categorised according to the nature of the terpyridyl ligand; in fact they fall into three distinct categories which are now described along with the reason for investigating their photophysical properties.



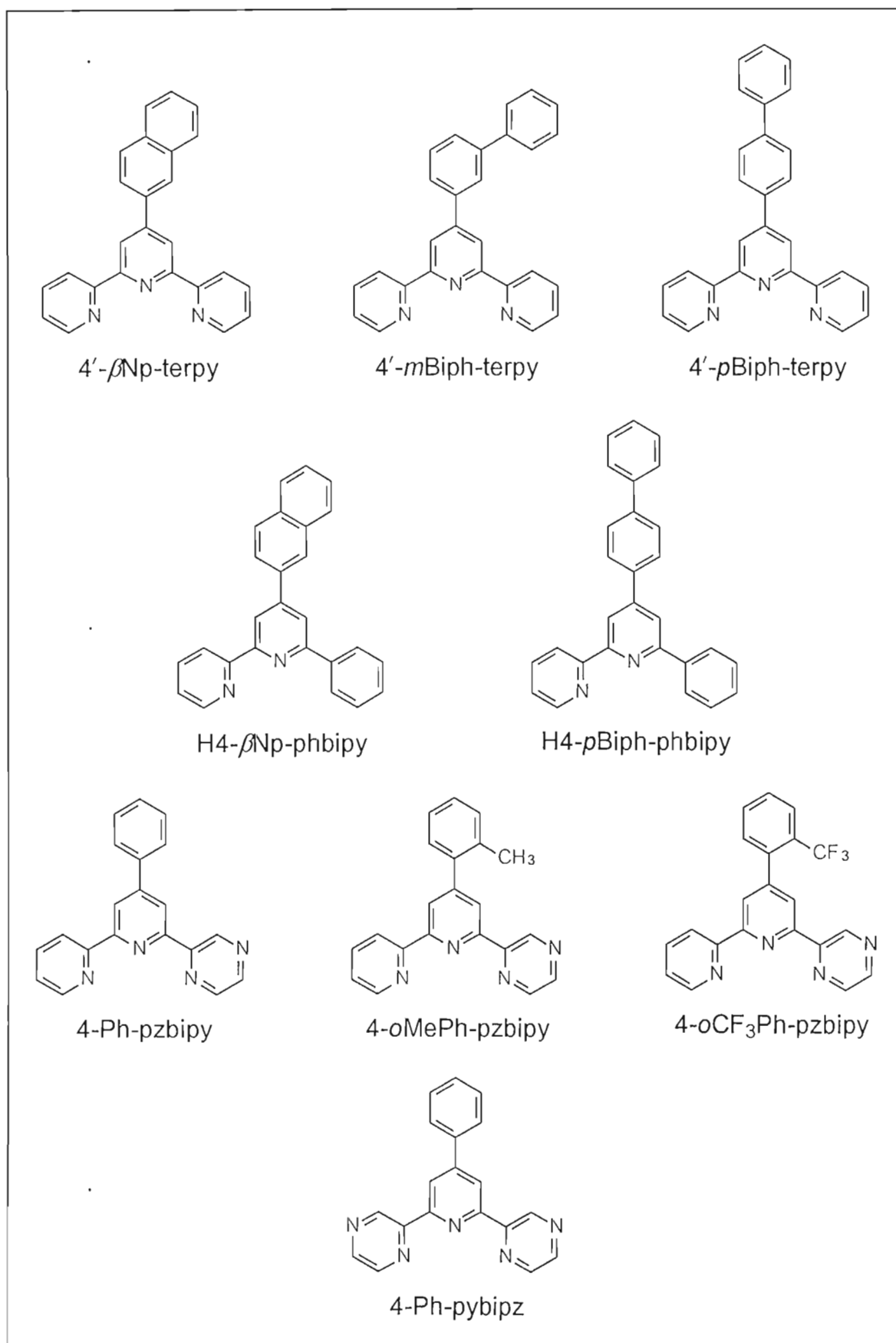


**Figure 1.5** Ligands synthesised in this work and their abbreviations.

In the first category we report the synthesis of 4'-(R)-2,2':6',2''-terpyridines {R =  $\beta$ -naphthyl (4'- $\beta$ Np-terpy), *m*-biphenyl (4'-*m*Biph-terpy), *p*-biphenyl (4'-*p*Biph-terpy)}. Ligand 4'- $\beta$ Np-terpy is directly related to the 4'- $\alpha$ -naphthyl-2,2':6',2''-terpyridine (4'- $\alpha$ Np-terpy) ligand synthesised in our laboratories by Summerton.<sup>111</sup> The compound [Pt(4'- $\alpha$ Np-terpy)Cl]<sup>+</sup> has an exceptionally long lifetime of 12  $\mu$ s for the emitting state in the non-coordinating solvent dichloromethane. We wished to determine the effect of  $\beta$ - rather than  $\alpha$ -substitution on the lifetime of the emitting state. It is expected that the greater freedom of rotation of the naphthyl group about the interannular bond in [Pt(4'- $\beta$ Np-terpy)Cl]<sup>+</sup> compound to influence the emitting state. The [Pt(4'- $\beta$ Np-terpy)Cl]<sup>+</sup> compound is thus synthesised as a model to probe the dynamics and contribution of the naphthyl group to the photophysical properties of the luminophore. To extend on this idea two terpyridyl ligands with extended  $\pi$ -conjugated aromatic systems in the terpyridyl 4'-position were synthesised, *i.e.*, ligands 4'-*m*Biph-terpy and 4'-*p*Biph-terpy. The 4'-*m*Biph-terpy ligand is asymmetric in that 2-fold symmetry about the Pt-N(bridgehead) axis is absent because of the presence of the *m*-biphenyl (rather than *p*-biphenyl) group in the 4'-position. Our hope was that this would lead to novel photophysical properties for the complexes of this ligand and, in particular, that the inherent asymmetry of the ligand would promote interesting stacking arrangements in the solid state. In general, adding phenyl rings to the basic terpyridyl backbone could enhance the emission lifetime as it has been found that introducing phenyl rings in the 4, 4' and 4'' positions *i.e.*, *para* to the nitrogens of terpyridine, considerably prolongs the lifetime of the excited state produced by irradiation of the terpyridyl ligand complex [Ru(terpy)<sub>2</sub>]<sup>2+</sup>.<sup>115, 116</sup> In summary, it is hoped the Pt(II) complexes of ligands 4'- $\beta$ Np-terpy, 4'-*m*Biph-terpy, and 4'-*p*Biph-terpy would possess long lifetimes for their emitting states.

Each of the ligands 4'- $\beta$ Np-terpy, 4'-*m*Biph-terpy and 4'-*p*Biph-terpy is neutral which opens up the possibility of synthesising salts of the [Pt(L)Cl]<sup>+</sup> (L = 4'- $\beta$ Np-terpy, 4'-*m*Biph-terpy or 4'-*p*Biph-terpy) cation with different counterions. As discussed above, varying the counterion can have a marked effect on the solid state luminescence properties of the compound. To this end hexafluoroantimonate, tetrafluoroborate and triflate salts were synthesised.

As an extension to the 4'- $\beta$ Np-terpy and 4'-*m*Biph-terpy ligands, the syntheses of the potentially orthometallating analogues, 4-R-6-phenyl-2,2'-bipyridine {R =  $\beta$ -naphthyl (H4-

$\beta$ Np-phbipy), *p*-biphenyl (H4-*p*Biph-phbipy)}, are reported. These ligands offer the same advantages as their terpyridyl counterparts. In addition, since they bond to platinum(II) in their deprotonated, anionic form they give rise to neutral complexes when the fourth ligand ( $\text{Cl}^-$ ) is also anionic. This has the advantage that mutual repulsion between the complexes should not prevent oligomerisation, either in solution or the solid state. Also, we hoped that the neutral complexes would have better solubility in non-polar solvents. Moreover, an important focus of this work has been to modify the electron distributions on or near the platinum centre. Carbon donor ligands are strong field ligands, high in the spectrochemical series. With a weak-field chloride ligand also bound to platinum, the contrast between the properties of the two ligands may result in interesting photophysical properties for the complex. Indeed, the effect on emission resulting from the combined action of weak and strong field ligands on the photophysical properties of platinum complexes has already been the subject of study (see section 1.2.2).

Another method of making adjustments to the 4'-phenyl-2,2':6',2''-terpyridine ligand is to replace one of the outer pyridine rings with a pyrazine heterocycle. Here we report the synthesis of 4-(2'''-R-phenyl)-6-(2'''-pyrazinyl)-bipyridines {R = H (4-Ph-pzbipy),  $\text{CH}_3$  (4-*o*MePh-pzbipy),  $\text{CF}_3$  (4-*o*CF<sub>3</sub>Ph-pzbipy)}. As an extension a ligand was synthesised in which both the outer pyridine rings of 4'-phenyl-2,2':6',2''-terpyridine are exchanged for pyrazine rings with the synthesis of 4-phenyl-2,6-bis(2'-pyrazinyl)-pyridine (4-Ph-pybipz). The inclusion of aza-enriched pyrazine rings to the ligand's binding domain with platinum was also designed to perturb the electron distribution compared to the 4'-phenyl-2,2':6',2''-terpyridine case. Pyrazine is a weaker  $\sigma$ -donor but a superior  $\pi$ -acceptor ligand than pyridine.<sup>117</sup> This in itself should have a fundamental effect on the electron distribution at the platinum atom and hence on the photophysical properties of the complex.

## Chapter Two

## Ligand Synthesis

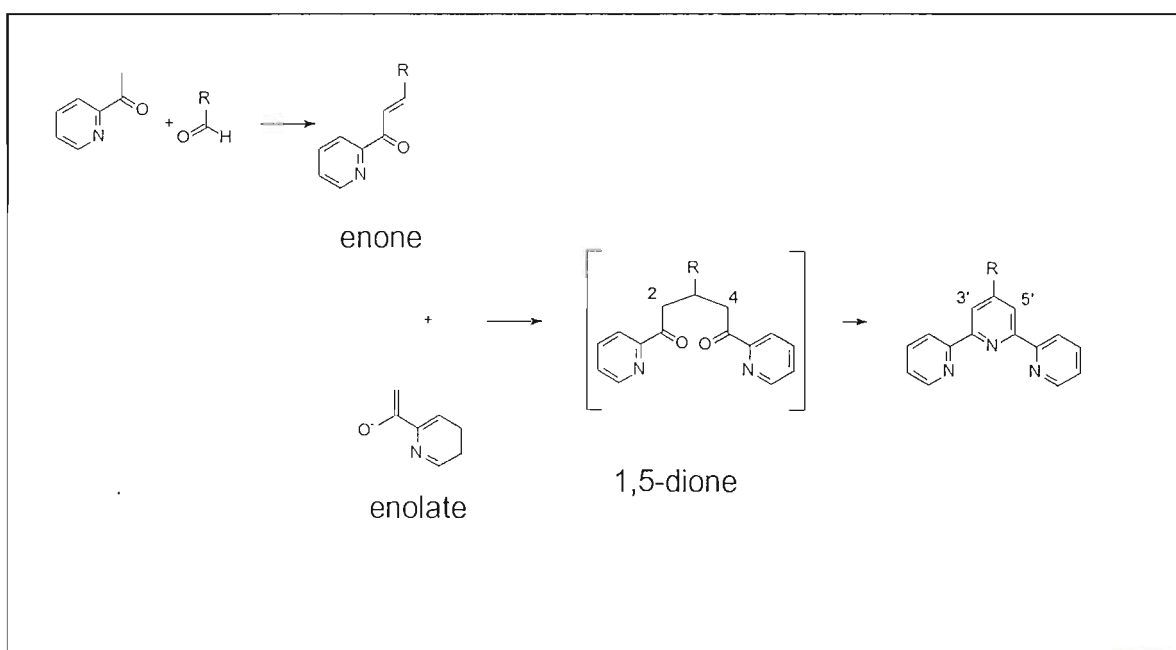
### 2.1 INTRODUCTION

The first report of the synthesis of 2,2':6',2''-terpyridine (terpy or terpyridine) was that by Morgan and Burstall in the 1930's. It was isolated in low yield (< 1.3 %) from a mixture of twenty or so oligopyridines<sup>118</sup>; the mixture had been produced through the oxidative coupling of pyridine by iron(III) chloride. In subsequent years, the widespread use of terpyridine as a planar tridentate ligand in coordination chemistry has led not only to vastly improved synthetic strategies for terpyridine itself, but also to a large number of high yielding syntheses of substituted terpyridines, often on gram or multigram scales. In a recent and comprehensive review, Cargill Thompson reported the range of methods currently available for the synthesis of terpyridine ligands<sup>119</sup>; two general strategies are reported here *viz.*, coupling methodologies and an approach involving ring assembly.

Initial methods aimed specifically at the synthesis of terpyridines focussed on coupling methodologies for the ligand assembly. Though ring assembly methods capable of making terpyridines have been available for some time<sup>120, 121</sup> they were not employed to this end until more recently.<sup>122</sup> (These latter methods will be discussed in greater detail below.) It was established that using the coupling approach, terpyridine could be prepared by copper (Cu<sup>0</sup>) mediated Ullman coupling of bromopyridines or by oxidative coupling of pyridines by the action of iodine.<sup>123</sup> Organometallic coupling methods developed more recently<sup>124, 125</sup> have produced markedly improved yields but often still result in intractable mixtures of different oligomers and regioisomers.

The second distinctive strategy for the synthesis of terpyridines involves the assembly of the central pyridine ring during the course of the final step of the synthesis. A few syntheses exist however, in which the final step involves the assembly of the outer pyridine ring.<sup>126 - 128</sup> One example of the former approach is provided by the synthesis of 4'-phenyl-2,2':6',2''-terpyridine carried out by Frank and Riener in 1950.<sup>122</sup> In fact the method employed by these two researchers is simply an extension of the Tschitschibabin method<sup>121</sup> developed as early as the

1920's for the synthesis of substituted pyridines. The Tschitschibabin<sup>121</sup> pyridine synthesis as well as that by Hantzsch<sup>120</sup>, both suitable for the assembly of the terpy moiety, were available prior to the efforts of Morgan and Burstall. However, the yields are low, with the method being further limited by requiring identical substituents in the 2- and 6-positions of the central pyridine ring. A three step terpyridine synthesis by Potts<sup>129</sup> led to considerably improved yields, but its use has been limited due to the necessity for the reductive removal of a thiomethyl group from the 4'-position on the ligand. Another problem encountered in this procedure is the difficulty experienced in removing the unpleasant smell of methanethiol (generated during the procedure) from the reaction product. These complications have been overcome by the method of Jameson and Guise.<sup>130</sup> Significantly the latter method is capable of terpyridine production on a multigram scale but unfortunately it is not suitable for introducing substituents in the 4'-position which is an important area of our work.

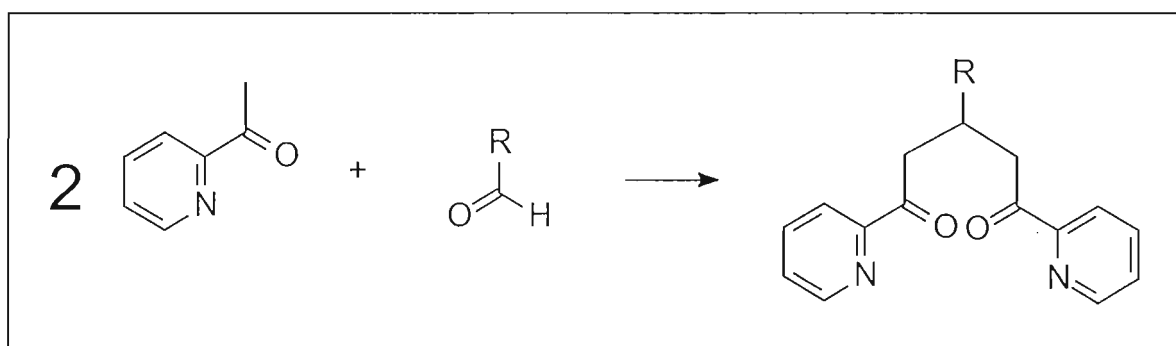


**Scheme 2.1** Reaction route showing generalised Kröhnke methodology.

The method of choice in this work is the Kröhnke synthesis<sup>131</sup> (see Scheme 2.1). It falls into the second category and involves the reaction of an enone with an enolate to form a pentane-1,5-dione intermediate (usually *in situ*) which undergoes ring closure by the action of an ammonia source, often ammonium acetate. The enone is formed by the Aldol condensation of 2-acetylpyridine with an aldehyde in basic medium to give an  $\alpha,\beta$ -unsaturated ketone *i.e.*, the enone. Clearly the choice of aldehyde determines the substituent in the 4'-position of the

terpyridine. Improved methods for the Aldol condensation by which the enones can be formed in ever higher yields have become available to complement the overall synthesis of terpyridyl and related ligands.<sup>132</sup> Advances in “Green Chemistry”<sup>133</sup> have been of benefit to the synthesis of enones which have been made under solventless conditions and in quantitative yields.<sup>134,135</sup> It is also useful to note that Mannich bases<sup>136</sup> are feasible substitutes for the enone if a terpyridine analogue lacking a substituent in the 4'-position is to be synthesised.<sup>105</sup>

It is sometimes possible to isolate the 1,5-dione directly from the Aldol condensation of twice molar amount of acetylpyridine with the aldehyde of choice (Scheme 2.2).<sup>137-139</sup>



**Scheme 2.2** Reaction scheme showing 2:1 addition to give a pentane-1,5-dione.

An advantage of this approach is that an enolate is no longer required. However, only symmetrical ligands can be produced using this method once the symmetrical 1,5-dione is reacted with an ammonia source. To this end Owlsley and coworkers have designed a synthesis specifically to produce 1,5-diones<sup>140</sup> that can then be reacted further with a source of ammonia to afford the ligand. Note that it is possible to distinguish the enones from the diones by <sup>1</sup>H NMR and IR spectroscopy should both be produced in an Aldol condensation reaction. In terms of the IR spectra the enones are distinguished from the diketones by the presence of prominent C=O stretching bands at about 1670 cm<sup>-1</sup> in the former case whereas they fall in the range 1698 - 1700 cm<sup>-1</sup> in the latter case. In terms of <sup>1</sup>H NMR spectra the diketones exhibit distinctive resonances due to their methine and methylene protons.

In cases where it is not possible to synthesize the 1,5-dione directly or if asymmetric substitution in the 2- and 6-positions of the central pyridine is required, the necessity to employ an enolate becomes unavoidable. The enolate usually takes the form of an acylpyridinium salt e.g., *N*-{1-(2'-pyridyl)-1-oxo-2-ethyl}pyridinium iodide (Figure 2.1).

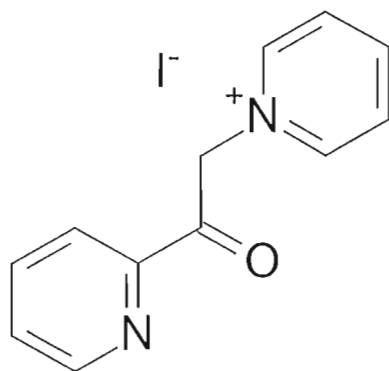
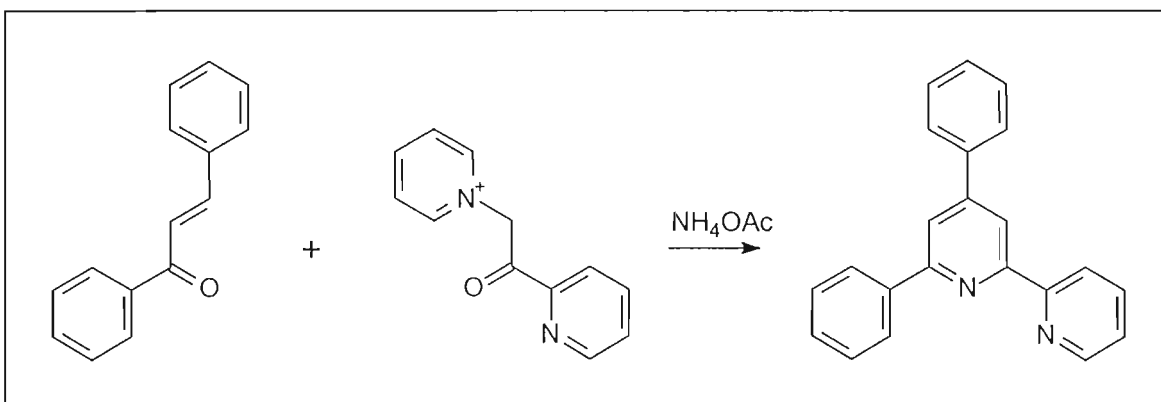


**Figure 2.1** *N*-{1-(2'-pyridyl)-1-oxo-2-ethyl}pyridinium iodide

The use of acylpyridinium salts in the synthesis of oligopyridines has been largely developed by Kröhnke and the utility of this procedure is described in his definitive review of the method.<sup>131</sup> The pyridinium salt is obtained by reaction of the appropriate methyl ketone with pyridine in the presence of iodine, an important result being the activation of the *N*-methylene protons of the salt compared to the parent methyl ketone, thus leading to markedly greater reactivity. Moreover, the pyridinium group has the added benefit of acting as an internal oxidant upon ring closure. In some cases the enone is not responsive to the pyridinium salt. In this event more rigorous conditions can be implemented by the use of the potassium enolate, which is prepared *in situ* by the action of potassium *t*-butoxide on the methyl ketone.<sup>141</sup>

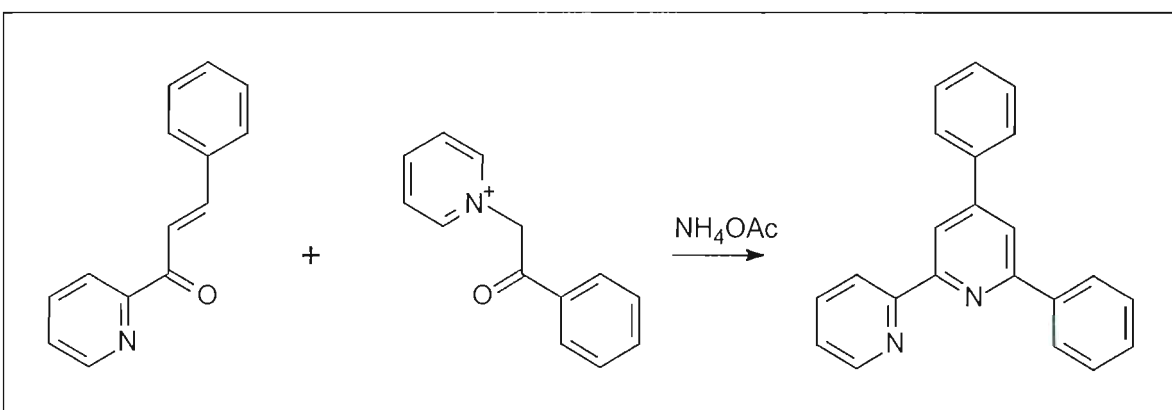
It is clear that if an asymmetric product is required, the new heterocycle, *i.e.*, a heterocycle other than pyridine, can be introduced *via* either the enone or the enolate. If, for instance, 6-phenyl-2,2'-bipyridine is to be prepared, the Kröhnke approach offers two possible routes. The desired product can be made either by the reaction of 1,3-diphenyl-prop-2-en-1-one with *N*-{1-(2'-pyridyl)-1-oxo-2-ethyl}pyridinium iodide<sup>111</sup> (Scheme 2.3a).





**Scheme 2.3a** One possible method to synthesize 6-phenyl-2,2'-bipyridine.

Alternatively the reaction of 1-(2'-pyridyl)-3-phenyl-prop-2-en-1-one with *N*-(1-phenyl-1-oxo-2-ethyl)pyridinium bromide<sup>107</sup> (Scheme 2.3b) could be attempted. In practice, for any particular ligand only one route tends to be viable and for this reason only one of the two approaches was used, the choice depending on the particular ligand. [Note that the syntheses of Potts<sup>129</sup> and Jameson and Guise<sup>130</sup> share this potential for performing syntheses that give asymmetric products *via* two possible routes.]



**Scheme 2.3b** Second method to synthesize 6-phenyl-2,2'-bipyridine.

In conclusion it is the inherent flexibility of the Kröhnke technique in terms of introducing new heterocycles and substituted heterocycles combined with the ease of introducing substituents in the 4'-position, that make it the method of choice for the synthesis of the ligands described in this work. An added advantage is that the reaction produces yields on a scale suitable for our requirements.

## 2.2 SYNTHESIS AND CHARACTERISATION OF THE TERPYRIDINE LIGANDS

The ligands synthesized in this work are listed with their abbreviations in Figure 1.5. All  $^1\text{H}$  NMR spectra were recorded in  $\text{CDCl}_3$  (unless otherwise stated) and spectral assignments were made with the aid of absolute value correlation spectroscopy (COSY) experiments. Inverse  $^{13}\text{C}$ - $\{^1\text{H}\}$  heteronuclear correlation (HETCOR) spectra formed the basis for the  $^{13}\text{C}$  NMR assignments made for non-quaternary carbon atoms. Where possible comparison with known chemical shifts allowed for the assignment of resonances arising from quaternary carbon atoms.

### 2.2.1 Synthesis and characterisation of terpyridine derivatives with an extended $\pi$ -conjugated system in the 4'-position

#### 2.2.1.1 4'-(R)-2,2':6',2''-terpyridines {R = $\beta$ -naphthyl (4'- $\beta$ Np-terpy), *m*-biphenyl (4'-*m*Biph-terpy), *p*-biphenyl (4'-*p*Biph-terpy)}

In the case of the 4'-R-substituted terpyridines an equivalent of 2-acetylpyridine was reacted with the R-aldehyde at 0 °C in ethanolic medium. The reactants underwent an Aldol condensation upon the addition of an equivalent of aqueous sodium hydroxide resulting in the precipitation of the desired enone, 1-(2'-pyridyl)-3-R-prop-2-en-1-one, as a pale yellow solid. The intermediary enone was characterized by mass spectrometry, IR and NMR spectroscopy and by elemental analysis. The IR spectrum of the enone exhibits a prominent peak at 1670  $\text{cm}^{-1}$  due to the C=O stretching vibration. The *trans* arrangement at the olefinic bond was confirmed by a  $^3J_{\text{HH}}$  coupling constant of 16.0 Hz. (A *cis* arrangement would result in a coupling constant with about half the magnitude of that of the *trans* system.)

Reaction of the enone with *N*-{1-(2'-pyridyl)-1-oxo-2-ethyl}pyridinium iodide (the enolate) in boiling ethanolic ammonium acetate resulted in an amber solution from which the desired terpyridine precipitated on cooling as a dirty white solid. The product was recrystallised from ethanol to give fine white needles (or yellow flakes in the naphthyl case) of the pure ligand (Yield: 32-61 %).

Elemental analysis was in accord with the proposed formulation. The loss of the carbonyl functionality was evidenced by the absence of prominent features in the 1602 to 1900  $\text{cm}^{-1}$  region of the IR spectrum. The fully aromatised system was manifested in an NMR spectrum that showed no resonances below  $\delta$  7.2. In all cases resonances associated with the well established terpyridine system<sup>38, 139</sup> appeared (Table 2.1). The downfield end of the spectrum consists of a singlet between  $\delta$  8.4 and  $\delta$  8.85 and two doublets each at  $\delta$  8.7 and  $\delta$  8.65. These signals may be assigned to  $\text{H}^{3',5'}$ ,  $\text{H}^{6,6''}$  and  $\text{H}^{3,3''}$  respectively. The multiplet at  $\sim \delta$  7.8 may be attributed to  $\text{H}^{4,4''}$ , while  $\text{H}^{5,5''}$  conspicuously (in the case of these three ligands) appears upfield at  $\sim \delta$  7.3 as a quartet of doublets. Remaining peaks can be assigned to the substituent in the 4'-position.

**Table 2.1** <sup>1</sup>H NMR chemical shifts for the 2,2':6,2''-terpyridine moiety<sup>a, b, c</sup>

	$\text{H}^{3,3''}$	$\text{H}^{4,4''}$	$\text{H}^{5,5''}$	$\text{H}^{6,6''}$	$\text{H}^{3',5'}$
terpy <sup>38</sup>	8.62	7.82	7.33	8.70	8.46, m
4'-Ph-terpy <sup>139</sup>	8.68	7.89	7.35	8.71	8.75, s
4'- $\beta$ Np-terpy	8.68	7.86	7.34	8.74	8.85, s
4'- <i>m</i> Biph-terpy	8.65	7.83	7.30	8.71	8.77, s
4'- <i>p</i> Biph-terpy	8.66	7.84	7.32	8.72	8.78, s

<sup>(a)</sup> Protons numbered according to Figure 2.2

<sup>(b)</sup> Shifts measured relative to TMS as internal standard in  $\text{CDCl}_3$ , ( $\delta$ ), ppm.

<sup>(c)</sup> s = singlet

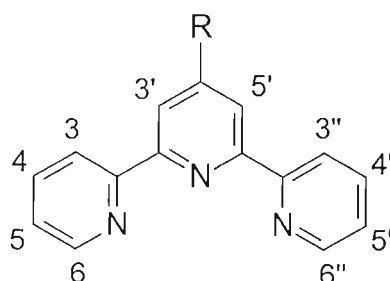


**Figure 2.2** Terpyridine moiety showing numbering scheme used.

Note that synthesis and characterisation of the *para*-biphenyl-substituted ligand, 4'-*p*BiPh-terpy, has subsequently been reported by Hannon *et al.*<sup>142</sup> The synthetic approach and characterisation agree completely with the work presented here.

### 2.2.1.2 4-R-6-phenyl-2,2'-bipyridines {R = $\beta$ -naphthyl (H4- $\beta$ Np-phbipy), *p*-biphenyl (H4-*p*Biph-phbipy)}

The Kröhnke-type synthesis was slightly modified for the synthesis of the desired ligands. The phenyl ring is introduced by incorporating the phenyl functionality into the enone (as opposed to the enolate as implemented recently by Campagna *et al.*<sup>107</sup>). The enone therefore takes the form 1-(phenyl)-3-R-prop-2-en-1-one and is synthesized as a pale yellow solid by Aldol condensation of acetophenone with the properly substituted aldehyde. Yields in excess of 70 % were obtained. The enones were recrystallised from ethanol with 1-(phenyl)-3-( $\beta$ -naphthyl)-prop-2-en-1-one isolated as a pale yellow powder in this step (Yield: 84 %). The *p*-biphenyl substituted enone forms large pale yellow needle-like crystals in 55 % yield.

Characterisation of the product by means of elemental analysis, <sup>1</sup>H NMR, IR spectroscopy and mass spectrometry confirmed it to be the desired enone. The mass spectrum shows a molecular ion peak (M<sup>+</sup>) in the case of both enones, the carbonyl functionality being evident as a distinctive peak in the IR spectrum at ~ 1660 cm<sup>-1</sup>. The *E*-configuration of the vinylic protons results in a characteristic <sup>3</sup>J<sub>HH</sub> coupling constant of ~ 16 Hz.

The ligand was obtained by refluxing the enone with *N*-{1-(2'-pyridyl)-1-oxo-2-ethyl}pyridinium iodide in absolute ethanol in the presence of a vast excess of ammonium acetate, and was isolated by allowing it to precipitate from the dark brown mixture on cooling. Ammonia was given off during the refluxing stage. The product was recrystallised from ethanol as pale yellow hairy crystals (Yield: 31 - 60 %).

Although it was not possible to obtain a mass spectrum of the product, the results of the elemental analysis are in agreement with the proposed structure. The IR spectrum shows no evidence of a carbonyl stretching band between 1600 and 1900 cm<sup>-1</sup> in accord with the cyclisation required for the successful synthesis of the ligand.

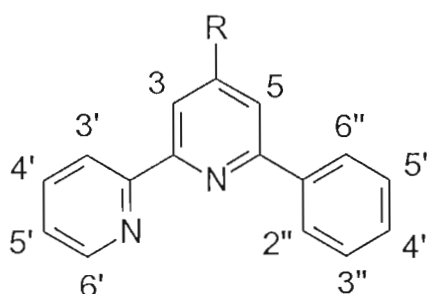
Evidence for complete aromatisation is the total absence of <sup>1</sup>H NMR signals upfield of  $\delta$  7.2. Proton resonances from the potentially *C,N,N*-orthometallating phenyl-bipyridine binding domain closely correspond to assignments made for related compounds<sup>111, 143</sup> (Table 2.2).

**Table 2.2** <sup>1</sup>H NMR shifts for the 6-phenyl-2,2'-bipyridine moiety<sup>a, b</sup>

	H <sup>3</sup>	H <sup>5</sup>	H <sup>3'</sup>	H <sup>4'</sup>	H <sup>5'</sup>	H <sup>6'</sup>	H <sup>2'',6''</sup>	H <sup>3'',5'',4''</sup>
phbipy <sup>143</sup>	8.36	7.79	8.63	7.85	7.32	8.69	8.14	7.55
4-Ph-phbipy <sup>111</sup>	8.64	7.98	8.66	7.82	7.31	8.68	8.20	7.53 - 7.49
H4-βNp-phbipy	8.77	8.09	8.71	7.86	7.33	8.74	8.24	7.53
H4-pBiph-phbipy	8.69	8.02	8.69	7.86	7.29	8.72	8.21	7.51

<sup>(a)</sup> Protons numbered according to Figure 2.3

<sup>(b)</sup> Shifts measured relative to TMS as internal standard in CDCl<sub>3</sub>, (δ), ppm.

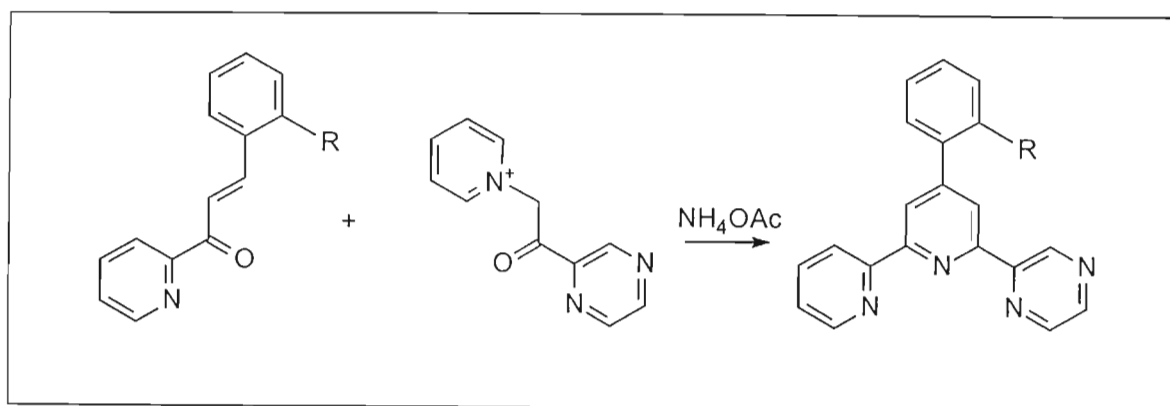
**Figure 2.3** Phenyl-bipyridine moiety showing numbering scheme used.

Peaks due to H<sup>3</sup>, H<sup>3'</sup> and H<sup>6'</sup> are concentrated in the δ 8.36 - δ 8.77 region of the spectrum and can be distinguished by performing a COSY experiment. The H<sup>2''</sup> and H<sup>6''</sup> protons afford a distinctive doublet of doublets between δ 8.14 and δ 8.24. The H<sup>5</sup> signal also occurs as an obvious doublet but at δ 8.0. In close resemblance to the H<sup>4,4''</sup> and H<sup>5,5''</sup> resonances of terpyridine (*vide supra*), the H<sup>4'</sup> and H<sup>5'</sup> resonances appear at ~ δ 7.85 and ~ δ 7.30 respectively, as expected, with half the integral seen on the terpyridine spectrum. Amongst the mass of peaks between δ 7.3 and δ 7.9, the COSY experiment can distinguish the remaining *meta*- and *para*-proton (H<sup>3'',4'',5''</sup>) resonances of the phenyl moiety, usually at approximately δ 7.52. The group in the 4'-position accounts for the remaining resonances.

## 2.2.2 Synthesis and characterisation of terpyridine analogues incorporating the pyrazine functionality

### 2.2.2.1 4-(2'''-R-phenyl)-6-(2''-pyrazinyl)-bipyridines {R = H (4-Ph-pzbipy), CH<sub>3</sub> (4-*o*MePh-pzbipy), CF<sub>3</sub> (4-*o*CF<sub>3</sub>Ph-pzbipy)}

In order to assemble the desired 6-(2''-pyrazinyl)-bipyridine the Kröhnke method was further extended to allow for the incorporation of the pyrazine ring. The pyrazine functionality was introduced *via* the enolate with the synthesis of *N*-{1-pyrazinyl-1-oxo-2-ethyl}pyridinium iodide (PZPI) by adaptation of the method for the assembly of the well known *N*-{1-(2'-pyridyl)-1-oxo-2-ethyl}pyridinium iodide.<sup>131</sup> For the synthesis of the enones, [1-(2'-pyridyl)-3-(2''-R-phenyl)-prop-2-en-1-one (R = H, CH<sub>3</sub>, CF<sub>3</sub>)], special care was taken to ensure that it was not possible for 2:1 addition to take place (as illustrated in Scheme 2.2). This product would react preferentially from this step forward resulting in a progressive buildup of undesirable terpyridyl adducts with each subsequent reaction step. Thus in the synthesis of [1-(2'-pyridyl)-3-phenyl-prop-2-en-1-one] four equivalents of aldehyde were reacted with acetylpyridine with much reduced reaction times, thereby ensuring kinetic control. The method of Summerton proved satisfactory in the formation of the other two enones.<sup>111</sup> The pure enones were refluxed with PZPI in ethanolic ammonium acetate for 90 minutes (25 minutes in the R = CH<sub>3</sub> case). The desired heterocycle precipitated from the dark amber solution as a cream coloured solid. Recrystallisation of the impure material from ethanol produced pale yellow brown blocks (Yield: 21 - 43 %). The overall reaction is illustrated in Scheme 2.4.



**Scheme 2.4** Synthetic route to pyrazinyl-bipyridine derivatives.

Elemental analysis for C, H and N was consistent with the proposed formulation of each ligand, as is the appearance of a molecular ion peak ( $M^+$ ) in the mass spectrum of the ligands. The absence of any peaks between 1610 and 1900  $\text{cm}^{-1}$  in the IR spectrum confirms the loss of the carbonyl groups and the complete reaction of the enone.

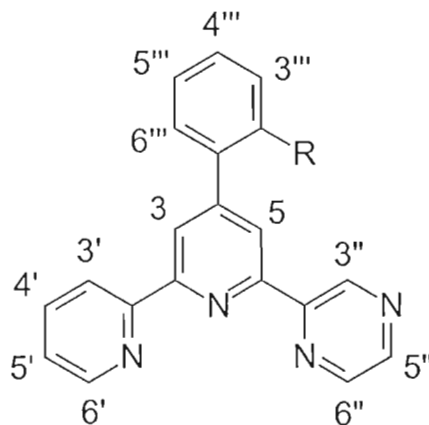


**Figure 2.4** Pyrazinyl-bipyridine moiety showing numbering scheme used.

The  $^1\text{H}$  NMR spectrum of **4-*o*MePh-pz**bipy** shows a singlet at  $\delta$  2.34 attributable to the protons of the methyl group in the *ortho* position of the phenyl ring. No further peaks below  $\delta$  7.2 for all three spectra confirms the complete aromaticity expected for the remaining parts of the molecule. The presence of the pyrazine ring results in a fairly distinctive set of resonances. The downfield region shows a lone finely split singlet at  $\delta$  9.86 due to  $\text{H}^{3''}$  which is far more deshielded than any other proton of the compound. The signal with the nearest chemical shift only occurs in the region between  $\delta$  8.64 and  $\delta$  8.71 and is assigned to  $\text{H}^{6'}$  and  $\text{H}^{3'}$ . The resonances due to the  $\text{H}^{5''}$  and  $\text{H}^{6''}$  protons are distinguishable as an intense signal between  $\delta$  8.57 and  $\delta$  8.62 while the  $\text{H}^3$  and  $\text{H}^5$  resonances are each found as a doublet ( $^4J_{\text{HH}} \sim 1.6$  Hz) between  $\delta$  8.39 and  $\delta$  8.78. The resonances below  $\delta$  8.0 can be assigned to the remaining protons of the structure.**

Drew *et al.* have synthesized a similar asymmetric pyrazinyl-bipyridyl ligand in the form of 4-(*para*-heptyloxyphenyl)-6-pyrazinyl-2,2'-bipyridine.<sup>144</sup> The Kröhnke method was also used, but unlike the approach used to synthesize ligands in this work, the pyrazine functionality was incorporated into the enone and the ligand assembled by the reaction of 1-(2'-pyridyl)-3-(*para*-heptyloxyphenyl)-prop-2-en-1-one with *N*-{1-(2'-pyridyl)-1-oxo-2-ethyl}pyridinium iodide

in the presence of ammonium acetate.<sup>144</sup>

#### 2.2.2.2 4-phenyl-2,6-bis(2'-pyrazinyl)-pyridine (4-Ph-pybipz)

An unorthodox method was used to synthesize the bis-pyrazine substituted ligand. As it is a symmetric molecule the initial strategy focussed on attempts to assemble the 1,5-dione in a similar way to that employed by Constable *et al.* for the synthesis of the similarly symmetrical 4'-phenyl-2,2':6',2''-terpyridine.<sup>138</sup> Thus two equivalents of acetylpyrazine were reacted with one equivalent of benzaldehyde in the presence of an equivalent of base. The reaction was carried out at ambient temperatures and left to stir overnight. Upon workup the reaction produced a white powder which could not be identified. Despite this workup the white powder still appeared to consist of a mixture of compounds from NMR spectral evidence.

However, analysis by GC/MS revealed only one product with a molecular ion ( $M^+$ ) peak of  $m/z$  310 corresponding to the mass of 1-pyrazinyl-3-phenyl-prop-2-en-1-one. This suggests that each mole of benzaldehyde reacts with only one mole of acetylpyrazine to yield the enone. On the other hand, it is also possible that thermal retro-reactions during the mass spectrometry experiment reduced the desired 1,5-dione to the enone. Assignment is therefore not concrete.

The white solid has a prominent C=O stretching band at  $1684\text{ cm}^{-1}$  in its IR spectrum. At this wavelength it falls between the characteristic carbonyl stretches of the enone and dione which generally have IR absorbances at  $\sim 1665$  and  $\sim 1698\text{ cm}^{-1}$  respectively. The IR spectrum is therefore also inconclusive.

The  $^1\text{H}$  NMR spectrum shows numerous resonances ranging from  $\delta$  1.0 to  $\delta$  10.0. Multiplets at  $\delta$  3.5 and  $\delta$  5.4 resemble the signals one would expect for the methine and methylene protons of the dione. On this basis the white powder was treated accordingly and refluxed overnight in the presence of an excess ammonium acetate. (This was done in a manner analogous to the method of reference 134.) This procedure had very little effect, with the white powder recovered largely unaltered. The  $^1\text{H}$  NMR spectrum clearly shows resonances associated with the successful formation of the ligand, but in very small amounts. As a result, the white powder as well as attempts to synthesize the ligand *via* the dione intermediate were



temporarily abandoned.

It was decided to adopt a similar approach to that used to synthesise the *mono*-pyrazinyl ligands described in section 2.2.2.1 (*vide supra*) *i.e.*, by synthesizing an enone intermediate to react with PZPI for the formation of the ligand. The enone was prepared by reacting benzaldehyde with a single equivalent of acetylpyrazine in the presence of sodium hydroxide at 0 °C over the course of three hours. (Leaving the mixture to react overnight produces the same white powder described above.) Unfortunately the enone forms as a sticky solid which is difficult to purify and impossible to work with. Thus the physical properties of the enone rendered the method unviable.

As a last resort the white powder described above was treated as if it were the enone. As such it was refluxed with PZPI in the presence of an excess of ammonium acetate. Quite contrary to expectations the reaction produced a brown microcrystalline solid (after recrystallisation) which, upon analysis, proved to be the required ligand. Note that the method finally employed consistently affords the ligand in yields of about 25 %.

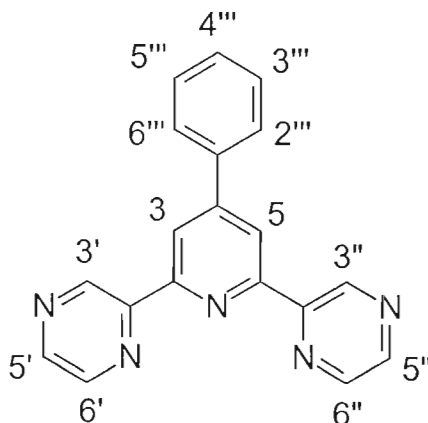


**Figure 2.5** 4-phenyl-2,6-bis(2'-pyrazinyl)-pyridine (4-Ph-pybipz) showing numbering scheme used.

The successful formation of the ligand (4-Ph-pybipz), in 24 % yield, is confirmed by GC/MS, showing a molecular ion ( $M^+$ ) of  $m/z$  311. Elemental analysis agreed with the formulation of the ligand and the IR spectrum confirmed the loss of the carbonyl functionality. The  $^1H$  NMR

spectrum only showed signals in the aromatic region of the spectrum. The H<sup>3',3''</sup> resonances are again evident as a split singlet ( $^4J_{\text{HH}}$  0.91 Hz) far downfield at  $\delta$  9.85. The magnetically equivalent protons of the pyridyl ring (H<sup>3',5'</sup>) have a singlet resonance at  $\delta$  8.71. Interestingly the remaining pyrazinyl protons (H<sup>5',5'',6',6''</sup>) appear as a single signal in CDCl<sub>3</sub> solution at  $\delta$  8.64. However, when deuterated benzene is the solvent, the signals of H<sup>5',5''</sup> and H<sup>6',6''</sup> appear as separate signals at  $\delta$  8.08 and  $\delta$  8.20 respectively. The remaining resonances between  $\delta$  7.4 and  $\delta$  7.9 are attributed to the phenyl protons.

## 2.3 EXPERIMENTAL

All reactions were carried out in air. Acetophenone was purchased from Riedel de Haen, while benzaldehyde, *o*-tolualdehyde, and  $\alpha,\alpha,\alpha$ -trifluorotolualdehyde (*o*) were obtained from Aldrich. These chemicals were all purified by distillation. Ammonium acetate was dried in a vacuum desiccator over  $P_2O_5$  for several days prior to use. *m*-Biphenylcarboxaldehyde was prepared from *m*-bromobiphenyl by literature methods.<sup>145</sup> The ligand precursors [1-(2'-pyridyl)-3-(2''-R-phenyl)-prop-2-en-1-one (R = CH<sub>3</sub>, CF<sub>3</sub>)]<sup>111</sup> and *N*-{1-(2'-pyridyl)-1-oxo-2-ethyl}pyridinium iodide<sup>131</sup> were also synthesised by methods taken from the literature, while acetylpyrazine, 2-acetylpyridine, *p*-biphenylcarboxaldehyde and  $\beta$ -naphthaldehyde were used as supplied (Aldrich).

### 2.3.1 4'-(R)-2,2':6',2''-terpyridines {R = $\beta$ -naphthyl (4'- $\beta$ Np-terpy), *m*-biphenyl (4'-*m*Biph-terpy), *p*-biphenyl (4'-*p*Biph-terpy)}

#### 2.3.1.1 Synthesis of 1-(2''-pyridyl)-3-R-prop-2-en-1-one

A mixture of 2-acetylpyridine (2.42 g, 20 mmol) and  $\beta$ -naphthaldehyde (or R-carboxaldehyde) (20 mmol) in absolute ethanol (100 ml) was cooled to 0 °C. Sodium hydroxide (20 ml, 1.0 M) was added dropwise and the reaction mixture stirred at 0 °C for 3 hours. The pale yellow product was precipitated with ice-water, filtered, washed with 50 % aqueous ethanol and dried *in vacuo*.

1-(2''-pyridyl)-3-( $\beta$ -naphthyl)-prop-2-en-1-one: Yield 4.72 g (91 %), m.p. 143 - 145 °C. GC/MS: *m/z* 259 (M<sup>+</sup>). (Found: C, 83.1; H, 5.1; N, 5.3. Calc. for C<sub>18</sub>H<sub>13</sub>NO: C, 83.4; H, 5.1; N, 5.4 %). IR  $\nu$  (CO) 1670 cm<sup>-1</sup>. <sup>1</sup>H NMR (CDCl<sub>3</sub>)  $\delta$  8.40(1H, AB, <sup>3</sup>J<sub>HH</sub> 16.0 Hz, CHAr) 8.08(1H, AB, <sup>3</sup>J<sub>HH</sub> 16.0 Hz, CHCO).

1-(2''-pyridyl)-3-(*m*-biphenyl)-prop-2-en-1-one: Yield 4.62 g (81 %), m.p. 122 - 125 °C. GC/MS: *m/z* 285 (M<sup>+</sup>). IR  $\nu$  (CO) 1672 cm<sup>-1</sup>. <sup>1</sup>H NMR (CDCl<sub>3</sub>)  $\delta$  8.37(1H, AB, <sup>3</sup>J<sub>HH</sub> 16.0 Hz, CHAr) 8.00(1H, AB, <sup>3</sup>J<sub>HH</sub> 16.0 Hz, CHCO).

1-(2''-pyridyl)-3-(*p*-biphenyl)-prop-2-en-1-one: Yield 4.79 g (84 %), m.p. 127 - 130 °C. GC/MS: *m/z* 285 (M<sup>+</sup>). (Found: C, 84.0; H, 5.2; N, 4.8. Calc. for C<sub>20</sub>H<sub>15</sub>NO: C, 84.2; H, 5.3; N, 4.9 %). IR  $\nu$  (CO) 1666 cm<sup>-1</sup>. <sup>1</sup>H NMR (CDCl<sub>3</sub>)  $\delta$  8.35(1H, AB, <sup>3</sup>J<sub>HH</sub> 16.0 Hz, CHAr) 7.63(1H, AB, <sup>3</sup>J<sub>HH</sub> 16.0 Hz, CHCO).

### 2.3.1.2 Synthesis of 4'-(R)-2,2':6',2''-terpyridines {R = $\beta$ -naphthyl (4'- $\beta$ Np-terpy), *m*-biphenyl (4'-*m*Biph-terpy), *p*-biphenyl (4'-*p*Biph-terpy)}

A mixture of 1-(2''-pyridyl)-3-R-prop-2-en-1-one (2.0 mmol), *N*-{1-(2'-pyridyl)-1-oxo-2-ethyl}pyridinium iodide (0.72 g, 2.2 mmol) and ammonium acetate (10 g, excess) was heated to reflux in absolute ethanol (8 ml). After 70 minutes the mixture was allowed to cool. The resultant precipitate was filtered and washed with 50 % aqueous ethanol on the same day. The impure product was then carefully washed with ethanol (95 %), leaving a white solid (pale yellow in the naphthyl substituted case) on the frit. The product was recrystallised from ethanol (95 %) and dried *in vacuo*. The naphthyl substituted ligand forms pale yellow flakes while the biphenyl substituted ligands form fine pale yellow-white needles.

4'-( $\beta$ -naphthyl)-2,2':6',2''-terpyridine (4'- $\beta$ Np-terpy): Yield 0.44 g (61 %), m.p. 209 - 211 °C. (Found: C, 83.7; H, 4.6; N, 12.0. Calc. for C<sub>25</sub>H<sub>17</sub>N<sub>3</sub>: C, 83.5; H, 4.8; N, 11.7 %).

Spectroscopic data for 4'- $\beta$ Np-terpy	
<sup>1</sup> H NMR (CDCl <sub>3</sub> )	8.85(2H, s, H <sup>3',5'</sup> ) 8.74(2H, m, H <sup>6',6''</sup> ) 8.68(2H, m, H <sup>3',3''</sup> ) 8.39(1H, br s, naphthyl H) 8.10 - 7.92(4H, m, naphthyl H's) 7.86(2H, td, H <sup>4,4''</sup> ) 7.52(2H, m, naphthyl H's) 7.34(2H, qd, H <sup>5,5''</sup> )
<sup>13</sup> C NMR (CDCl <sub>3</sub> )	155.9 - 156.3(4C, ds, C <sup>2,2',6',2''</sup> ) 150.2(1C, s, C <sup>4'</sup> ) 149.2(2C, s, C <sup>6,6''</sup> ) 136.9(2C, s, C <sup>4,4''</sup> ) 133.5 - 136.9(3C, ts, naphthyl quat. C's) 128.6(2C, ds, naphthyl CH's) 127.6(1C, s, naphthyl CH's) 126.6(2C, ds, naphthyl CH's) 126.4(1C, s, naphthyl CH) 125.0(1C, s, naphthyl CH) 123.8(2C, s, C <sup>5,5''</sup> ) 121.4(2C, s, C <sup>3,3''</sup> ) 119.0(2C, s, C <sup>3',5'</sup> )

IR	776(w) 733(m) 756(m) 791(m) 825(m) 870(m) 1442(m) 1466(m) 1542(m) 1560(s) 1586(s) 1599(w)
UV/vis (MeCN)	256, 267sh, 281 ( $\pi$ - $\pi^*$ )

4'-(*m*-biphenyl)-2,2':6',2''-terpyridine (**4'-*m*Biph-terpy**): Yield 0.25 g (32 %), m.p. 171 - 173 °C. (Found: C, 83.9; H, 4.9; N, 10.8. Calc. for C<sub>27</sub>H<sub>19</sub>N<sub>3</sub>: C, 84.1; H, 5.0; N, 10.9 %).

Spectroscopic data for 4'- <i>m</i> Biph-terpy	
<sup>1</sup> H NMR (CDCl <sub>3</sub> )	8.77(2H, s, H <sup>3',5'</sup> ) 8.71(2H, m, H <sup>6,6''</sup> ) 8.65(2H, m, H <sup>3,3''</sup> ) 8.07(1H, t, H <sup>2''</sup> ) 7.85 and 7.66(2H, m's, H <sup>4'',6''</sup> ) 7.83(2H, m, H <sup>4,4''</sup> ) 7.65(2H, m, H <sup>2''',6'''</sup> ) 7.54(1H, m, H <sup>5''</sup> ) 7.46(2H, m, H <sup>3''',5'''</sup> ) 7.38(1H, m, H <sup>4'''</sup> ) 7.30(2H, qd, H <sup>5,5''</sup> )
<sup>13</sup> C NMR (CDCl <sub>3</sub> )	155.9 - 156.1(4C, ds, C <sup>2,2',6',2''</sup> quat. C's) 150.2(1C, s, C <sup>4'</sup> ) 149.0(2C, s, C <sup>6,6''</sup> ) 139.0 - 142.0(3C, ts, phenyl quat. C's) 136.8(2C, s, C <sup>4,4''</sup> ) 129.3 and 127.5(2C, ds, C <sup>4''',6'''</sup> ) 128.7(2C, s, C <sup>2''',6'''</sup> ) 127.8(1C, s, C <sup>4'''</sup> ) 127.3(2C, s, C <sup>3''',5'''</sup> ) 126.2(1C, s, C <sup>5''</sup> ) 126.0(1C, s, C <sup>2''</sup> ) 123.7(2C, s, C <sup>5,5''</sup> ) 121.3(2C, s, C <sup>3,3''</sup> ) 118.9(2C, s, C <sup>3',5'</sup> )
IR	618(w) 660(w) 698(m) 733(m) 760(s) 789(s) 878(w) 1441(w) 1468(m) 1543(m) 1562(s) 1582(s) 1599(w)
UV/vis (MeCN)	252, 274sh, 319sh ( $\pi$ - $\pi^*$ )

4'-(*p*-biphenyl)-2,2':6',2''-terpyridine (**4'-*p*Biph-terpy**): Yield 0.29 g (38 %), m.p. 200 - 202 °C. (Found: C, 84.3; H, 4.9; N, 10.9. Calc. for C<sub>27</sub>H<sub>19</sub>N<sub>3</sub>: C, 84.1; H, 5.0; N, 10.9 %).

Spectroscopic data for 4'- <i>p</i> Biph-terpy	
<sup>1</sup> H NMR (CDCl <sub>3</sub> )	8.78(2H, s, H <sup>3',5'</sup> ) 8.72(2H, m, H <sup>6,6''</sup> ) 8.66(2H, m, H <sup>3,3''</sup> ) 7.97 and 7.71(4H, m, H <sup>2'',3'',5'',6''</sup> ) 7.84(2H, td, H <sup>4,4''</sup> ) 7.65(2H, m, H <sup>3''',5'''</sup> ) 7.44(2H, m, H <sup>2''',6'''</sup> ) 7.39(1H, m, H <sup>4'''</sup> ) 7.32(2H, qd, H <sup>5,5''</sup> )
<sup>13</sup> C NMR (CDCl <sub>3</sub> )	156.4 - 156.8(4C, ds, C <sup>2,2',6',2''</sup> quat. C's) 150.2(1C, s, C <sup>4'</sup> quat. C) 149.7(2C, s, C <sup>6,6''</sup> ) 137.5 - 142.3(3C, ts, phenyl quat. C's) 137.4, (2C, s, C <sup>4,4''</sup> ) 129.4(2C, s, C <sup>2''',6'''</sup> ) 128.2 and 128.1(4C, ds, C <sup>2'',3'',5'',6''</sup> ) 128.17(1C, s, C <sup>4'''</sup> ) 127.7(2C, s, C <sup>3''',5'''</sup> ) 124.4(2C, s, C <sup>5,5''</sup> ) 121.9(2C, s, C <sup>3,3''</sup> ) 119.2(2C, s, C <sup>3',5'</sup> )
IR	682(w) 738(w) 764(s) 789(m) 1443(m) 1472(s) 1489(w) 1544(m) 1560(s) 1582(s) 1601(w)
UV/vis (MeCN)	255sh, 288 (π-π*)

### 2.3.2 4-R-6-phenyl-2,2'-bipyridine {R = β-naphthyl (H4-βNp-phbipy), *p*-biphenyl (H4-*p*Biph-phbipy)}

#### 2.3.2.1 Synthesis of 1-(phenyl)-3-R-prop-2-en-1-one

A suspension of R-carboxaldehyde (20 mmol) in absolute ethanol (50 ml) was cooled to 0 °C. Acetophenone (2.40 g, 20 mmol) was diluted in ethanol (10 ml) and added to the cooled mixture. After stirring for 2 minutes at 0 °C, sodium hydroxide (20 ml, 1.0 M) was added dropwise and the mixture allowed to stir for a further 3 hours at 0 °C. Once stirring was complete the product was precipitated from the solution by the addition of large quantities of ice-water. The pale yellow product was filtered and thoroughly washed on the frit with 50 % aqueous ethanol. The 1-(phenyl)-3-(β-naphthyl)-prop-2-en-1-one was isolated as a pale yellow

powder. Repeated recrystallisation from 80 % aqueous ethanol gave 1-(phenyl)-3-(*p*-biphenyl)-prop-2-en-1-one as large flat yellow needles. The enones were then dried *in vacuo*.

1-(phenyl)-3-( $\beta$ -naphthyl)-prop-2-en-1-one: Yield 4.34 g (84 %), m.p. 162 - 164 °C. GC/MS:  $m/z$  258 ( $M^+$ ). IR  $\nu$  (CO) 1661  $\text{cm}^{-1}$ .  $^1\text{H NMR}$  ( $\text{CDCl}_3$ )  $\delta$  7.97(1H, AB,  $^3J_{\text{HH}}$  15.7 Hz, CHCO) 7.63(1H, AB,  $^3J_{\text{HH}}$  15.7 Hz, CHAr).

1-(phenyl)-3-(*p*-biphenyl)-prop-2-en-1-one: Yield 3.13 g (55 %), m.p. 113 - 114 °C. GC/MS:  $m/z$  284 ( $M^+$ ). (Found: C, 89.0; H, 5.5; N, 0.0. Calc. for  $\text{C}_{21}\text{H}_{16}\text{O}$ : C, 88.7; H, 5.7; N, 0.0 %). IR  $\nu$  (CO) 1664  $\text{cm}^{-1}$ .  $^1\text{H NMR}$  ( $\text{CDCl}_3$ )  $\delta$  7.85(1H, AB,  $^3J_{\text{HH}}$  15.7 Hz, CHCO) 7.56(1H, AB,  $^3J_{\text{HH}}$  15.7 Hz, CHAr).

### 2.3.2.2 Synthesis of 4-R-6-phenyl-2,2'-bipyridine {R = $\beta$ -naphthyl (H4- $\beta$ Np-phbipy), *p*-biphenyl (H4-*p*Biph-phbipy)}

The ligand precursors 1-phenyl-3-R-prop-2-en-1-one (2.0 mmol) and *N*-{1-(2'-pyridyl)-1-oxo-2-ethyl}pyridinium iodide (0.72 g, 2.2 mmol) were added to a 100 ml round bottom flask. Ammonium acetate (10 g, excess) and absolute ethanol (8 ml) were added, the mixture heated to reflux for 60 minutes (90 minutes in the biphenyl case) and allowed to cool. The ligand precipitated from the amber reaction mixture upon cooling as a dirty white solid which was filtered off and washed on the frit with 50 % aqueous ethanol. The impure ligand was recrystallised from ethanol (95 %) to give a pale yellow powder. The biphenyl substituted ligand (H4-*p*Biph-phbipy) forms as fine pale yellow needles.

4-( $\beta$ -naphthyl)-6-phenyl-2,2'-bipyridine (H4- $\beta$ Np-phbipy): Yield 0.22 g (31 %), m.p. 153 - 155 °C. (Found: C, 87.1; H, 4.9; N, 7.8. Calc. for  $\text{C}_{26}\text{H}_{18}\text{N}_2$ : C, 87.1; H, 5.1; N, 7.8 %).

Spectroscopic data for H4-βNp-phbipy	
<sup>1</sup> H NMR (CDCl <sub>3</sub> )	8.77(1H, d, H <sup>3</sup> ) 8.74(1H, m, H <sup>6</sup> ) 8.71(1H, m, H <sup>3</sup> ) 8.29(1H, m, naphthyl H) 8.24(2H, m, H <sup>2",6"</sup> ) 8.09(1H, d, H <sup>5</sup> ) 7.84 - 8.00(4H, m, naphthyl H's) 7.86(1H, m, H <sup>4</sup> ) 7.53 (3H, m, phenyl H's) 7.58 - 7.46(2H, m, naphthyl H's) 7.33(1H, qd, H <sup>5</sup> )
<sup>13</sup> C NMR (CDCl <sub>3</sub> )	150.0 - 157.1(4C, qs, pyridyl quat. C's) 149.0(1C, s, C <sup>6</sup> ) 139.4(1C, s, phenyl quat. C) 136.8(1C, s, C <sup>4</sup> ) 135.9(1C, s, naphthyl quat. C) 133.4(2C, ds, naphthyl quat. C's) 126.5 - 129.1(5C, ts, phenyl CH's) 124.8 - 128.7(7C, ps, naphthyl CH's) 123.8(1C, s, C <sup>5</sup> ) 121.5(1C, s, C <sup>3</sup> ) 118.6(1C, s, C <sup>5</sup> ) 117.5(1C, s, C <sup>3</sup> )
IR	610(w) 636(w) 689(m) 731(m) 764(m) 794(m) 860(m) 1398(s) 1472(m) 1497(m) 1545(s) 1581(s) 1597(s)
UV/vis (MeCN)	261, 279sh (π-π*)

4-(*p*-biphenyl)-6-phenyl-2,2'-bipyridine (**H4-*p*Biph-phbipy**): Yield 0.46 g (60 %), m.p. 183 - 184 °C. (Found: C, 87.4; H, 5.1; N, 7.2. Calc. for C<sub>28</sub>H<sub>20</sub>N<sub>2</sub>: C, 87.5; H, 5.2; N, 7.3 %).

Spectroscopic data for H4- <i>p</i> Biph-phbipy	
<sup>1</sup> H NMR (CDCl <sub>3</sub> )	8.72(1H, m, H <sup>6</sup> ) 8.69(1H, d, H <sup>3</sup> ) 8.69(1H, m, H <sup>3</sup> ) 8.21(2H, m, H <sup>2",6"</sup> ) 8.02(1H, d, H <sup>5</sup> ) 7.91(2H, m, H <sup>2",6"</sup> ) 7.86(1H, m, H <sup>4</sup> ) 7.74(2H, m, H <sup>3",5"</sup> ) 7.35 - 7.55(8H, m, terminal phenyl H's) 7.29(1H, qd, H <sup>5</sup> )
<sup>13</sup> C NMR (CDCl <sub>3</sub> )	149.7 - 157.2(4C, qs, pyridyl quat. C's) 149.1(1C, s, C <sup>4</sup> ) 137.5 - 141.9(4C, qs, phenyl quat. C's) 136.9(1C, s, C <sup>4</sup> ) 127.1 - 129.5(8C, m, terminal phenyl CH's) 127.7(4C, ds, C <sup>2",3",5",6"</sup> ) 127.1(2C, s, C <sup>2",6"</sup> ) 123.8(1C, s, C <sup>5</sup> ) 121.5(1C, s, C <sup>3</sup> ) 118.3(1C, s, C <sup>5</sup> ) 117.3(1C, s, C <sup>3</sup> )



IR	628(w) 640(w) 687(m) 731(m) 764(s) 793(m) 838(w) 1382(m) 1477(m) 1541(m) 1563(s) 1584(s) 1599(m)
UV/vis (MeCN)	290 ( $\pi$ - $\pi^*$ )

### 2.3.3 4-(2'''-R-phenyl)-6-(2''-pyrazinyl)-bipyridines {R = H (4-Ph-pzbipy), CH<sub>3</sub> (4-*o*MePh-pzbipy), CF<sub>3</sub> (4-*o*CF<sub>3</sub>Ph-pzbipy)}

#### 2.3.3.1 Synthesis of 1-(2'-pyridyl)-3-phenyl-prop-2-en-1-one

Benzaldehyde (2.12 g, 20 mmol) and 2-acetylpyridine (2.42 g, 20 mmol) were dissolved in absolute ethanol (60 ml) and the solution cooled to 0 °C. Sodium hydroxide (20 ml, 1.0 M) was added dropwise with stirring. The mixture was stirred for a further 25 minutes and the product precipitated with large quantities of ice-water. The resultant pale yellow solid was filtered, washed on the frit with 80 % aqueous ethanol and dried *in vacuo*.

1-(2'-pyridyl)-3-phenyl-prop-2-en-1-one: Yield 2.41 g (58 %), m.p. 72 - 74 °C. GC/MS: *m/z* 209 (M<sup>+</sup>). IR  $\nu$  (CO) 1672 cm<sup>-1</sup>. <sup>1</sup>H NMR (CDCl<sub>3</sub>):  $\delta$  8.32 (1H, AB, <sup>3</sup>J<sub>HH</sub> 16.1 Hz, CHAr) 7.95(1H, AB, <sup>3</sup>J<sub>HH</sub>, 16.1 Hz, CHCO)

#### 2.3.3.2 Synthesis of 1-(2'-pyridyl)-3-(2'''-R-phenyl)-prop-2-en-1-one (R = CH<sub>3</sub>, CF<sub>3</sub>)

The ligand precursors 1-(2'-pyridyl)-3-(2'''-CH<sub>3</sub>-phenyl)-prop-2-en-1-one and 1-(2'-pyridyl)-3-(2'''-CF<sub>3</sub>-phenyl)-prop-2-en-1-one were synthesized from methods taken from the literature.<sup>111</sup>

#### 2.3.3.3 Synthesis of *N*-{1-pyrazinyl-1-oxo-2-ethyl}pyridinium iodide (PZPI)

Acetylpyrazine (4.76 g, 39 mmol) was added to a suspension of iodine (5.0 g, 39 mmol) in pyridine (15 ml). The mixture was refluxed for 90 minutes, allowed to cool, and the black precipitate filtered off, washed with a small amount of cold pyridine and dried *in vacuo*. The crude product was purified by refluxing in a minimum volume of ethanol in the presence of

deactivated charcoal (*ca.* 1-2% by weight) and filtered through Celite®. The desired product precipitated as golden flakes upon cooling.

*N*-{1-pyrazinyl-1-oxo-2-ethyl}pyridinium iodide (PZPI): Yield 6.12 g (48 %), IR  $\nu(\text{CO})$  1705  $\text{cm}^{-1}$ . (Found: C, 40.1; H, 2.9; N, 12.7. Calc. for  $\text{C}_{11}\text{H}_{10}\text{N}_3\text{OI}$ : C, 40.4; H, 3.1; N, 12.8 %).

#### 2.3.3.4 Synthesis of 4-(2'''-R-phenyl)-6-(2''-pyrazinyl)-2,2'-bipyridines {R = H (4-Ph-pzbipy), CH<sub>3</sub> (4-*o*MePh-pzbipy), CF<sub>3</sub> (4-*o*CF<sub>3</sub>Ph-pzbipy)}

Ammonium acetate (10 g, excess) was added to a suspension of 1-(2'-pyridyl)-3-(2''-R-phenyl)-prop-2-en-1-one (2.0 mmol) and *N*-{1-pyrazinyl-1-oxo-2-ethyl}pyridinium iodide (0.72 g, 2.2 mmol) in absolute ethanol (8 ml). The mixture was heated to reflux for 90 minutes (25 minutes in the R = CH<sub>3</sub> case) and allowed to cool. The impure ligand precipitated as a dirty white solid which was crystallised from ethanol (95 %) to produce off-white blocks of analytically pure ligand which was dried *in vacuo*.

4-phenyl-6-(2''-pyrazinyl)-2,2'-bipyridine (**4-Ph-pzbipy**): Yield 0.27 g (43 %), m.p. 217 - 219 °C. GC/MS:  $m/z$  310 ( $\text{M}^+$ ). (Found: C, 77.6; H, 4.4; N, 17.7. Calc. for  $\text{C}_{20}\text{H}_{14}\text{N}_4$ : C, 77.4; H, 4.5; N, 18.1 %).

Spectroscopic data for 4-Ph-pzbipy	
<sup>1</sup> H NMR (CDCl <sub>3</sub> )	9.86(1H, d, H <sup>3''</sup> ) 8.78(1H, d, H <sup>5'</sup> ) 8.71(1H, m, H <sup>6'</sup> ) 8.66(1H, m, H <sup>3</sup> ) 8.65(1H, m, H <sup>3'</sup> ) 8.62(2H, m, H <sup>5'',6''</sup> ) 7.81 - 7.92(2H, m, phenyl H's) 7.85(1H, m, H <sup>4'</sup> ) 7.44 - 7.55(3H, m, phenyl H's) 7.35(1H, qd, H <sup>5'</sup> )
<sup>13</sup> C NMR (CDCl <sub>3</sub> )	150.5 - 156.2(5C, ps, pyridyl and pyrazinyl quat. C's) 149.1(1C, s, C <sup>6'</sup> ) 143.5 - 144.5(3C, ts, pyrazinyl CH's) 138.1(1C, s, phenyl quat. C) 137.0(1C, s, C <sup>4'</sup> ) 127.2 - 129.3(5C, ts, phenyl CH's) 124.0(1C, s, C <sup>5'</sup> ) 121.4(1C, s, C <sup>3'</sup> ) 119.5(1C, s, C <sup>5'</sup> ) 119.2(1C, s, C <sup>3'</sup> )

IR	619(m) 667(w) 692(m) 737(w) 759(sh) 765(s) 793(m) 1377(s) 1441(m) 1551(s) 1567(s) 1600(w)
UV/vis (MeCN)	250, 278, 316sh ( $\pi$ - $\pi^*$ )

4-(2'''-CH<sub>3</sub>-phenyl)-6-(2''-pyrazinyl)-2,2'-bipyridine (**4-*o*MePh-pzbipy**): Yield 0.23 g (35 %), m.p. 174 - 176 °C. GC/MS: *m/z* 324 (M<sup>+</sup>). (Found: C, 77.7; H, 4.9; N, 17.2. Calc. for C<sub>21</sub>H<sub>16</sub>N<sub>4</sub>: C, 77.8; H, 5.0; N, 17.3 %).

Spectroscopic data for 4- <i>o</i> MePh-pzbipy	
<sup>1</sup> H NMR (CDCl <sub>3</sub> )	9.86(1H, d, H <sup>3''</sup> ) 8.65(1H, m, H <sup>6'</sup> ) 8.64(1H, m, H <sup>3'</sup> ) 8.57(2H, d, H <sup>5'',6''</sup> ) 8.51(1H, d, H <sup>5'</sup> ) 8.39(1H, d, H <sup>3'</sup> ) 7.84(1H, td, H <sup>4'</sup> ) 7.20 - 7.40(5H, m, H <sup>5'</sup> and phenyl H's) 2.34(3H, s, methyl H's)
<sup>13</sup> C NMR (CDCl <sub>3</sub> )	151.0 - 155.6(5C, ps, pyridyl and pyrazinyl quat. C's) 149.1(1C, s, C <sup>6'</sup> ) 144.3(1C, s, pyrazinyl CH) 143.5(2C, ss, pyrazinyl CH's) 139.1(1C, s, phenyl quat. C) 136.8(1C, s, C <sup>4'</sup> ) 135.0(1C, s, phenyl quat. C) 125.9 - 130.5(4C, qs, phenyl CH's) 123.9(1C, s, C <sup>5'</sup> ) 122.1(1C, s, C <sup>5'</sup> ) 121.8(1C, s, C <sup>3'</sup> ) 121.2(1C, s, C <sup>3'</sup> ) 20.3(1C, s, CH <sub>3</sub> )
IR	623(w) 642(w) 729(m) 740(m) 764(s) 793(w) 849(w) 1379(s) 1468(s) 1491(w) 1543(m) 1564(m) 1588(s) 1605(w)
UV/vis (MeCN)	247, 279 ( $\pi$ - $\pi^*$ )

4-(2'''-CF<sub>3</sub>-phenyl)-6-(2''-pyrazinyl)-2,2'-bipyridine (**4-*o*CF<sub>3</sub>Ph-pzbipy**): Yield 0.16 g (21 %), m.p. 298 - 301 °C. GC/MS: *m/z* 378 (M<sup>+</sup>). (Found: C, 66.9; H, 3.3; N, 14.7. Calc. for C<sub>21</sub>H<sub>13</sub>N<sub>4</sub>F<sub>3</sub>: C, 66.7; H, 3.5; N, 14.8 %).

Spectroscopic data for 4- <i>o</i> CF <sub>3</sub> Ph-pzbipy	
<sup>1</sup> H NMR (CDCl <sub>3</sub> )	9.88(1H, d, H <sup>3''</sup> ) 8.67(2H, m, H <sup>3',6'</sup> ) 8.60(2H, m, H <sup>5'',6''</sup> ) 8.40 - 8.53(2H, dm, H <sup>3,5</sup> ) 7.88(1H, m, H <sup>4'</sup> ) 7.40 - 7.85(4H, m, phenyl H's) 7.34(1H, qd, H <sup>5</sup> )
<sup>13</sup> C NMR (CDCl <sub>3</sub> )	150.0 - 155.5(5C, ps, pyridyl and pyrazinyl quat. C's) 149.2(1C, s, C <sup>6'</sup> ) 143.5 - 144.6(3C, ts, pyrazinyl CH's) 138.6{1C, s(low intensity), C <sup>1''</sup> } 137.0(1C, s, C <sup>4'</sup> ) 128.4 - 131.6(3C, ts, phenyl CH's) 128.2(1C, q, <sup>2</sup> J <sub>CF</sub> 30.6 Hz, C <sup>2''</sup> ) 126.2(1C, q, <sup>3</sup> J <sub>CF</sub> 5.3 Hz, C <sup>3''</sup> ) 124.1(1C, s, C <sup>5'</sup> ) 124.0(1C, q, <sup>1</sup> J <sub>CF</sub> 273.9 Hz, CF <sub>3</sub> ) 121.5 - 122.0(2C, ss, C <sup>3,5</sup> ) 121.4(1C, s, C <sup>3'</sup> )
IR	619(w) 672(w) 743(m) 794(m) 773(s) 854(w) 1269(m) 1313(vs) 1381(s) 1468(m) 1585(s) 1601(m)
UV/vis (MeCN)	242, 277 (π-π*)

#### 2.3.4 Synthesis of 4-phenyl-2,6-bis(2'-pyrazinyl)-pyridine (4-Ph-pybizp)

A suspension of acetylpyrazine (4.89 g, 40 mmol) in absolute ethanol (50 ml) was cooled to 0 °C. After addition of benzaldehyde (2.12 g, 20 mmol), sodium hydroxide (40 ml, 1.0 M) was added dropwise with stirring. The mixture was stirred at 0 °C for three hours and then at ambient temperature overnight. Ice-water was used to precipitate a solid from the reaction mixture. The solid was thoroughly washed on the frit with 50 % aqueous ethanol until the last trace of pink was removed from the reaction product. This left a white solid on the frit which was recrystallised from ethanol. This white solid (0.42 g) and *N*-{1-pyrazinyl-1-oxo-2-ethyl}pyridinium iodide (0.72 g, 2.2 mmol) with ammonium acetate (10 g, excess) was refluxed in a 1:1 mixture of ethanol:glacial acetic acid (10 ml). After 3 hours the reaction mixture was allowed to cool resulting in the precipitation of a dirty brown solid. The brown solid was filtered and washed with 80 % aqueous ethanol. Recrystallisation of the brown solid from ethanol (95 %) resulted in brown microcrystalline ligand which was dried *in vacuo*.

4-phenyl-2,6-bis(2'-pyrazinyl)-pyridine (**4-Ph-pybipz**): Yield 1.62 g (24 % based on PZPI), m.p. 251 - 253 °C. GC/MS:  $m/z$  311 ( $M^+$ ). (Found: C, 73.1; H, 4.1; N, 22.5. Calc. for  $C_{26}H_{18}N_2$ : C, 73.3; H, 4.2; N, 22.5 %).

Spectroscopic data for 4-Ph-pybipz	
$^1H$ NMR ( $CDCl_3$ )	9.85(2H, m, $H^{3,3'}$ ) 8.71(2H, s, $H^{3,5}$ ) 8.64(4H, m, $H^{5',5'';6,6''}$ ) 7.82 - 7.88(2H, m, phenyl H's) 7.42 - 7.58(3H, m, phenyl H's)
$^1H$ NMR (benzene- $d_6$ )	9.98(2H, m, $H^{3,3'}$ ) 8.84(2H, s, $H^{3,5}$ ) 8.20(2H, m, $H^{6,6''}$ ) 8.08 (2H, m, $H^{5',5''}$ ) 7.50(2H, m, $H^{2'',6''}$ ) 7.12(3H, m, $H^{3'',4'',5''}$ )
$^{13}C$ NMR ( $CDCl_3$ )	150.5 - 154.5(5C, ts, pyridyl and pyrazinyl quat. C's) 143.5 - 144.8(6C, ts, pyrazinyl CH's) 137.7(1C, s, $C^{1''}$ ) 127.0 - 129.5(5C, ts, phenyl CH's) 119.8(2C, s, $C^{3,5}$ )
IR	575(w) 621(m) 690(m) 766(s) 827(w) 852(m) 889(w) 1375(s) 1427(s) 1471(s) 1498(w) 1521(m) 1602(m)
UV/vis (MeCN)	249, 284 ( $\pi$ - $\pi^*$ )

## Chapter Three

**Synthesis and photophysical properties of terpyridyl ligand complexes of platinum(II)****3.1 INTRODUCTION**

In work done previously in our laboratories, Summerton synthesised the  $[\text{Pt}\{4'-(\alpha\text{-naphthyl})\text{-}2,2':6',2''\text{-terpyridine}\}\text{Cl}]\text{X}$   $\{[\text{Pt}(4'\text{-}\alpha\text{Np-terpy})\text{Cl}]\text{X}\}$  ( $\text{X}^- = \text{SbF}_6^-, \text{BF}_4^-, \text{CF}_3\text{SO}_3^-$ ) set of complexes.<sup>111</sup> The  $\alpha$ -substituted naphthyl group, in the 4'-position of the terpyridyl unit, is not expected to be coplanar with the terpyridyl unit because of the considerable steric interactions between the proton in the naphthyl 8-position (*i.e.*, the adjacent  $\alpha$ -proton) and the protons on the terpyridyl fragment (see Figure 3.1). (This interaction of substituents in adjacent  $\alpha$ -positions is known as a *peri*-interaction.) Subsequent studies of the photophysical properties showed that the complex has an exceptionally long-lived emitting state in dichloromethane ( $\text{CH}_2\text{Cl}_2$ ) solution of  $17 \mu\text{s}$ <sup>32, 111</sup> which is significantly longer than the lifetime of 850 ns recorded for  $[\text{Ru}(\text{bipy})_3]^{2+}$  ( $\text{bipy} = 2,2'\text{-bipyridine}$ ) in degassed acetonitrile solution at room temperature.<sup>146</sup> The question arose as to what extent the *peri*-interaction and the consequent restricted rotation about the interannular bond is responsible for the prolonged emission lifetime. With this in mind the naphthyl ring in the 4'-position was substituted in the  $\beta$  as opposed to the  $\alpha$ -position to provide a ligand with the same naphthyl group but with a reduced steric interaction with the terpyridyl system. We report here the synthesis and photophysical properties of a selection of salts of a platinum(II) complex of this ligand *viz.*,  $[\text{Pt}(4'\text{-}\beta\text{Np-terpy})\text{Cl}]^+$  where  $4'\text{-}\beta\text{Np-terpy} = 4'\text{-}(\beta\text{-naphthyl})\text{-}2,2':6',2''\text{-terpyridine}$ .

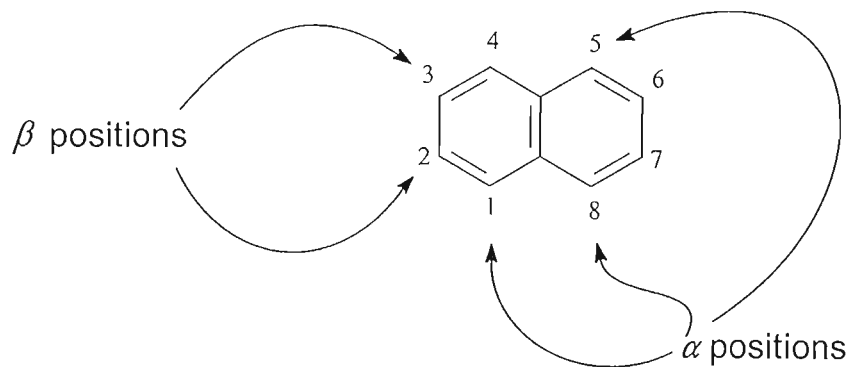


**Figure 3.1** *Numbering and nomenclature of naphthyl rings.*

Also reported is the synthesis and photophysical properties of salts of  $[\text{Pt}(4'\text{-}m\text{Biph-terpy})\text{Cl}]^+$   $\{4'\text{-}m\text{Biph-terpy} = 4'\text{-}(m\text{-biphenyl})\text{-}2,2':6',2''\text{-terpyridine}\}$  and  $[\text{Pt}(4'\text{-}p\text{Biph-terpy})\text{Cl}]^+$   $\{4'\text{-}p\text{Biph-terpy} = 4'\text{-}(p\text{-biphenyl})\text{-}2,2':6',2''\text{-terpyridine}\}$ . These two luminophores are distinguished by having either a *meta*- or *para*-biphenyl group in the 4'-position of the terpyridyl moiety (see Figure 3.2). Of primary interest was to determine what effect the replacement of a  $\beta$ -naphthyl with a biphenyl group would have on the photophysical properties of the associated complex. Certainly an effect on the electronic structure of the ligand is expected given the higher degree of  $\pi$ -conjugation in the fused ring ( $\beta$ -naphthyl) moiety as opposed to the biphenyl moieties. To what extent this would play a role in determining the photophysical properties of the complex as a whole remained to be determined. On the other hand the *peri*-interaction described above is not expected to be important since steric interactions between  $\text{H}^{2''}$  and  $\text{H}^{6''}$  of the biphenyl substituent with the  $\text{H}^{3'}$  and  $\text{H}^{5'}$  protons of the terpyridyl moiety, will be the same as those involving the  $\text{H}^{1''}$  and  $\text{H}^{3''}$  protons of the  $\beta$ -naphthyl moiety. In short, all three luminophores  $[\text{Pt}(4'\text{-}\beta\text{Np-terpy})\text{Cl}]^+$ ,  $[\text{Pt}(4'\text{-}m\text{Biph-terpy})\text{Cl}]^+$  and  $[\text{Pt}(4'\text{-}p\text{Biph-terpy})\text{Cl}]^+$  should exhibit the same degree of rotational freedom about the interannular bond in the 4'-position of the terpyridyl unit.

Of secondary interest is to what extent, if any, *meta*- as opposed to *para*-substitution affects the nature of the excited state. Substitution in the *ortho*-position has been avoided since, apart from producing sterically crowded luminophores, substitution in this position would be accompanied by a twist in interannular bonds, forcing a loss of conjugation and the extended delocalisation which it was hoped would be a feature of the  $[\text{Pt}(4'\text{-}m\text{Biph-terpy})\text{Cl}]^+$  and  $[\text{Pt}(4'\text{-}p\text{Biph-terpy})\text{Cl}]^+$  luminophores.

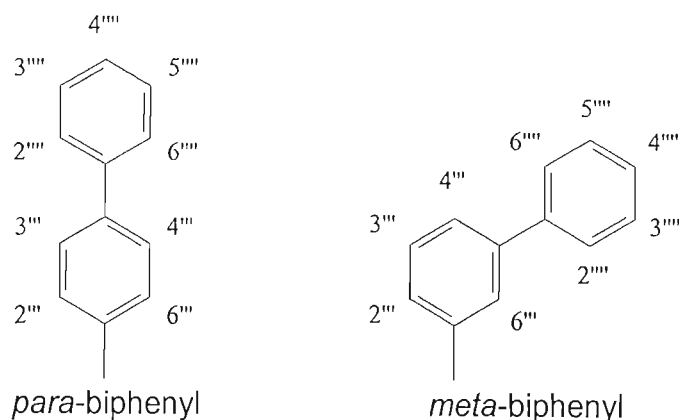


**Figure 3.2** Numbering and nomenclature of biphenyl rings in 4'-position of terpyridyl ligand.



The preceding remarks apply strictly to measurements of absorption and emission spectra in fluid solution and in a dilute glass. As will be shown from measurements made in a more concentrated glass and in the solid state, intermolecular interactions can also play an important role in determining the photophysical properties of the compound.

## 3.2 RESULTS AND DISCUSSION

### 3.2.1 [Pt(4'- $\beta$ Np-terpy)Cl]X [X<sup>-</sup> = SbF<sub>6</sub><sup>-</sup> (1), BF<sub>4</sub><sup>-</sup> (2), CF<sub>3</sub>SO<sub>3</sub><sup>-</sup> (3)]

{where 4'- $\beta$ Np-terpy = 4'-( $\beta$ -naphthyl)-2,2':6',2"-terpyridine}

#### 3.2.1.1 Synthesis and characterisation of [Pt(4'- $\beta$ Np-terpy)Cl]X [X<sup>-</sup> = SbF<sub>6</sub><sup>-</sup> (1), BF<sub>4</sub><sup>-</sup> (2), CF<sub>3</sub>SO<sub>3</sub><sup>-</sup> (3)]

The coordination of the tridentate terpyridyl ligand to platinum(II) was first reported in 1934 by Morgan and Burstall.<sup>63</sup> The method involved refluxing potassium tetrachloroplatinate(II) with terpyridine in an aqueous solution to give the doubly hydrated product [Pt(terpy)Cl]Cl.2H<sub>2</sub>O. This method is time consuming and suffers from a poor yield due to the formation of the insoluble Magnus-type salt, [Pt(terpy)Cl]<sub>2</sub>[PtCl<sub>4</sub>], which precipitates from the reaction mixture and is thus precluded from reacting further. Through the work of Mureinik and Bidani<sup>147</sup> slight improvements were made to this method culminating in 1980 in the publication by Howe-Grant and Lippard<sup>83</sup> of another modification of the basic synthetic route established by Morgan and Burstall. Che and coworkers applied the method of Howe-Grant and Lippard<sup>83</sup> in their preparation of [Pt(terpy)Cl]CF<sub>3</sub>SO<sub>3</sub>.<sup>28</sup> Counterion metathesis was effected in aqueous medium by refluxing [Pt(terpy)Cl]Cl.2H<sub>2</sub>O (made by the method of Lippard *et al.*) in the presence of an equivalent of silver triflate. In a similar way Gray and coworkers prepared a range of chloro(terpyridine)platinum(II) compounds, each with a different counterion in the outer coordination sphere of platinum.<sup>29</sup> Gray *et al.* were able to precipitate their compounds from solution by the use of a large excess of the sodium or ammonium salt containing the appropriate anion instead of the silver salt used by Che and coworkers.<sup>28</sup> The method of Howe-Grant and Lippard is regarded as the definitive synthesis of [Pt(terpy)Cl]Cl.2H<sub>2</sub>O, and successive adjustments to the original route merely served to

improve the yield. The process still suffers from long reaction times (2 - 3 days) and is susceptible to the formation of mixed products. Long reaction times have been overcome with the use of microwave techniques to facilitate the coordination. Mingos and coworkers have demonstrated that it is possible to perform this reaction in 1 minute by applying microwave dielectric heating effects.<sup>148</sup> The greatest disadvantage of the method for the work presented here, however, is the difficulty experienced in coordinating substituted terpyridines, especially hydrophobic substituted terpyridines, to platinum(II).<sup>68</sup>

Annibale and coworkers pioneered a new approach to the synthesis of chloro(terpyridine)platinum(II) complexes with the use of  $[\text{Pt}(1,5\text{-COD})\text{Cl}_2]$  (where 1,5-COD = 1,5-cyclooctadiene) as a starting material.<sup>149</sup> This compound is warmed in aqueous medium for 15 minutes in the presence of an equimolar amount of terpyridine to give  $[\text{Pt}(\text{terpy})\text{Cl}]\text{Cl}\cdot 2\text{H}_2\text{O}$  in a nearly quantitative yield. This idea was extended by Lowe and Vilaivan<sup>68</sup> with their recommendation of  $[\text{Pt}(1,5\text{-COD})\text{I}_2]$  as a starting material and utilising a two-step synthesis. The method provides high yields and short reaction times which have been attributed to the strong *trans*-labilising effect of 1,5-cyclooctadiene on the platinum centre in the starting material. In addition, reaction conditions are mild and the products easily isolated and purified. A significant disadvantage of the method of Howe-Grant and Lippard<sup>83</sup> was also overcome as Lowe and Vilaivan demonstrated that their method was capable of facile coordination of platinum to a range of substituted terpyridines to platinum(II).<sup>68</sup>

The method employed in this work for coordinating the terpyridyl ligand is different from those described above and follows an approach previously applied in our laboratories.<sup>47, 53, 54</sup> A counterion for the final product is selected and the silver salt of that counterion used as a starting material. The neutral compound  $[\text{Pt}(\text{PhCN})_2\text{Cl}_2]$  is treated with an equimolar amount of the appropriate silver salt in refluxing acetonitrile. {It is also possible to use the acetonitrile coordinated adduct *viz.*  $[\text{Pt}(\text{MeCN})_2\text{Cl}_2]$ , but given the commercial availability of  $[\text{Pt}(\text{PhCN})_2\text{Cl}_2]$  it would be wasteful to incorporate an additional step in preparing  $[\text{Pt}(\text{MeCN})_2\text{Cl}_2]$ .<sup>150</sup>} Silver abstracts a chlorine atom from the platinum reactant to precipitate as silver chloride, its former anion most likely introduced to the outer coordination sphere of the platinum species in solution. The silver chloride is filtered off and the filtrate containing platinum species of the type  $[\text{Pt}(\text{PhCN})_{2-x}(\text{MeCN})_x\text{Cl}]^+$  ( $x = 1$  or  $2$ ), added to an equimolar

amount of 4'-( $\beta$ -naphthyl)-2,2':6',2''-terpyridine (4'- $\beta$ Np-terpy) in acetonitrile. The mixture containing the ligand is again refluxed and then filtered hot to remove any trace of silver chloride. Air and moisture stable, analytically pure products precipitate upon cooling as orange ( $\text{SbF}_6^-$  and  $\text{BF}_4^-$ ) and yellow ( $\text{CF}_3\text{SO}_3^-$ ) solids. Precipitation can be induced by the partial removal of solvent under reduced pressure. The complexes were recrystallized from hot acetonitrile as an additional purification step. Repeated attempts were made to grow single crystals of each of the three complexes,  $[\text{Pt}(4'\text{-}\beta\text{Np-terpy})\text{Cl}]\text{SbF}_6$ ,  $[\text{Pt}(4'\text{-}\beta\text{Np-terpy})\text{Cl}]\text{BF}_4$  and  $[\text{Pt}(4'\text{-}\beta\text{Np-terpy})\text{Cl}]\text{CF}_3\text{SO}_3$  by three methods: a refluxing acetonitrile solution of the complex was slowly cooled to room temperature; a saturated acetonitrile solution was left to slowly evaporate at ambient temperatures; and finally, diethyl ether was allowed to diffuse into an acetonitrile solution containing the complex of interest. None of these methods yielded single crystals which were suitable for X-ray diffraction studies.

Elemental analysis for C, H and N confirms the formulation of each of the three platinum salts containing 4'- $\beta$ Np-terpy synthesised in this study as  $[\text{Pt}(4'\text{-}\beta\text{Np-terpy})\text{Cl}]\text{SbF}_6$  (**1**),  $[\text{Pt}(4'\text{-}\beta\text{Np-terpy})\text{Cl}]\text{BF}_4$  (**2**) and  $[\text{Pt}(4'\text{-}\beta\text{Np-terpy})\text{Cl}]\text{CF}_3\text{SO}_3$  (**3**). The  $^1\text{H}$  NMR spectra of the three salts are similar and the spectrum obtained for the hexafluoroantimonate salt in deuterated dimethylsulfoxide ( $\text{DMSO-d}_6$ ) is briefly described as a representative example and a complete listing of chemical shifts for each compound is provided in the experimental section of this chapter. Resonances were assigned by comparison to the signals from the free ligand and with the aid of an absolute value correlation spectroscopy (COSY) experiment. Protons are numbered according to the numbering scheme introduced in Chapter 2. The  $\text{H}^{3,5'}$  protons occur the furthest downfield as a singlet at  $\delta$  8.76. The next three upfield signals at  $\delta$  8.61, 8.56 and 8.44 are assigned to the pyridyl protons  $\text{H}^{3,3'}$ ,  $\text{H}^{6,6'}$  and  $\text{H}^{4,4'}$  respectively. The presence of the remaining pyridyl proton ( $\text{H}^{5,5'}$ ) signals at  $\delta$  7.67 are obscured under naphthyl proton peaks but were also distinguished by means of a COSY experiment. Remaining resonances are assigned to protons on the naphthyl substituent.

Solid state infrared spectra were recorded of each of the three salts as KBr pellets. The spectra are essentially the same, prominent peaks due to vibrations associated with the counterions providing the only variation. A listing of the most salient peaks is provided in Table 3.10 at the end of this chapter.

### 3.2.1.2 Photophysical properties of [Pt(4'- $\beta$ Np-terpy)Cl]X [ $X^- = \text{SbF}_6^-$ (1), $\text{BF}_4^-$ (2), $\text{CF}_3\text{SO}_3^-$ (3)]

Aspects of the work described in this section have already been published.<sup>32</sup> In particular the solution photophysical studies of the [Pt(4'- $\beta$ Np-terpy)Cl]<sup>+</sup> chromophore have been published in conjunction with the photophysical properties of related complexes that also have large fused aromatic rings as the substituent in the 4'-position of the terpyridyl ligand.

#### *Fluid solution absorption spectroscopy*

Room temperature UV/vis absorption studies were carried out on each of the three complexes. Not surprisingly the counterion has no effect on the absorption spectra and for this reason a single discussion is given.

The complexes dissolve in acetonitrile and dichloromethane and at low concentrations give yellow solutions that provide absorptions which are stable in intensity and energy for at least a week. The absorption spectrum of [Pt(4'- $\beta$ Np-terpy)Cl]<sup>+</sup> in MeCN is provided in Figure 3.3 with the absorption data being listed in Table 3.11 at the end of this chapter. Absorptions in acetonitrile follow Beer's Law in the concentration range studied (5 - 50  $\mu\text{M}$ ), indicating dissolution into monomeric ions. The spectrum can be regarded in terms of two sets of absorptions. The first consists of intense absorptions in the UV region and the second of a moderately intense vibrationally structured band at the high energy end of the visible region, in particular in acetonitrile a band maximising at 411 nm is observed which has a shoulder at 394 nm. This pattern closely parallels measurements previously made on [Pt(terpy)Cl]<sup>+</sup> and [Pt(4'-Ph-terpy)Cl]<sup>+</sup> (where 4'-Ph-terpy is 4'-phenyl -2,2':6',2''-terpyridine).<sup>27 - 32, 42, 53</sup> The absorptions in the UV region occur as an intense absorption at 284 nm and a structured band between 300 and 350 nm. The 284 nm peak is mirrored by a band at 281 nm for the free ligand under similar conditions. Coordination of the terpyridyl ligand necessitates conversion from the *trans-trans* configuration adopted by the free ligand to the *cis-cis* form resulting in a reduction in the energy at which  $\pi-\pi^*$  absorptions occur.<sup>151, 152</sup> This allows us to account for

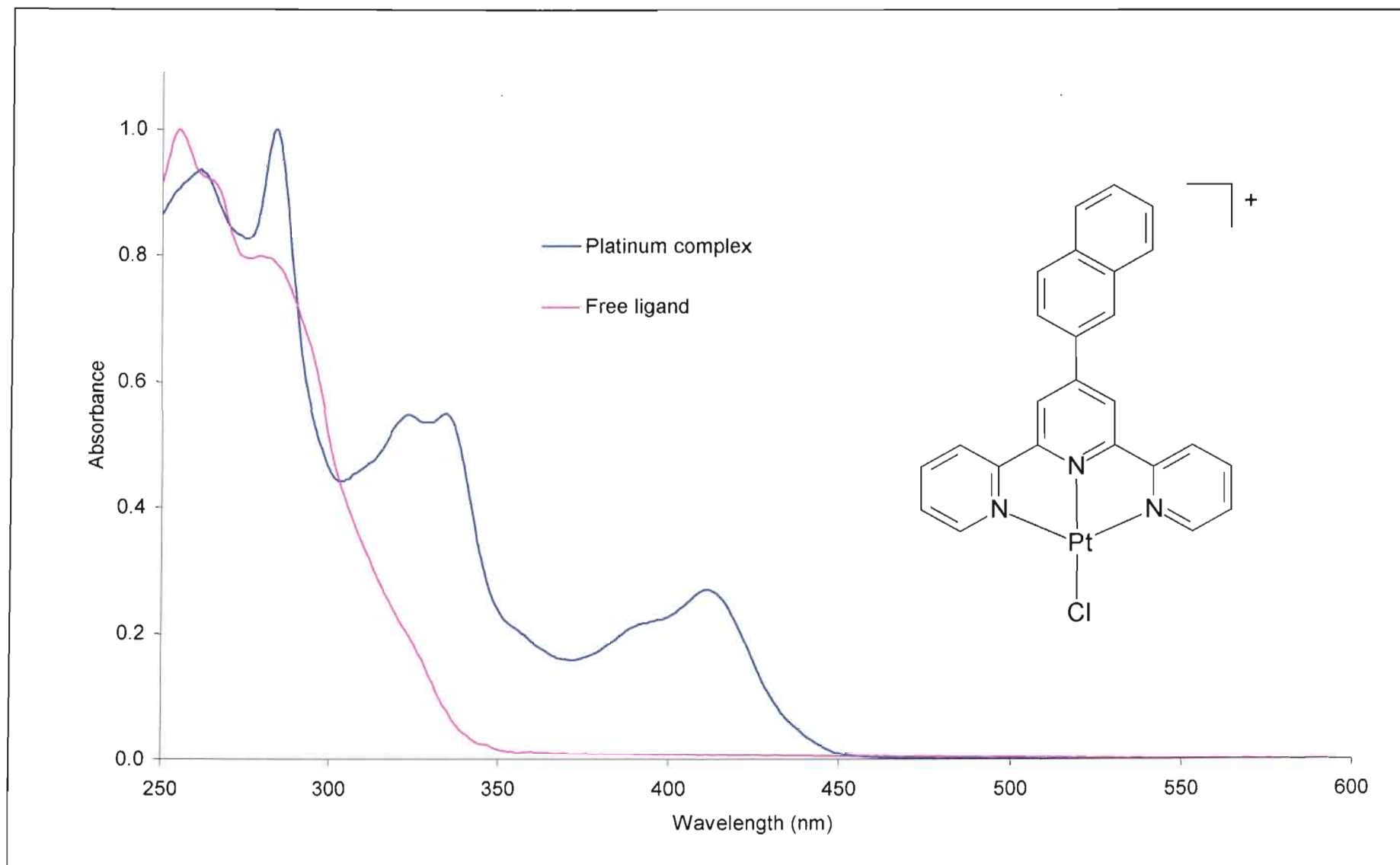


**Figure 3.3** Acetonitrile solution absorption spectra of the  $[Pt(4'-\beta Np\text{-terpy})Cl]^+$  and  $4'-\beta Np\text{-terpy}$  chromophores recorded at 298 K.

the absorption bands observed in the 330 nm region of the absorption spectrum of  $[\text{Pt}(4'\text{-}\beta\text{Np-terpy})\text{Cl}]^+$ . These points in conjunction with assignments previously made for spectra of the  $[\text{Pt}(\text{terpy})\text{Cl}]^+$  and  $[\text{Pt}(4'\text{-Ph-terpy})\text{Cl}]^+$  chromophores (see section 1.2.1.1 in Chapter 1) led to the assignment of the absorptions between 280 and 380 nm to  $^1(\pi \rightarrow \pi^*)$  transitions associated with the coordinated 4'-( $\beta$ -naphthyl)-2,2':6',2''-terpyridine (4'- $\beta$ Np-terpy) ligand.

The bands in the visible region between 380 and 430 nm although less intense than the  $^1(\pi\text{-}\pi^*)$  transitions ( $\epsilon 1 \times 10^4 \text{ M}^{-1}\cdot\text{cm}^{-1}$ ) are far more intense than d-d ligand field (LF) absorptions (for d-d transitions we expect  $\epsilon < 1000 \text{ M}^{-1}\cdot\text{cm}^{-1}$ ), allowing us to discount this possibility.<sup>27</sup> Moreover, the energy of these bands depends on the solvent and occurs at 411 nm in acetonitrile and at 427 nm in dichloromethane. This change in energy is consistent with absorption to give a charge-transfer excited state that would experience a net reduction in dipole moment in a polar solvent like acetonitrile and hence occur at higher energy in this medium.<sup>27,30,32</sup> This evidence in conjunction with assignments made for similar bands in the literature<sup>27-29,32</sup> allow us to ascribe the bands to a charge-transfer transition, in particular to a  $[\text{5d}(\text{Pt}) \rightarrow \pi^*(4'\text{-}\beta\text{Np-terpy})]$  metal-to-ligand charge transfer  $^1(\text{MLCT})$  transition.

The room temperature absorption spectrum of the closely related complex  $[\text{Pt}\{4'-(\alpha\text{-naphthyl})\text{-}2,2':6',2''\text{-terpyridine}\}\text{Cl}]^+$   $\{[\text{Pt}(4'\text{-}\alpha\text{Np-terpy})\text{Cl}]^+\}$  in acetonitrile is reproduced from the work of Michalec, Summerton and McMillin *et al.*<sup>32</sup> in Figure 3.3a. The main absorbance features compare well with the spectrum of the  $[\text{Pt}(4'\text{-}\beta\text{Np-terpy})\text{Cl}]^+$  chromophore recorded under the same conditions, there being only minor differences in the relative intensities of the bands in the 300 - 350 nm region of the spectrum.<sup>32</sup> Indeed Summerton's assignment of the absorption bands are the same as those given above for  $[\text{Pt}(4'\text{-}\beta\text{Np-terpy})\text{Cl}]^+$ . An important point to note is that the molar absorptivity of the low energy CT absorptions for  $[\text{Pt}(4'\text{-}\beta\text{Np-terpy})\text{Cl}]^+$  ( $14100 \text{ M}^{-1}\cdot\text{cm}^{-1}$  at 411 nm in acetonitrile) is significantly higher than those for  $[\text{Pt}(4'\text{-}\alpha\text{Np-terpy})\text{Cl}]^+$  ( $7300 \text{ M}^{-1}\cdot\text{cm}^{-1}$  at 406 nm<sup>32, 111</sup>), indicating the greater likelihood of the former chromophore being nearly planar in the ground state. This conclusion is consistent with the reduced *peri*-interaction present in the  $\beta$ -naphthyl, as opposed to the  $\alpha$ -naphthyl, derivative.

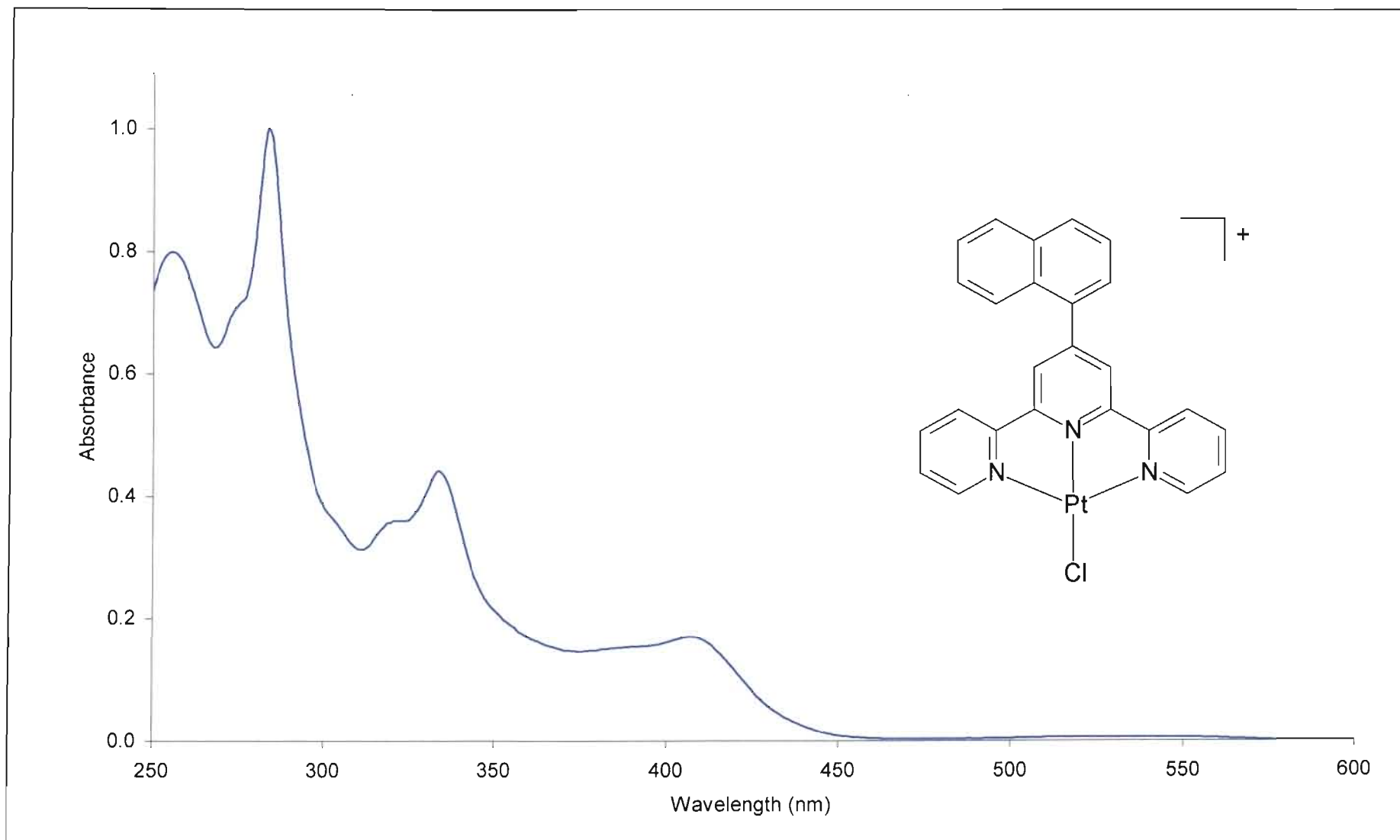


**Figure 3.3a** The acetonitrile solution absorption spectrum of the  $[Pt(4'\text{-}\alpha\text{Np-terpy})Cl]^+$  chromophore recorded at 298 K. (From the work of Summerton.<sup>111</sup>)

### *Fluid solution emission spectroscopy*

Emission spectra were recorded in solution (at room temperature and in a low temperature rigid glass) and in the solid state, the emission data being presented in Table 3.12 and Table 3.13 respectively at the end of this chapter. The emission in fluid solution will be discussed first. As expected, the counterion has no effect on the emission in solution and, for this reason, the emission spectrum of the hexafluoroantimonate salt will be discussed as representative of the  $[\text{Pt}(4'\text{-}\beta\text{Np-terpy})\text{Cl}]^+$  luminophore in solution.

No emission could be detected from an acetonitrile solution of the  $[\text{Pt}(4'\text{-}\beta\text{Np-terpy})\text{Cl}]^+$  luminophore. However, the non-coordinating solvent dichloromethane allows for an appreciable emission signal. The emission profile in a 20  $\mu\text{M}$  solution of dichloromethane (Figure 3.4) shows a structured band with a 0-0 transition at 570 nm and progressions at 615 and 670 nm. An emission lifetime of 11.9  $\mu\text{s}$  has been recorded.

In assigning an emission origin the following observations and deductions about the emission profile are made. First, we note the vibrational structure with a spacing of between 1000 and 1400  $\text{cm}^{-1}$ . Resolved vibrational spacings of this magnitude are consistent with the deposition of energy in the C=C and C=N stretching vibrations of an aromatic system and are typical of an intraligand (IL)  $\pi\text{-}\pi^*$  contribution to the excited state.<sup>29,61</sup> However, a MLCT contribution to the emitting state is also expected because of the absence of any detectable emission when the measurement is made in a coordinating solvent such as acetonitrile. This kind of solvent dependence is exactly what is expected for a MLCT state, since the MLCT absorption increases the metal's formal oxidation state, leaving the metal centre open to solvent attack with a concomitant non-radiative deactivation of the excited state.<sup>48</sup> Such solvent dependence is *not* expected of a pure IL ( $\pi\text{-}\pi^*$ ) emission nor for intraligand charge transfer (ILCT) emission (*vide infra*). Pure IL emission is also unlikely because the energy of the 0-0 transition falls below the range expected for such an emission. In this regard consider the following. Chassot, Balzani *et al.* have studied emission from complexes of the type  $[\text{Pt}(\text{Phpy})_2(\text{CH}_2\text{Cl})\text{Cl}]$  (where the Phpy ligand is the anionic C-deprotonated form of 2-phenylpyridine). The emission is assigned as entirely ligand centred *i.e.*,  $^3\text{IL}(\pi\text{-}\pi^*)$  for two



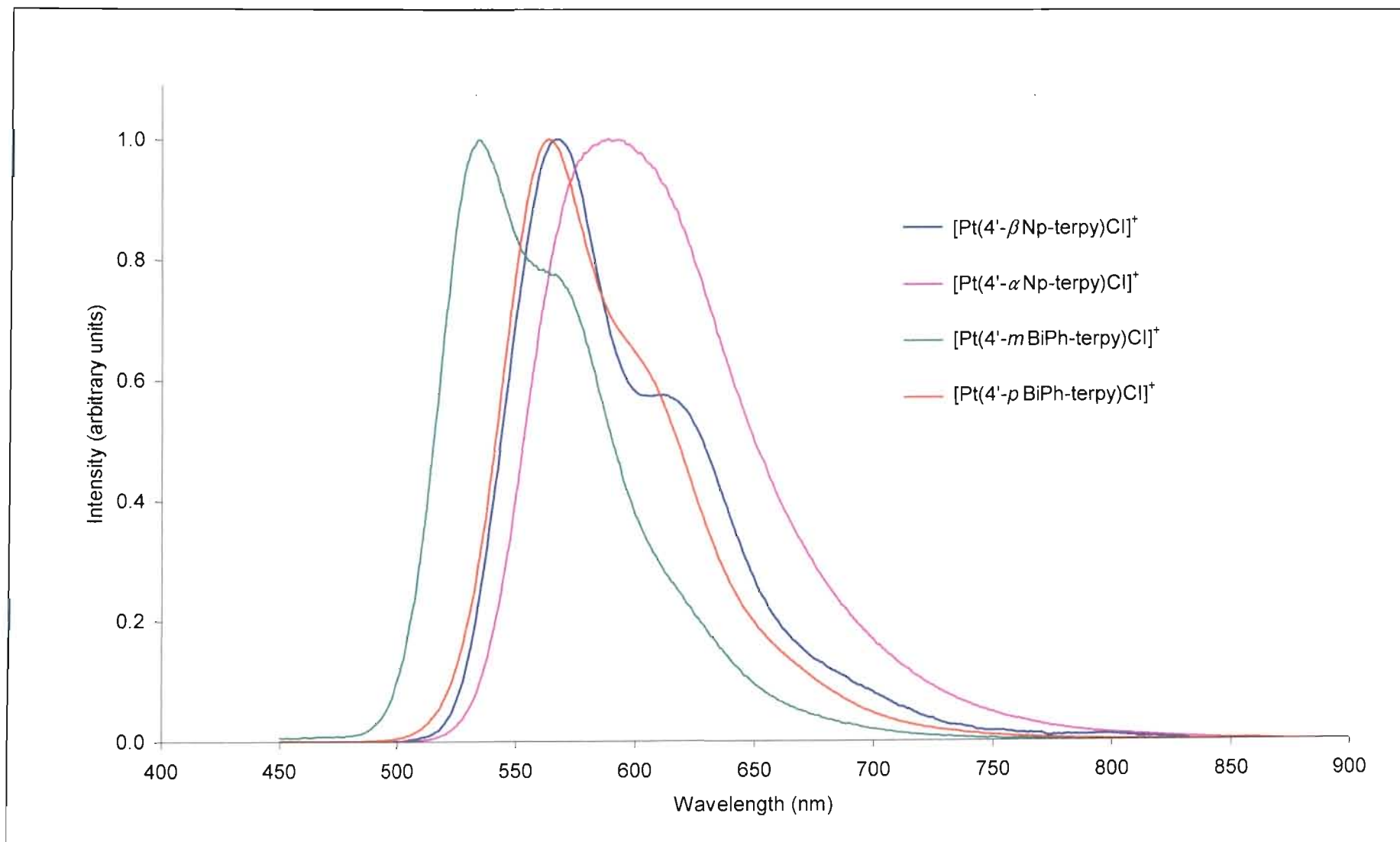


**Figure 3.4** Dichloromethane solution emission spectra of the  $[\text{Pt}(4'\text{-}R\text{-terpy})\text{Cl}]^+$  luminophores recorded at 298 K. ( $R = \beta\text{Np}$ ,  $\alpha\text{Np}$ ,  $m\text{BiPh}$  and  $p\text{BiPh}$ )

main reasons. First the 0-0 transitions at *ca.* 450 nm fall at very similar energies to those of the protonated Phpy free ligand.<sup>43</sup> Second, with the platinum metal in the IV oxidation state MLCT contributions to the excited state are considered unlikely. Their conclusions are corroborated by emission lifetimes longer than 300  $\mu$ s. By comparison with this “pure” ligand centred emitter, emission from [Pt(4'- $\beta$ Np-terpy)Cl]<sup>+</sup> is much lower in energy, a stabilisation attributed to MLCT processes contributing to the character of the excited state.

The emission lifetime of 11.9  $\mu$ s recorded for the complex in dichloromethane provides further evidence for the composition of the excited state. Though the lifetime is not as long as that of 16.6  $\mu$ s recorded for the 4'- $\alpha$ Np-terpy derivative under the same conditions,<sup>32</sup> it is similar and considerably longer than the lifetime of 85 ns recorded in dichloromethane at room temperature for [Pt(4'-Ph-terpy)Cl]<sup>+</sup>.<sup>32</sup> Michalec, Summerton and McMillin *et al.* have associated the long emission lifetimes of complexes such as [Pt(4'- $\alpha$ Np-terpy)Cl]<sup>+</sup>, [Pt(4'- $\beta$ Np-terpy)Cl]<sup>+</sup>, [Pt(4'-Phe9-terpy)Cl]<sup>+</sup> and [Pt(4'-Pyre1-terpy)Cl]<sup>+</sup> (where Phe9 denotes 9-phenanthrenyl and Pyre1 denotes 1-pyrenyl) with the presence of a *fused-ring* substituent in the 4'-position of the terpyridyl ligand and, in particular, with an emissive excited state that takes on some intraligand charge transfer (ILCT) character.<sup>32</sup> Since the fused ring substituent is easily ionised, the ILCT transition is from the HOMO on the fused ring to the  $\pi^*$ -LUMO on the terpyridyl fragment. In conclusion, the best assignment of the emitting state is one that is an admixture of <sup>3</sup>IL, <sup>3</sup>MLCT and <sup>3</sup>ILCT character. (The triplet assignment follows from the long lifetime.) Indeed, this is the same assignment as that made by Michalec, Summerton and McMillin *et al.* to the emission recorded in dichloromethane for all of the above complexes that have in common fused-ring substituents in the 4'-position of the terpyridyl moiety.<sup>32</sup>

Interestingly, the vibrational structure in the emission spectrum of the [Pt(4'- $\alpha$ Np-terpy)Cl]<sup>+</sup> complex is less well resolved than that in the [Pt(4'- $\beta$ Np-terpy)Cl]<sup>+</sup> complex.<sup>32</sup> The explanation probably follows from the fact that the  $\beta$ -naphthyl substituent is more nearly coplanar with the terpyridyl fragment than the  $\alpha$ -naphthyl substituent, because of the reduced *peri*-interactions in the former case. This would lead to a lowering of the energy of the IL( $\pi$ - $\pi^*$ ) absorption and to a concomitant increased contribution of the  $\pi$ - $\pi^*$  component to the emitting state. As noted above a more resolved vibrational structure is generally associated with IL( $\pi$ - $\pi^*$ ) emission.<sup>28</sup> Also noteworthy is that the energy of the 0-0 transition in the [Pt(4'-

$\alpha$ Np-terpy)Cl]<sup>+</sup> complex is somewhat lower than the corresponding transition in the [Pt(4'- $\beta$ Np-terpy)Cl]<sup>+</sup> complex *cf.* wavelengths for the emission maxima of 588 nm and 570 nm respectively.<sup>32</sup> The origin of this difference is uncertain. We tentatively suggest that it is due to an increased contribution of the ILCT component to an emitting state that is stabilised in some way by the reduced planarity of the 4'- $\alpha$ Np-terpy ligand. Certainly, this would be consistent with the slightly longer lifetime of 16.6  $\mu$ s recorded for the [Pt(4'- $\alpha$ Np-terpy)Cl]<sup>+</sup> complex.<sup>32</sup>

### *Glass emission spectroscopy*

Emission spectra of the [Pt(4'- $\beta$ Np-terpy)Cl]<sup>+</sup> luminophore have been recorded in a rigid glassy medium at 77 K, specifically in 1:5:5 (v/v) DMF/MeOH/EtOH (DME). The emission spectrum of the triflate salt {[Pt(4'- $\beta$ Np-terpy)Cl]CF<sub>3</sub>SO<sub>3</sub>} in a DME glass at 77 K at various concentrations is illustrated in Figure 3.5; spectra recorded for the other salts are entirely similar. {Glass emission spectra of [Pt(4'- $\beta$ Np-terpy)Cl]<sup>+</sup> have also been recorded by the group of McMillin in frozen butyronitrile.<sup>32</sup>} Note that the appearance of the spectrum depends on the concentration of the complex in solution. As the concentration increases aggregation takes place in solution and the aggregated species give rise to a distinctive emission. Emission from aggregates is at no stage intense enough to be the dominant emission, partly due to an inherently weak emission and partly due to the limiting solubility of [Pt(4'- $\beta$ Np-terpy)Cl]CF<sub>3</sub>SO<sub>3</sub> in DME which means that a large concentration of aggregated luminophores is never achieved. Thus emission from monomers is the overwhelming radiative pathway. However, as shown below, it is possible to avoid population of the monomer excited state by using a lower excitation energy, in which case, the emission from the aggregated species is highlighted. Emission from the monomers will be discussed first, followed by an analysis of the emission by the aggregates.

When the concentration of the solution is in the 0.1 to 10  $\mu$ M range and the excitation wavelength is below 450 nm (*i.e.* at relatively high energy), we see a structured band with maxima at 547, 585sh and 630 nm (essentially identical to spectra recorded in butyronitrile at 77 K and reported in the literature<sup>32</sup>). Varying the solution concentration in this range only results in intensity, and no variation in band profile is observed. The emission has a radiative

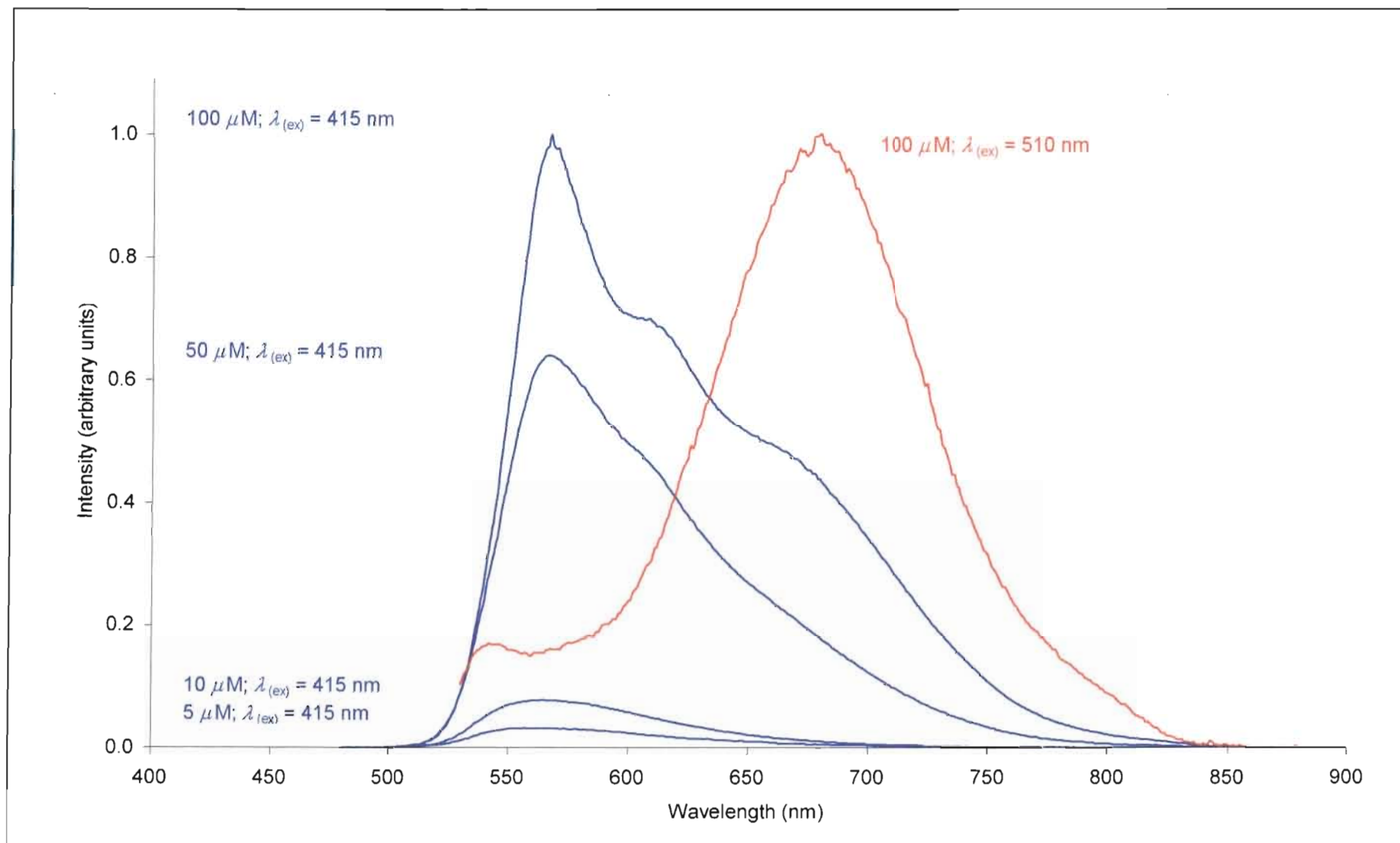


**Figure 3.5** Solution emission spectra of  $[Pt(4'\text{-}\beta\text{Np-terpy})Cl]^+$  recorded in a rigid DME glass at 77 K. (Intensities at different excitation energies adjusted to achieve equal maxima.)

lifetime of 47.0  $\mu\text{s}$ . Excitation spectra monitored at 520 nm match the basic low energy features of the room temperature dichloromethane absorption spectrum (*vide supra*), when the excitation spectrum is recorded at wavelengths shorter than 610 nm (see Figure 3.6).

With the exception of the emission lifetime the features of the dilute glass emission spectrum recorded in DME at 77 K are identical to those of emission in a dichloromethane solution at room temperature. Hence the same assignment is made *i.e.* emission is assigned to a configurationally mixed excited state with  $^3\text{IL}$ ,  $^3\text{MLCT}$  and  $^3\text{ILCT}$  character. The difference in emission lifetime between the fluid (11.9  $\mu\text{s}$ ) and glass (47.0  $\mu\text{s}$ ) solutions is attributed to the minimisation of radiationless processes at 77 K.

We now turn to evidence for the presence of aggregates in solution of relatively high concentration. Specifically, when the concentration is raised above 50  $\mu\text{M}$  and with excitation at wavelengths longer than 490 nm a less intense structureless emission emerges with  $\lambda_{\text{em}}(\text{max})$  at *ca.* 690 nm. (When an excitation wavelength longer than 490 nm is used and concentration is below 50  $\mu\text{M}$ , the low temperature glass is essentially non-emissive.) The radiative lifetime of the 690 nm emission is 1.9  $\mu\text{s}$ , significantly less than the 47  $\mu\text{s}$  recorded for the emission at higher energies. Excitation spectra monitoring emission at wavelengths shorter than 610 nm match absorption spectra recorded at relatively low concentration (5 - 35  $\mu\text{M}$ ). However, excitation spectra obtained by monitoring at wavelengths longer than 610 nm reveal a new, very broad band centred at roughly 520 nm (see Figure 3.6). This distinct, new band appears gradually, at the expense of bands between 360 and 410 nm. These findings indicate that there is an additional emitting species luminescing at wavelengths longer than 610 nm, which is distinct from emission by monomeric species. It is suggested that this additional emission source arises from aggregated species present only in the more concentrated solutions.

Gray and coworkers have undertaken a detailed study of the emission of  $[\text{Pt}(\text{terpy})\text{Cl}]^+$  in a glassy DME solution at 77 K.<sup>29</sup> The authors identify three different emissions depending on the concentration of the solution and on the excitation energy that is used (see Table 3.1). Similar emission behaviour for this and related luminophores in a rigid glassy medium has subsequently been reported by Campagna, Monsú Scolaro *et al.*<sup>42</sup>, in particular for the  $[\text{Pt}(4'$

**Table 3.1** Comparison of emissions obtained in rigid glassy medium at 77 K.

Compound	IL $\pi$ - $\pi^*$				Excimeric emission				MMLCT			
	conc ( $\mu$ M)	$\lambda_{ex}$ (nm)	$\lambda_{em}(\max)$ (nm)	$\tau$ ( $\mu$ s)	conc ( $\mu$ M)	$\lambda_{ex}$ (nm)	$\lambda_{em}(\max)$ (nm)	$\tau$ ( $\mu$ s)	conc ( $\mu$ M)	$\lambda_{ex}$ (nm)	$\lambda_{em}(\max)$ (nm)	$\tau$ ( $\mu$ s)
[Pt(terpy)Cl] <sup>+</sup>	< 10	337 <sup>M/E, 42</sup>	<u>470</u> <sup>BuCN, 28</sup> <u>470</u> <sup>M/E, 42</sup> 470, 506, 546, <u>580</u> <sup>BuCN, 32</sup>	15.0	> 6	337 <sup>42</sup>	~ 600 <sup>29</sup> ~ 670 <sup>M/E, 42</sup>	3.1	> 10	547	720 <sup>DME, 29</sup> 730 <sup>M/E, 42</sup>	2.0 <sup>42</sup>
[Pt(4'-Ph-terpy)Cl] <sup>+</sup>	40	350 <sup>M/E, 42</sup>	<u>515</u> <sup>M/E, 42</sup> <u>505</u> <sup>BuCN, 53</sup> 503, 540, <u>582</u> <sup>BuCN, 32</sup>	15.0	> 10	< 480	~ 650 <sup>M/E, 42</sup> 622 <sup>BuCN, 53</sup>	3.7	100	> 500	690 <sup>M/E, 42</sup> 726 <sup>BuCN, 53</sup>	2.6 <sup>42</sup>
[Pt(4'- $\beta$ Np-terpy)Cl] <sup>+</sup>	< 10	< 450	<u>545, 583,</u> <u>633</u> <sup>DME</sup> 542, 583, <u>625</u> <sup>BuCN, 32</sup>	47.0	-	-	-	-	> 50	> 490	696 <sup>DME</sup>	1.9
[Pt(4'- $\alpha$ Np-terpy)Cl] <sup>+</sup>	-	-	<u>540, 587</u> <sup>BuCN, 32</sup>	-	-	-	-	-	-	-	-	-
[Pt(4'- <i>m</i> Biph-terpy)Cl] <sup>+</sup>	< 10	< 440	510, <u>550,</u> 590sh <sup>DME</sup>	< 20	>10	470	~ 600	-	> 25	> 470	~ 670	1.9
[Pt(4'- <i>p</i> Biph-terpy)Cl] <sup>+</sup>	< 0.5	< 450	<u>550, 583,</u> 640sh <sup>DME</sup>	2.9	>20	460	~ 600	-	> 50	> 490	~ 685	1.9

Underlined values refer to the most intense emission bands within a manifold.

(BuCN) Solvent used is butyronitrile

(DME) Solvent used is 1:5:5 (v/v) DMF/MeOH/EtOH

(M/E) Solvent used is 4:1 (v/v) MeOH/EtOH

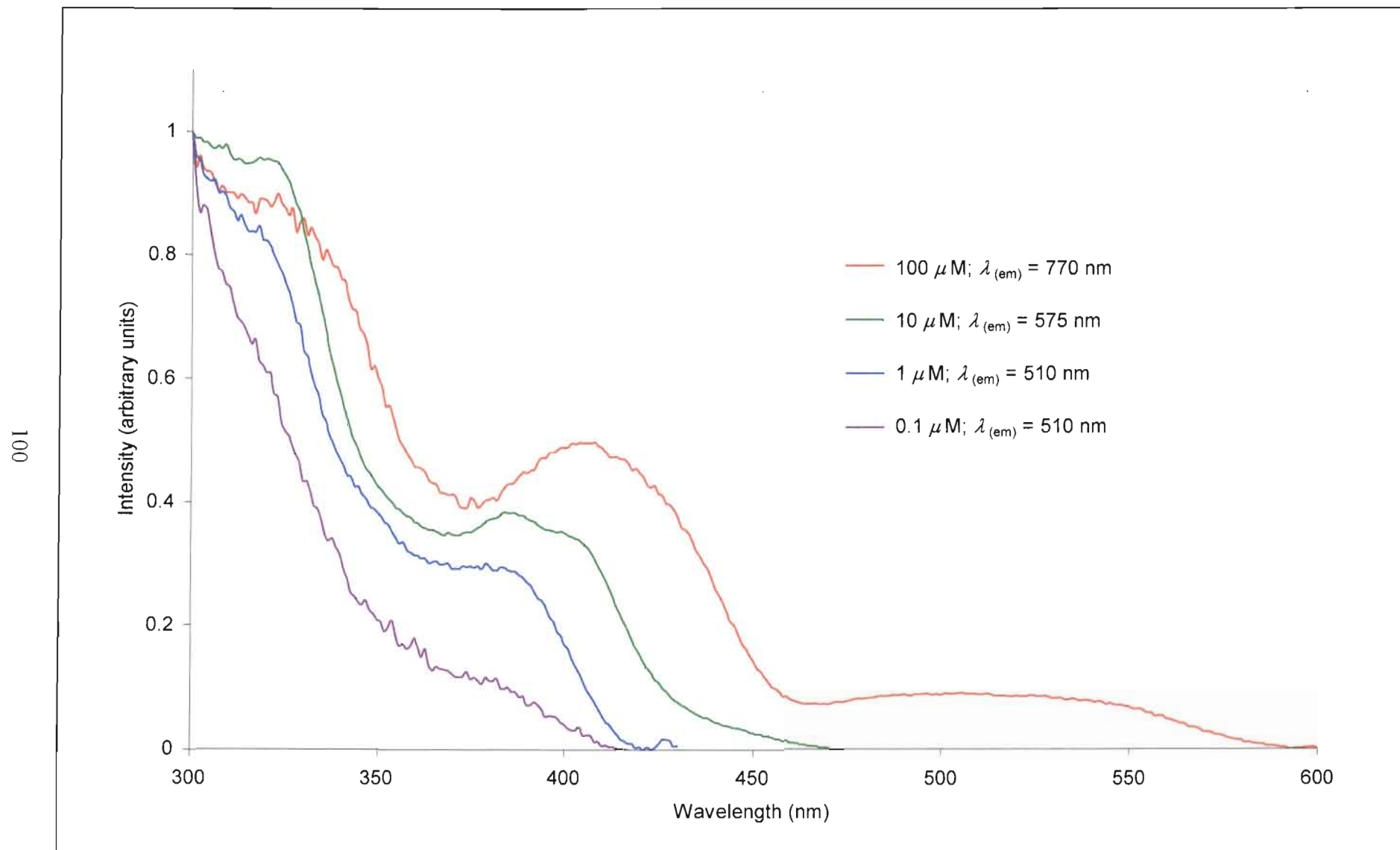


**Figure 3.6** Solution excitation spectra of  $[Pt(4'-\beta Np-terpy)Cl]^+$  recorded in a rigid DME glass at 77 K.

Ph-terpy)Cl]<sup>+</sup> luminophore. The first emission is from the most dilute solutions (with concentrations less than 10 μM) and occurs at highest energy {0-0 transition at 470 nm for [Pt(terpy)Cl]<sup>+</sup> and at 515 nm for [Pt(4'-Ph-terpy)Cl]<sup>+</sup> in frozen butyronitrile}. It is the longest-lived (τ > 10 μs) and has been assigned to π-π\* emission localised to the ligand. Campagna, Monsú Scolaro *et al.* also contend that there is a degree of MLCT character present in order to justify relatively modest emission lifetimes compared to pure ligand centred emitters.<sup>42</sup> This emission is paralleled by the monomer emission observed here for [Pt(4'-βNp-terpy)Cl]<sup>+</sup> with its most intense band at 547 nm.

The second emission exhibited by [Pt(terpy)Cl]<sup>+</sup> and assigned as <sup>3</sup>MMLCT in origin by Gray *et al.*, occurs at the lowest energies {λ<sub>em</sub>(max) > 670 nm} and in a single unstructured band. This emission is only evident from measurements on the most concentrated solutions and when an excitation wavelength longer than 500 nm is used.<sup>29</sup> These findings have been endorsed by Campagna, Monsú Scolaro *et al.* in addition to making similar findings for the [Pt(4'-Ph-terpy)Cl]<sup>+</sup> luminophore. Of importance is that the <sup>3</sup>MMLCT emission for both luminophores occurs at very similar energies despite a significant stabilisation in the monomeric emission energy of [Pt(4'-Ph-terpy)Cl]<sup>+</sup> compared to the unsubstituted luminophore, [Pt(terpy)Cl]<sup>+</sup>.<sup>42</sup> This is not surprising given that the interacting portions of the inner coordination spheres of the cations in [Pt(terpy)Cl]<sup>+</sup> and [Pt(4'-Ph-terpy)Cl]<sup>+</sup> are identical. For the same reason the energy of a <sup>3</sup>MMLCT transition is not expected to be significantly different for [Pt(4'-βNp-terpy)Cl]<sup>+</sup>. Thus the lowest energy emission observed at *ca.* 695 nm in concentrated solutions of [Pt(4'-βNp-terpy)Cl]<sup>+</sup> is assigned to a <sup>3</sup>MMLCT state. (The triplet assignment follows from the lifetime of *ca.* 2 μs.) Assuming the <sup>3</sup>MMLCT assignment is correct the implication is that d<sub>z<sup>2</sup></sub>(Pt)-d<sub>z<sup>2</sup></sub>(Pt) interactions are responsible for holding adjacent cations together as aggregates.

#### *Solid state absorption and emission spectroscopy*

Room temperature absorption spectra were recorded in the solid state for the three salts [Pt(4'-βNp-terpy)Cl]X [X<sup>-</sup> = SbF<sub>6</sub><sup>-</sup> (**1**), BF<sub>4</sub><sup>-</sup> (**2**), CF<sub>3</sub>SO<sub>3</sub><sup>-</sup> (**3**)]. The spectrum recorded for [Pt(4'-βNp-terpy)Cl]CF<sub>3</sub>SO<sub>3</sub> (presented in Figure 3.7) is representative of the spectra of [Pt(4'-βNp-



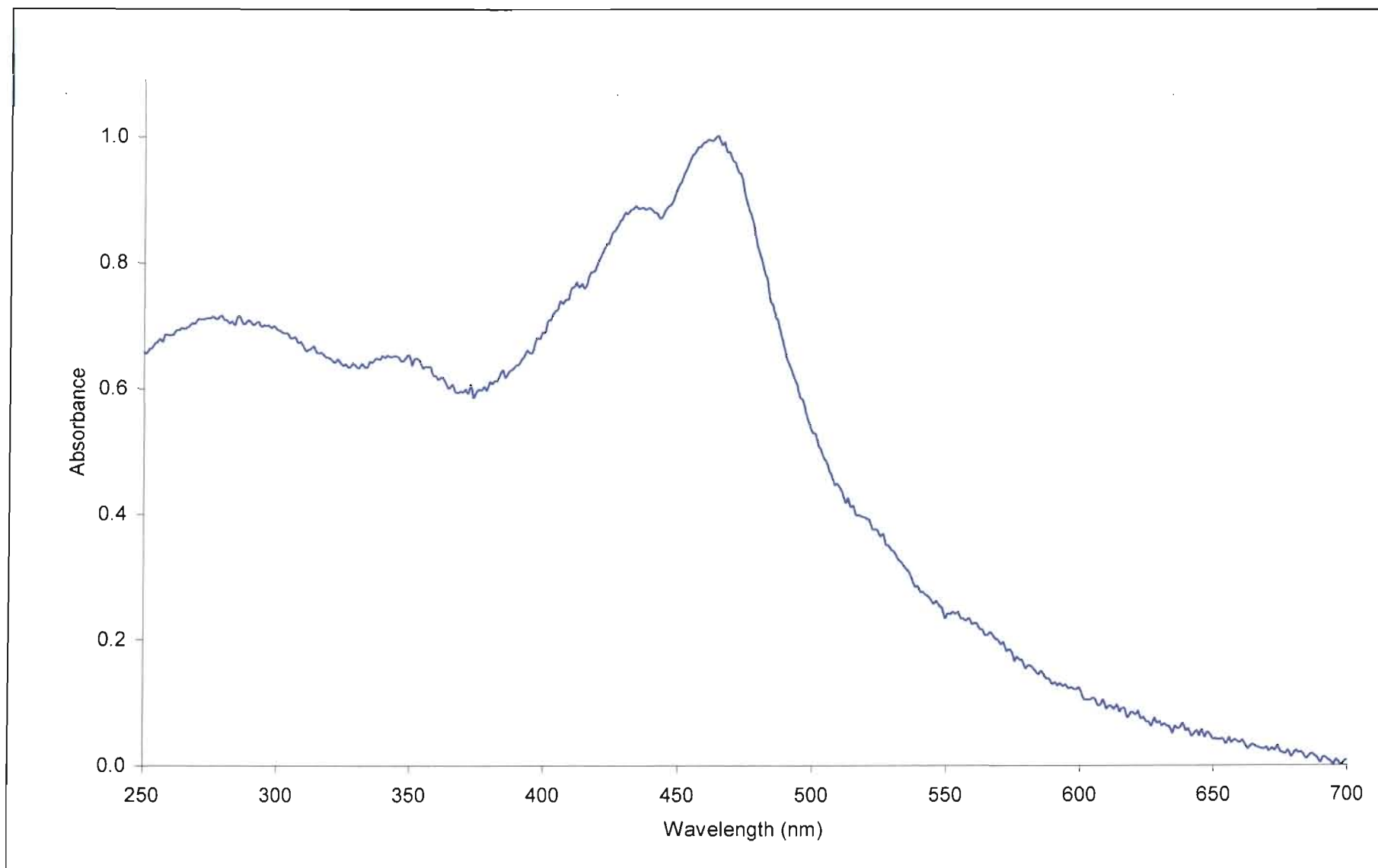


**Figure 3.7** Solid state absorption spectrum of  $[Pt(4'\text{-}\beta\text{Np-terpy)Cl]CF}_3\text{SO}_3$  recorded at 298 K.

terpy)Cl]SbF<sub>6</sub> and [Pt(4'-βNp-terpy)Cl]BF<sub>4</sub> and this discussion therefore applies to those salts as well. A summary of the solid state absorption maxima is compiled in Table 3.13 at the end of this chapter. A prominent absorption maximum is found at *ca.* 460 nm which is assigned to a monomeric MLCT absorption by analogy with the absorption band recorded at 411 nm in fluid solution (*vide supra*). (The lower energy at which the band occurs in the solid state compared to the fluid absorption described previously is attributed to stabilisation brought about by the lack of any solvent effect.) This band is independent of the counterion, consistent with its association with the monomeric luminophore {*viz.* [Pt(4'-βNp-terpy)Cl]<sup>+</sup>}.

The solid state emission behaviour of the three platinum salts [Pt(4'-βNp-terpy)Cl]X [X<sup>-</sup> = SbF<sub>6</sub><sup>-</sup> (**1**), BF<sub>4</sub><sup>-</sup> (**2**), CF<sub>3</sub>SO<sub>3</sub><sup>-</sup> (**3**)] is essentially similar and the emission of the triflate salt, [Pt(4'-βNp-terpy)Cl]CF<sub>3</sub>SO<sub>3</sub>, (shown in Figure 3.8) will form the basis of this discussion. Spectral data for the solid state emission of all three salts are presented in Table 3.13 at the end of this chapter.

At ambient temperatures the solid state emission spectrum of [Pt(4'-βNp-terpy)Cl]CF<sub>3</sub>SO<sub>3</sub> consists of a vibrationally structured band having three fairly well defined progressions. The 0-0 transition occurs at 578 nm with subsequent maxima at 621 and *ca.* 670 nm and has an emission lifetime of 390 ns. Reducing the temperature to 80 K has a startling effect on the emission exhibited by the salts. Below 240 K a new structured emission of lower energy gradually begins to appear at the expense of the room temperature emission; this lower energy emission has maxima at 612, 674 and 740 nm (see Figure 3.9). Altering the excitation wavelength between 450 and 560 nm has no effect on the emission profile either at 280 or at 80 K. The luminescent lifetime of emission at 80 K is significantly longer than that at ambient temperatures and was found to be *ca.* 4 μs.

The similarity of the room temperature solid and solution emission spectra strongly suggests that the origin of the room temperature emission in the solid state is the same as that in solution. Hence the room temperature solid state luminescence of the three platinum salts [Pt(4'-βNp-terpy)Cl]X [X<sup>-</sup> = SbF<sub>6</sub><sup>-</sup> (**1**), BF<sub>4</sub><sup>-</sup> (**2**), CF<sub>3</sub>SO<sub>3</sub><sup>-</sup> (**3**)] is also ascribed to relaxation from an excited state in which there is configurational mixing between states of <sup>3</sup>IL, <sup>3</sup>MLCT

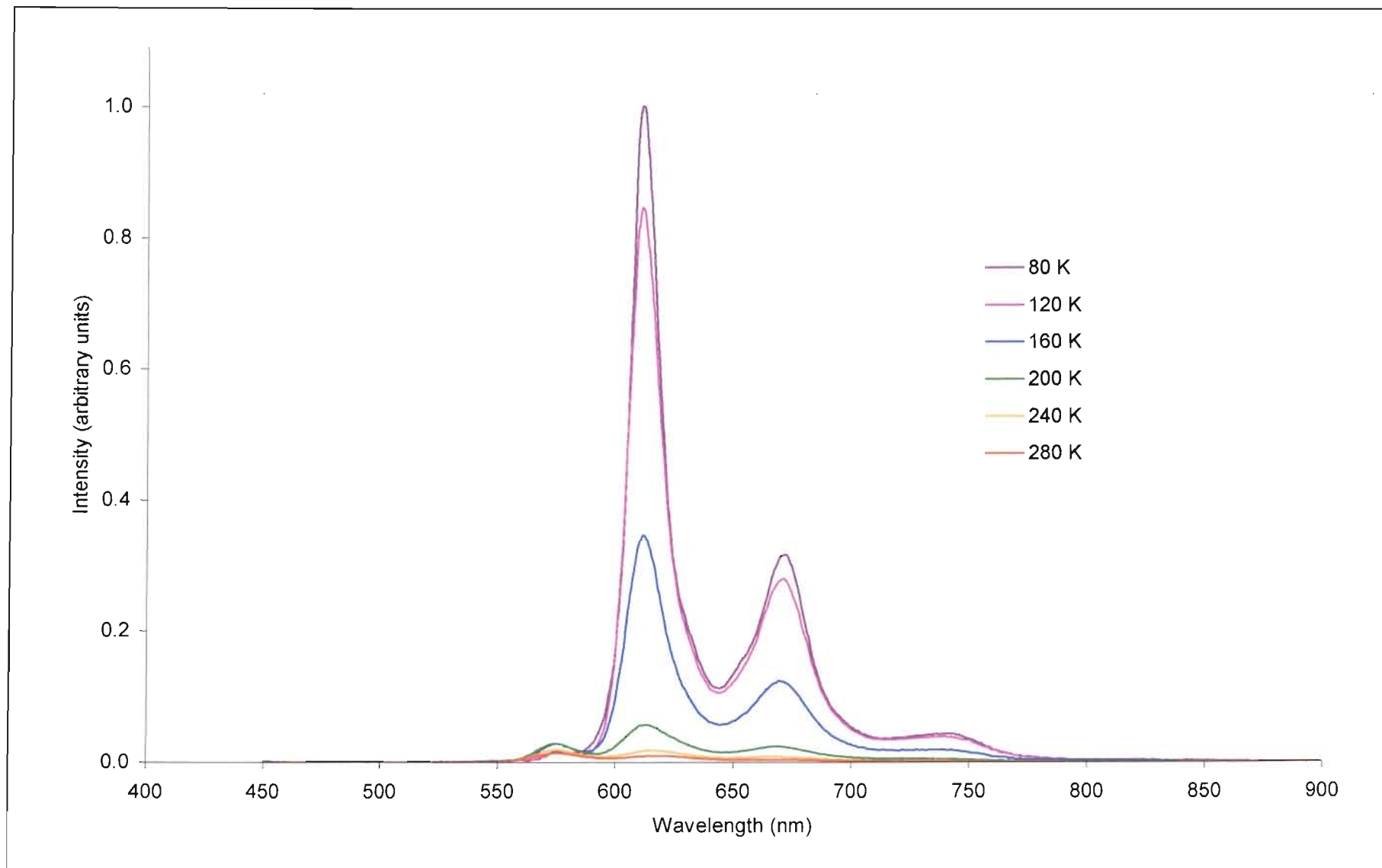


**Figure 3.8** Solid state emission spectra of  $[Pt(4'\text{-}\beta\text{Np-terpy)Cl]CF}_3\text{SO}_3$ .

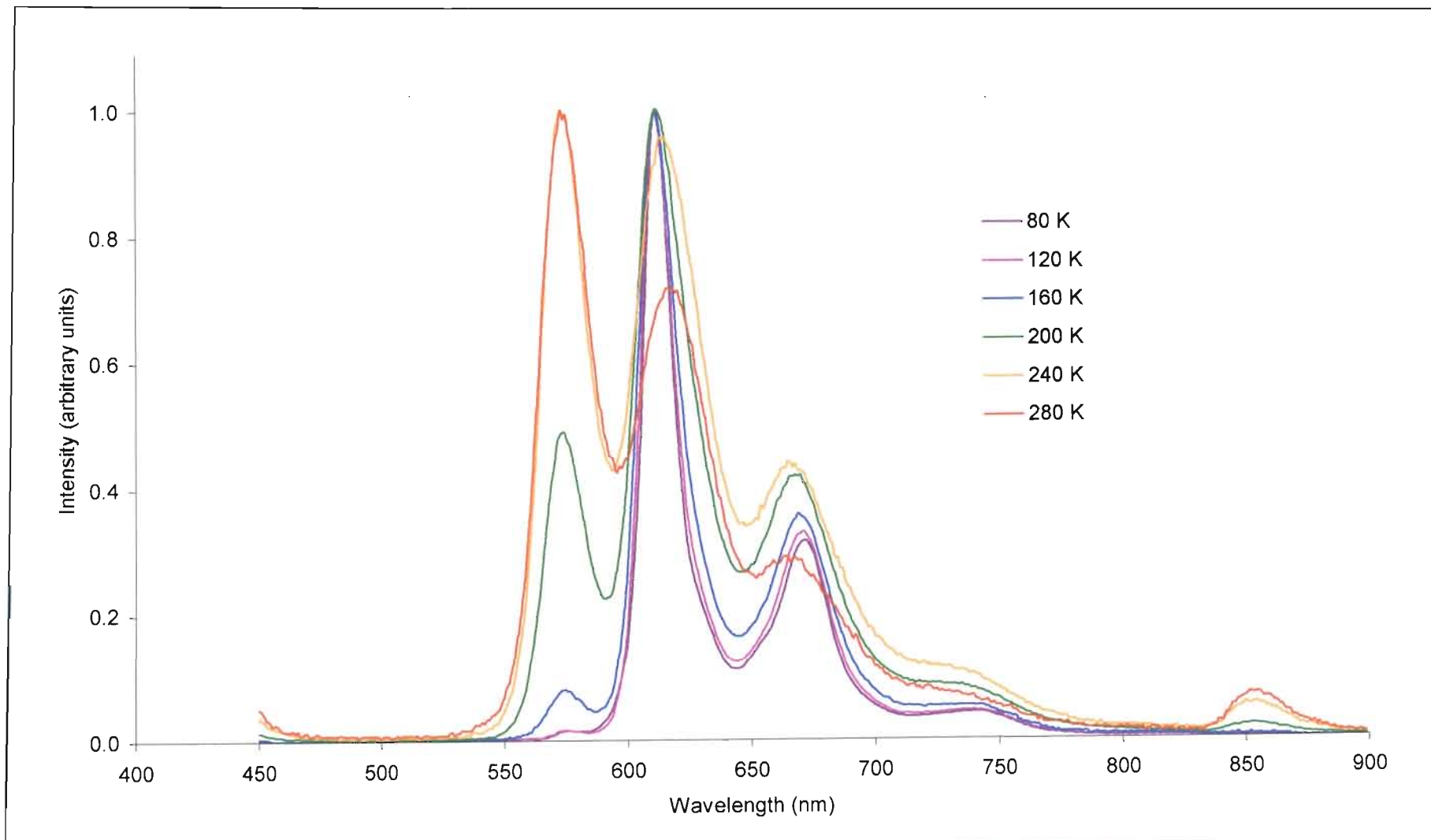


**Figure 3.9** Solid state emission spectra of  $[Pt(4'\text{-}\beta\text{Np-terpy)Cl]CF}_3\text{SO}_3$   
(Intensities adjusted to achieve equal maxima.)

and  $^3\text{ILCT}$  character. We note that the lifetimes are lower than in fluid solution but are nevertheless consistent with the triplet assignments. Given the obvious similarity of the fluid and solid emission it follows that the  $[\text{Pt}(4'\text{-}\beta\text{Np-terpy})\text{Cl}]^+$  luminophores exist as isolated monomers at room temperature in the solid state.

The basic features of the low temperature solid emission are the same except that the emission is at lower energies (*cf.* 580 vs 545 nm). This suggests that the same assignment of mixed  $^3\text{IL}$ ,  $^3\text{MLCT}$  and  $^3\text{ILCT}$  character applies *i.e.*, at 80 K the emission remains monomeric in nature. We now have to address the issue of a reduction in energy as the temperature is reduced. A possible explanation is that the cations adopt a more planar conformation as the temperature is reduced. To be precise, the inevitable compression of the unit cell volume that accompanies cooling of a crystal, could force the  $4'\text{-}\beta\text{Np}$  group closer to coplanarity with the terpyridyl moiety. Such a conformational change would lead to a reduction in the energy of the ligand acceptor  $\pi^*$ -orbital due to the more extensive electron delocalisation over the luminophore. It is proposed that the greater delocalisation alters the admixture of states contributing to the configurationally mixed state. Specifically, a stronger ligand-centred contribution results, that is manifested in the prominent structure displayed by the band at 80 K and the shift to lower energies. It is important to emphasise that, though plausible, this explanation must be regarded as speculation, given the absence of crystal structure determinations over the measured temperature range of 80 - 280 K.

### **3.2.2 [Pt(4'-*m*Biph-terpy)Cl]X [X<sup>-</sup> = SbF<sub>6</sub><sup>-</sup> (4), BF<sub>4</sub><sup>-</sup> (5), CF<sub>3</sub>SO<sub>3</sub><sup>-</sup> (6)]**

**{where 4'-*m*Biph-terpy = 4'-(*meta*-biphenyl)-2,2':6',2''-terpyridine}**

#### **3.2.2.1 Synthesis and characterisation of [Pt(4'-*m*Biph-terpy)Cl]X [X<sup>-</sup> = SbF<sub>6</sub><sup>-</sup> (4), BF<sub>4</sub><sup>-</sup> (5), CF<sub>3</sub>SO<sub>3</sub><sup>-</sup> (6)]**

Coordination of the 4'-(*m*-biphenyl)-2,2':6',2''-terpyridine (4'-*m*Biph-terpy) ligand to platinum(II) followed the same procedure as that used for the coordination of the 4'-( $\beta$ -naphthyl)-2,2':6',2''-terpyridine ligand (4'- $\beta$ Np-terpy). A chloride group is abstracted from  $[\text{Pt}(\text{PhCN})_2\text{Cl}_2]$  by refluxing it overnight in acetonitrile in the presence of an equivalent of the

appropriate silver salt. Silver chloride precipitates as an off-white solid which is filtered off once reflux is complete and the filtrate is then added to an equimolar amount of 4'-*m*Biph-terpy. The mixture is again refluxed overnight, the desired products precipitating from the reaction mixture as orange {[Pt(4'-*m*Biph-terpy)Cl]SbF<sub>6</sub>} and [Pt(4'-*m*Biph-terpy)Cl]CF<sub>3</sub>SO<sub>3</sub>} and yellow {[Pt(4'-*m*Biph-terpy)Cl]BF<sub>4</sub>} solids. Further precipitation is induced by partial solvent removal under reduced pressure. The product is filtered and washed on a frit with copious quantities of diethyl ether followed by small amounts of cold acetonitrile to give an air and moisture stable, analytically pure product. Recrystallisation from hot acetonitrile served as an additional purification step. Elemental analysis for C, H and N confirms empirical formulae corresponding to [Pt(C<sub>27</sub>H<sub>19</sub>N<sub>3</sub>)Cl]SbF<sub>6</sub> (**4**), [Pt(C<sub>27</sub>H<sub>19</sub>N<sub>3</sub>)Cl]BF<sub>4</sub> (**5**) and [Pt(C<sub>27</sub>H<sub>19</sub>N<sub>3</sub>)Cl]CF<sub>3</sub>SO<sub>3</sub> (**6**).

Proton NMR spectra of [Pt(4'-*m*Biph-terpy)Cl]SbF<sub>6</sub>, [Pt(4'-*m*Biph-terpy)Cl]BF<sub>4</sub> and [Pt(4'-*m*Biph-terpy)Cl]CF<sub>3</sub>SO<sub>3</sub> were recorded in DMSO-d<sub>6</sub>. The spectra are all essentially similar and that of [Pt(4'-*m*Biph-terpy)Cl]SbF<sub>6</sub> is discussed as representative of the other two salts. A listing of the chemical shifts is provided in the experimental section of this chapter. A prominent singlet appears at  $\delta$  8.76 and is ascribed to the H<sup>3,5'</sup> protons. Further upfield a signal at  $\delta$  8.60 is assigned to the degenerate protons in the H<sup>3</sup> and H<sup>3''</sup> positions. The remaining signals from protons on the terpyridyl fragment *viz.*, H<sup>4,4''</sup>, H<sup>5,5''</sup> and H<sup>6,6''</sup> are obscured by the overlapping signals of protons on the *m*-biphenyl moiety but can be distinguished by a COSY experiment and are found at  $\delta$  8.29, 7.65 and 8.38 respectively.

A solid state infrared spectrum of the complex as a KBr pellet was recorded and shows prominent peaks at 658 cm<sup>-1</sup> {[Pt(4'-*m*Biph-terpy)Cl]SbF<sub>6</sub>}, 1032 cm<sup>-1</sup> {[Pt(4'-*m*Biph-terpy)Cl]BF<sub>4</sub>} and 1268, 1155 and 1028 cm<sup>-1</sup> {[Pt(4'-*m*Biph-terpy)Cl]CF<sub>3</sub>SO<sub>3</sub>} associated with the anions. The remaining noteworthy peaks are summarised in Table 3.10 at the end of this chapter.

### 3.2.2.2 Structural characterisation of [Pt(4'-*m*Biph-terpy)Cl]SbF<sub>6</sub>.CH<sub>3</sub>CN (**4a**)

Yellow-orange crystals of the title compound suitable for X-ray diffraction studies were grown by dissolving the salt in acetonitrile and allowing the solvent to evaporate at ambient temperatures in air over a period of days. The crystals formed as light orange rectangular blocks that are stable for approximately two hours once removed from the mother liquor. After this time the crystals revert to a finely divided orange material like that isolated from the reaction mixture, presumably due to the loss of solvent from the crystal lattice. If the crystals are retained in the mother liquor they appear to be stable for a period of weeks. The data collection was performed at 173 K and within 24 h in order to prevent transformation to the finely divided material.

The compound crystallises in the centrosymmetric triclinic space group  $P\bar{1}$  with two formula units per unit cell. Thus each asymmetric unit consists of the cation (the luminophore), the anion and a solvent molecule. The unit cell dimensions and a list of other pertinent crystallographic data are given in Table 3.14 at the end of this chapter. Table 3.16 contains a list of interatomic distances and interatomic angles can be found in Table 3.17, also at the end of the chapter.

A perspective view of the cation including the atom labelling scheme is given in Figure 3.10. The coordination geometry around the platinum centre is essentially square-planar. Excluding the *m*-biphenyl unit, the greatest deviation by any non-hydrogen atom in the cation from the mean plane through the platinum, chlorine and three nitrogen atoms (henceforth referred to as the plane of the binding domain) is by carbon atom C2, which lies 0.12 Å from the plane. Distortions arise due to the geometric constraints imposed by the chelating terpyridyl ligand since it does not have an ideal tridentate bite for Pt(II).<sup>2</sup> This effect is manifested in a platinum-to-bridgehead-nitrogen (Pt-N2) distance of 1.933(3) Å, which is about 0.1 Å shorter than the Pt-N1 and Pt-N3 bond lengths of 2.030(3) and 2.027(4) Å respectively. Such a short bond between platinum and the nitrogen of the central pyridine ring leads to significant overlap between the nitrogen lone pair and the Pt  $\sigma$ -orbital.<sup>69</sup> The respective platinum-nitrogen bond lengths agree favourably with those of similar chloro(terpyridine)platinum(II) structures

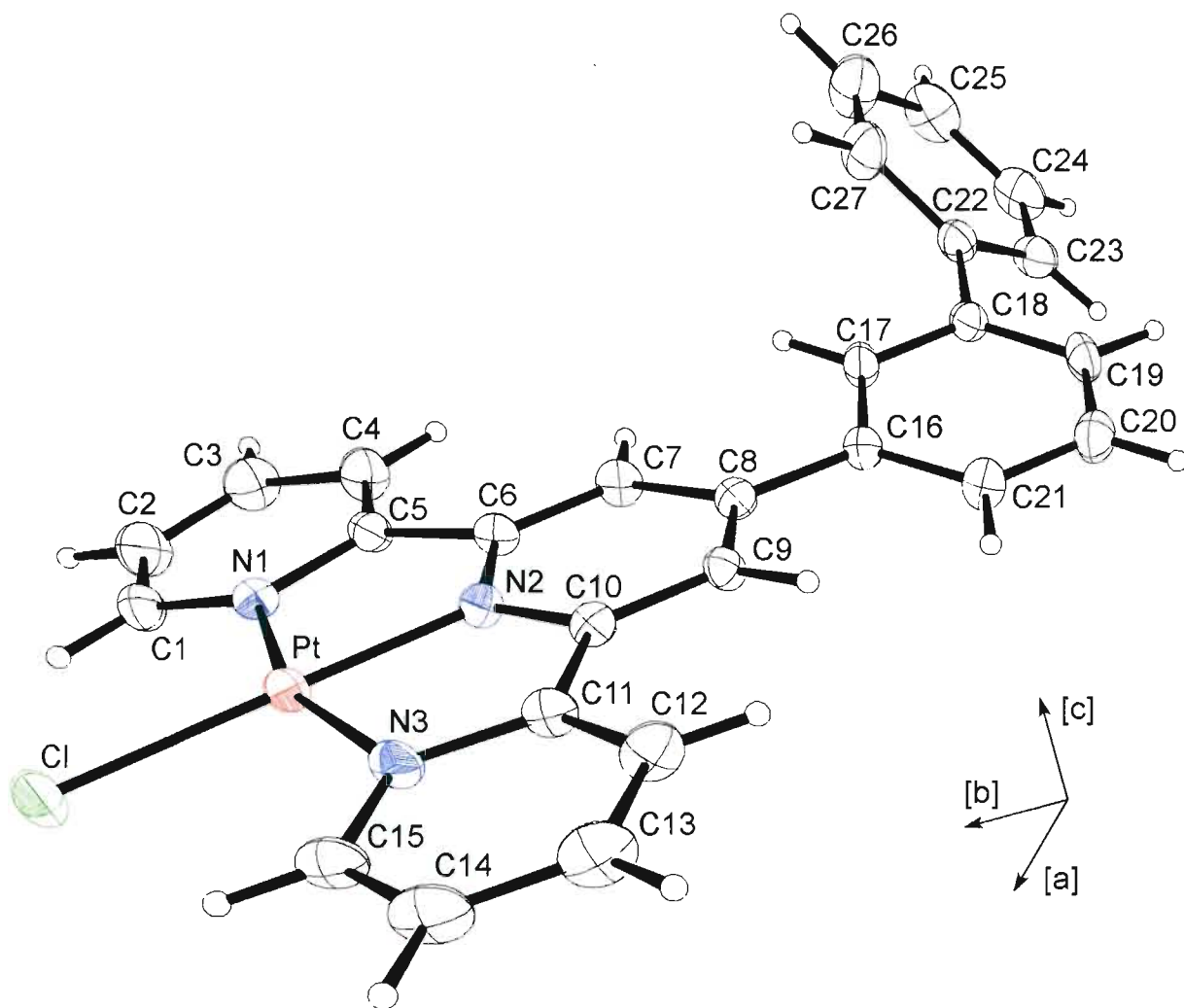


**Figure 3.10** Molecular geometry and numbering scheme used for the  $[Pt(4'-mBiph-terpy)Cl]^+$  cation.



reported in the literature. For comparison the data from three relevant literature examples are summarised in Table 3.2 to emphasise this point. The Pt-Cl bond length of 2.305(1) Å is also found to be in good agreement with the corresponding separations found in related structures.<sup>27, 29, 53</sup>

**Table 3.2** Bond distances at the binding domain of similar terpyridyl complexes of platinum(II) with a chloride ligand in the fourth coordination site.

COMPLEXES	Pt-N1 (Å) Pt-N3 (Å)	Pt-N2 <sup>a</sup> (Å)	Pt-Cl (Å)
[Pt(4'- <i>m</i> Biph-terpy)Cl]SbF <sub>6</sub> .CH <sub>3</sub> CN ( <b>4a</b> )	2.030(3) 2.027(4)	1.933(3)	2.305(1)
[Pt(terpy)Cl]CF <sub>3</sub> SO <sub>3</sub> <sup>27</sup>	2.018(5) 2.030(5)	1.930(4)	2.307(1)
[Pt(terpy)Cl]ClO <sub>4</sub> <sup>29</sup>	1.976(16) <sup>b</sup> 2.003(18) 2.033(15) 2.018(6)	1.952(15) 1.933(15)	2.302(7) 2.301(6)
[Pt(4'-Ph-terpy)Cl]BF <sub>4</sub> .CH <sub>3</sub> CN <sup>53</sup>	2.008(9) <sup>b</sup> 2.024(9) 2.040(9) 2.014(10)	1.929(10) 1.935(9)	2.296(3) 2.313(2)

(a) N2 is the central (bridgehead) nitrogen atom of the terpyridyl ligand.

(b) In these complexes the asymmetric unit consists of two distinct molecules.

The distortion of the coordination geometry around the platinum centre in order to accommodate the terpyridyl ligand is further emphasised by the bond angles subtended at the platinum centre. Instead of the ideal 90 °, distortions reduce the N1-Pt-N2 and N3-Pt-N2 angles to 80.9(2) and 80.7(2) ° respectively. Once again these values compare well with corresponding angles reported for similar structures (see Table 3.3).

**Table 3.3** Distortion from ideal square-planar coordination geometry as indicated by angles between Pt-N bonds subtended at the platinum centre.

COMPLEXES	N1-Pt-N2 <sup>a</sup> (°)	N2-Pt-N3 <sup>a</sup> (°)
[Pt(4'- <i>m</i> Biph-terpy)Cl]SbF <sub>6</sub> .CH <sub>3</sub> CN ( <b>4a</b> )	80.9(2)	80.7(2)
[Pt(terpy)Cl]CF <sub>3</sub> SO <sub>3</sub> <sup>27</sup>	81.1(2)	80.8(1)
[Pt(terpy)Cl]ClO <sub>4</sub> <sup>29</sup>	82.0(4) <sup>b</sup>	80.6(4)
	80.7(4)	80.9(4)
[Pt(4'-Ph-terpy)Cl]BF <sub>4</sub> .CH <sub>3</sub> CN <sup>53</sup>	81.9(6) <sup>b</sup>	81.8(7)
	79.8(6)	81.4(6)

(a) N2 is the central (bridgehead) nitrogen atom of the terpyridyl ligand.

(b) In these complexes the asymmetric unit consists of two distinct molecules.

Coordination to platinum seems to result in a slight shortening of the bonds linking the pyridyl rings *viz.*, C5-C6 and C10-C11 which have lengths of 1.474(6) and 1.475(5) Å respectively compared to the corresponding bonds in the free terpyridine {1.49(1) Å}<sup>153</sup> and uncoordinated 4'-phenyl-terpyridine {1.49(1) Å}<sup>138</sup> ligands. This is in spite of the fact that tridentate coordination to the metal necessitates a *cis-cis* conformation of pyridyl rings as opposed to the less sterically interacting *trans-trans* conformation typical of uncoordinated terpyridyl ligands.<sup>138, 153 - 156</sup>

Steric interactions between the phenyl rings are not influenced by coordination and hence any steric repulsions can be reduced by a twist about the C8-C16 and C18-C22 interannular bonds. (The lengths of these carbon-carbon bonds are 1.487(5) and 1.486(6) Å for C8-C16 and C18-C22 respectively.) The rotation about the interannular bonds is balanced by two counteracting factors *viz.* the need to minimise steric interactions and the need to maximise  $\pi$ -conjugation by promoting coplanarity.<sup>53, 138</sup> As a result the dihedral angle formed between the first (*meta*-substituted) phenyl ring (C16 - C21) and the plane of the binding domain is 14.7(1)°. The non-bonded separations between the protons of this phenyl ring (C16 - C21) and the protons of the central pyridine ring are both *ca.* 2.05 Å. In the structure described here the rotation of the first phenyl ring is also influenced by the way in which the terminal phenyl ring (C22 - C27) is accommodated in the rest of the lattice. The dihedral angle of the terminal phenyl ring

with the first phenyl ring is  $38.3^\circ$  resulting in a non-bonded proton separation for H19...H27 and H17...H23 of 2.30 and 2.34 Å respectively.

The luminophores pack face-to-face in parallel layers in the crystal. Figure 3.11 shows five cations packed in adjacent layers. Molecules in adjacent layers are related by a centre of symmetry and hence the co-planar portions of the molecules are parallel to those on the neighbouring level. In each level the luminophores are arranged head-to-tail in rows at an angle of  $2.94(1)^\circ$  to the Pt-Cl bond. The plane on which the luminophores lie (defined by the mean plane of the platinum atoms in each level) slopes gently and is inclined at  $2.74(1)^\circ$  to the plane of the binding domain of each molecule. Luminophores are shielded from luminophores in adjacent rows of the same level by interposing hexafluoroantimonate anions and solvent molecules. In this arrangement each luminophore is surrounded by four nearest neighbours, labelled A, B, C and D as shown in Figure 3.11.

Of the four nearest neighbours, only one (A) packs in such a way as to allow for a intermolecular metal-metal interaction. The luminophores thus pack as metal-metal dimers throughout the crystal. The interaction of a luminophore with each of its four closest neighbours will now be discussed.

The luminophore at A is related to the central luminophore by a centre of symmetry situated midway along the [c]-axis. As a result the molecules pack face-to-face and in a head-to-tail fashion. The Pt-Cl and Pt-N2 bonds of the adjacent molecules are eclipsed with a Pt-Cl...Pt'-N2' torsion angle of  $0.14(1)^\circ$ . The spacing between the mean planes defined by the binding domain of each molecule is  $3.29(1) \text{ \AA}$ . This is within the limit of intermolecular  $\pi$ - $\pi$  interactions<sup>56</sup>, although direct overlap in this case is limited to orbitals of the C1, C2...C14', C15' carbon atoms of the outer pyridine rings (see Figure 3.12). Of greater significance to the interactions of the luminophore with its counterpart in position A is the proximity of the two metal centres. As can be seen in Figure 3.12, which is viewed normal to the plane of the binding domain, the metal atom  $d_{z^2}$ -orbitals do not overlap directly although the direct Pt...Pt distance is  $3.356(2) \text{ \AA}$ . This is well within the upper limit of  $3.554 \text{ \AA}$  proposed by Gray *et al.* for a significant  $d_{z^2}(\text{Pt})\cdots d_{z^2}(\text{Pt}')$  interaction.<sup>157</sup> The slight lateral offset of *ca.*  $0.66 \text{ \AA}$  would

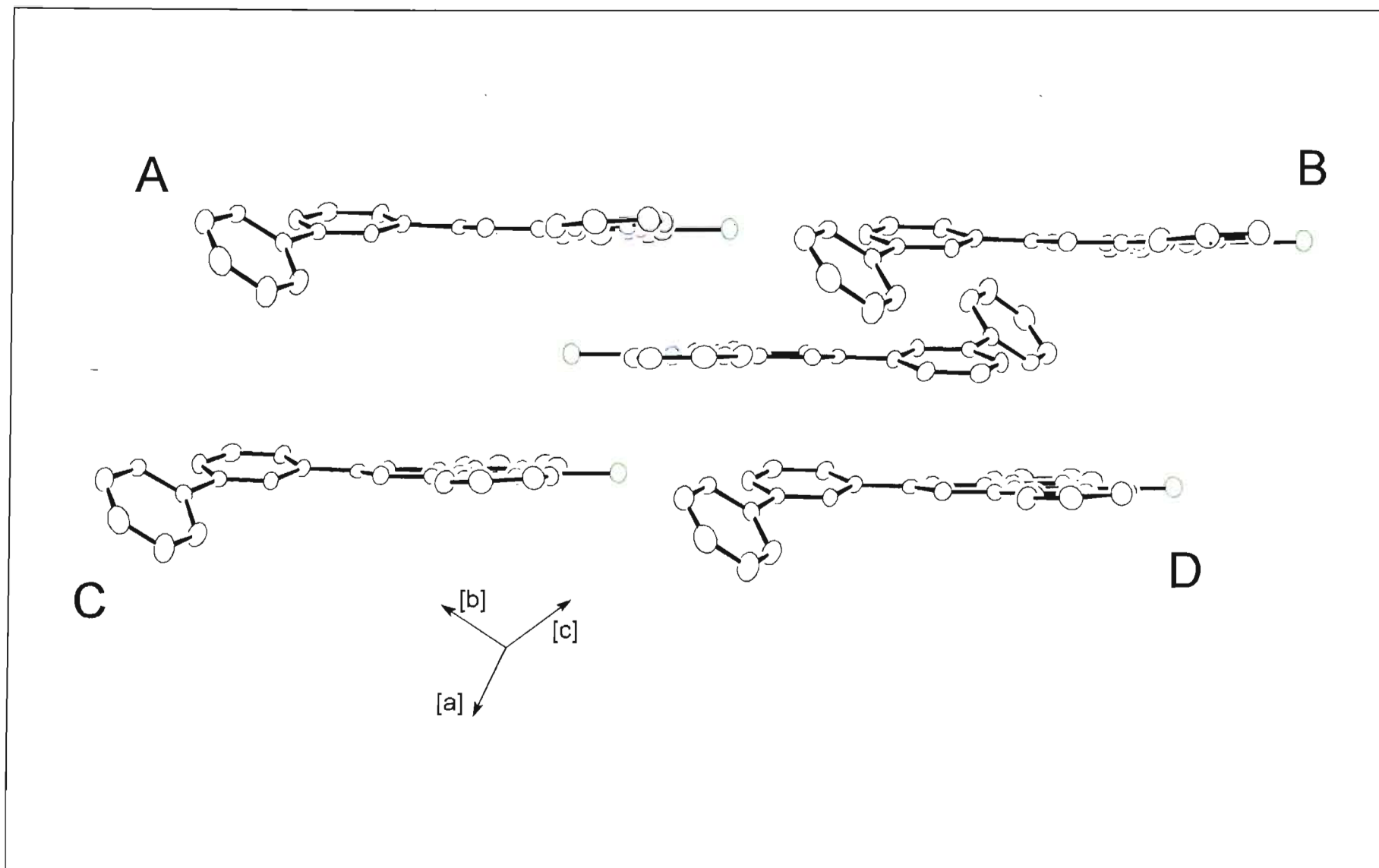


**Figure 3.11** View of the  $[Pt(4'-mBiph-terpy)Cl]^+$  cation with each of its four nearest neighbours in positions labelled A, B, C and D.

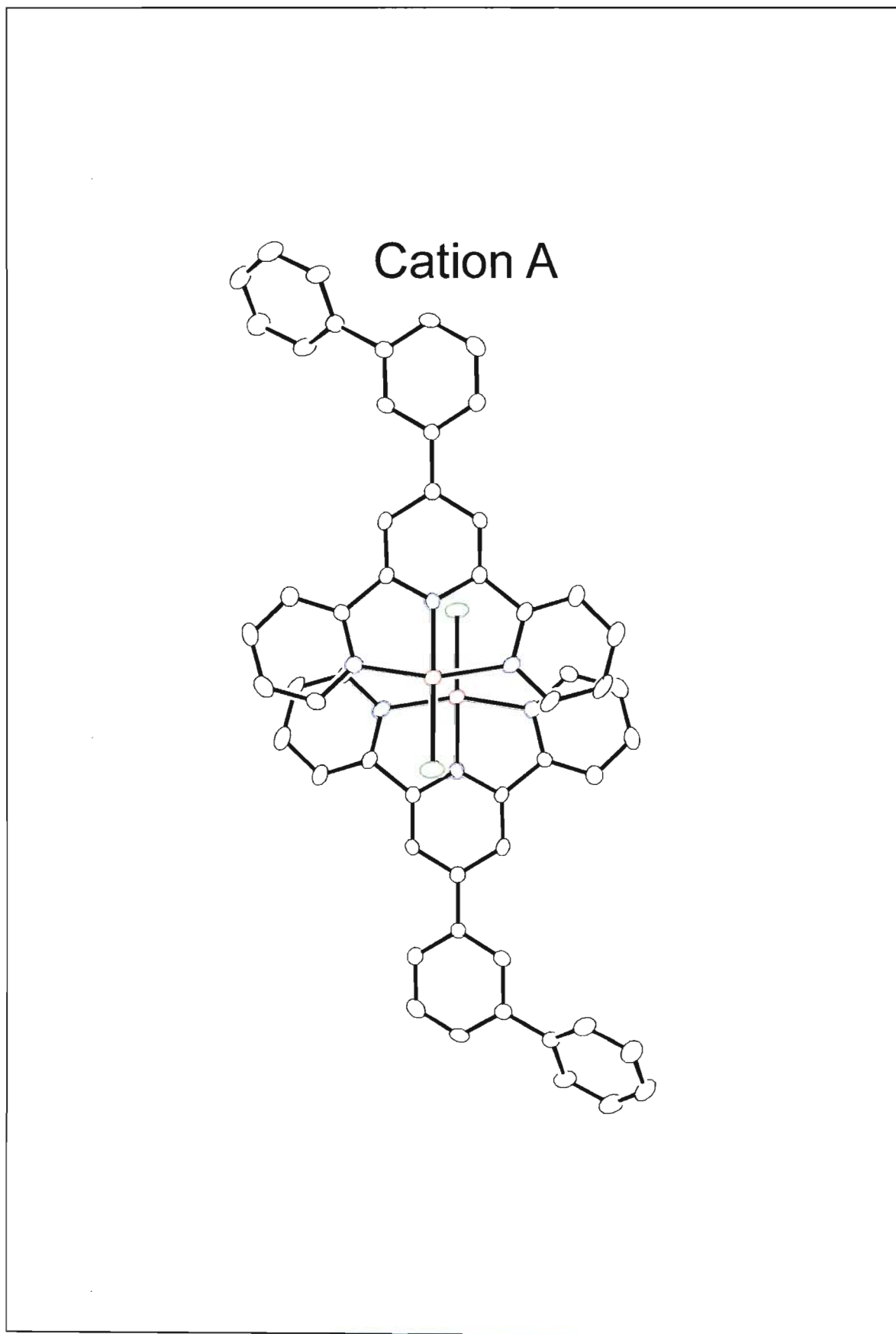


**Figure 3.12** *Overlap of a  $[Pt(4'-mBiph-terpy)Cl]^-$  luminophore with its counterpart in position A.*

detract from the extent of intermolecular metal orbital interaction, although it still seems to be of sufficient significance to promote the close metal-metal packing between these two [Pt(4'-*m*Biph-terpy)Cl]<sup>+</sup> units. It is these close metal-metal contacts that Gray and coworkers conclude to be the dominant factor in determining the formation of linear chains<sup>157</sup>, and clearly this determinant is also at work here in facilitating the type of interaction each luminophore has with its counterpart in position A. It is also this association of each luminophore with one of four of its closest neighbours which leads to the description of the solid as consisting of packed dimeric pairs, termed a “dimer structure” by Miskowski and Houlding.<sup>30</sup>

Cation B is related to the central luminophore by a centre of symmetry at the centre of the unit cell. As can be seen in Figure 3.13 a twist about the C8-C16 bond directs the biphenyl moiety of each luminophore towards the plane of the other. This steric intrusion is accommodated by the biphenyl fragments “pointing” away from each other due to the centre of symmetry by which they are related. As a result the cations related in this way have the shortest intermolecular separation of the four possible interactions with the mean planes defined by the binding domains lying just 2.95(1) Å apart (Figure 3.13). This is again well within the limit of intermolecular  $\pi$ - $\pi$  interactions although contact is limited to carbon atoms C16 and C21. Since the interactions are so limited the close packing is probably more as a consequence of the way in which the biphenyl fragments are accommodated by fitting into the cavity behind the biphenyl rings on the opposing molecule.

Cation C is related to the central cation by a centre of symmetry situated at the centre of the [ac]-face of the unit cell. The interplanar spacing of the two mean planes defined by the binding domain is 3.24(1) Å (Figure 3.14). There is however no direct overlap between the luminophores and it is unlikely that they interact in any way.

Lastly, each luminophore has a nearby counterpart in the position labelled D (the overlap is depicted in Figure 3.15) which is related by a centre of symmetry located at the centre of the [bc]-face of the unit cell. The average planes defined by the respective binding domains are 3.58(1) Å apart. The aromatic portions of the molecules are overlaid at a slight lateral offset, in accord with rules set out by Hunter and Sanders on the nature of  $\pi$ - $\pi$  interactions.<sup>56</sup>

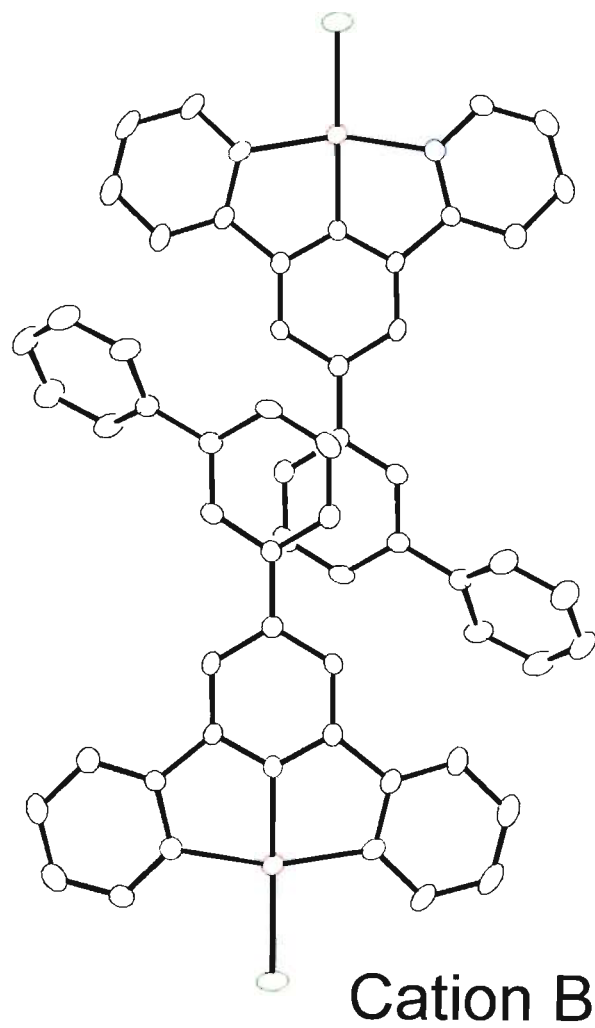


**Figure 3.13** *Overlap of a  $[Pt(4'-mBiph-terpy)Cl]^+$  luminophore with its counterpart in position B.*

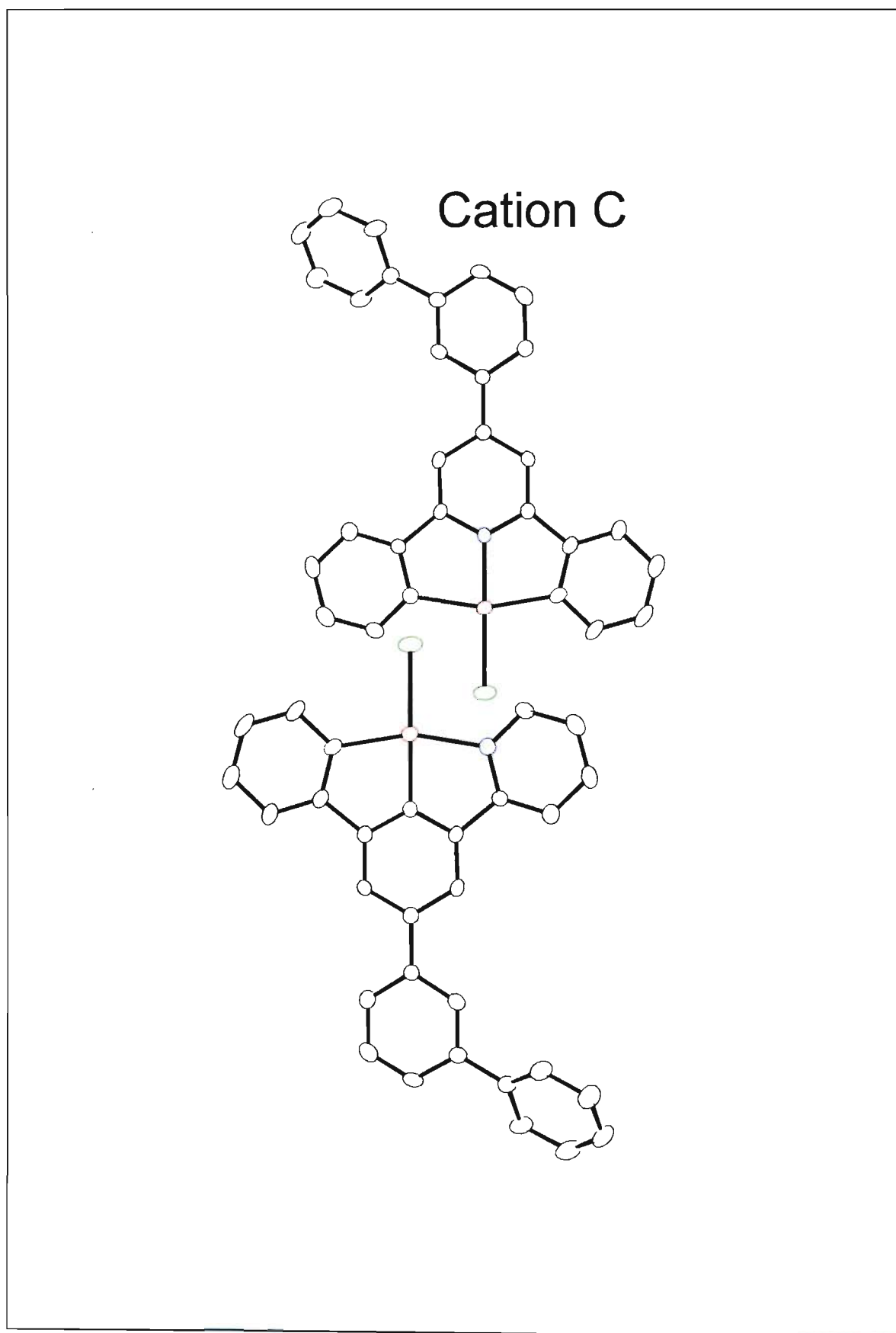


**Figure 3.14** *Overlap of a  $[Pt(4'-mBiph-terpy)Cl]^+$  luminophore with its counterpart in position C.*



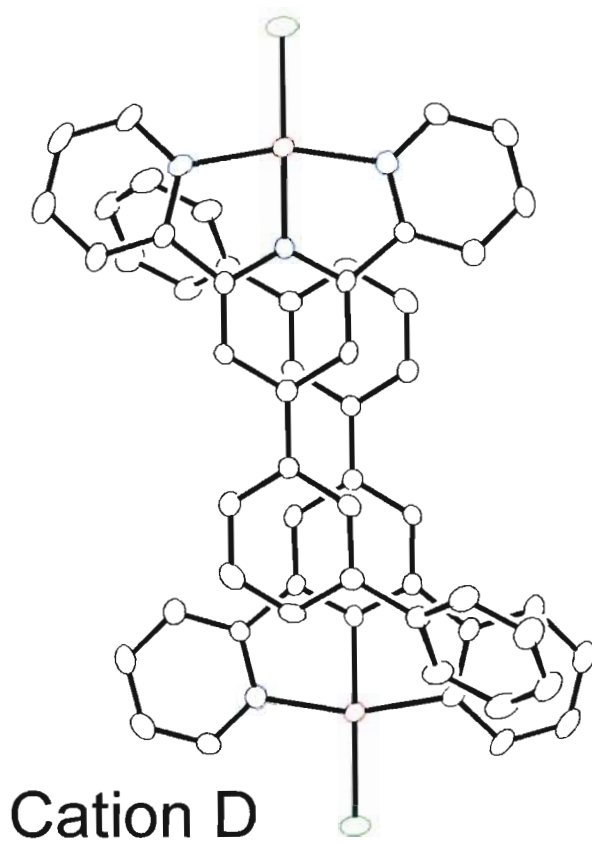


**Figure 3.15** *Overlap of a  $[Pt(4'-mBiph-terpy)Cl]^+$  luminophore with its counterpart in position D.*

Although overlap of the biphenyl fragment of one molecule with the terpyridyl system of the other appears to be more extensive than in the previous systems of overlap, the effects of this overlap are slightly offset by a twist about the C8-C16 interannular bond which directs the biphenyl fragment away from the adjoining molecule. This results in carbon atom C20 lying closest to the average plane of molecule D at a distance of 3.14(1) Å. Intermolecular  $\pi$ - $\pi$  interactions are probably weakened by the dihedral angles at which the phenyl rings are inclined which prohibits direct orbital overlap. This effect would be especially pronounced in the terminal phenyl ring which is inclined at a greater angle than the *meta*-substituted phenyl ring.

### 3.2.2.3 Photophysical studies on [Pt(4'-*m*Biph-terpy)Cl]X [ $X^- = \text{SbF}_6^-$ (4), $\text{BF}_4^-$ (5), $\text{CF}_3\text{SO}_3^-$ (6)]

#### *Fluid solution absorption spectroscopy*

Absorption spectra of [Pt(4'-*m*Biph-terpy)Cl]SbF<sub>6</sub>, [Pt(4'-*m*Biph-terpy)Cl]BF<sub>4</sub> and [Pt(4'-*m*Biph-terpy)Cl]CF<sub>3</sub>SO<sub>3</sub> were recorded in both acetonitrile and dichloromethane solution at ambient temperatures. The spectrum of [Pt(4'-*m*Biph-terpy)Cl]SbF<sub>6</sub> in acetonitrile is shown in Figure 3.16 with the absorption data obtained in both media being provided in Table 3.11 at the end of this chapter. The spectra are independent of the counterion and the spectrum of [Pt(4'-*m*Biph-terpy)Cl]SbF<sub>6</sub> is discussed as representative of the other two salts. Absorptions follow Beer's law in the 0.5 - 5 mM concentration range indicating that complete dissociation takes place in solution. In acetonitrile the spectrum consists of two intense absorption bands at 256 and 282 nm as well as a vibrationally structured band between 290 and 350 nm; the vibronic intervals of ~ 1400 - 1700 cm<sup>-1</sup> correspond to vibrational frequencies associated with the terpyridyl ligand. At lower energy there is a moderately intense band which attains its peak intensity at 404 nm and which also exhibits a shoulder at 384 nm. The absorption spectrum measured in dichloromethane exhibits a shift of the absorption bands to lower energies. This shift is especially pronounced for the peaks occurring at wavelengths longer than 370 nm.

The absorption behaviour of the [Pt(4'-*m*Biph-terpy)Cl]<sup>+</sup> chromophore follows a pattern

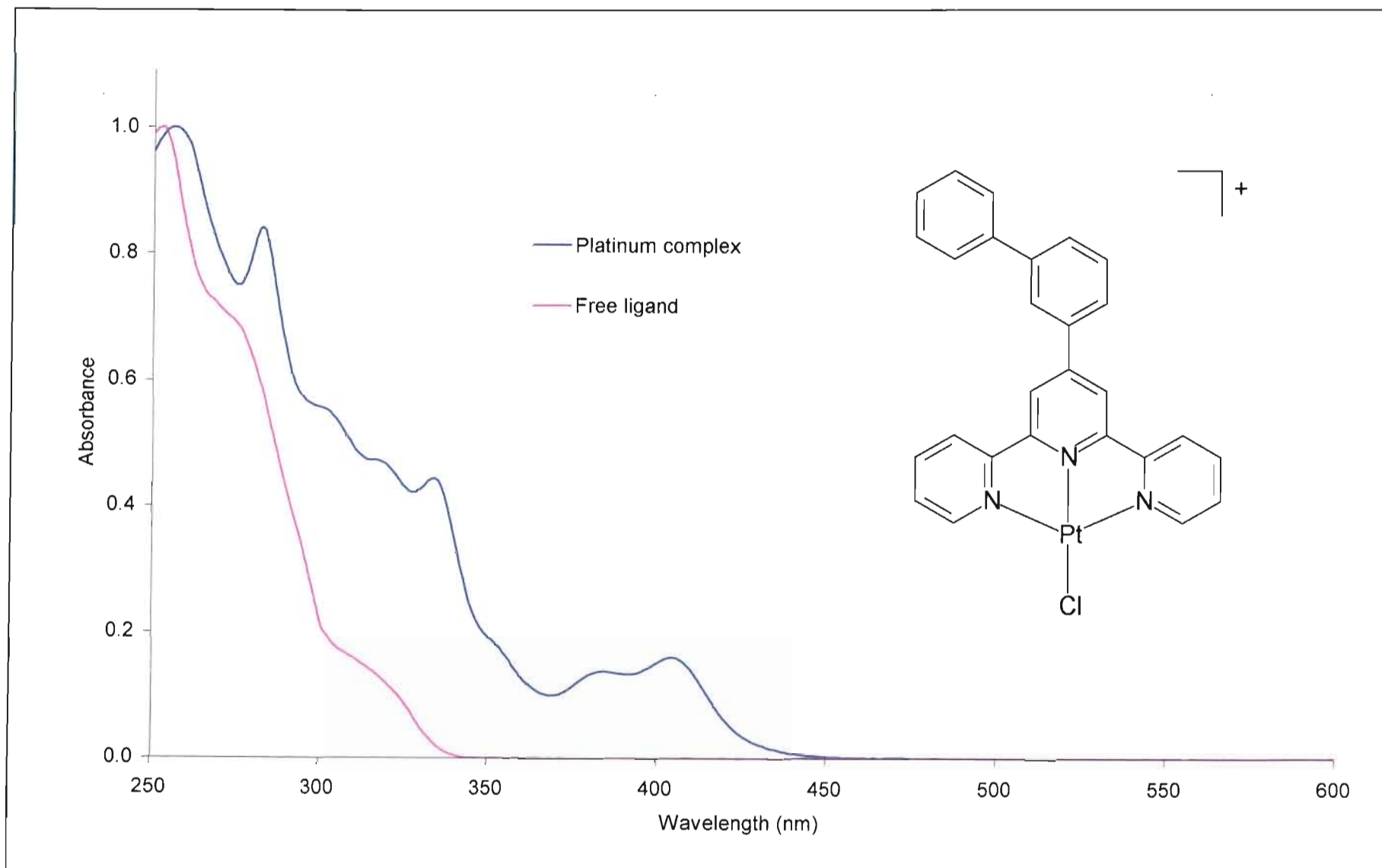


**Figure 3.16** Acetonitrile solution absorption spectra of the  $[Pt(4'-mBiph-terpy)Cl]^+$  and 4'-mBiph-terpy chromophores recorded at 298 K.

similar to that observed for  $[\text{Pt}(4'\text{-}\beta\text{Np-terpy})\text{Cl}]^+$  in solution (see section 3.2.1.2). Assignment of the absorption bands is therefore identical. The vibronically structured absorptions from 280 to 350 nm are assigned to  $^1\text{IL} (\pi\text{-}\pi^*)$  absorptions of the ligand 4'-*m*Biph-terpy. The high energy absorption at 256 nm is also assigned to transitions localised to the ligand as the energy of this band correlates with that of the most intense absorption of the free ligand.

The behaviour of the bands at wavelengths longer than 370 nm is consistent with absorptions due to charge-transfer transitions. In particular the absorptions are assigned to  $^1\text{MLCT}$  transitions.

Solid state absorption spectra have been recorded for each of the three salts with each salt showing its own particular set of absorbances. These measurements in the solid state will be discussed in conjunction with the emission seen for that salt (*vide infra*).

#### *Fluid solution emission spectroscopy*

A complete listing of all emission data measured both in solution and in the solid state is provided in Tables 3.11 and 3.12 respectively at the end of this chapter.

Measurements of the emission spectrum of  $[\text{Pt}(4'\text{-}m\text{Biph-terpy})\text{Cl}]^+$  in fluid solution at room temperature were made in acetonitrile and dichloromethane. No emission was detected on irradiation of a solution of  $[\text{Pt}(4'\text{-}m\text{Biph-terpy})\text{Cl}]^+$  in acetonitrile using excitation wavelengths of between 400 and 560 nm. The complex was however found to be emissive in deoxygenated dichloromethane and the spectrum of this emission is presented in Figure 3.4. The complex luminesces in a vibronically structured emission profile with the most intense band at highest energy (536 nm) with subsequent progressions at 570 and *ca.* 625 nm. The emission decay is mono-exponential and has a magnitude of 115 ns. Excitation matches absorption.

This emission behaviour is essentially identical to that of  $[\text{Pt}(4'\text{-Ph-terpy})\text{Cl}]^+$ <sup>31, 32</sup> and of a range of chloro(terpyridyl)platinum(II) complexes which have the terpyridyl ligand substituted in the 4'-position with both electron withdrawing (CN, SO<sub>2</sub>Me) and electron donating groups (SMe, NMe<sub>2</sub>).<sup>30</sup> In all these complexes emission in room temperature fluid solution has been

assigned to an excited state of mixed orbital parentage involving a combination of MLCT and IL ( $\pi$ - $\pi^*$ ) states and denoted a  $^3[(d,\pi) - \pi^*]$  transition. By analogy the solution emission of  $[\text{Pt}(4\text{'-}m\text{Biph-terpy})\text{Cl}]^+$  is therefore assigned to a  $^3[(d,\pi) - \pi^*]$  transition, which has its origin in a configurationally mixed state. The complete lack of emission from an acetonitrile solution containing the  $[\text{Pt}(4\text{'-}m\text{Biph-terpy})\text{Cl}]^+$  luminophore reinforces such an assignment since emission involving partial oxidation of the metal centre is vulnerable to solvent induced exciplex quenching.<sup>48</sup> Also consistent with the assignment are i) the vibrational structure with a spacing of between 1200 and 1400  $\text{cm}^{-1}$  and ii) the energy of the 0-0 progression that is too low for pure IL ( $\pi$ - $\pi^*$ ) transitions.<sup>37, 43</sup>

The  $[\text{Pt}(4\text{'-}Ph\text{-terpy})\text{Cl}]^+$  luminophore has an emission lifetime of 85 ns measured in dichloromethane that is not very different from the lifetime of 115 ns recorded in the same solvent for  $[\text{Pt}(4\text{'-}m\text{Biph-terpy})\text{Cl}]^+$ . Clearly the addition of a phenyl ring in the *meta*-position has little effect on the lifetime of the emitting state. These lifetimes are in stark contrast with the emission lifetimes of  $[\text{Pt}(4\text{'-}\beta\text{Np-terpy})\text{Cl}]^+$  and  $[\text{Pt}(4\text{'-}\alpha\text{Np-terpy})\text{Cl}]^+$  and of other large fused ring systems such as phenanthroline and pyrene<sup>32</sup> all of which are significantly greater than 10  $\mu\text{s}$  measured under the same conditions. The presence of a fused-ring substituent is associated with a significant lifetime enhancement brought about by prominent ILCT character in the excited state.<sup>32</sup> In the case of  $[\text{Pt}(4\text{'-}m\text{Biph-terpy})\text{Cl}]^+$  there is neither a particularly long emission lifetime nor a fused-ring substituent in the 4'-position and hence we do not believe that ILCT processes play any significant role in the emission of this complex.

#### *Glass emission spectroscopy*

The emission of  $[\text{Pt}(4\text{'-}m\text{Biph-terpy})\text{Cl}]^+$  in a dilute glass medium was studied by dissolution of  $[\text{Pt}(4\text{'-}m\text{Biph-terpy})\text{Cl}]\text{CF}_3\text{SO}_3$  in a DME {1:5:5 (v/v) DMF/MeOH/EtOH} solvent mixture with the measurements recorded in the rigid glass at 77 K. Emission from the hexafluoroantimonate and tetrafluoroborate salts is identical and no additional discussion will be provided. The emission behaviour of  $[\text{Pt}(4\text{'-}m\text{Biph-terpy})\text{Cl}]^+$  in a rigid glassy medium at 77 K is concentration dependent and very similar to that of  $[\text{Pt}(\text{terpy})\text{Cl}]^+$  and  $[\text{Pt}(4\text{'-}Ph\text{-terpy})\text{Cl}]^+$  recorded under similar conditions.<sup>29, 42</sup> In the 0.1 - 30  $\mu\text{M}$  concentration range {30  $\mu\text{M}$  constitutes the limiting solubility of  $[\text{Pt}(4\text{'-}m\text{Biph-terpy})\text{Cl}]\text{CF}_3\text{SO}_3$  in DME at ambient

temperatures} and with an excitation wavelength shorter than 440 nm, emission is in a vibronically structured band with the 0-0 transition at *ca.* 510 nm. Additional progressions occur at lower energy with the most intense band at 550 nm and a weaker band at 590 nm (see Figure 3.17). The Huang-Rhys factor (defined as  $I_{0-1}/I_{0-0}$ ) measured for the 30  $\mu\text{M}$  solution is *ca.* 2.3. Unfortunately, an accurate measurement of the emission lifetime could not be made. Raising the concentration to 30  $\mu\text{M}$  and using excitation wavelengths longer than 490 nm results in emission in a fairly narrow (fwhm  $\approx 2300\text{ cm}^{-1}$ ) structureless band with a maximum at 671 nm and with a luminescence lifetime of 1.9  $\mu\text{s}$ . The latter emission is exclusively present when an excitation wavelength longer than 540 nm is used. When the concentration is above 10  $\mu\text{M}$ , it is also possible to isolate a third luminescence by using an excitation wavelength of 470 nm. Emission is in a broad band (fwhm  $\approx 4100\text{ cm}^{-1}$ ) centred at  $\sim 600\text{ nm}$ . Each emission will now be discussed in turn. Relevant emission data are abridged in Table 3.1.

The high energy structured emission that develops at 510 nm is very similar in terms of energy to the monomeric emission exhibited by  $[\text{Pt}(4'\text{-Ph-terpy})\text{Cl}]^+$ .<sup>32, 42, 53</sup> By analogy and taking into account the assignment made in fluid solution for the 4'-*m*Biph-terpy derivative, emission is assigned to excitation of the monomer to a state of mixed orbital parentage, with contributions from IL and MLCT states, *i.e.*, a  $^3[(d,\pi) \leftarrow \pi^*]$  transition. The fact that the most intense vibrational progression is the 0-1 transition rather than the 0-0 transition could be a reflection of strong IL character of the excited state.<sup>21, 41</sup> This is however not reflected in the emission lifetime (of under 10  $\mu\text{s}$ ) which is similar to that of  $[\text{Pt}(\text{terpy})\text{Cl}]^+$  and  $[\text{Pt}(4'\text{-Ph-terpy})\text{Cl}]^+$ <sup>42</sup> and is certainly nowhere near that of 47  $\mu\text{s}$  recorded for  $[\text{Pt}(4'\text{-}\beta\text{Np-terpy})\text{Cl}]^+$  under the same conditions. The fact that  $[\text{Pt}(4'\text{-}m\text{Biph-terpy})\text{Cl}]^+$  emits at higher energy than  $[\text{Pt}(4'\text{-}\beta\text{Np-terpy})\text{Cl}]^+$ , and yet has a shorter emission lifetime, is in apparent violation of the energy gap law for radiationless transitions<sup>57</sup> which predicts that the opposite trend should be true. The explanation is linked simply to the dissimilar make-up of each state, with the excited state of  $[\text{Pt}(4'\text{-}\beta\text{Np-terpy})\text{Cl}]^+$  including ILCT character due to the presence of the easily ionisable fused-ring substituent.<sup>32</sup>

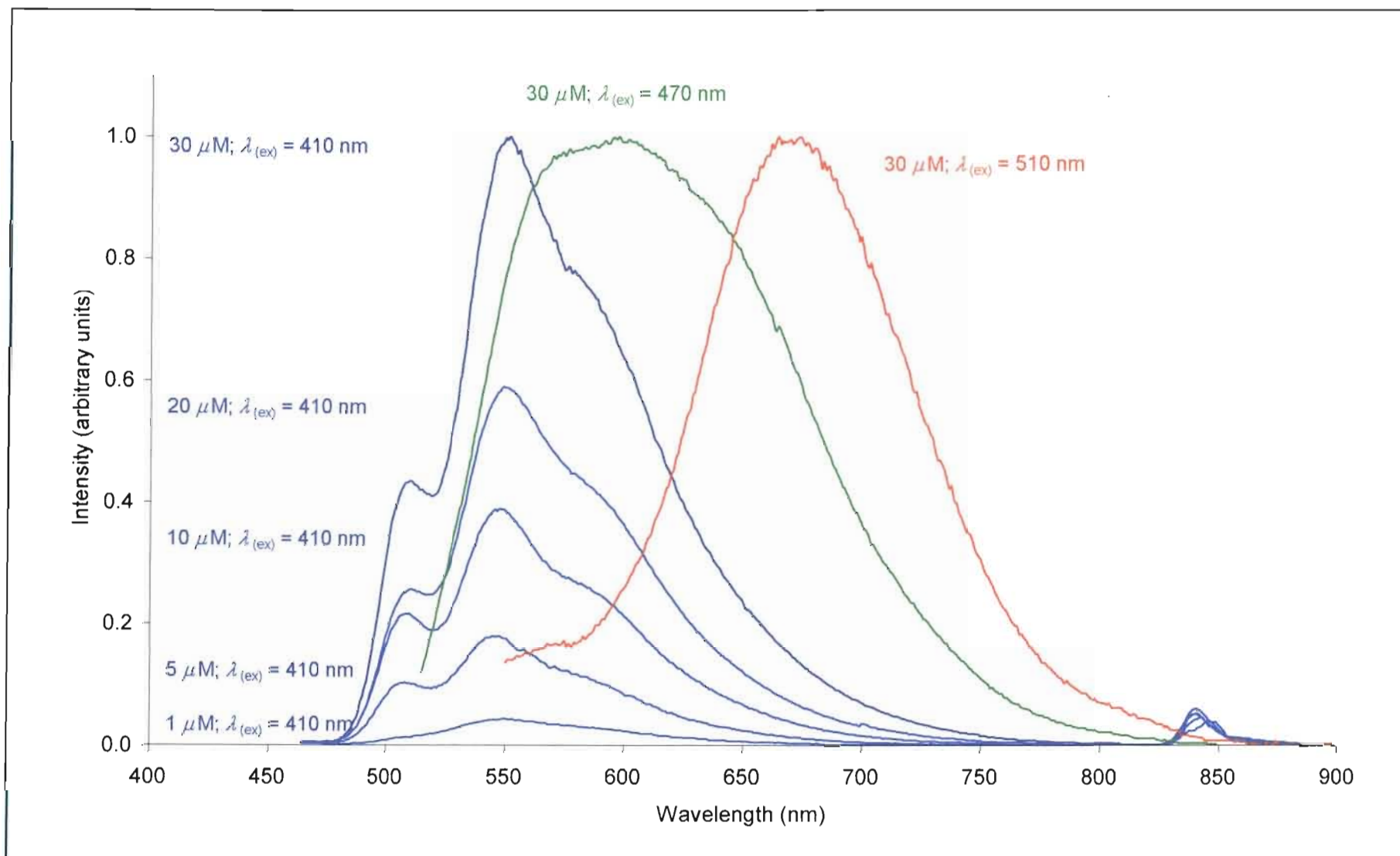


**Figure 3.17** Solution emission spectra of  $[Pt(4'-mBiph-terpy)Cl]^+$  recorded in DME glass at 77 K. (Intensities at different excitation energies adjusted to achieve equal maxima.)

Raising the concentration to at least 25  $\mu\text{M}$  and exciting at wavelengths longer than 490 nm, makes it possible to isolate emission from aggregated species in solution. By analogy with the emission of  $[\text{Pt}(4'\text{-Ph-terpy})\text{Cl}]^+$ <sup>42, 53, 32</sup> the structureless emission with  $\lambda_{\text{em}}(\text{max})$  at 670 nm is ascribed to a <sup>3</sup>MMLCT excited state arising from the direct overlap of platinum  $d_{z^2}$ -orbitals of the metal centres of neighbouring luminophores. The overlap necessary for this type of emission is possible for  $[\text{Pt}(4'\text{-}m\text{Biph-terpy})\text{Cl}]^+$ , as seen from the solvent supported crystal structure presented in section 3.2.2.2 (overlap with luminophores in position A). This emission is exclusively present if excitation is at wavelengths longer than 540 nm.

A point of difference between the 77 K glass emissions of  $[\text{Pt}(4'\text{-}\beta\text{Np-terpy})\text{Cl}]^+$  and  $[\text{Pt}(4'\text{-}m\text{Biph-terpy})\text{Cl}]^+$  is the presence of broad, structureless emission of intermediate energy centred at 600 nm when the solution concentration is above 10  $\mu\text{M}$  and an excitation wavelength of 470 nm is used. By analogy with the work of Gray *et al.* of a similar emission reported for  $[\text{Pt}(\text{terpy})\text{Cl}]^+$  recorded under similar conditions,<sup>29</sup> this emission is assigned to an excimeric excited state arising from the partial overlap of the organic fragments of adjacent molecules.

Excitation spectra of  $[\text{Pt}(4'\text{-}m\text{Biph-terpy})\text{Cl}]^+$  were recorded in a rigid glass at 77 K (see Figure 3.18) and these match absorption spectra recorded in fluid solution at ambient temperatures (*vide supra*). As for  $[\text{Pt}(4'\text{-}\beta\text{Np-terpy})\text{Cl}]^+$ , when the excitation is recorded in a high concentration glass solution and monitored at wavelengths longer than 610 nm the onset of a low energy band centred at *ca.* 500 nm in the excitation spectrum is observed. This band is ascribed to aggregative species in solution.

#### *Solid state absorption and emission spectroscopy*

All solid state emission data are condensed and presented in Table 3.13 at the end of this chapter. Unlike the complexes  $[\text{Pt}(4'\text{-}\beta\text{Np-terpy})\text{Cl}]\text{SbF}_6$  (**1**),  $[\text{Pt}(4'\text{-}\beta\text{Np-terpy})\text{Cl}]\text{BF}_4$  (**2**) and  $[\text{Pt}(4'\text{-}\beta\text{Np-terpy})\text{Cl}]\text{CF}_3\text{SO}_3$  (**3**) which share basic features in their solid state absorption and emission spectra, the photophysical behaviour from each of the three salts derived from the 4'-*m*Biph-terpy ligand, is distinct and the emissions from  $[\text{Pt}(4'\text{-}m\text{Biph-terpy})\text{Cl}]\text{SbF}_6$  (**4**),



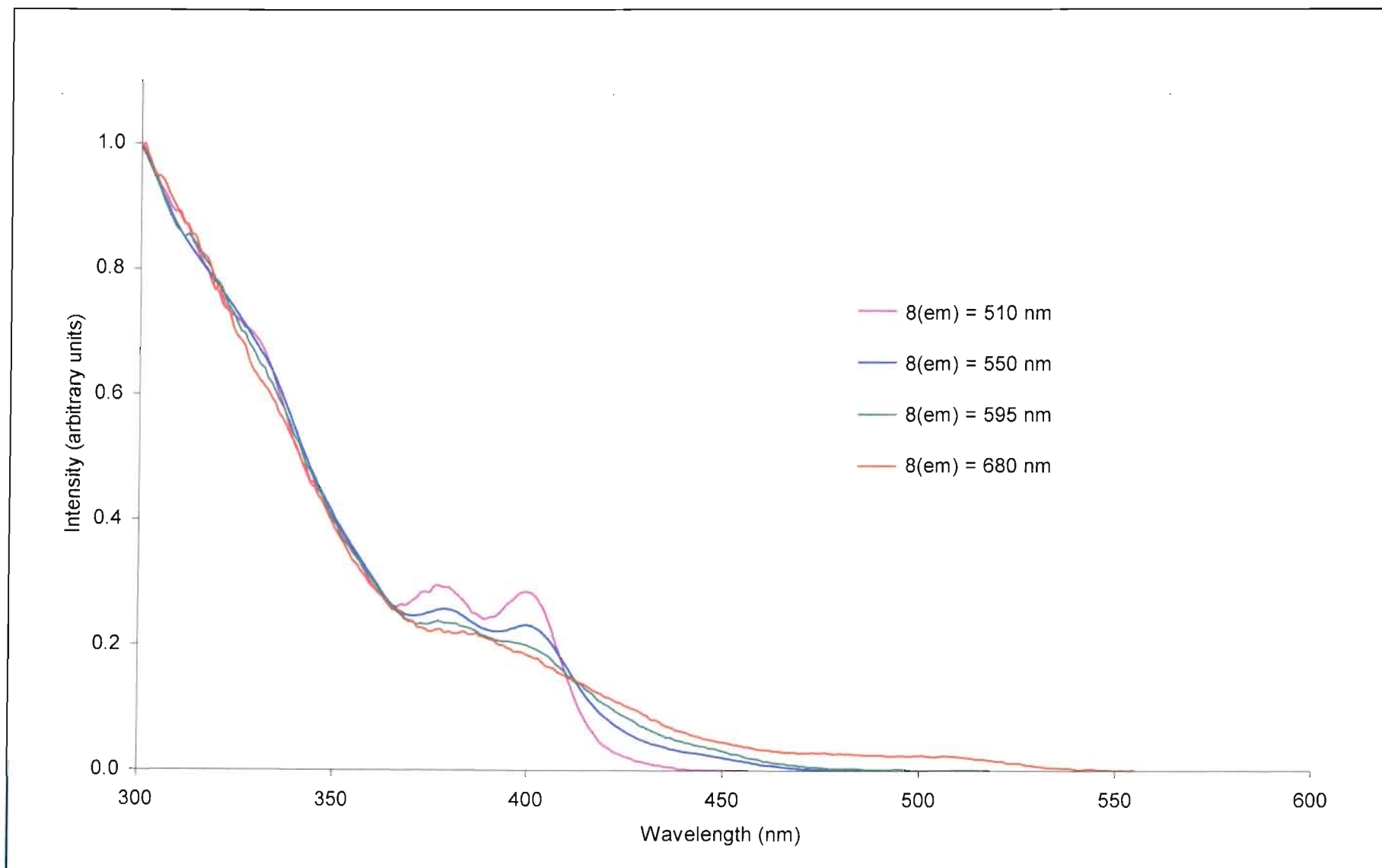


**Figure 3.18** Excitation spectra of  $[Pt(4'-mBiph-terpy)Cl]^+$  recorded in a  $30 \mu M$  DME glass at 77 K.

[Pt(4'-*m*Biph-terpy)Cl]BF<sub>4</sub> (**5**) and [Pt(4'-*m*Biph-terpy)Cl]CF<sub>3</sub>SO<sub>3</sub> (**6**) will each be discussed in turn.

The hexafluoroantimonate salt, [Pt(4'-*m*Biph-terpy)Cl]SbF<sub>6</sub>, exists in two forms. One is a pale yellow-orange solvated crystalline material with the formulation [Pt(4'-*m*Biph-terpy)Cl]SbF<sub>6</sub>·CH<sub>3</sub>CN for which the crystal structure was described in section 3.2.2.2. Of course the material also exists in its non-solvated form and each form gives a distinct luminescence. Emission from the latter form will be described first. In this case photophysical measurements were performed on the analytically pure, finely divided orange microcrystalline powder isolated after workup of the reaction mixture. Neither the elemental analysis nor the <sup>1</sup>H NMR spectroscopy experiments show any evidence for the inclusion of solvent in the material.

#### *Solid state absorption and emission spectroscopy of [Pt(4'-*m*Biph-terpy)Cl]SbF<sub>6</sub>*

A solid state absorption spectrum was recorded for [Pt(4'-*m*Biph-terpy)Cl]SbF<sub>6</sub> which shows its lowest energy absorption at 525 nm and a higher energy band at 443 nm. A solid state absorption spectrum was also recorded of the related salt, [Pt(4'-*m*Biph-terpy)Cl]TFPB which has the very large non-coordinating counterion tetrakis[3,5-(trifluoromethylphenyl)]borate (TFPB) in its outer coordination sphere. (The salt was made by anion metathesis of [Pt(4'-*m*Biph-terpy)Cl]SbF<sub>6</sub> in the presence of the sodium salt of TFPB.) Coulombic attraction would ensure that TFPB anions are interspersed between luminophores and the large size of the anion is expected to prevent any aggregation of [Pt(4'-*m*Biph-terpy)Cl]<sup>+</sup> luminophores in the solid state. Thus the solid state absorption of [Pt(4'-*m*Biph-terpy)Cl]TFPB should be free of any energy stabilisation brought about by interacting luminophores. Indeed the solid state absorption spectrum of [Pt(4'-*m*Biph-terpy)Cl]TFPB shows a single strong absorption maximum at *ca.* 435 nm, similar to the absorption at 443 nm of [Pt(4'-*m*Biph-terpy)Cl]SbF<sub>6</sub>. As a result of this similarity we assign the 443 nm absorption band of [Pt(4'-*m*Biph-terpy)Cl]SbF<sub>6</sub> to a CT transition of the monomer, an assignment also based in part on the energy of the band and by comparison with absorption recorded in fluid solution. Since the absorption spectrum of [Pt(4'-*m*Biph-terpy)Cl]TFPB shows no bands corresponding to the

absorption of  $[\text{Pt}(4\text{'-}m\text{Biph-terpy})\text{Cl}]\text{SbF}_6$  at 525 nm, it is suggested that this band indicates the presence of stabilised energy levels brought about by aggregative phenomena in the solid state. This aggregation can either be due to inter-luminophore Pt...Pt interactions or from inter-luminophore  $\pi$ - $\pi$  interactions.

Emission spectra of  $[\text{Pt}(4\text{'-}m\text{Biph-terpy})\text{Cl}]\text{SbF}_6$  in the solid state have been recorded over a range of temperatures between 80 and 298 K and these data are presented in Figure 3.19. At 280 K the emission of  $[\text{Pt}(4\text{'-}m\text{Biph-terpy})\text{Cl}]\text{SbF}_6$  is in a fairly broad (fwhm = 2693  $\text{cm}^{-1}$ ) structureless band with maximum intensity at 640 nm. Reducing the temperature to 80 K results in a prominent increase in intensity and a slight reduction in the width of the band (fwhm = 1625  $\text{cm}^{-1}$ ). Of greater consequence is a shift to lower energy of the emission maximum to 623 nm. Emission lifetimes at ambient temperatures and at 80 K are 250 ns and 1.6  $\mu\text{s}$  respectively.

Gray *et al.* have studied the solid emission from a range of chloroplatinum(II)terpyridine complexes, different only in the nature of the counterion.<sup>29</sup> In particular the solid state emission behaviour of the complexes with formulation:  $[\text{Pt}(\text{terpy})\text{Cl}]\text{X}$  [ $\text{X}^- = \text{ClO}_4^-$  (red form precipitated from aqueous solution),  $\text{ClO}_4^-$  (orange-red form recrystallized from DMF/ether),  $\text{Cl}^-$ ,  $\text{CF}_3\text{SO}_3^-$  and  $\text{PF}_6^-$ ] have been investigated. All show a blue shift in peak emission intensity as the temperature is reduced. The groups of Che *et al.*<sup>28</sup> and Field *et al.*<sup>47</sup> have also studied the triflate salt under the same conditions and both groups found a red emission shift with falling temperature. (Different sample preparation has been proposed to rationalise this apparently anomalous emission behaviour.<sup>47</sup>) Of these salts it is the emission behaviour observed by Gray and coworkers<sup>29</sup> for the orange triflate salt,  $[\text{Pt}(\text{terpy})\text{Cl}]\text{CF}_3\text{SO}_3$ , which most closely parallels that of  $[\text{Pt}(4\text{'-}m\text{Biph-terpy})\text{Cl}]\text{SbF}_6$ . The former complex displays a broad (fwhm  $\approx$  4250  $\text{cm}^{-1}$ ) structureless emission with its maximum at 640 nm at room temperature. At 80 K the band narrows (fwhm  $\approx$  1470  $\text{cm}^{-1}$ ) and its maximum is blue shifted to 625 nm.<sup>29</sup> Gray *et al.* rationalise emission from all the salts in their study by suggesting emission from multiple electronic states, their relative contribution depending on temperature.<sup>29</sup> The 80 K emission is assigned to a MMLCT state based in part on the close intermolecular contacts (3.328 Å) observed by Che *et al.* in the X-ray crystal structure of  $[\text{Pt}(\text{terpy})\text{Cl}]\text{CF}_3\text{SO}_3$ .<sup>28</sup>

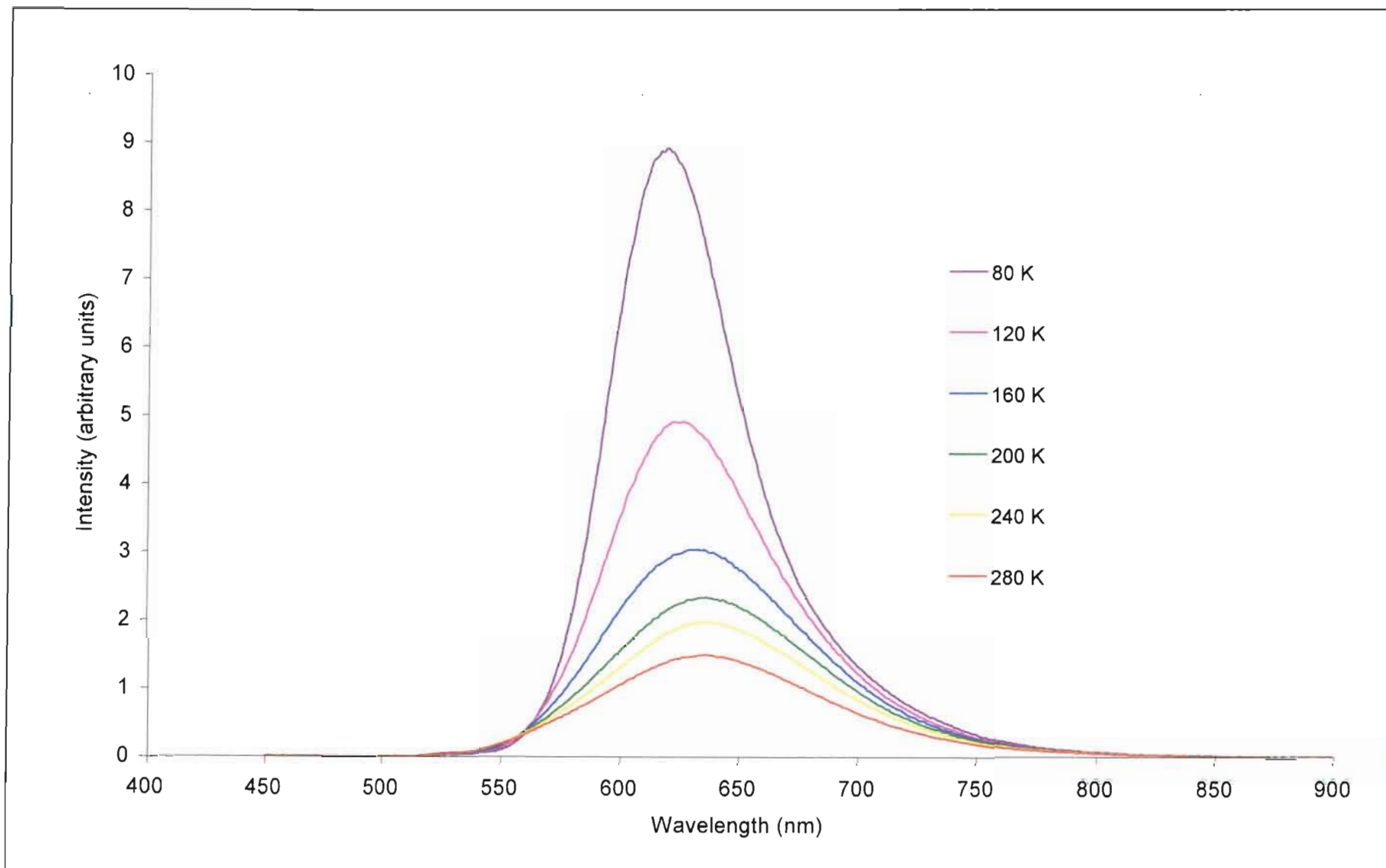


**Figure 3.19** Solid state emission spectra of  $[Pt(4'-mBiph-terpy)Cl]SbF_6$  (4).

Further justification is found in the emission band shape and energy which comply with previously reported MMLCT emissions.<sup>21, 41</sup> However, Gray *et al.* do not believe the Pt...Pt contacts necessary for MMLCT emission persist for this salt at ambient temperatures and an excimeric emission is proposed to account for the room temperature emission with maximum intensity at 640 nm.

Another important point arising from the combined findings by the groups of Che<sup>28</sup>, Gray<sup>29</sup> and Field<sup>47</sup> is that the emission measurements recorded at the lowest temperatures of all three groups agree. This suggests that this low temperature emission is the most representative of the excited state of the complex in question. {The consensus is in favour of the existence of a MMLCT state, a point reinforced by a crystal structure of the [Pt(terpy)Cl]CF<sub>3</sub>SO<sub>3</sub> complex in which [Pt(terpy)Cl]<sup>+</sup> luminophores pack in dimeric units which have a Pt...Pt separation of 3.328 Å.} Extrapolating that point to the complex under investigation here, points to a MMLCT excited state as the primary low energy excited state of [Pt(4'-*m*Biph-terpy)Cl]SbF<sub>6</sub> at the lowest temperatures.

The most obvious dissimilarity of the emission behaviour of [Pt(4'-*m*Biph-terpy)Cl]SbF<sub>6</sub> compared to that of [Pt(terpy)Cl]CF<sub>3</sub>SO<sub>3</sub> reported by Gray *et al.*<sup>29</sup> is the broadness of the room temperature emission by the unsubstituted luminophore as evidenced by a band with a fwhm of 4250 cm<sup>-1</sup> compared to that of 1625 cm<sup>-1</sup> for [Pt(4'-*m*Biph-terpy)Cl]SbF<sub>6</sub>. This behaviour is sufficiently different to prompt suspicion that identical processes are not at work in the emission of both complexes. On this basis the band profile of the room temperature emission of [Pt(4'-*m*Biph-terpy)Cl]SbF<sub>6</sub> is more consistent with MMLCT emission.

Consequently it is also not believed that the blue shift in the emission maximum observed for [Pt(4'-*m*Biph-terpy)Cl]SbF<sub>6</sub> has the same origins as that observed by Gray and coworkers<sup>29</sup> and propose that metal-metal contacts are maintained at the lowest temperatures. However, in the absence of a crystal structure, in particular a variable temperature X-ray structure determination we can only speculate as to the origin of the blue shift. The blue shift can be rationalised by slippage which results in emitting dimers that are slightly more separated at low temperatures than at ambient temperatures. Conceivably this increased separation occurs by anions that “wedge” between luminophores from either side due to a lattice contraction normal to the Pt-Pt axis of emitting dimers.

### *Solid state emission of [Pt(4'-mBiph-terpy)Cl]SbF<sub>6</sub>.CH<sub>3</sub>CN*

Collecting photophysical data for the acetonitrile solvated form of [Pt(4'-mBiph-terpy)Cl]SbF<sub>6</sub>, namely [Pt(4'-mBiph-terpy)Cl]SbF<sub>6</sub>.CH<sub>3</sub>CN (**4a**) for which a structure is reported in section 3.2.2.2 of this chapter, proved tricky due to decay of the orange-yellow crystals to the non-solvated orange powder. This crystal decay prevented the determination of a solid state absorption spectrum of [Pt(4'-mBiph-terpy)Cl]SbF<sub>6</sub>.CH<sub>3</sub>CN. However, it was possible to record variable temperature emission spectra as well as time-resolved emission spectra for [Pt(4'-mBiph-terpy)Cl]SbF<sub>6</sub>.CH<sub>3</sub>CN. In all cases close visual examinations were made of each sample prior to the commencement of a photophysical experiment to ensure sample homogeneity and to prevent the inclusion of decayed crystals.

Variable temperature emission spectra (presented in Figure 3.20) were recorded by removing the crystals from the mother liquor, placing them on filter paper to draw off the excess solvent and then transferring the bulk material directly to the spectrometer. Since the crystals were found only to deteriorate visibly after a period of hours, we do not believe the uniformity of the material was affected by solvent loss from the crystal lattice. At this point it is also worth reminding the reader that the solid state structure determination took place at 173 K, a point to keep in mind when assignments of emission bands are considered with reference to the crystal structure.

At ambient temperatures two weak and very broad bands are discernable in the emission spectrum of [Pt(4'-mBiph-terpy)Cl]SbF<sub>6</sub>.CH<sub>3</sub>CN at 557 and 650 nm. As the temperature is reduced the higher energy band at *ca.* 560 nm increases in intensity to become a sharp peak once 80 K is reached, with its energy largely unchanged. There is also the emergence of what appears to be a second vibrational progression from the same excited state manifold at 612 nm which only becomes properly discernable at temperatures below 160 K. (At 80 K the vibrational spacing between the two highest energy bands is  $\sim 1800\text{ cm}^{-1}$ , which is probably the upper limit of the range of frequencies that are expected for ligand breathing modes.) The band maximum at 650 nm shows a conspicuous shift to lower energies as the temperature is reduced, eventually showing a  $\lambda_{(\text{cm})\text{max}}$  of 670 nm at 80 K. Emission in this temperature range

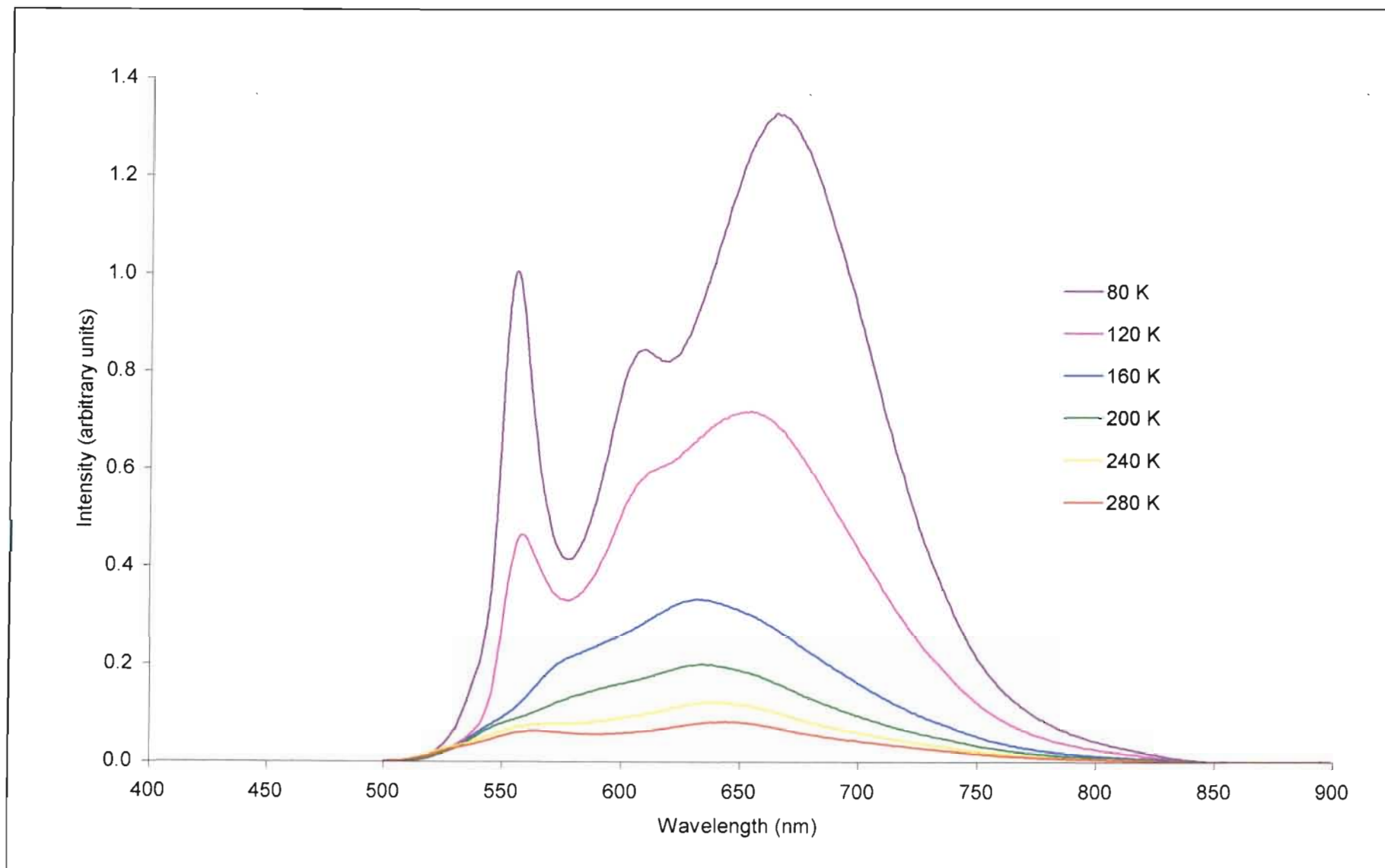


**Figure 3.20** Solid state emission spectra of  $[Pt(4'-mBiph-terpy)Cl]SbF_6 \cdot CH_3CN$

is essentially unaffected by varying the excitation wavelength between 430 and 505 nm. (An excitation of 430 nm was used to give the spectra presented in Figure 3.20.)

The emission gives the immediate impression of deriving from multiple emission origins *i.e.*, emission from more than one excited state is apparently occurring in this sample. The sharpness and temperature independent energy of the bands at highest energy is typical of emission associated with radiative decay from a  $\pi$ - $\pi^*$  excited state. In contrast, the red shift with falling temperature of the lowest energy band is a feature typifying emission from a MMLCT state as is the much lower energy.

Before proceeding to formalise the assignment, consider the following, low temperature (77 K) solid state emission reported for  $[\text{Pt}(i\text{-biq})(\text{CN})_2]$  (where *i*-biq is 2,2'-biisoquinoline) by Kato and coworkers<sup>158, 159</sup> which shows similar features to that of  $[\text{Pt}(4'\text{-}m\text{Biph-terpy})\text{Cl}]\text{SbF}_6\cdot\text{CH}_3\text{CN}$ . The emission spectrum consists of a band with four distinguishable peaks with varying widths. Band maxima occur at 569(sharp), 596(sharp), 630(broad) and 645(shoulder) nm. Kato *et al.* were able to isolate the longest-lived component ( $\tau \approx 300 \mu\text{s}$ ) which emits at 77 K in a structured band with the maximum at 596 nm constituting the 0-0 transition of this component. The broader emission band at lower energy is assigned to a <sup>3</sup>MMLCT excited state based on a X-ray crystal structure which shows a Pt...Pt separation of 3.34 Å.<sup>159</sup> Kato *et al.* assign simultaneous emission from multiple sources in the solid state to  $\pi$ - $\pi^*$  and MMLCT states that are of similar energy and suggest that the states work competitively in order to bring about the observed emission. It would seem that the same is true of the solid state emission by  $[\text{Pt}(4'\text{-}m\text{Biph-terpy})\text{Cl}]\text{SbF}_6\cdot\text{CH}_3\text{CN}$ . However, in contrast to the emission from  $[\text{Pt}(4'\text{-}m\text{Biph-terpy})\text{Cl}]\text{SbF}_6\cdot\text{CH}_3\text{CN}$ ,  $[\text{Pt}(i\text{-biq})(\text{CN})_2]$  shows no red-shift in the lowest energy band as the temperature is reduced.<sup>158, 159</sup> Instead the unit cell is shown to contract along an axis perpendicular to the Pt...Pt stacking direction as the temperature is reduced from 293 to 210 K. Thus there is no lowering of the gap between the platinum atoms and no destabilisation of the HOMO and stabilisation of the LUMO (predicted by Che *et al.*<sup>28</sup>) which would result in a reduction of the energy gap for the MMLCT excitation.

By analogy with the observations made by Kato and coworkers for the solid state emission of  $[\text{Pt}(i\text{-biq})(\text{CN})_2]$ <sup>158, 159</sup> the solid state emission of  $[\text{Pt}(4'\text{-}m\text{Biph-terpy})\text{Cl}]\text{SbF}_6\cdot\text{CH}_3\text{CN}$  is



assigned to multiple sources which emit simultaneously. As such, the high energy structured emission (at 557 nm) is assigned to ligand centred  $^3(\pi-\pi^*)$  transitions due to the sharpness of the bands and their energy which occurs in the energy regime at which monomeric emission was observed in the 77 K glass (*vide supra*). The lowest energy band is assigned to the presence of an  $^3\text{MMLCT}$  excited state due to the energy of the emission but also in large part due to the red emission shift as the temperature is reduced, characteristic of this type of emission.<sup>45</sup> Moreover, Gray *et al.* regard 3.554 Å as the upper limit for significant Pt...Pt  $d_{z^2}$ -orbital overlap<sup>157</sup> and hence the upper limit at which Pt...Pt interactions are effective in producing MMLCT emission. The X-ray crystal structure of  $[\text{Pt}(4'\text{-}m\text{Biph-terpy})\text{Cl}]\text{SbF}_6 \cdot \text{CH}_3\text{CN}$  recorded at 173 K (see section 3.2.2.2) shows the presence of dimeric units in which the direct Pt...Pt separation between each luminophore and its counterpart in position A is 3.356(2) Å. On this basis the inter-luminophore platinum  $d_{z^2}$ -orbital interaction is highly probable.

Without variable temperature X-ray crystal structure determinations of  $[\text{Pt}(4'\text{-}m\text{Biph-terpy})\text{Cl}]\text{SbF}_6 \cdot \text{CH}_3\text{CN}$ , it is not possible to confirm a shortening of the Pt...Pt distance as the temperature is reduced. The shift to lower emission energy of the long wavelength band as the temperature of  $[\text{Pt}(4'\text{-}m\text{Biph-terpy})\text{Cl}]\text{SbF}_6 \cdot \text{CH}_3\text{CN}$  is reduced can probably be regarded as sufficient evidence for a lattice contraction in the direction of the Pt...Pt stack.

It is also important to address the emission band with a maximum at 612 nm with its most prominent participation visible at 80 K. It is possible that this band is a lower energy vibrational progression of the ligand centred emission (0-0 transition at 557 nm) evident at the highest energies. However, as noted above, the unsolvated complex,  $[\text{Pt}(4'\text{-}m\text{Biph-terpy})\text{Cl}]\text{SbF}_6$ , emits at *ca.* 625 nm at 80 K (assigned as MMLCT) and it may be that some of the unsolvated species is contributing to the overall emission by the sample. In short, it is possible that the sample of  $[\text{Pt}(4'\text{-}m\text{Biph-terpy})\text{Cl}]\text{SbF}_6 \cdot \text{CH}_3\text{CN}$  was contaminated by trace amounts of  $[\text{Pt}(4'\text{-}m\text{Biph-terpy})\text{Cl}]\text{SbF}_6$  despite all attempts to avoid this problem.

#### *Solid state absorption and emission spectroscopy of $[\text{Pt}(4'\text{-}m\text{Biph-terpy})\text{Cl}]\text{BF}_4$*

The solid state photophysical properties of  $[\text{Pt}(4'\text{-}m\text{Biph-terpy})\text{Cl}]\text{BF}_4$  will now be discussed.

An absorption spectrum has been recorded in the solid state showing band maxima at 443 and at 525 nm, essentially identical to the solid state absorption regime of [Pt(4'-*m*Biph-terpy)Cl]SbF<sub>6</sub>. The absorption assignment is therefore no different. The band at 443 nm is thought to be due to a monomeric charge transfer transition, while absorption at 525 nm is proposed to occur from aggregated species. It is not possible to speculate as to the nature of the interactions giving rise to the 525 nm absorption based only on the solid state absorption spectrum, and absorptions at these energies could arise either from intermolecular  $\pi$ - $\pi$  interactions or from extended Pt-Pt interactions in the solid state.

Variable temperature emission spectra of [Pt(4'-*m*Biph-terpy)Cl]BF<sub>4</sub> have been recorded in the 80 - 280 K temperature range and are reproduced in Figure 3.21. At 280 K the spectrum consists of a series of peaks with maxima at 545(sharp), 580(broad), 653(broad) and 715(broad) nm. Reducing the temperature to 80 K results in a completely different emission profile. Intensities at each of the maxima increase, just at different rates, and where the broad band at 653 nm emitted at highest intensity at 280 K, a new band emerges at 120 K, becoming the dominant emission, with  $\lambda_{em}(max)$  at 621 nm at 80 K. Excitation at a wavelength of 400 nm has been used in Figure 3.21, but variable temperature emission spectra were also recorded over the same temperature range but using excitation wavelengths of 450 and 490 nm. In no case was the intensity response to temperature the same.

The basic features of the emission exhibited by [Pt(4'-*m*Biph-terpy)Cl]BF<sub>4</sub> correspond with those of emission from [Pt(4'-*m*Biph-terpy)Cl]SbF<sub>6</sub>.CH<sub>3</sub>CN. Emission at room temperature is in a structured band and as the temperature is reduced bands at highest energy develop into very narrow, sharp features. In addition the wavelength of the most intense band at 80 K (620 nm) falls into the energy range of a MMLCT emission, in particular this emission energy corresponds very well with the 80 K MMLCT emission observed for the non-solvated [Pt(4'-*m*Biph-terpy)Cl]SbF<sub>6</sub> complex. In the emission spectra of [Pt(4'-*m*Biph-terpy)Cl]BF<sub>4</sub> the emergence of the band at 620 nm is not as obvious as in the case of [Pt(4'-*m*Biph-terpy)Cl]SbF<sub>6</sub>.CH<sub>3</sub>CN, being obscured beneath emission from surrounding bands. Based on these similar features, emission from [Pt(4'-*m*Biph-terpy)Cl]BF<sub>4</sub> is also assigned to simultaneous emission from <sup>3</sup>MMLCT and <sup>3</sup>( $\pi$ - $\pi^*$ ) excited states (see above discussion).

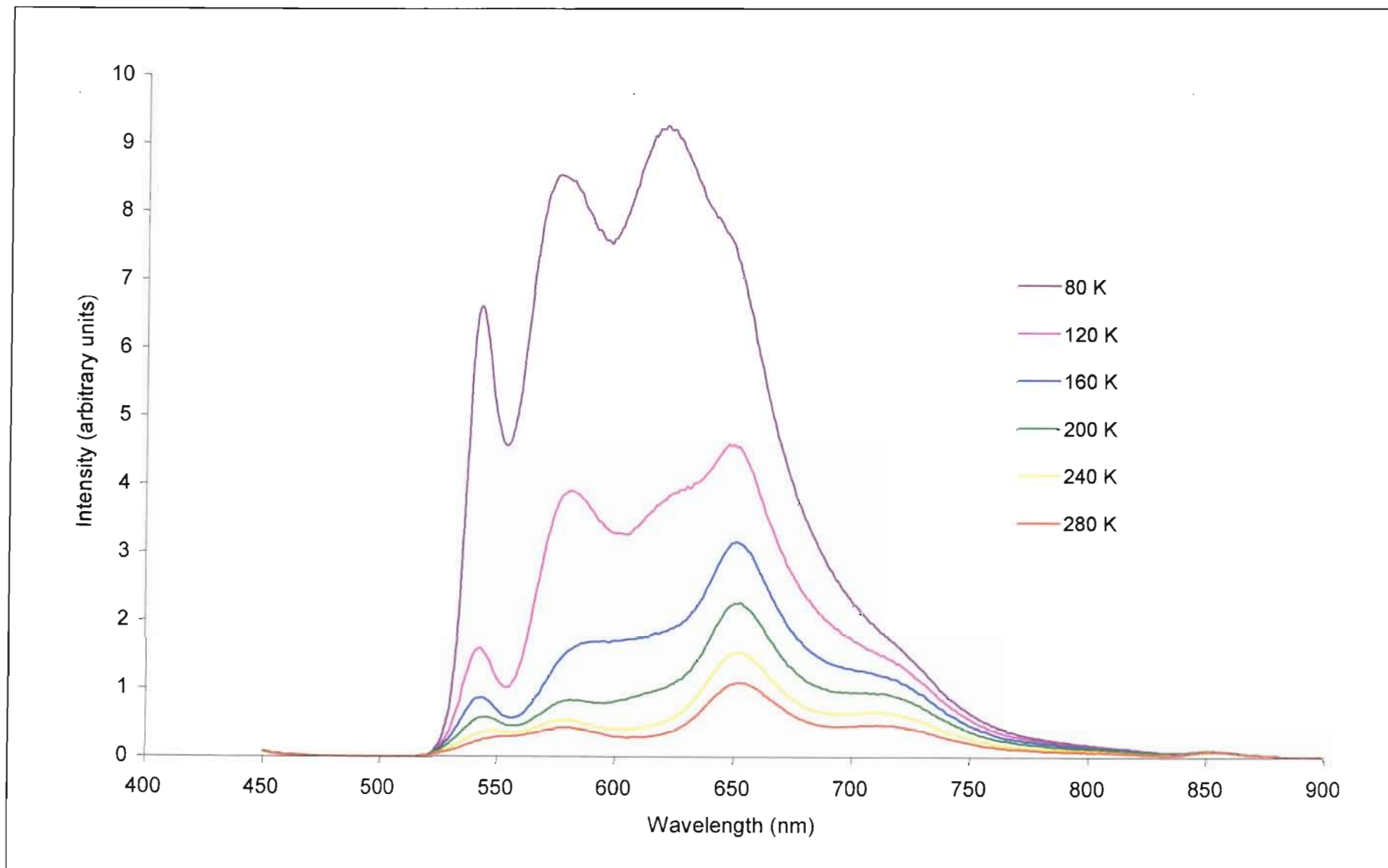


**Figure 3.21** Solid state emission spectra of  $[Pt(4'-mBiph-terpy)Cl]BF_4$  (5).

The basic features of the solid state absorption and luminescence of [Pt(4'-mBiph-terpy)Cl]CF<sub>3</sub>SO<sub>3</sub> are the same as those of [Pt(4'-mBiph-terpy)Cl]BF<sub>4</sub>. Absorption and emission maxima coincide and it is just the relative intensities at each wavelength that differ. The solid state emission spectrum of [Pt(4'-mBiph-terpy)Cl]CF<sub>3</sub>SO<sub>3</sub> recorded at a range of temperatures is reproduced in Figure 3.22. As can be seen the 620 nm band is far more prominent in the emission profile of this salt and we suggest that the excited state bringing about this emission represents a more favourable deactivation pathway in the case of [Pt(4'-mBiph-terpy)Cl]CF<sub>3</sub>SO<sub>3</sub>. Given the broadness of the band at 280 K which is atypical of a MMLCT emission, it is possible that the 620 nm emission at this temperature is more excimeric in character than that of [Pt(4'-mBiph-terpy)Cl]BF<sub>4</sub> under the same conditions. The important point though is that at 80 K the emission component of [Pt(4'-mBiph-terpy)Cl]BF<sub>4</sub> and [Pt(4'-mBiph-terpy)Cl]CF<sub>3</sub>SO<sub>3</sub> at this energy is almost identical to that of [Pt(4'-mBiph-terpy)Cl]SbF<sub>6</sub>, *i.e.* <sup>3</sup>MMLCT in nature. As for [Pt(4'-mBiph-terpy)Cl]SbF<sub>6</sub> however {and in contrast to [Pt(4'-mBiph-terpy)Cl]BF<sub>4</sub>} the energy is distinctly blue-shifted as the temperature falls. As before, additional bands are rationalised in terms of simultaneous emission from an additionally populated energy level. Again, we propose that contraction for this solid is along an axis normal to the Pt...Pt stacking direction to account for the blue emission shift with falling temperature. The magnitude of the shift (657 to 625 nm) could be indicative of a relatively inefficient packing architecture at ambient temperatures compared to that of [Pt(4'-mBiph-terpy)Cl]SbF<sub>6</sub>.

### **3.2.3 [Pt(4'-pBiph-terpy)Cl]X [X<sup>-</sup> = SbF<sub>6</sub><sup>-</sup> (7), BF<sub>4</sub><sup>-</sup> (8), CF<sub>3</sub>SO<sub>3</sub><sup>-</sup> (9)]**

**{where 4'-pBiph-terpy = 4'-(para-biphenyl)-2,2':6',2''-terpyridine}**

#### **3.2.3.1 Synthesis and characterisation of [Pt(4'-pBiph-terpy)Cl]X [X<sup>-</sup> = SbF<sub>6</sub><sup>-</sup> (7), BF<sub>4</sub><sup>-</sup> (8), CF<sub>3</sub>SO<sub>3</sub><sup>-</sup> (9)]**

The approach to the synthesis of the three platinum(II) complexes, [Pt(4'-pBiph-terpy)Cl]X [X<sup>-</sup> = SbF<sub>6</sub><sup>-</sup> (7), BF<sub>4</sub><sup>-</sup> (8), CF<sub>3</sub>SO<sub>3</sub><sup>-</sup> (9)] {4'-pBiph-terpy = 4'-(p-biphenyl)-2,2':6',2''-

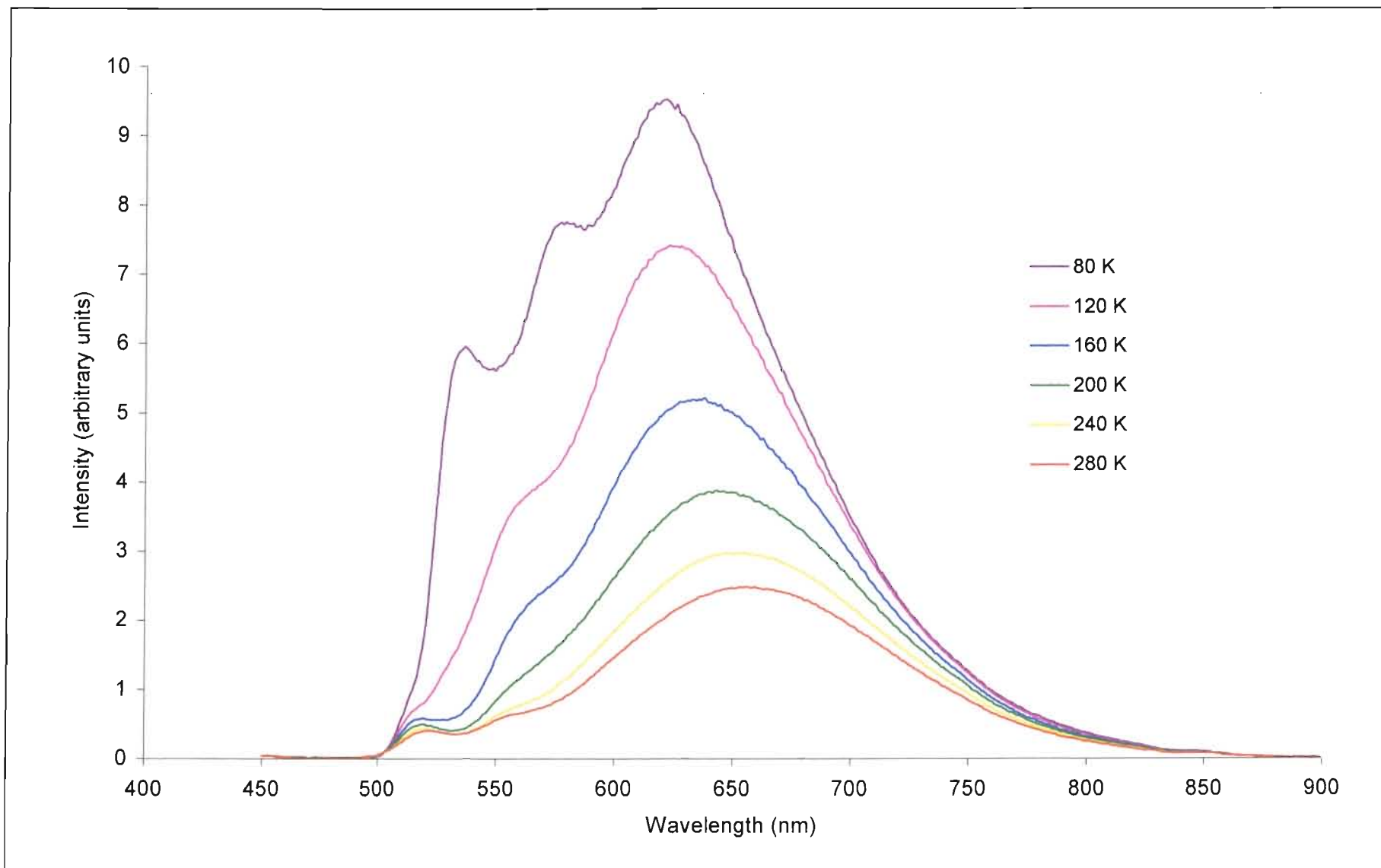


**Figure 3.22** Solid state emission spectra of  $[Pt(4'-mBiph-terpy)Cl]CF_3SO_3$  (6).

terpyridine}, is identical to that for the synthesis of  $[\text{Pt}(4'\text{-}\beta\text{Np-terpy})\text{Cl}]\text{X}$  and  $[\text{Pt}(4'\text{-}m\text{Biph-terpy})\text{Cl}]\text{X}$  described in sections 3.2.1.1 and 3.2.2.1 of this work. Equimolar amounts of  $[\text{Pt}(\text{PhCN})_2\text{Cl}_2]$  and the appropriate silver salt incorporating the desired counterion were refluxed overnight in acetonitrile under an inert atmosphere of nitrogen. Upon completion, the creamy white silver chloride precipitate was filtered off and the filtrate added to an equivalent of the ligand 4'-*p*Biph-terpy suspended in acetonitrile before the resultant mixture was again refluxed overnight under nitrogen. The hot solution was filtered to remove the last traces of silver chloride and the desired complexes  $[\text{Pt}(4'\text{-}p\text{Biph-terpy})\text{Cl}]\text{SbF}_6$  (**7**),  $[\text{Pt}(4'\text{-}p\text{Biph-terpy})\text{Cl}]\text{BF}_4$  (**8**), and  $[\text{Pt}(4'\text{-}p\text{Biph-terpy})\text{Cl}]\text{CF}_3\text{SO}_3$  (**9**) precipitated upon cooling as pale orange, yellow and bright orange complexes respectively. Further precipitation was encouraged by the partial removal of solvent under reduced pressure. Recrystallisation of each compound from boiling acetonitrile served as a final purification step and yielded analytically pure products. In performing this step the tetrafluoroborate salt,  $[\text{Pt}(4'\text{-}p\text{Biph-terpy})\text{Cl}]\text{BF}_4$ , was also found to exist in a red crystalline form in addition to the original yellow form. It is possible to selectively produce either of the two forms by controlling the cooling rate of the solution from which the compound is recrystallized. Rapid cooling produces the yellow powdery form whereas very slow cooling afforded the red form. Although the red crystals appear externally to be perfect and single rectangular blocks, each one that was subjected to Weissenberg X-ray photography proved to be twinned. Hence no X-ray structure determination was undertaken.

Elemental analysis for C, H, and N confirmed the empirical formulation of each salt as  $[\text{Pt}(\text{C}_{27}\text{H}_{19}\text{N}_3)\text{Cl}]\text{X}$  [ $\text{X}^- = \text{SbF}_6^-$  (**7**),  $\text{BF}_4^-$  (**8**),  $\text{CF}_3\text{SO}_3^-$  (**9**)]. A proton NMR spectrum of each of the complexes was recorded in deuterated DMSO and the spectrum of the tetrafluoroborate salt is briefly described here as representative of the other two salts. Signals were assigned by comparison with the  $^1\text{H}$  NMR spectrum of the free ligand (see Chapter 2) and with the aid of a COSY experiment. A prominent singlet furthest downfield at  $\delta$  8.60 is ascribed to the degenerate resonances of the two protons of the central pyridyl ring in the terpyridyl fragment ( $\text{H}^{3,5}$ ). Upfield of this singlet, two doublets ( $\delta$  8.48 and  $\delta$  8.30) and a triplet ( $\delta$  8.21) are assigned to the  $\text{H}^{3,3'}$ ,  $\text{H}^{6,6'}$  and  $\text{H}^{4,4'}$  protons of the outer pyridine rings respectively. The signal of the remaining protons of the terpyridyl system ( $\text{H}^{5,5'}$ ) is obscured by peaks from the phenyl

protons but can be distinguished by the COSY experiment at  $\delta$  7.60. Remaining resonances can be ascribed to the protons of the *para*-biphenyl substituent and a comprehensive listing can be found in the experimental section of this chapter.

An infrared spectrum of each salt as a KBr pellet was recorded. The spectra show distinctive peaks associated with the counterion of each salt but are otherwise identical. The most salient peaks are listed in Table 3.10 at the end of this chapter.

### 3.2.3.2 Photophysical studies on [Pt(4'-*p*Biph-terpy)Cl]X [ $X^- = \text{SbF}_6^-$ (7), $\text{BF}_4^-$ (8), $\text{CF}_3\text{SO}_3^-$ (9)]

#### *Fluid solution absorption spectroscopy*

Not unexpectedly the room temperature solution absorption spectra of the three platinum complexes [Pt(4'-*p*Biph-terpy)Cl]SbF<sub>6</sub>, [Pt(4'-*p*Biph-terpy)Cl]BF<sub>4</sub> and [Pt(4'-*p*Biph-terpy)Cl]CF<sub>3</sub>SO<sub>3</sub> were identical despite their different counterions. The spectrum of the hexafluoroantimonate salt in acetonitrile will therefore be discussed as a representative example. This spectrum is reproduced in Figure 3.23 and the spectral data are provided in Table 3.11 at the end of this chapter. The spectrum is composed in the first instance of an intense peak at 284 nm and a vibrationally structured band between 300 and 375 nm. At longer wavelengths there is a moderately intense band maximising at 410 nm, with a shoulder at 390 nm. This absorption pattern is typical of similar platinum terpyridyl complexes of this kind<sup>27-29</sup>, including those described in sections 3.2.1.2 and 3.2.2.2 of this chapter, and hence the assignment of the absorption origin is no different. The interval between each feature of the vibrationally structured band in the 300 - 375 nm range is ~ 1200 - 1400 cm<sup>-1</sup>. This is typical of the vibrational spacing of  $\pi$ - $\pi^*$  transitions as the vibronic interval corresponds with the C=N and C=C stretching vibrations associated with the skeletal stretching of the heterocyclic ligand. In addition the sharp peak at *ca.* 280 nm occurs at a very similar energy to the most intense absorption of the free ligand (4'-*p*Biph-terpy). The peaks in the 280 - 375 nm range are therefore also assigned to  $\pi$ - $\pi^*$  transitions localised to the organic framework of the terpyridyl ligand.

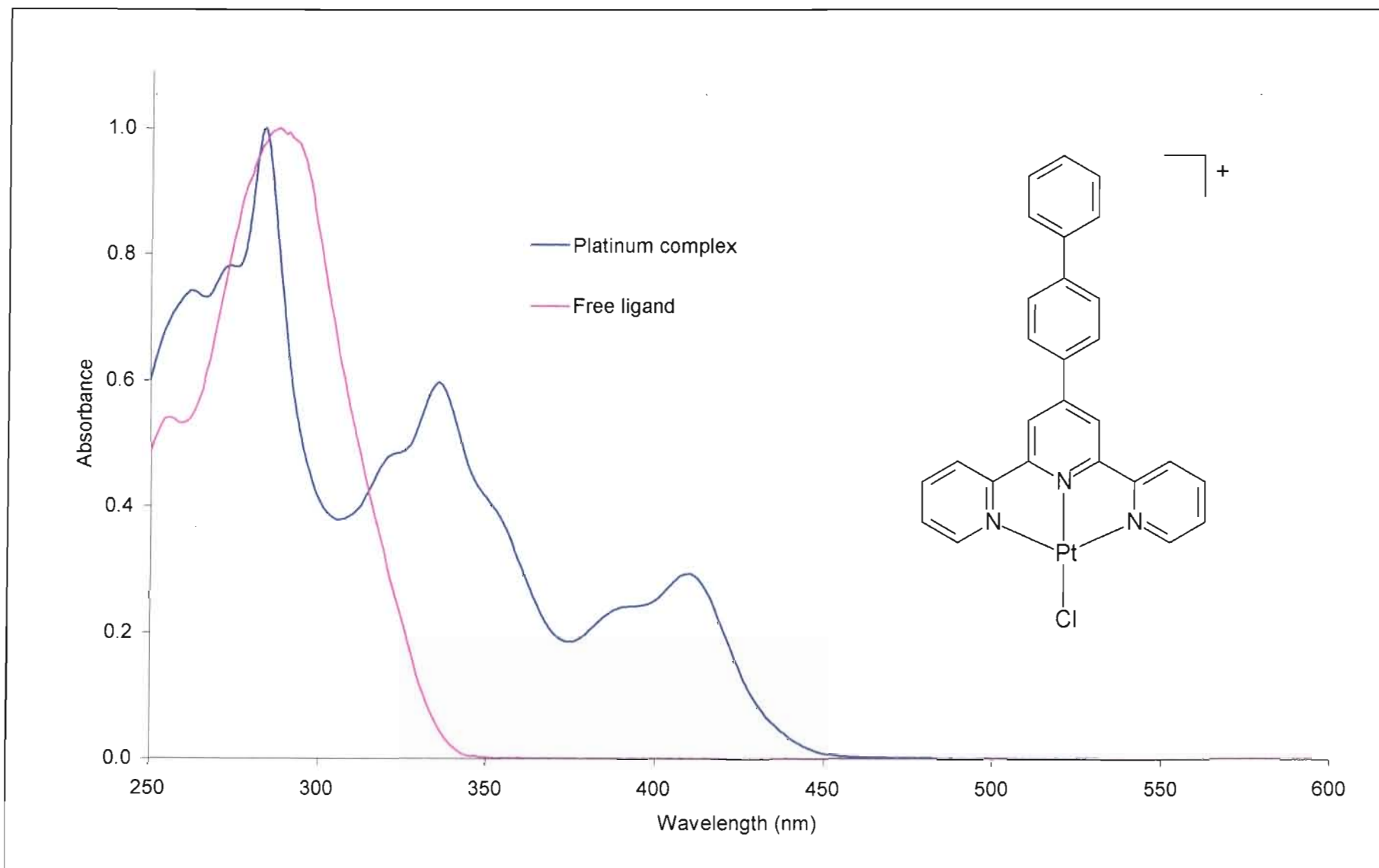


**Figure 3.23** Acetonitrile solution absorption spectra of the  $[Pt(4'-pBiph-terpy)Cl]^+$  and 4'-pBiph-terpy chromophores recorded at 298 K.



The two less intense broad bands at wavelengths above 375 nm are assigned to MLCT transitions based on the energy, intensity (relative to the  $\pi$ - $\pi^*$  bands) and shape of the bands which correspond to those observed by previous authors in the absorption spectrum of the  $[\text{Pt}(\text{terpy})\text{Cl}]^+$  chromophore measured in acetonitrile solution.<sup>27-29</sup> The charge-transfer nature of these bands is indicated by the shift to lower energy of this band when the solvent is the less polar dichloromethane.

#### *Fluid solution emission spectroscopy*

An excitation spectrum of  $[\text{Pt}(4'\text{-}p\text{Biph-terpy})\text{Cl}]^+$  was recorded that matches the absorption spectrum in dichloromethane. This confirms that emission is from a single species in solution.

The emission spectrum of the  $[\text{Pt}(4'\text{-}p\text{Biph-terpy})\text{Cl}]^+$  luminophore was recorded at room temperature in both acetonitrile and dichloromethane solutions; emission in acetonitrile is only barely detectable and the solution can effectively be regarded as non-emissive. The emission spectrum of a 20  $\mu\text{M}$  solution of the hexafluoroantimonate salt of  $[\text{Pt}(4'\text{-}p\text{Biph-terpy})\text{Cl}]^+$  in dichloromethane is shown in Figure 3.4, the spectra of the other two salts being identical. A complete listing of the emission data is given in Table 3.12 at the end of this chapter. As shown in Figure 3.4 the emission attains its peak intensity at 562 nm with poorly resolved progressions at *ca.* 605 and 650 nm, corresponding to vibrational spacings of  $\sim 1000 - 1300 \text{ cm}^{-1}$ . A structured emission of this type is indicative of IL ( $\pi$ - $\pi^*$ ) character in the emitting state. Two factors point to the presence of MLCT character in the emissive excited state as well. Firstly, the energy of the 0-0 transition is lower than expected for a pure IL state and, secondly, the emission is quenched in a coordinating solvent. All of the above features are similar to those observed in the fluid emission exhibited by the 4'-*m*Biph-terpy derivative and by the  $[\text{Pt}(4'\text{-Ph-terpy})\text{Cl}]^+$  chromophore.<sup>32</sup> (Data from these and related luminophores is summarised in Table 3.4.)

However, there are noteworthy differences. We note that emission exhibited by the 4'-*p*Biph-terpy derivative is at significantly lower energies than that found for  $[\text{Pt}(4'\text{-}m\text{Biph-terpy})\text{Cl}]^+$  and  $[\text{Pt}(4'\text{-Ph-terpy})\text{Cl}]^+$  *cf.* 0-0 transitions of 562, 536 and 535 nm respectively. Also evident is that the lifetime of 4  $\mu\text{s}$  for the emitting state is forty times longer than the values of 0.12

and 0.09  $\mu\text{s}$  measured for the 4'-*m*Biph-terpy and 4'-Ph-terpy derivatives respectively. Possible reasons for the differences will now be discussed.

**Table 3.4** Summary of emission data recorded in dichloromethane solution at 298 K.

Compound	$\lambda_{\text{em}}$ (max) of 0-0 transition (nm)	Huang- Rhys factor	$\tau$ ( $\mu\text{s}$ )	Assignment
[Pt(4'-Ph-terpy)Cl] <sup>+</sup> <sup>32</sup>	535	0.88	0.09	<sup>3</sup> [IL/MLCT]
[Pt(4'- <i>m</i> Biph-terpy)Cl] <sup>+</sup>	536	0.77	0.12	<sup>3</sup> [IL/MLCT]
[Pt(4'- <i>p</i> Biph-terpy)Cl] <sup>+</sup>	562	0.65	4	<sup>3</sup> [IL/ILCT/MLCT]
[Pt(4'- $\beta$ Np-terpy)Cl] <sup>+</sup>	570	0.58	11.9	<sup>3</sup> [IL/ILCT/MLCT]
[Pt(4'- $\alpha$ Np-terpy)Cl] <sup>+</sup> <sup>32, 111</sup>	588	-	16.6	<sup>3</sup> [IL/ILCT/MLCT]

Starting with the very different lifetimes for [Pt(4'-*p*Biph-terpy)Cl]<sup>+</sup> and [Pt(4'-*m*Biph-terpy)Cl]<sup>+</sup> we note that the energy gap law is violated since the lowest energy state *viz.* that of [Pt(4'-*p*Biph-terpy)Cl]<sup>+</sup> is the longest lived.<sup>57</sup> This leads to the conclusion that the composition of the excited state is different for the two species. One possibility is that the emitting state for the [Pt(4'-*p*Biph-terpy)Cl]<sup>+</sup> luminophore contains relatively more IL than MLCT character, as compared to the emitting state for the [Pt(4'-*m*Biph-terpy)Cl]<sup>+</sup> luminophore. This suggestion is consistent with the longer lifetime measured for the [Pt(4'-*p*Biph-terpy)Cl]<sup>+</sup> luminophore since, all things being equal, ligand localised states of the  $\pi$ - $\pi^*$  type are expected to have longer emission lifetimes than MLCT ( $d$ - $\pi^*$ ) states.<sup>37, 43</sup> However, we consider this explanation for the unexpectedly long lifetime for the [Pt(4'-*p*Biph-terpy)Cl]<sup>+</sup> luminophore to be unlikely for the following reasons. First, a higher percentage of IL character in the emitting state would lead to an increase in the energy of the emitting state, not the observed decrease. Second, the Huang-Rhys ratio of 0.65 for the [Pt(4'-*p*Biph-terpy)Cl]<sup>+</sup> luminophore is significantly less than the Huang-Rhys ratio of 0.77 for the [Pt(4'-*m*Biph-terpy)Cl]<sup>+</sup> luminophore (see Table 3.4). Smaller Huang-Rhys ratios are usually taken to imply a reduction in the contribution of ligand localised transitions ( $\pi$ - $\pi^*$  in this case) to an excited state.<sup>21, 41</sup> A second and, in our opinion, more plausible explanation to the unexpectedly high emission lifetime of 4  $\mu\text{s}$  recorded for the [Pt(4'-*p*Biph-terpy)Cl]<sup>+</sup> luminophore is that the

character is present in the emitting state in addition to IL and MLCT character. This contrasts the situation for the  $[\text{Pt}(4'\text{-}m\text{Biph-terpy})\text{Cl}]^+$  derivative where the emitting state has been assigned as mixed  $^3\text{IL}/^3\text{MLCT}$  only (see earlier discussion).

The addition of ILCT character in the emitting state for the  $[\text{Pt}(4'\text{-}p\text{Biph-terpy})\text{Cl}]^+$  luminophore would be expected to i) increase the lifetime of the excited state responsible for the emission,<sup>32</sup> ii) reduce the energy of that excited state<sup>32</sup> and iii) lead to a reduction in the Huang-Rhys factor for the structured band profile.<sup>21,41</sup> This is exactly as is observed. It is on this basis that we conclude our assignment of the emitting state for  $[\text{Pt}(4'\text{-}p\text{Biph-terpy})\text{Cl}]^+$  to one containing an admixture of  $^3\text{IL}$ ,  $^3\text{MLCT}$  and some  $^3\text{ILCT}$  character. Moreover, Michalec *et al.* identify ILCT character in the excited state of  $[\text{Pt}(4'\text{-}p\text{OMePh-terpy})\text{Cl}]^+$  luminophore {where 4'-*p*OMePh-terpy denotes 4'-(*para*-OMe-phenyl)-2,2':6',2''-terpyridine}<sup>32</sup>, which is another luminophore where the phenyl ring in the 4'-position is substituted in the *para*-position, in this case with a methoxy group. This is in contrast to the excited state of the 4'-phenyl substituted luminophore,  $[\text{Pt}(4'\text{-Ph-terpy})\text{Cl}]^+$ , which does not show evidence of an ILCT excitation.<sup>32</sup>

The question now arises: Why is there a difference in the makeup of the excited state that gives rise to emission by the  $[\text{Pt}(4'\text{-}m\text{Biph-terpy})\text{Cl}]^+$  and  $[\text{Pt}(4'\text{-}p\text{Biph-terpy})\text{Cl}]^+$  luminophores? We first note that the differences cannot be ascribed to steric effects and, in particular, to differences in the steric interactions between the hydrogens of the central phenyl ring and those of the central pyridine ring of the terpyridyl moiety. The same degree of rotational freedom is expected to apply to the interannular bond between the central phenyl ring and the attached pyridine ring in both the  $[\text{Pt}(4'\text{-}m\text{Biph-terpy})\text{Cl}]^+$  and  $[\text{Pt}(4'\text{-}p\text{Biph-terpy})\text{Cl}]^+$  cations. Our conclusion is that the cause of the differences is electronic in origin. In this regard we note that aromatic substituents specifically activate positions on the phenyl ring to which they are attached that are *para* to the substituent.<sup>160</sup> In particular, aromatic substituents activate *para*-positions to electrophilic substitution, an effect normally referred to as an “inductive” effect.<sup>160</sup> This implies a very different electron density distribution at the carbon atoms of the phenyl ring bonded to the terpyridyl unit for the 4'-*m*Biph-terpy and 4'-*p*Biph-terpy derivatives. Inevitably this will lead to differences in the relative energies of the IL, MLCT and ILCT transitions and therefore to their contributions to the configurationally

IL, MLCT and ILCT transitions and therefore to their contributions to the configurationally mixed state. Unfortunately, in the absence of detailed calculations, it is not possible to make a more quantitative interpretation of the experimental observations. However, it is clear that by simply replacing a *m*BiPh-group with a *p*BiPh group in the 4'-position of the terpyridyl unit there is a dramatic effect on the emission properties associated with the platinum complex.

To our knowledge there are at present no other studies of this type in which attempts to harness inductive effects to bring about changes in the nature of the excited state. The difficulty of substitution of a phenyl ring in the *meta*-position could be partly responsible for the dearth of suitably substituted luminophores.

#### *Glass emission spectroscopy*

Measurements of the luminescence properties of  $[\text{Pt}(4'\text{-}p\text{BiPh-terpy})\text{Cl}]^+$  were made in a DME glass at 77 K on solutions ranging in concentration from 0.1 to 150  $\mu\text{M}$ . Results at 150  $\mu\text{M}$  are shown in Figure 3.24 and complete data are tabulated at the end of this chapter.

Emission is concentration dependent and, as in the case of  $[\text{Pt}(4'\text{-}m\text{BiPh-terpy})\text{Cl}]^+$ , three differing emission sources have been identified. A structured emission with maxima at *ca.* 550, 680 and 630(shoulder) nm is evident in solutions of  $[\text{Pt}(4'\text{-}p\text{BiPh-terpy})\text{Cl}]^+$  at low concentration and when the excitation wavelength is shorter than 450 nm. The emission has a radiative lifetime of *ca.* 3  $\mu\text{s}$ . By raising the concentration above 20  $\mu\text{M}$  it is possible to isolate a broad (fwhm  $\sim 4400\text{ cm}^{-1}$ ) unstructured emission with  $\lambda_{\text{em}}(\text{max})$  at 620 nm provided an excitation wavelength between 460 and 480 nm is used. A third emission source is possible when solutions more concentrated than 50  $\mu\text{M}$  are used and excitation is at wavelengths longer than 490 nm. Emission in these cases is in a relatively narrow (fwhm  $\sim 2300\text{ cm}^{-1}$ ) unstructured band with an energy that is concentration dependent. Specifically the emission maximum increases from 680 to 688 to 695 nm {with  $\lambda_{\text{ex}}(\text{max}) = 520\text{ nm}$ } as the concentration in DME is increased from 50 to 100 to 150  $\mu\text{M}$ . This emission feature has a radiative lifetime of 1.9  $\mu\text{s}$ .

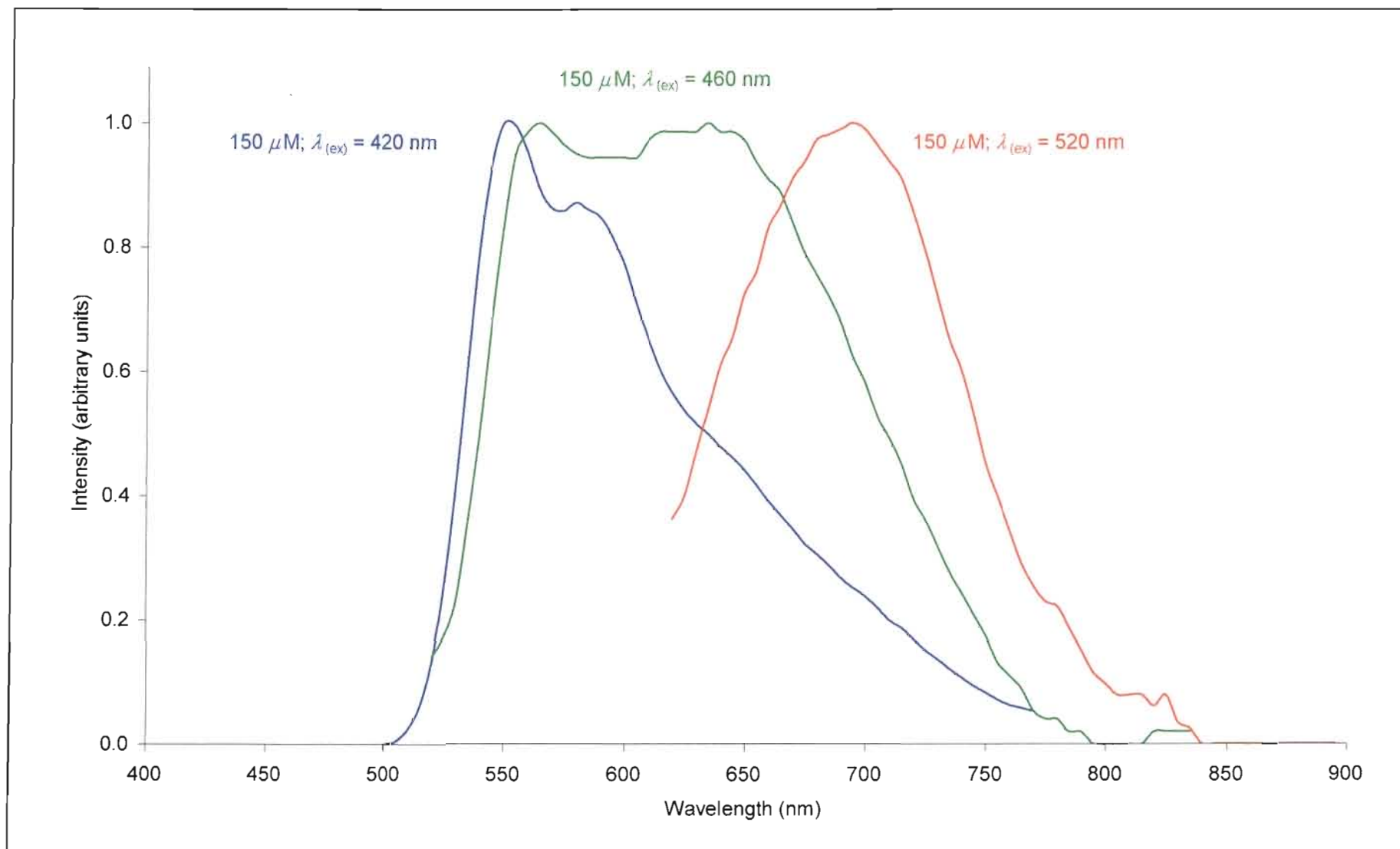


**Figure 3.24** Solution emission spectra of  $[Pt(4'-pBiph-terpy)Cl]^+$  recorded in DME glass at 77 K. (Intensities at different excitation energies adjusted to achieve equal maxima.)

As in the case of  $[\text{Pt}(4'\text{-Ph-terpy})\text{Cl}]^+$  and  $[\text{Pt}(4'\text{-}m\text{Biph-terpy})\text{Cl}]^+$ , the structured emission at highest energies is assigned to radiative decay from an excited state localised to the monomer that is of mixed orbital parentage. In particular, the emission is characterised by contributions from intraligand  ${}^3\text{IL } {}^3(\pi\text{-}\pi^*)$ ,  ${}^3\text{ILCT}$  and  ${}^3\text{MLCT}$  states.

The broad unstructured emission with maximum at  $\sim 600$  nm shows a band profile which may still contain contributions from the monomeric emission. However, emission at this energy, present only in more concentrated solutions and in such a broad band is assigned to an excimeric excited state resulting from interactions of the organic fragments of partially overlapping luminophores. This assignment is made by analogy with emission from the  $[\text{Pt}(4'\text{-}m\text{Biph-terpy})\text{Cl}]^+$  luminophore recorded in rigid glassy medium and the work by Gray *et al.* on the unsubstituted ligand complex  $[\text{Pt}(\text{terpy})\text{Cl}]^+$ .<sup>29</sup>

The third emission source occurring in the most concentrated solutions displays behaviour that is regarded as characteristic of emission from a MMLCT excited state. Clearly at higher concentrations  $d_{z^2}\text{-}d_{z^2}$  interactions between two platinum atoms becomes possible due to aggregation of the luminophores. This is shown in Figure 3.24 where increasing the concentration results in a red shift in the emission maximum.

#### *Solid state absorption and emission spectroscopy*

The focus now moves to the solid state absorption and emission spectra of compounds in which platinum(II) has been coordinated to 4'-*p*Biph-terpy. Emission from the hexafluoroantimonate salt (**7**), the tetrafluoroborate salt (**8**) and the triflate salt (**9**) will each be discussed in turn. The emission data for all three salts are summarised in Table 3.13 at the end of this chapter.

#### *Solid state absorption and emission spectroscopy of $[\text{Pt}(4'\text{-}p\text{Biph-terpy})\text{Cl}]\text{SbF}_6$*

The  $[\text{Pt}(4'\text{-}p\text{Biph-terpy})\text{Cl}]\text{SbF}_6$  salt is pale orange in colour when viewed under white light.

A solid state absorption spectrum of [Pt(4'-*p*Biph-terpy)Cl]SbF<sub>6</sub> shows a prominent band at *ca.* 480 nm which is assigned to a charge transfer absorption similar to that observed in acetonitrile solution at 410 nm. Bands at higher energy correspond to  $\pi$ - $\pi^*$  absorptions of the coordinated ligand.

The variable temperature luminescence spectra of [Pt(4'-*p*Biph-terpy)Cl]SbF<sub>6</sub> are presented in Figure 3.25 where an excitation wavelength of 400 nm is used. At 280 K the compound emits in a vibrationally structured band with maxima at 566, 603 and *ca.* 660sh (see Figure 3.25) and which has a radiative lifetime of 870 ns. The vibrational spacing between the 0-0 and 0-1 transition is 1100 cm<sup>-1</sup> and the Huang-Rhys factor (defined as  $I_{0,1}/I_{0,0}$  and regarded as a measure of the ligand contribution to a state of mixed orbital parentage<sup>28</sup>) is  $\sim$  0.6. A Huang-Rhys factor significantly greater than unity is thought to indicate that the excited state is predominantly ligand-centred in nature.<sup>28</sup> Reducing the temperature to 80 K does not result in a systematic increase in emission intensity. Rather the intensity of the 566 nm maximum increases initially, reaching a local maximum at 240 K, then falling off dramatically to an overall minimum at 160 K before increasing steeply again to the maximum intensity at 80 K, the lowest temperature at which measurements were recorded.

Emission at 80 K is still in a vibrationally structured band, but with maxima slightly red shifted (by 4 nm for the 0-0 transition) to 570, 620 and *ca.* 670sh nm. The lifetime of radiative decay is significantly longer at 6.8  $\mu$ s. The vibrational spacing between the 0-0 and 0-1 bands at 80 K is 1400 cm<sup>-1</sup> and the Huang-Rhys factor has fallen to  $\sim$  0.4. Between 280 and 80 K the Huang-Rhys ratio varies unpredictably between 0.4 and 0.7.

When excitation is at slightly lower energies (in this case an excitation wavelength of 450 nm was used) the emission behaviour follows the same pattern, but is slightly different (see Figure 3.26). At 280 K emission is in a structured band with 0-0 transition at 576 nm with subsequent transitions at 612 and *ca.* 670 nm. As the temperature is reduced the intensity increases and the maxima shift slightly to 576, 623 and  $\sim$  670 nm. Emission intensities increase more systematically and the band profile undergoes similar changes to those observed when the excitation wavelength was 400 nm. The Huang-Rhys ratio at 280 K is  $\sim$  0.6, but falls monotonically to 0.4 as temperature is reduced to 80 K. At the same time the vibrational spacing increases from  $\sim$  1100 to  $\sim$  1320 cm<sup>-1</sup>.

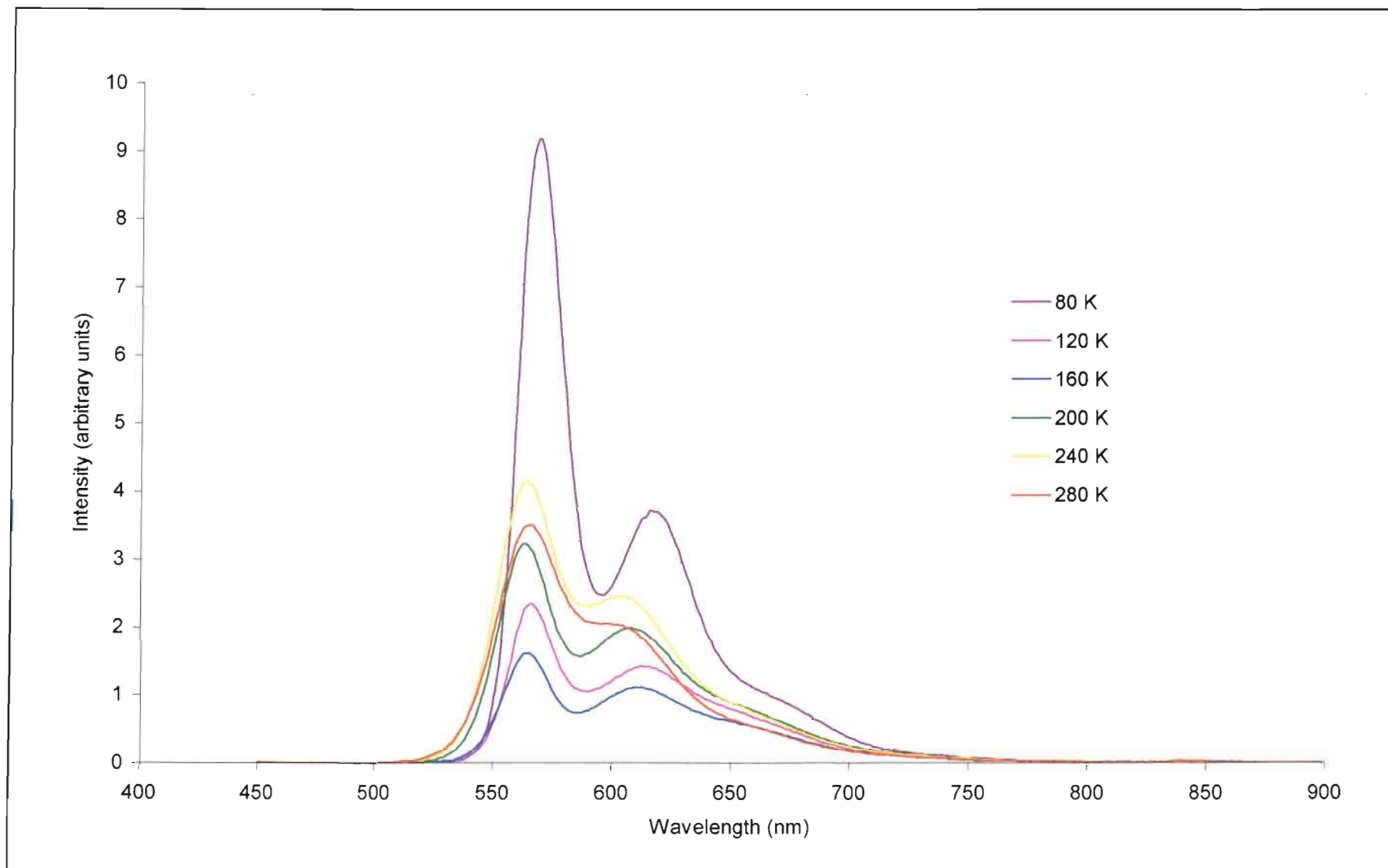


**Figure 3.25** Solid state emission spectra of  $[Pt(4'-pBiph-terpy)Cl]SbF_6 (Z)$  ( $\lambda_{ex(max)} = 400nm$ ).



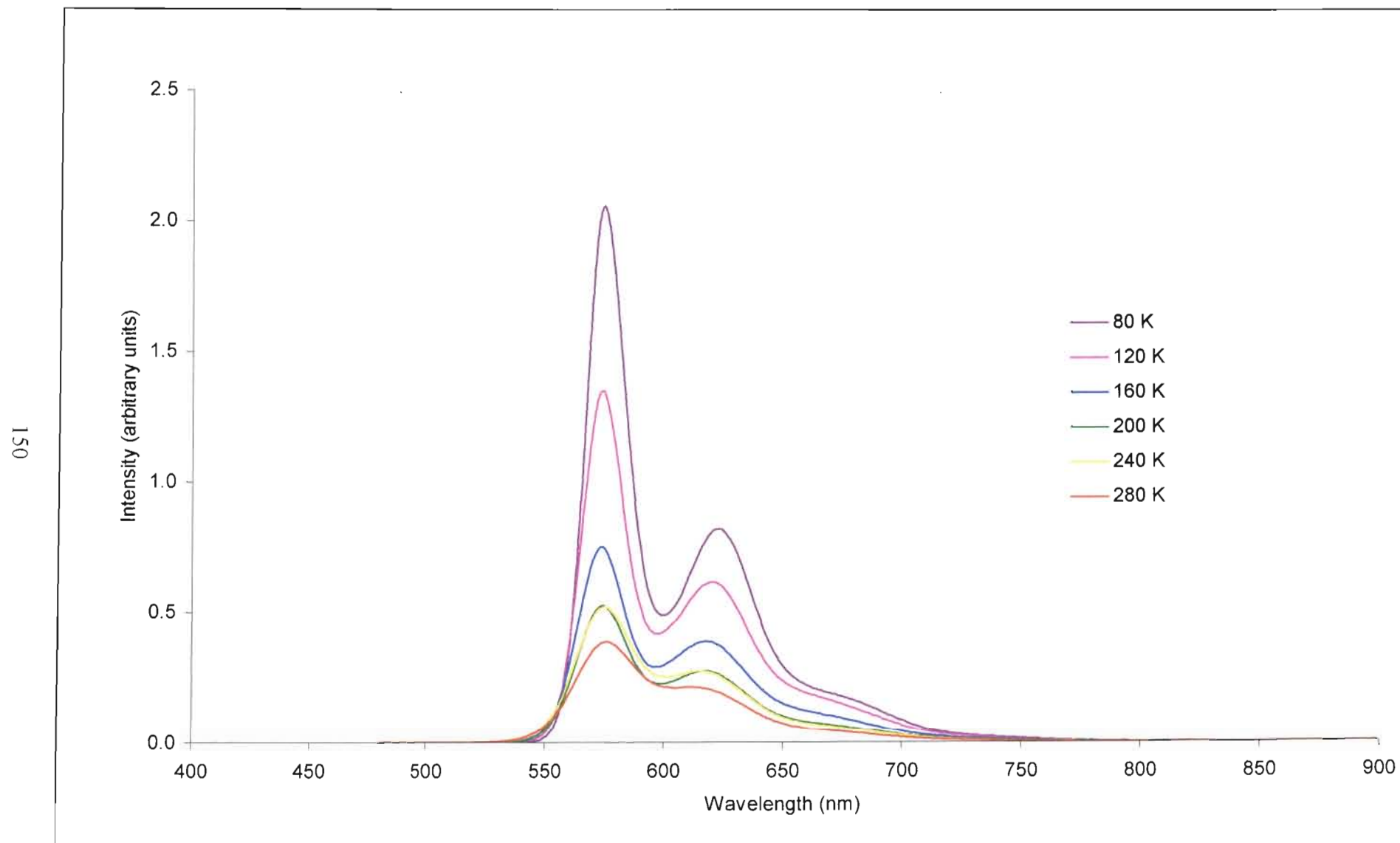


**Figure 3.26** Solid state emission spectra of  $[Pt(4'-pBiph-terpy)Cl]SbF_6$  (**7**)  $\{\lambda_{ex}(max) = 450nm\}$ .

Although the emission changes with temperature appear random at first, examination of the band profile, without taking into account the intensity changes, shows a systematic change from the emission profile at room temperature to that at 80 K (see Figure 3.27). The room temperature emission spectrum is typified by a vibrationally structured band with a spacing between the 0-0 and 0-1 transitions of less than  $1250\text{ cm}^{-1}$  and a Huang-Rhys ratio of approximately 0.6. In contrast, emission at the lowest temperatures (80 K) is characterised by a vibrationally structured band with a vibrational spacing larger than  $1250\text{ cm}^{-1}$  and a Huang-Rhys factor ranging between 0.4 and 0.7. The energy of the 0-0 transition for emission at room temperature and at 80 K are very similar and it is the Huang-Rhys factor and the vibrational spacing which appear to be a diagnostic feature of emission at each temperature. Changing the temperature between 280 and 80 K results in a gradual transformation in the emission features between the extremes described above for the respective temperatures.

In summary the solid emission exhibited by  $[\text{Pt}(4'\text{-}p\text{Biph-terpy})\text{Cl}]\text{SbF}_6$  at all temperatures is typical of monomer emission. Indeed, the energies of the vibrational progressions measured in the solid are similar to those recorded in fluid and glassy solutions. Accordingly the same assignment to the emitting state is made to one of mixed orbital parentage containing  $^3\text{IL}$ ,  $^3\text{MLCT}$  and some  $^3\text{ILCT}$  character.

In explaining the difference between the emission features of  $[\text{Pt}(4'\text{-}p\text{Biph-terpy})\text{Cl}]\text{SbF}_6$  at room and at low temperatures we propose that the temperature change is accompanied by changes in the dihedral angles between the various aromatic rings, which in turn changes the makeup of the configurationally mixed excited state, with overall planarity associated with more ligand centred character. The changes in dihedral angle are probably forced by the contraction of lattice that occurs on cooling a crystal. The difference between emission at ambient and the lowest temperatures is then due to dissimilar contributions from each of the IL, ILCT and MLCT components making up the excited state. Another possibility is that one of the IL, ILCT or MLCT states deactivates through thermal population of a nearby state that is non-radiative and which is therefore not directly observed. However, its presence can be deduced from its effect on the composition of the emitting state itself. In the absence of crystal structure determinations at various temperatures these explanations, though plausible, cannot be confirmed.

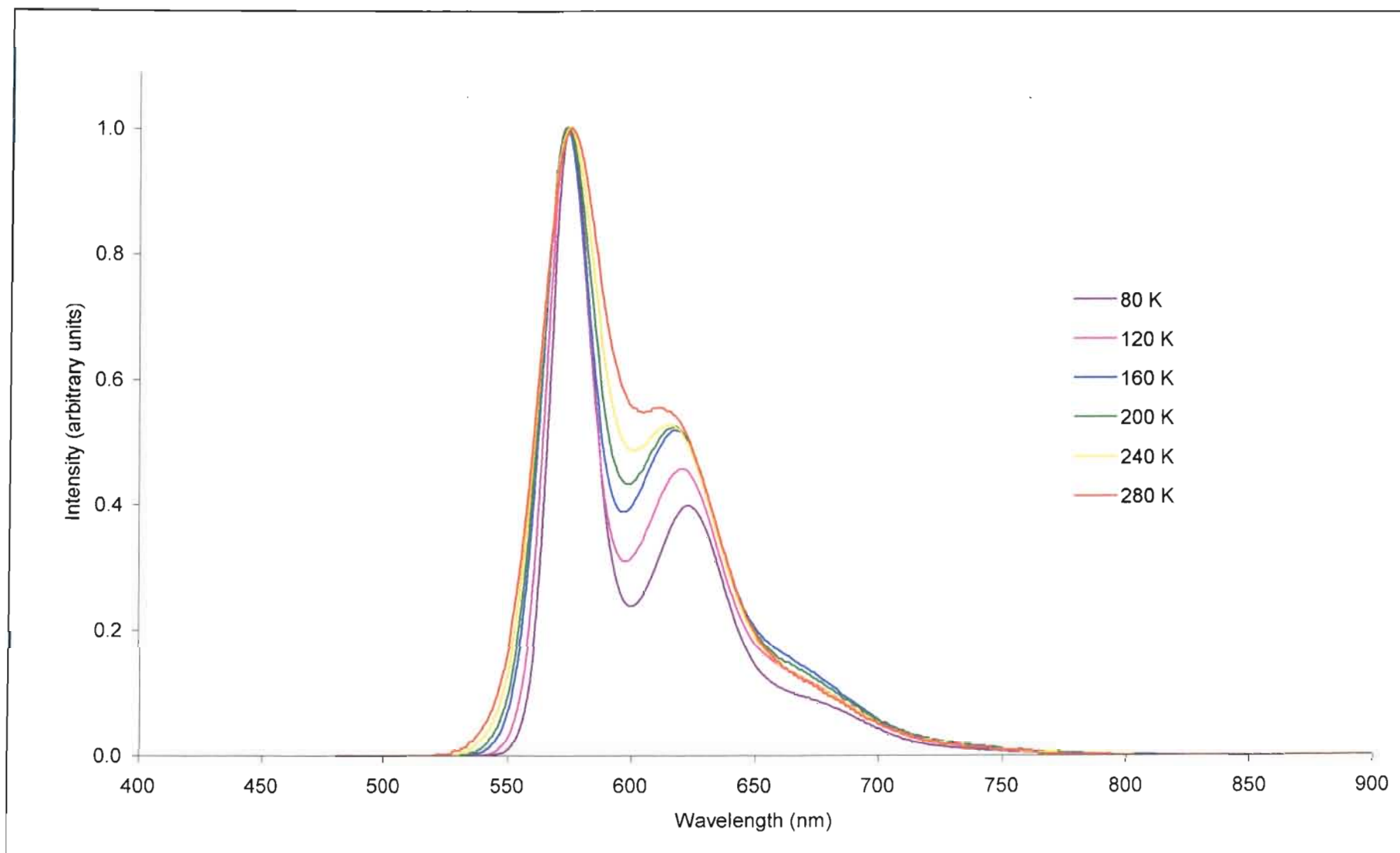


**Figure 3.27** Solid state emission spectra of  $[Pt(4'-pBiph-terpy)Cl]SbF_6$  (7)  $\{\lambda_{ex}(max) = 450nm\}$ . (Intensities adjusted arbitrarily to a value of 1.)

This is the same scenario as proposed to account for the solid state emissions from  $[\text{Pt}(4'\text{-}\beta\text{Np-terpy})\text{Cl}]\text{SbF}_6$  earlier in this chapter, and again we have a salt that is pale orange in colour and which emits from a configurationally mixed excited state. The difference here is that there is not a noticeable difference in energy between states dominating at each extreme in temperature.

#### *Solid state absorption and emission spectroscopy of $[\text{Pt}(4'\text{-}p\text{Biph-terpy})\text{Cl}]\text{BF}_4$*

The  $[\text{Pt}(4'\text{-}p\text{Biph-terpy})\text{Cl}]\text{BF}_4$  complex consists of the same  $[\text{Pt}(4'\text{-}p\text{Biph-terpy})\text{Cl}]^+$  luminophore, but with a tetrafluoroborate anion in the outer coordination sphere. The compound exists in two forms, one a yellow microcrystalline powder and the other a red crystalline powder. The photophysical properties of the yellow form will be discussed first.

A solid state absorption spectrum was recorded of a sample of the yellow form of  $[\text{Pt}(4'\text{-}p\text{Biph-terpy})\text{Cl}]\text{BF}_4$  and the most prominent low energy absorption band occurs at 436 nm. This absorption is present at a similar energy as that of  $[\text{Pt}(4'\text{-}m\text{Biph-terpy})\text{Cl}]\text{BF}_4$  and  $[\text{Pt}(4'\text{-}m\text{Biph-terpy})\text{Cl}]\text{CF}_3\text{SO}_3$  and hence is assigned to the same origin, that of a charge transfer state localised to the monomer.

Emission spectra recorded of the yellow microcrystalline salt are presented in Figure 3.28 and the emission behaviour is immediately reminiscent of the solid state emission recorded for the salts of the  $[\text{Pt}(4'\text{-}\beta\text{Np-terpy})\text{Cl}]^+$  cation described earlier in this section. At 280 K emission is in a vibronically structured band with maxima at 555, 597 and 647 nm. Emission decay was not found to be mono-exponential, but was measured at the tail-end at 2.8  $\mu\text{s}$ . Reducing the temperature to 80 K results in the onset of a new structured emission with maxima at 574, 623 and 677 nm. Vibrational spacing between these bands is between 1300 and 1400  $\text{cm}^{-1}$ , evidence of a ligand contribution to the excited state since this spacing corresponds to ligand stretching modes as observed by infrared spectroscopy. The room temperature band is still visible, but now as a shoulder at 552 nm. The luminescence intensity at this temperature still does not fall off exponentially but sampled at the tail-end decay was measured at 28.0  $\mu\text{s}$ . The similarity of this emission behaviour to that observed in the solid state for salts of the  $[\text{Pt}(4'\text{-}\beta\text{Np-terpy})\text{Cl}]^+$  cation results in the same description of the emission origin *viz.* emission

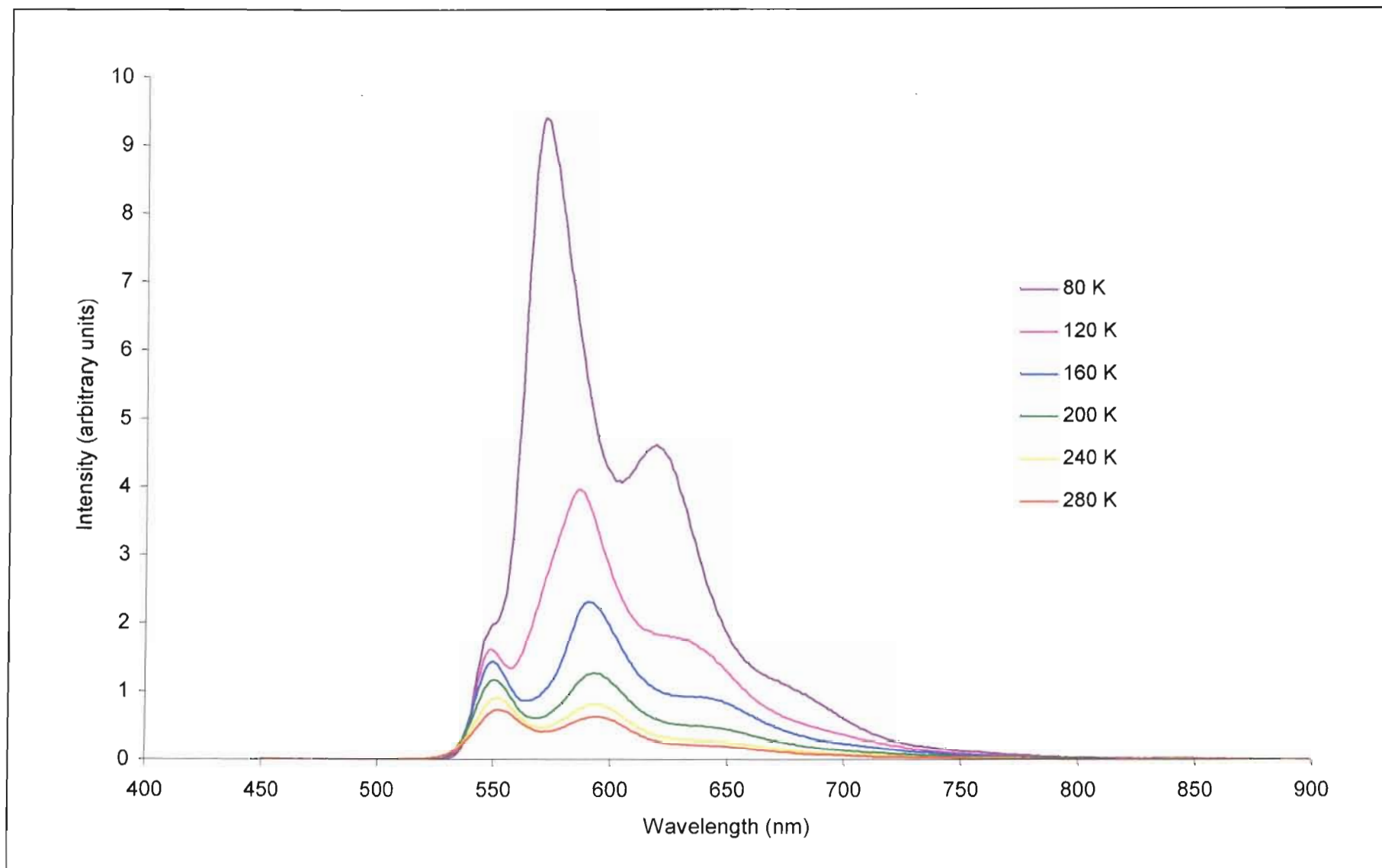


**Figure 3.28** Solid state emission spectra of the yellow form of  $[Pt(4'-pBiph-terpy)Cl]BF_4$  (**8**).

arising from a single configurationally mixed state with the relative contributions to the state changing with the lattice contraction. Significantly the 80 K maxima coincide very well with those found for the hexafluoroantimonate salt,  $[\text{Pt}(4'\text{-}p\text{Biph-terpy})\text{Cl}]\text{SbF}_6$ , measured under the same conditions.

*Solid state emission spectroscopy of the red form of  $[\text{Pt}(4'\text{-}p\text{Biph-terpy})\text{Cl}]\text{BF}_4$*

We now discuss the luminescence from the crystalline red form of the tetrafluoroborate salt of  $[\text{Pt}(4'\text{-}p\text{Biph-terpy})\text{Cl}]^+$ .

A solid state absorption spectrum has been recorded for the red form of  $[\text{Pt}(4'\text{-}p\text{Biph-terpy})\text{Cl}]\text{BF}_4$  which shows a prominent absorption band with peak intensity at *ca.* 560 nm. This is significantly lower in energy than the lowest energy absorption band in the solid state spectrum of  $[\text{Pt}(4'\text{-}p\text{Biph-terpy})\text{Cl}]\text{SbF}_6$  which has been assigned to absorption by the monomeric species. In conjunction with the red colour of the salt, we associated the very low absorption energy with aggregation of luminophores in the solid state.<sup>21</sup>

The luminescence spectra of the red form of  $[\text{Pt}(4'\text{-}p\text{Biph-terpy})\text{Cl}]\text{BF}_4$  recorded over a range of temperatures between 80 and 280 K are reproduced in Figure 3.29. At 280 K emission is in a single, narrow (fwhm  $\approx 2130\text{ cm}^{-1}$ ) asymmetric peak, devoid of vibrational structure and with a maximum intensity at 683 nm, essentially the energy at which the MMLCT emission was observed in a rigid glassy medium at 77 K. At 120 K the emission profile is very similar, but has shifted significantly to an even lower energy. Further reducing the temperature results in a further narrowing of the band profile (to a fwhm of  $\approx 1920\text{ cm}^{-1}$  at 80 K) and a lengthening in its emission wavelength to 720 nm. In addition a new emission gradually becomes evident at 586 nm as the temperature is reduced from 120 to 80 K.

The intensity of the band displays an unusual relationship with temperature. As the temperature falls from 280 K, the luminescence intensity shows an initial increase, reaching a maximum at 240 K, before falling to an overall minimum intensity by 90 K and then slightly improving again. Tests of the instrument response using different samples ruled out instrument error and the behaviour appears to be intrinsic to the salt. The reason for this peculiar result is not known.

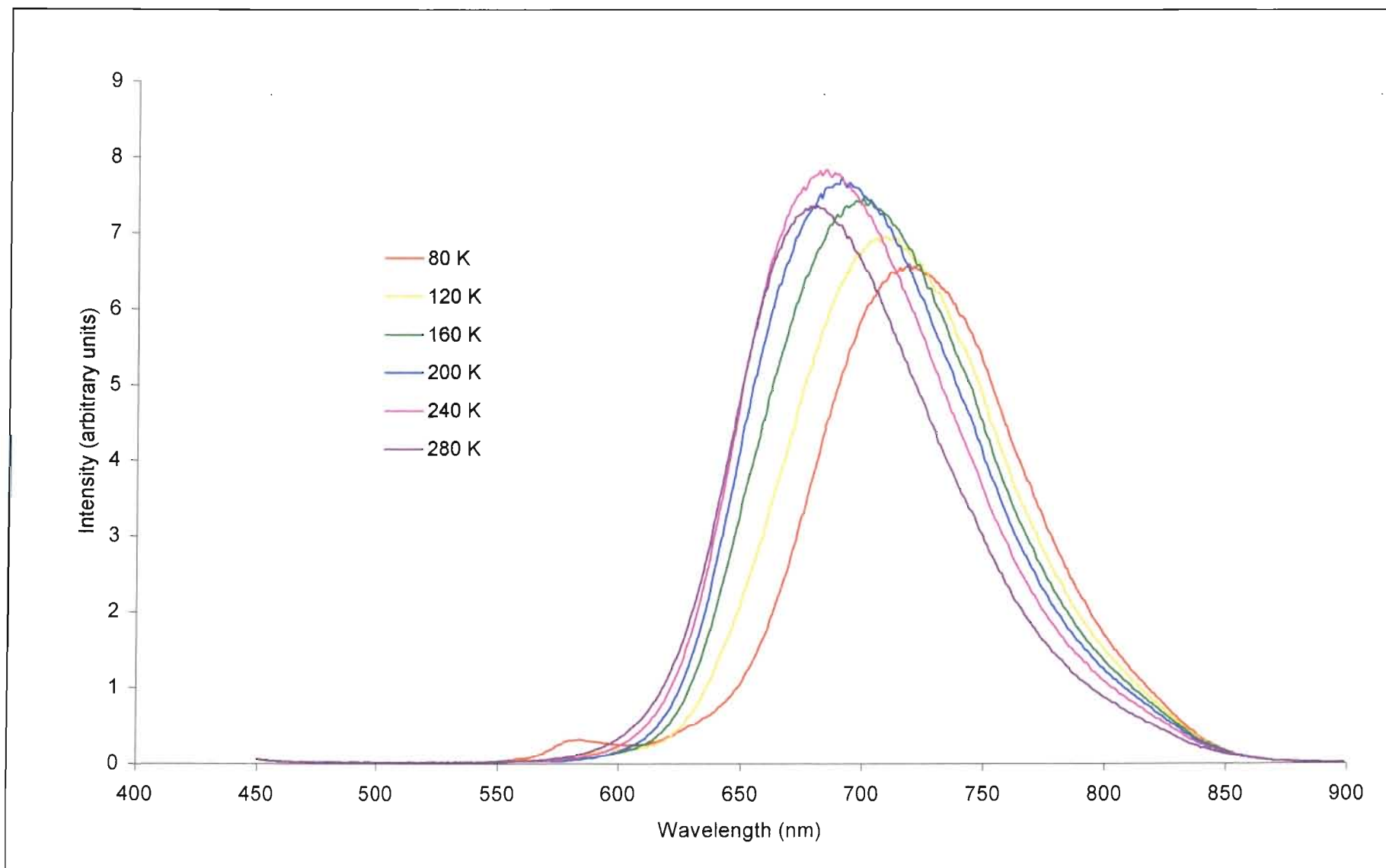


**Figure 3.29** Solid state emission spectra of the red form of  $[Pt(4'-pBiph-terpy)Cl]BF_4$  (**8**).

The presence of a narrow, asymmetric band that is stabilised in energy as the temperature falls is indicative of radiative decay from a MMLCT excited state.<sup>29</sup> The most striking feature of the luminescence is its low energy, which is likely to be brought about by extended Pt...Pt interactions in the solid state which significantly stabilise the excited state. This assignment is consistent with that made for the very low energy absorption band observed in the solid state absorption spectrum.

There is no precedent in previously reported MMLCT emissions for the appearance of a band analogous to that at 586 nm which is present at the lowest temperatures. It is somewhat lower in energy than the monomeric emission recorded in a DME glass at 77 K which shows its peak emission intensity at *ca.* 550 nm. This is sufficient evidence to rule out the presence of isolated emitting monomers in the solid state. Falling where it does, lower in energy than the monomer yet higher in energy than the MMLCT emission, in addition to its presence at only the lowest temperatures makes excimer emission a plausible origin for this emission. At temperatures below 120 K, where the 586 nm band becomes evident, luminophores appear to still be approaching each other as the temperature is reduced further. This can be seen by a MMLCT emission energy that is consistently falling with temperature. We speculate that the emission is excimeric in origin and that it results from the interaction of one (or both) phenyl rings on adjacent luminophores to produce an excimeric excited state in addition to the dominant MMLCT emission. Hannon and coworkers have coordinated the same 4'-*p*Biph-terpy ligand to a variety of metals and have shown that the biphenyl portions of the complexes promote the assembly of supramolecular structures in the solid state through  $\pi$ - $\pi$  interactions.<sup>142</sup> It is likely that the same effect is present here to produce extended  $\pi$ -stacking, and hence excimeric emission in the solid state of the red form of [Pt(4'-*p*Biph-terpy)Cl]BF<sub>4</sub>. An excimeric emission assignment for the band at 586 nm suggests that a complete charge separation between the biphenyl and platinum-terpyridyl fragments of luminophores becomes possible as molecular orbitals localised *between* adjacent luminophores begin to form.

Platinum(II) complexes containing  $\alpha, \alpha'$ -diimine<sup>46, 157, 161</sup> and terpyridyl<sup>29, 53, 162</sup> ligands have a propensity for existing with more than one packing architecture in the solid state *i.e.*, for polymorphism. In an investigation of the factors promoting linear chain formation in complexes of platinum(II), Gray *et al.* make the point that the solid state arrangement is



brought about by the relative stability of the various packing arrangements which in turn are influenced by factors unique for each compound.<sup>157</sup> Thus more than one arrangement with sufficient stability could exist and appear as polymorphism. Additional stable crystalline forms could also be brought about by solvent inclusion. This does not seem to be the case here as neither the <sup>1</sup>H NMR spectroscopic results nor the elemental analysis for C, H and N shows any evidence of included acetonitrile in either the red or yellow polymorphs. It is noteworthy that the two platinum(II) complexes [Pt(4'-Ph-terpy)Cl]BF<sub>4</sub> and [Pt(bipy)Cl<sub>2</sub>] (where bipy is 2,2'-bipyridine) both exist in a red and a yellow form.<sup>53, 163</sup> In both cases a X-ray crystal structure of the red form shows stacked luminophores with extended Pt...Pt interactions which brings about a MMLCT emitting state.<sup>41, 46, 53</sup> A X-ray structure determination of the yellow form of [Pt(bipy)Cl<sub>2</sub>] shows the complete absence of any metal-metal contact. Predictably emission from the yellow forms of both complexes confirm this absence of a close metal contact, with the emission origins localised to the monomer.<sup>41, 53</sup> By analogy the likelihood therefore exists that the same effects are at work in the solid state emission from the red form of [Pt(4'-pBiph-terpy)Cl]BF<sub>4</sub> and, in particular, that there is a significant platinum d<sub>2</sub>...d<sub>2</sub> orbital interaction between adjacent luminophores in the red form of [Pt(4'-pBiph-terpy)Cl]BF<sub>4</sub>.

*Solid state absorption and emission spectroscopy of [Pt(4'-pBiph-terpy)Cl]CF<sub>3</sub>SO<sub>3</sub>*

Finally we report the solid state photophysical properties of the bright orange triflate salt of [Pt(4'-pBiph-terpy)Cl]<sup>+</sup> viz. [Pt(4'-pBiph-terpy)Cl]CF<sub>3</sub>SO<sub>3</sub>. An absorption spectrum recorded in the solid state shows a prominent peak at 475 nm which is assigned to a charge transfer transition within the monomer by comparison with the solution spectra and with the absorption spectra of the other two salts incorporating the [Pt(4'-pBiph-terpy)Cl]<sup>+</sup> luminophore. At lower energy there is also a weak but discernable band centred at 560 nm which is assigned to absorption from aggregated species in the solid state.

Emission at 280 K is in a narrow (fwhm ≈ 2400 cm<sup>-1</sup>), asymmetric, structureless band centred at 627 nm. (See Figure 3.30.) An emission lifetime of 510 ns is recorded at ambient temperatures. The emission energy falls essentially linearly as the temperature is reduced from 280 to 80 K, reaching its longest wavelength emission at 686 nm. The band narrows concurrently, reaching a minimum of ca. 1800 cm<sup>-1</sup> at the lowest temperature. At this temperature the emission lifetime is 1.5 μs.

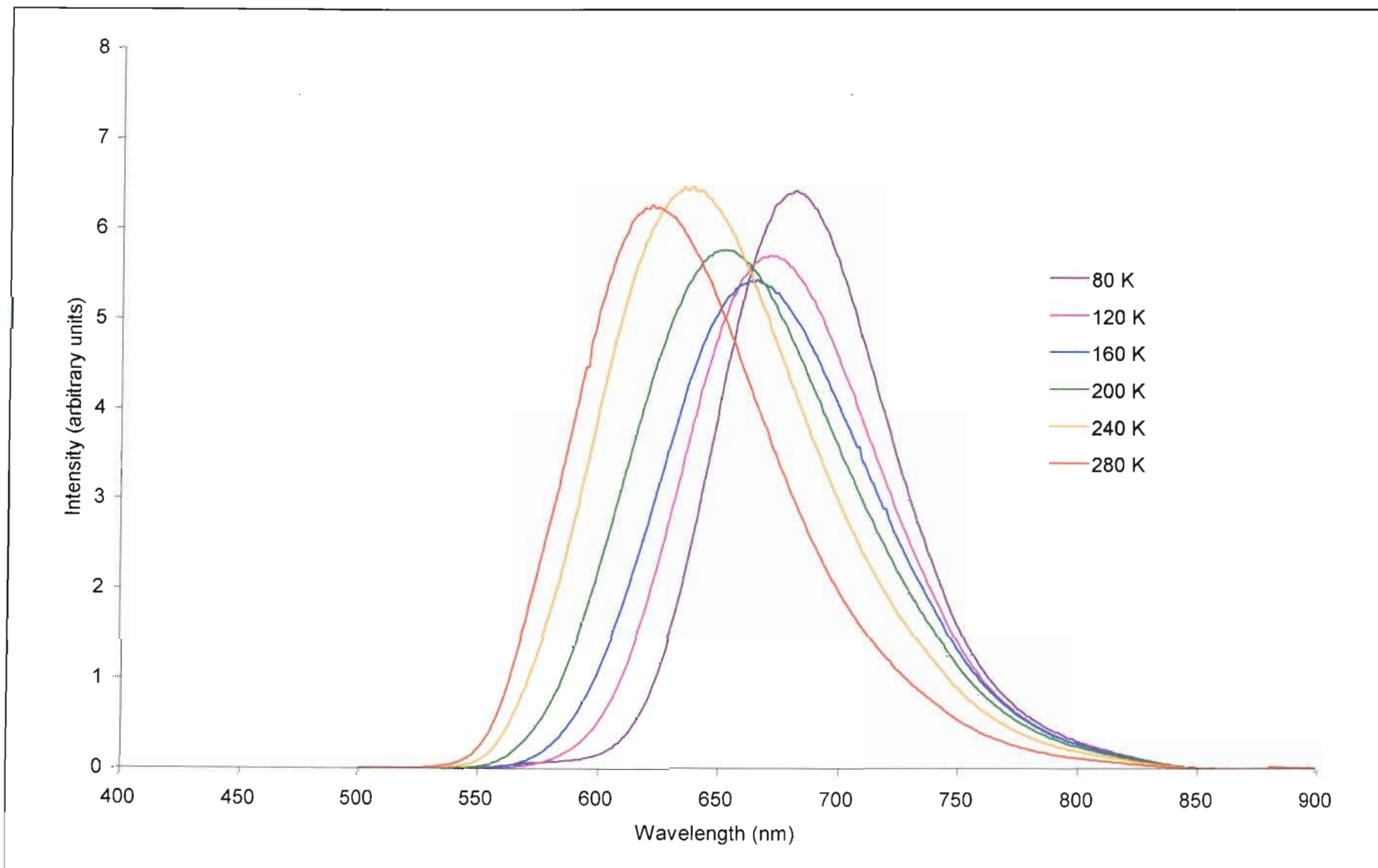


**Figure 3.30** Solid state emission spectra of  $[Pt(4'-pBiph-terpy)Cl]CF_3SO_3$  (9).

As for the red form of  $[\text{Pt}(4'\text{-}p\text{Biph-terpy})\text{Cl}]\text{BF}_4$ , peak intensities do not follow a pattern. Variable temperature emission spectra were repeated three times; twice using a 510 nm excitation and once with an excitation wavelength of 470 nm. Curiously emission intensities were not reproducible in any instance. The reason for this unusual behaviour is not understood. Importantly the emission maxima were identical on every occasion.

Excitation spectra indicate the presence of a band centred at 560 nm, matching a band of similar energy in the absorption spectrum indicating that the observed emission occurs from a single species. Significantly this excitation band does not fall at the energy at which the monomer absorbs, but at a lower energy where bands in the solid state absorption spectrum have been assigned to absorbance from aggregated species.

An unstructured emission profile is inconsistent with emission from excited states with significant ligand character. In any event, the energy of emission from  $[\text{Pt}(4'\text{-}p\text{Biph-terpy})\text{Cl}]\text{CF}_3\text{SO}_3$  is too low for any form of ligand centred emission. A narrow structureless asymmetric band is most often associated with emission from an intermolecular excited state brought about by close platinum-platinum interactions, *i.e.* a MMLCT state. Although somewhat higher in energy than the MMLCT emission observed for the red form of  $[\text{Pt}(4'\text{-}p\text{Biph-terpy})\text{Cl}]\text{BF}_4$ , emission from  $[\text{Pt}(4'\text{-}p\text{Biph-terpy})\text{Cl}]\text{CF}_3\text{SO}_3$  still falls into the energy range at which MMLCT emission is possible. Significantly the red emission shift which accompanies temperature reduction is a diagnostic feature of MMLCT emission and based on this observation, emission from  $[\text{Pt}(4'\text{-}p\text{Biph-terpy})\text{Cl}]\text{CF}_3\text{SO}_3$  is assigned to such an excited state.

### 3.3 SUMMARY AND CONCLUSIONS

The study of chloro(terpyridine)platinum(II) complexes with extensively  $\pi$ -conjugated substituents in the 4'-position of the terpyridyl ligand was prompted by the unusually long emission lifetime of the  $[\text{Pt}(4'\text{-}\alpha\text{Np-terpy})\text{Cl}]^+$  luminophore in a non-coordinating solvent, recorded at *ca.* 17  $\mu\text{s}$ .<sup>32</sup> A transition metal complex with such a long emission lifetime generates hope for photocatalysts, especially if it were possible to produce a similar compound with an even longer-lived excited state. The  $[\text{Pt}(4'\text{-}\alpha\text{Np-terpy})\text{Cl}]^+$  {where 4'- $\alpha\text{Np-terpy}$  = 4'-( $\alpha$ -naphthyl)-2,2':6',2''-terpyridine} luminophore has an  $\alpha$ -naphthyl substituent in the 4'-position of the terpyridyl ligand; indeed the long lifetime is associated with the presence of this group. However, its precise role in stabilising the excited state was not understood. Our approach to gaining a better understanding has been to synthesise closely related systems, in particular complexes with similar substituents in the 4'-position of the terpyridyl ligand and to investigate their luminescence properties. To this end investigations have been undertaken on the luminescence properties of nine platinum(II) terpyridyl complexes. These are  $[\text{Pt}(4'\text{-}\beta\text{Np-terpy})\text{Cl}]\text{X}$  [ $\text{X}^- = \text{SbF}_6^-$  (**1**),  $\text{BF}_4^-$  (**2**),  $\text{CF}_3\text{SO}_3^-$  (**3**)] {where 4'- $\beta\text{Np-terpy}$  = 4'-( $\beta$ -naphthyl)-2,2':6',2''-terpyridine},  $[\text{Pt}(4'\text{-}m\text{Biph-terpy})\text{Cl}]\text{X}$  [ $\text{X}^- = \text{SbF}_6^-$  (**4**),  $\text{BF}_4^-$  (**5**),  $\text{CF}_3\text{SO}_3^-$  (**6**)] {where 4'- $m\text{Biph-terpy}$  = 4'-(*meta*-biphenyl)-2,2':6',2''-terpyridine}, and  $[\text{Pt}(4'\text{-}p\text{Biph-terpy})\text{Cl}]\text{X}$  [ $\text{X}^- = \text{SbF}_6^-$  (**7**),  $\text{BF}_4^-$  (**8**),  $\text{CF}_3\text{SO}_3^-$  (**9**)] {where 4'- $p\text{Biph-terpy}$  = 4'-(*para*-biphenyl)-2,2':6',2''-terpyridine}.

The discussion of results collected in this study will commence with an overview of the monomeric emissions recorded in room temperature fluid solution and in a dilute rigid glassy medium at 77 K. This is followed by a discussion of the solid state photophysical properties of each of the salts.

#### *Emission from room temperature fluid solution*

The room temperature emission data recorded in fluid solution for each of the three luminophores *viz.*  $[\text{Pt}(4'\text{-}\beta\text{Np-terpy})\text{Cl}]^+$ ,  $[\text{Pt}(4'\text{-}m\text{Biph-terpy})\text{Cl}]^+$  and  $[\text{Pt}(4'\text{-}p\text{Biph-terpy})\text{Cl}]^+$  are summarised in Table 3.4 (reproduced here). In addition the data from the closely related

[Pt(4'- $\alpha$ Np-terpy)Cl]<sup>+</sup> and [Pt(4'-Ph-terpy)Cl]<sup>+</sup> luminophores are presented alongside that of complexes described in this work. Complexes in the table are ordered according to their respective emission energies.

**Table 3.4** Summary of emission data recorded in dichloromethane solution at 298 K.

Compound	$\lambda_{em}(\text{max})$ of 0-0 transition (nm)	Huang- Rhys factor	$\tau$ ( $\mu\text{s}$ )	Assignment
[Pt(4'-Ph-terpy)Cl] <sup>+</sup> <sup>32</sup>	535	0.88	0.09	<sup>3</sup> [IL/MLCT]
[Pt(4'- <i>m</i> Biph-terpy)Cl] <sup>+</sup>	536	0.77	0.12	<sup>3</sup> [IL/MLCT]
[Pt(4'- <i>p</i> Biph-terpy)Cl] <sup>+</sup>	562	0.65	4	<sup>3</sup> [IL/ILCT/MLCT]
[Pt(4'- $\beta$ Np-terpy)Cl] <sup>+</sup>	570	0.58	11.9	<sup>3</sup> [IL/ILCT/MLCT]
[Pt(4'- $\alpha$ Np-terpy)Cl] <sup>+</sup> <sup>32, 111</sup>	588	-	16.6	<sup>3</sup> [IL/ILCT/MLCT]

In each case an acetonitrile solution of the luminophore is non-emissive, but emission is observed in deoxygenated dichloromethane solution, providing an indication of the MLCT character present in the excited state that makes the emission prone to solvent induced exciplex quenching. Emission in deoxygenated dichloromethane is in a structured band {except in the case of [Pt(4'- $\alpha$ Np-terpy)Cl]<sup>+</sup>} with its 0-0 transition at wavelengths shorter than 590 nm. In all cases monomer emission is from a configurationally mixed excited state. This excited state has in common for all the luminophores an <sup>3</sup>IL ( $\pi$ - $\pi^*$ ) and a <sup>3</sup>MLCT ( $d$ - $\pi^*$ ) contribution. What distinguishes the emitting states for the different luminophores are the relative contributions of <sup>3</sup>IL and <sup>3</sup>MLCT character to the excited state and, more significantly, the presence or absence of an <sup>3</sup>ILCT contribution. The presence of ILCT character is evidenced by long emission lifetimes for the emitting state ranging from 4.0  $\mu\text{s}$  for [Pt(4'-*p*Biph-terpy)Cl]<sup>+</sup> to 16.6  $\mu\text{s}$  for [Pt(4'- $\alpha$ Np-terpy)Cl]<sup>+</sup>. In the former case, the ILCT component has its origin in inductive effects associated with the terminal phenyl group occupying a position on the central phenyl ring that is *para* to the interannular bond to the terpyridyl moiety. In the case of the two naphthyl derivatives, it is the presence of an easily ionisable fused ring system that is responsible for ILCT character in the emitting state. We conclude that a long

lifetime for a platinum complex is “guaranteed” by coordination to the platinum of a terpyridyl ligand that is substituted in the 4'-position by a fused-ring system. Further confirmation of this conclusion is provided by a 64  $\mu\text{s}$  lifetime recorded in dichloromethane for the  $[\text{Pt}(4'\text{-Pyre1-terpy})\text{Cl}]^+$  luminophore {where 4'-Pyre1-terpy denotes 4'-(1-pyrenyl-2,2':6',2''-terpyridine)}.<sup>31</sup>  
<sup>32</sup> However, as the example of the 4'-*p*Biph-terpy derivative shows, other factors may lead to an ILCT contribution to the excited state and hence to a longer emission lifetime.

Also worthy of comment are the Huang-Rhys factors listed in Table 3.4. These show a systematic decrease down the list of complexes, reflecting the change in composition of the emitting state and, in particular, the increasing contribution of charge transfer character (MLCT and/or ILCT) to the excited state. (Unfortunately, it was not possible to extend this analysis to the 4'- $\alpha$ Np-terpy derivative in view of the lack of vibrational structure in its emission band profile.) As previously noted, were it not for the change in the makeup of the emitting state for the series of complexes, the energy gap law would be violated since the law predicts that emission lifetimes should decrease (not increase) as the energy of the emission decreases.

We now address the difference in the fluid solution emission behaviour brought about by bonding the naphthyl ring *via* its  $\beta$ - as opposed to its  $\alpha$ -position. The lifetime is somewhat longer for  $[\text{Pt}(4'\text{-}\alpha\text{Np-terpy})\text{Cl}]^+$  and two possibilities arise. The difference in lifetime can either be ascribed to an unequal rotational barrier of the naphthyl group relative to the rest of the luminophore, or there is a difference in the inductive effect brought about by  $\beta$ - as opposed to  $\alpha$ -substitution of the naphthyl ring. The difference in inductive influences of the  $\alpha$ -naphthyl ring compared to a  $\beta$ -naphthyl ring are expected to be negligible, and both  $\alpha$ -naphthyl and  $\beta$ -naphthyl groups can be regarded merely as electron rich systems. Thus a more likely cause for the difference in excited state lifetimes would be the greater steric rotational barrier about the interannular bond in the 4'-position in the  $[\text{Pt}(4'\text{-}\alpha\text{Np-terpy})\text{Cl}]^+$  luminophore due to the *peri*-interaction associated with substitution of the naphthyl ring in the  $\alpha$ -position. A restricted rotation would influence the nature of the excited state by interrupting the extent of electron delocalisation between the naphthyl and platinum-terpyridyl moieties. It is this restricted rotation present in the  $[\text{Pt}(4'\text{-}\alpha\text{Np-terpy})\text{Cl}]^+$  luminophore to which we ascribe the difference in the precise composition of the excited states of the two complexes and hence in the differing

emission lifetimes. Of course steric interference to the rotation of the interannular bond in the 4'-position is also present for the  $\beta$ -naphthyl substituted luminophores, just to a far lesser extent. Conjugation in the  $\beta$ -naphthyl substituted luminophore is thus expected to be more extensive than in the case of  $\alpha$ -naphthyl substitution as the naphthyl group is more likely to be nearly coplanar with the platinum-terpyridyl fragment, allowing a greater electron delocalisation over the entire luminophore. It is interesting that this more extensive electron delocalisation over the terpyridyl ligand seems to be manifested in a greater  $\pi$ - $\pi^*$  contribution to the nature of the excited state, evident in a more structured emission band for the  $\beta$ -naphthyl derivative.

#### *Glass emission spectra*

The emission behaviour in a DME glass of the three luminophores,  $[\text{Pt}(4'\text{-}\beta\text{Np-terpy})\text{Cl}]^+$ ,  $[\text{Pt}(4'\text{-}m\text{Biph-terpy})\text{Cl}]^+$  and  $[\text{Pt}(4'\text{-}p\text{Biph-terpy})\text{Cl}]^+$  are all essentially similar, in that they all exhibit three concentration dependent emissions. At the lowest concentrations emission from the monomeric luminophores is in a structured band with a 0-0 transition at a wavelength shorter than 570 nm. As the concentration is raised it is possible to identify a MMLCT emission at the lowest energies, usually emitting in a structureless band with  $\lambda_{\text{em}}(\text{max})$  at wavelengths longer than 650 nm. With care it is also possible to detect emission from excimeric species in a broad structureless band at intermediate energies as the concentration is raised and before the MMLCT emission establishes itself as the dominant emission. Conditions were not optimized to study this emission in detail. Similar emission behaviour has previously been reported by both Gray *et al.*<sup>29</sup> and by Campagna and coworkers<sup>42</sup> in studying the emission in rigid glassy medium of  $[\text{Pt}(\text{terpy})\text{Cl}]^{+29,42}$  and related luminophores.<sup>42</sup> As such this emission behaviour is neither new or unexpected, but serves to aid our understanding of the excited state.

The data in Table 3.5 summarises the monomeric emission recorded for the same set of luminophores in a dilute glassy solution. Emission in each case is in a structured band with 0-0 transition in the 510 - 550 nm range. The excited state assignment in a dilute glassy solution is the same as that made in a room temperature dichloromethane solution (*vide supra*). Unfortunately a detailed analysis of trends in the emission energies and lifetimes is not

possible since the spectra were not all recorded in the same medium. Further complications are the absence of reliable lifetime data for the  $[\text{Pt}(4'\text{-}m\text{Biph-terpy})\text{Cl}]^+$  and some uncertainty in the precise values of the energies of the 0-0 transitions for the  $[\text{Pt}(4'\text{-}\beta\text{Np-terpy})\text{Cl}]^+$  and  $[\text{Pt}(4'\text{-}p\text{Biph-terpy})\text{Cl}]^+$  complexes. Nevertheless we believe that the excited state assignments are consistent with the available data though, clearly, some modification to the exact compositions of the emitting state will occur when the solvent is changed from dichloromethane to a glass.

**Table 3.5** Monomeric emission data recorded in a dilute glassy DME solution at 77 K.

Compound	$\lambda_{\text{em}}(\text{max})$ of 0-0 transition (nm)	Huang-Rhys factor	$\tau$ ( $\mu\text{s}$ )	Assignment
$[\text{Pt}(4'\text{-Ph-terpy})\text{Cl}]^{+32}$	470 <sup>BuCN</sup>	0.7	15	<sup>3</sup> [IL/MLCT]
$[\text{Pt}(4'\text{-}m\text{Biph-terpy})\text{Cl}]^+$	510 <sup>DME</sup>	2.3	- <sup>a</sup>	<sup>3</sup> [IL/MLCT]
$[\text{Pt}(4'\text{-}p\text{Biph-terpy})\text{Cl}]^+$	550 <sup>DME</sup>	0.8 - 0.9	2.9	<sup>3</sup> [IL/ILCT/MLCT]
$[\text{Pt}(4'\text{-}\beta\text{Np-terpy})\text{Cl}]^+$	550 <sup>DME</sup>	0.7	47	<sup>3</sup> [IL/ILCT/MLCT]
$[\text{Pt}(4'\text{-}\alpha\text{Np-terpy})\text{Cl}]^{+32, 111}$	540 <sup>BuCN</sup>	0.8	-	<sup>3</sup> [IL/ILCT/MLCT]

(BuCN) Solvent used is butyronitrile.

(DME) Solvent used is 1:5:5 (v/v) DMF/MeOH/EtOH

(a) A reliable emission lifetime could not be measured.

A brief summary of the lowest energy emission recorded in concentrated solutions of various luminophores is provided in Table 3.6. In all cases emission has been assigned to a MMLCT excited state brought about by  $d_{z^2}$ -orbital overlap of the platinum centres on adjacent luminophores. There is precedent for this type of emission from both the  $[\text{Pt}(\text{terpy})\text{Cl}]^+$ -<sup>29,42</sup> and  $[\text{Pt}(4'\text{-Ph-terpy})\text{Cl}]^+$ -luminophores,<sup>42</sup> although emission in these cases has been reported using a lower energy excitation wavelength. Noteworthy are the emission lifetimes which all fall in the 1.6 - 2.6  $\mu\text{s}$  range, typical of MMLCT emission at 77 K.<sup>29,42,54</sup> In the cases of  $[\text{Pt}(4'\text{-}\beta\text{Np-terpy})\text{Cl}]^+$ ,  $[\text{Pt}(4'\text{-}m\text{Biph-terpy})\text{Cl}]^+$  and  $[\text{Pt}(4'\text{-}p\text{Biph-terpy})\text{Cl}]^+$  the emission lifetimes are essentially identical, recorded at 1.9  $\mu\text{s}$ . This similarity in emission lifetimes, regardless of the



nature of the luminophore stands in stark contrast to the monomeric emission in fluid solution (see Table 3.5) that shows highly variable emission lifetimes depending on the nature of the luminophore, in particular on the ligand that was used. This similarity is easily explained in terms of the type of molecular orbital involved in producing the observed emission. The transition bringing about a MMLCT excited state involves molecular orbitals localised to the chloro(terpyridyl)platinum(II) binding domain. The 4'-substituent which distinguishes the ligands plays no part in bringing about the molecular orbital configuration responsible for this emission.

**Table 3.6** Summary of MMLCT emission data recorded in rigid glassy solution at 77 K.

Compound	Excitation wavelength (nm)	Emission maximum (nm)	$\tau$ ( $\mu$ s)
[Pt(terpy)Cl] <sup>+</sup> 42	540	730 <sup>M/E, 42</sup>	2
[Pt(4'-Ph-terpy)Cl] <sup>+</sup> 42	540	690 <sup>M/E, 42</sup>	2.6
[Pt(4'- <i>m</i> Biph-terpy)Cl] <sup>+</sup>	510	671 <sup>DME</sup>	1.9
[Pt(4'- <i>p</i> Biph-terpy)Cl] <sup>+</sup>	510	685 <sup>DME</sup>	1.9
[Pt(4'- $\beta$ Np-terpy)Cl] <sup>+</sup>	490	696 <sup>DME</sup>	1.9

(M/E) Solvent used is 4:1 (v/v) MeOH/EtOH  
(DME) Solvent used is 1:5:5 (v/v) DMF/MeOH/EtOH

#### *Solid state emission spectra*

The solid state emission displayed by the eleven complex salts which form part of this study can be divided into three groups according to emission type. The first group of complexes consist of those that exhibit an essentially monomeric emission in the solid state, very similar to the emission shown by the luminophore in dilute solution. Complexes falling into this group are all those which have 4'- $\beta$ Np-terpy as the coordinated ligand and also the hexafluoroantimonate and the yellow tetrafluoroborate salts of the [Pt(4'-*p*Biph-terpy)Cl]<sup>+</sup> luminophore. The solid state emission properties for the complexes in the first group are summarised in Table 3.7.

**Table 3.7** Solid state spectroscopic data of complexes in Group I.<sup>a</sup>

Compound	Colour	$\lambda_{\text{abs}}(\text{max})$	$\lambda_{\text{em}}(\text{max})$ (nm)	$\tau$ (ns)
		(nm)	[77 K]	[77 K]
[Pt(4'- $\beta$ Np-terpy)Cl]SbF <sub>6</sub> ( <b>1</b> )	orange	<u>470</u> , <i>ca.</i> 520, <i>ca.</i> 560	<u>572</u> , 615, 663, [ <u>596</u> , 655, 723]	395 <sup>#</sup> [3800]
[Pt(4'- $\beta$ Np-terpy)Cl]BF <sub>4</sub> ( <b>2</b> )	orange	<u>460</u>	<u>582</u> , 621, 670 [ <u>622</u> , 684, 750]	360 <sup>#</sup> [3900]
[Pt(4'- $\beta$ Np-terpy)Cl]CF <sub>3</sub> SO <sub>3</sub> ( <b>3</b> )	yellow	<u>460</u> , <i>ca.</i> 520, <i>ca.</i> 560	<u>578</u> , 621, 668 [ <u>612</u> , 674, 740]	390 <sup>#</sup> [4200]
[Pt(4'- <i>p</i> Biph-terpy)Cl]SbF <sub>6</sub> ( <b>7</b> )	pale orange	478	<u>566</u> , 603, <i>ca.</i> 660sh <sup>a</sup> [ <u>570</u> , 620, <i>ca.</i> 670sh] <sup>a</sup>  576, 612, <i>ca.</i> 670 <sup>b</sup> [576, 623, <i>ca.</i> 670] <sup>b</sup>	870 [6780] - -
[Pt(4'- <i>p</i> Biph-terpy)Cl]BF <sub>4</sub> ( <b>8</b> )	yellow	436	<u>555</u> , 597, 647 [552sh, <u>574</u> , 623, 677]	2780 <sup>#</sup> [28000] <sup>#</sup>

(a) These are complexes that exhibit monomer emission in the solid state.

(b)  $\lambda_{\text{em}}(\text{max}) = 400$  nm.

(c)  $\lambda_{\text{em}}(\text{max}) = 450$  nm.

Underlined values refer to the most intense bands within a manifold.

sh = shoulder.

# Biphasic decay, tail-end sampled.

Complexes showing emission that has its origin in an orbital brought about by close intermolecular Pt...Pt interactions *i.e.* from a MMLCT excited state, are placed in the second group which is represented by three complexes. These are the non-solvated form of [Pt(4'-*m*Biph-terpy)Cl]SbF<sub>6</sub>, the red form of [Pt(4'-*p*Biph-terpy)Cl]BF<sub>4</sub> and bright orange [Pt(4'-*p*Biph-terpy)Cl]CF<sub>3</sub>SO<sub>3</sub>. The emission properties for these complexes are summarised in Table 3.8. The last group of complexes show the most complex emission, brought about by simultaneous emission from MMLCT and monomer excited states. Complexes falling into this group are the acetonitrile solvated form of [Pt(4'-*m*Biph-terpy)Cl]SbF<sub>6</sub> *viz.*, [Pt(4'-*m*Biph-terpy)Cl]SbF<sub>6</sub>.CH<sub>3</sub>CN, and the tetrafluoroborate and triflate salts of the same luminophore.

Salient emission data can be found in Table 3.9. Emission from each group will now be discussed in turn.

The room temperature emission observed for complexes which appear to exhibit monomeric emission characteristics in the solid state is very similar to the dilute solution emission, except that the solid state emission occurs at slightly lower energies. Emission is in a structured band with two or three prominent progressions spaced 1200 - 1400  $\text{cm}^{-1}$  apart. As in solution the emission is assigned to a configurationally mixed excited state with contributions from IL, ILCT and MLCT transitions. It is interesting to note that each of the salts which exhibit emission from the monomer are either orange or yellow in colour. This relationship has previously been observed for platinum-polypyridyl complexes.<sup>53, 163</sup>

A reduction in temperature brings about a change in emission intensity and in the energy of the emission. This observation is attributed to the lattice contraction which results in a change in the composition of the configurationally mixed state. In particular, the lattice contraction is expected to induce different angles of rotation about the interannular bonds (one such bond when the ligand is 4'- $\beta$ Np-terpy and two such bonds when the ligand is 4'-*p*Biph-terpy) changing the overall planarity of the luminophore in a way that will inevitably lead to changes in the composition of the excited state. To be precise three changes in the monomeric emission profile can be indentified. These are: i) a change in the Huang-Rhys factor ii) a shift in energy and iii) slight changes in the vibrational spacing. The change in the Huang-Rhys factor is perhaps the most significant since this alteration is most indicative of a change in the admixture of states which makes up the configurationally mixed excited state. In particular, a more planar luminophore would facilitate a more extensive electron delocalisation over the luminophore and hence the ligand centred  $\pi$ - $\pi^*$  contribution would be stabilised and therefore constitute a stronger contribution to the excited state. Thus, although the overall assignment of the excited state is unaltered at low temperatures, the relative contributions making up the emitting state are clearly different.

**Table 3.8** Solid state spectroscopic data of complexes in Group II.<sup>a</sup>

Compound	Colour	$\lambda_{\text{abs}}(\text{max})$ (nm)	$\lambda_{\text{em}}(\text{max})$ (nm) [77 K]	fwhm ( $\text{cm}^{-1}$ ) [77 K]	$\tau$ (ns) [77 K]
[Pt(4'- <i>m</i> Biph-terpy)Cl]SbF <sub>6</sub> ( <b>4</b> )	orange	443, <u>525</u>	<u>640</u> [623]	2693 [1625]	250 <sup>#</sup> [1620]
[Pt(4'- <i>p</i> Biph-terpy)Cl]BF <sub>4</sub> ( <b>8</b> )	red	560	683 [586, <u>720</u> ]	2130 [1920]	- -
[Pt(4'- <i>p</i> Biph-terpy)Cl]CF <sub>3</sub> SO <sub>3</sub> ( <b>9</b> )	bright orange	<u>475</u> , 560	627 [684]	2400 [1800]	510 [1540]

(a) These are compounds that exhibit <sup>3</sup>MMLCT emission in the solid state.

Underlined values refer to the most intense bands within a manifold.

# Biphasic decay, tail-end sampled.

The MMLCT emission displayed by complexes falling into the second group (summarised in Table 3.8) is characterised by a dominant emission which is structureless and with a  $\lambda_{\text{em}}(\text{max})$  at wavelengths longer than 600 nm at both room temperature and at 77 K. The bands are typically narrow, with a fwhm < 2700  $\text{cm}^{-1}$  in all cases, narrowing even further as the temperature is reduced. In conjunction with a reduction in band width with temperature is a shift in emission maximum. Whether the shift is to lower or higher energy is unpredictable and depends on whether lattice contraction results in a reduction or in an increase in intermolecular Pt...Pt spacing. We predict that an increase in this distance would result in a blue emission shift and a red shift when the Pt...Pt distance is reduced in accordance with molecular orbital diagrams published by Che *et al.*<sup>28</sup> (see Figure 1.4).

Also significant is a solid state absorption spectrum which shows prominent maxima at wavelengths longer than 520 nm. This is considerably stabilised relative to the charge transfer absorption displayed in fluid solution and compared to the low energy absorption maxima displayed by the complexes in Group II *i.e.* relative to the monomer absorption energy.

The complexes are all darkly coloured, ranging from orange to deep red in colour. Darkly coloured complexes of this type reported previously have also been conclusively associated with MMLCT emission in the solid state and hence with platinum-platinum interactions in the solid state.<sup>46, 53, 163, 164</sup>

Finally, emission from the third group of complexes is summarised in Table 3.9.

**Table 3.9** *Solid state spectroscopic data of complexes in Group III.<sup>a</sup>*

Compound	Colour	$\lambda_{\text{abs}}(\text{max})$ (nm)	$\lambda_{\text{em}}(\text{max})$ (nm) [77 K]	$\tau$ (ns) [77 K]
[Pt(4'- <i>m</i> Biph-terpy)Cl]SbF <sub>6</sub> .CH <sub>3</sub> CN ( <b>4a</b> )	yellow-orange	-	565, <u>644</u> [557, 612, <u>666</u> ]	† [†]
[Pt(4'- <i>m</i> Biph-terpy)Cl]BF <sub>4</sub> ( <b>5</b> )	yellow	<u>443</u> , 525	545sh, 580, <u>653</u> , 715sh [543, 580, <u>621</u> , 650sh, 715sh]	† [†]
[Pt(4'- <i>m</i> Biph-terpy)Cl]CF <sub>3</sub> SO <sub>3</sub> ( <b>6</b> )	orange	<u>435</u> , 500	524, 556, <u>657</u> [540, 583, <u>625</u> ]	† [†]

(a) These are compounds that exhibit competitive (*i.e.* multiple emission) in the solid state, in particular from <sup>3</sup>MMLCT and <sup>3</sup>( $\pi$ - $\pi^*$ ) states.

Underlined values refer to the most intense bands within a manifold.

† Multiple emission components and lifetime determination not possible.

Emission from these complexes is typified by genuine multiple emission from two excited states which produce emission simultaneously. In each case one state has been assigned to a ligand centred origin and the other is <sup>3</sup>MMLCT in nature. The presence of the latter appears to be crucial in bringing about the multiple emission. Note that Kasha's rule is violated. According to this rule only emission from the lowest energy excited state (in this case the MMLCT state) should be observed.<sup>165</sup> For the compounds listed in Table 3.9 the two emitting states are of similar energy and, for this reason, we believe they are in thermal equilibrium with each other. On this basis the intensity of the ligand centred (IL) emission should decrease

relative to that of the MMLCT emission as the temperature is decreased. Unfortunately, it is impossible to discern such a trend since both types of emission are expected to increase in intensity when the temperature is lowered. Indeed, there are numerous examples of bipyridyl and terpyridyl ligand complexes for which the intensity of the solid emission increases with a decrease in temperature.<sup>29, 46, 53, 54</sup> Another complicating factor is that, being similar in energy, the IL and MMLCT bands overlap to a considerable extent. However our conclusion that multiple emission is observed in the solid state when monomer (IL) and MMLCT emission are similar in energy is borne out by the work of Kato *et al.* on the  $[\text{Pt}(i\text{-biq})]^{2+}$  systems (where *i*-biq is 2,2'-biisoquinoline).<sup>158, 159</sup>

## 3.4 EXPERIMENTAL

### 3.4.1 Synthetic procedures

#### 3.4.1.1 [Pt(4'- $\beta$ Np-terpy)Cl]X [ $X^-$ = SbF<sub>6</sub><sup>-</sup> (**1**), BF<sub>4</sub><sup>-</sup> (**2**), CF<sub>3</sub>SO<sub>3</sub><sup>-</sup> (**3**)]

{where 4'- $\beta$ Np-terpy = 4'-( $\beta$ -naphthyl)-2,2':6',2''-terpyridine}

The appropriate silver salt AgX (73 mg for  $X^-$  = SbF<sub>6</sub><sup>-</sup>; 41 mg for  $X^-$  = BF<sub>4</sub><sup>-</sup>; 54 mg for  $X^-$  = CF<sub>3</sub>SO<sub>3</sub><sup>-</sup>; 0.21 mmol), depending on the complex to be made, was dissolved in acetonitrile (5 ml) and added to a suspension of [Pt(PhCN)<sub>2</sub>Cl<sub>2</sub>] (100 mg, 0.21 mmol) in acetonitrile (10 ml). The mixture was refluxed overnight under an inert atmosphere before the resultant precipitate of AgCl was removed by filtration. An approximately equimolar amount of solid 4'-( $\beta$ -naphthyl)-2,2':6',2''-terpyridine (4'- $\beta$ Np-terpy) (75 mg, 0.20 mmol) was added and the mixture refluxed for 24 hrs. Once reflux was complete the mixture was filtered hot and the solvent partially removed under reduced pressure resulting in the precipitation of [Pt(4'- $\beta$ Np-terpy)Cl]X. The product was washed on the frit with copious amounts of diethyl ether and then smaller amounts of acetonitrile. The resulting powder was recrystallised from hot acetonitrile.

[Pt(4'- $\beta$ Np-terpy)Cl]SbF<sub>6</sub> (**1**): Yield 125 mg (72 %). Molecular mass 825.7 g.mol<sup>-1</sup>. [Calc. for C<sub>25</sub>H<sub>17</sub>ClF<sub>6</sub>N<sub>3</sub>PtSb: C, 36.37; H, 2.08; N, 5.09. Found: C, 36.85; H, 1.94; N, 5.06 %].

<sup>1</sup>H NMR for [Pt(4'- $\beta$ Np-terpy)Cl]SbF<sub>6</sub> (DMSO-d<sub>6</sub>):  $\delta$  8.76(2H, s, H<sup>3',5'</sup>) 8.61(1H, m, naphthyl H) 8.56(2H, m, H<sup>3,3''</sup>) 8.44(2H, m, H<sup>6,6''</sup>) 8.28(2H, m, H<sup>4,4''</sup>) 8.05(2H, s, naphthyl H's) 7.96(2H, m, naphthyl H's) 7.67(2H, m, H<sup>5,5''</sup>) 7.60 - 7.70(2H, m, naphthyl H's).

[Pt(4'- $\beta$ Np-terpy)Cl]BF<sub>4</sub> (**2**): Yield 105 mg (74 %). Molecular mass 676.7 g.mol<sup>-1</sup>. [Calc. for C<sub>25</sub>H<sub>17</sub>BClF<sub>4</sub>N<sub>3</sub>Pt: C, 44.37; H, 2.53; N, 6.21. Found: C, 43.78; H, 2.27; N, 6.07 %].

[Pt(4'- $\beta$ Np-terpy)Cl]CF<sub>3</sub>SO<sub>3</sub> (**3**): Yield 109 mg (70 %). Molecular mass 739.0 g.mol<sup>-1</sup>. [Calc. for C<sub>26</sub>H<sub>17</sub>ClF<sub>3</sub>N<sub>3</sub>O<sub>3</sub>PtS: C, 42.26; H, 2.32; N, 5.69. Found: C, 42.13; H, 2.06; N, 5.70 %].

### 3.4.1.2 [Pt(4'-*m*Biph-terpy)Cl]X [X<sup>-</sup> = SbF<sub>6</sub><sup>-</sup> (**4**), BF<sub>4</sub><sup>-</sup> (**5**), CF<sub>3</sub>SO<sub>3</sub><sup>-</sup> (**6**)]

{where 4'-*m*Biph-terpy = 4'-(*meta*-biphenyl)-2,2':6',2''-terpyridine}

The appropriate silver salt AgX (73 mg for X<sup>-</sup> = SbF<sub>6</sub><sup>-</sup>; 41 mg for X<sup>-</sup> = BF<sub>4</sub><sup>-</sup>; 54 mg for X<sup>-</sup> = CF<sub>3</sub>SO<sub>3</sub><sup>-</sup>; 0.21 mmol), depending on the complex to be made, was dissolved in acetonitrile (5 ml) and added to a suspension of [Pt(PhCN)<sub>2</sub>Cl<sub>2</sub>] (100 mg, 0.21 mmol) in acetonitrile (10 ml). The mixture was refluxed overnight under an inert atmosphere before the resultant precipitate of AgCl was removed by filtration. An approximately equimolar amount of solid 4'-(*meta*-biphenyl)-2,2':6',2''-terpyridine (4'-*m*Biph-terpy) (77 mg, 0.20 mmol) was added and the mixture refluxed for 24 hrs. Once reflux was complete the mixture was filtered hot and the solvent partially removed under reduced pressure resulting in the precipitation of [Pt(4'-*m*Biph-terpy)Cl]X. The product was washed on the frit with copious amounts of diethyl ether and then smaller amounts of acetonitrile. The resulting powder was recrystallised from hot acetonitrile.

[Pt(4'-*m*Biph-terpy)Cl]SbF<sub>6</sub> (**4**): Yield 129 mg (72 %). Molecular mass 851.7 g.mol<sup>-1</sup>. [Calc. for C<sub>27</sub>H<sub>19</sub>ClF<sub>6</sub>N<sub>3</sub>PtSb: C, 38.07; H, 2.25; N, 4.93. Found: C, 38.34; H, 1.99; N, 4.89 %].

<sup>1</sup>H NMR for [Pt(4'-*m*Biph-terpy)Cl]SbF<sub>6</sub> (DMSO-d<sub>6</sub>): δ 8.76(2H, s, H<sup>3',5'</sup>) 8.60(2H, d, H<sup>3,3''</sup>) 8.38(2H, m, H<sup>6,6''</sup>) 8.29(2H, td, H<sup>4,4''</sup>) 8.25 {1H, (signal obscured), H<sup>2''</sup>} 7.88 - 8.40(2H, m, H<sup>4'''</sup> and H<sup>6'''</sup>) 7.82(2H, m, H<sup>2''',6'''</sup>) 7.69(1H, m, H<sup>5''</sup>) 7.65(2H, m, H<sup>5,5''</sup>) 7.56(2H, m, H<sup>3''',5'''</sup>) 7.48(1H, m, H<sup>4'''</sup>).

[Pt(4'-*m*Biph-terpy)Cl]BF<sub>4</sub> (**5**): Yield 109 mg (73 %). Molecular mass 702.8 g.mol<sup>-1</sup>. [Calc. for C<sub>27</sub>H<sub>19</sub>BClF<sub>4</sub>N<sub>3</sub>Pt: C, 46.14; H, 2.72; N, 5.98. Found: C, 46.32; H, 2.50; N, 6.02 %].

[Pt(4'-*m*Biph-terpy)Cl]CF<sub>3</sub>SO<sub>3</sub> (**6**): Yield 123 mg (75 %). Molecular mass 765.1 g.mol<sup>-1</sup>. [Calc. for C<sub>28</sub>H<sub>19</sub>ClF<sub>3</sub>N<sub>3</sub>O<sub>3</sub>PtS: C, 43.96; H, 2.50; N, 5.49. Found: C, 44.05; H, 2.34; N, 5.52 %].



### 3.4.1.3 [Pt(4'-*p*Biph-terpy)Cl]X [X<sup>-</sup> = SbF<sub>6</sub><sup>-</sup> (7), BF<sub>4</sub><sup>-</sup> (8), CF<sub>3</sub>SO<sub>3</sub><sup>-</sup> (9)]

{where 4'-*p*Biph-terpy = 4'-(*para*-biphenyl)-2,2':6',2''-terpyridine}

The appropriate silver salt AgX (73 mg for X<sup>-</sup> = SbF<sub>6</sub><sup>-</sup>; 41 mg for X<sup>-</sup> = BF<sub>4</sub><sup>-</sup>; 54 mg for X<sup>-</sup> = CF<sub>3</sub>SO<sub>3</sub><sup>-</sup>; 0.21 mmol), depending on the complex to be made, was dissolved in acetonitrile (5 ml) and added to a suspension of [Pt(PhCN)<sub>2</sub>Cl<sub>2</sub>] (100 mg, 0.21 mmol) in acetonitrile (10 ml). The mixture was refluxed overnight under an inert atmosphere before the resultant precipitate of AgCl was removed by filtration. An approximately equimolar amount of solid 4'-(*para*-biphenyl)-2,2':6',2''-terpyridine (4'-*p*Biph-terpy) (77 mg, 0.20 mmol) was added and the mixture refluxed for 24 hrs. Once reflux was complete the mixture was filtered hot and the solvent partially removed under reduced pressure resulting in the precipitation of [Pt(4'-*p*Biph-terpy)Cl]X. The product was washed on the frit with copious amounts of diethyl ether and then smaller amounts of acetonitrile. The resulting powder was recrystallised from hot acetonitrile.

[Pt(4'-*p*Biph-terpy)Cl]SbF<sub>6</sub> (7): Yield 138 mg (77 %). Molecular mass 851.7 g.mol<sup>-1</sup>. [Calc. for C<sub>27</sub>H<sub>19</sub>ClF<sub>6</sub>N<sub>3</sub>PtSb: C, 38.07; H, 2.25; N, 4.93. Found: C, 38.19; H, 1.95; N, 4.94 %].

[Pt(4'-*p*Biph-terpy)Cl]BF<sub>4</sub> (8): Yield 111 mg (75 %). Molecular mass 702.8 g.mol<sup>-1</sup>. [Calc. for C<sub>27</sub>H<sub>19</sub>BClF<sub>4</sub>N<sub>3</sub>Pt: C, 46.14; H, 2.72; N, 5.98. Found: C, 45.92; H, 2.63; N, 5.92 %].

<sup>1</sup>H NMR for [Pt(4'-*p*Biph-terpy)Cl]BF<sub>4</sub> (DMSO-*d*<sub>6</sub>): δ 8.60 (2H, s, H<sup>3',5'</sup>) 8.48 (2H, m, H<sup>3,3''</sup>) 8.30 (2H, m, H<sup>6,6''</sup>) 8.21 (2H, td, H<sup>4,4''</sup>) 8.03 and 7.81 (4H, doublets, H<sup>2'',3'',5'',6''</sup>) 7.76 (2H, m, H<sup>2''',6'''</sup>) 7.60 (2H, m, H<sup>5,5''</sup>) 7.52 (2H, m, H<sup>3''',5'''</sup>) 7.46 (1H, m, H<sup>4'''</sup>)

[Pt(4'-*p*Biph-terpy)Cl]CF<sub>3</sub>SO<sub>3</sub> (9): Yield 116 mg (72 %). Molecular mass 765.1 g.mol<sup>-1</sup>. [Calc. for C<sub>28</sub>H<sub>19</sub>ClF<sub>3</sub>N<sub>3</sub>O<sub>3</sub>PtS: C, 43.96; H, 2.50; N, 5.49. Found: C, 43.50; H, 2.27; N, 5.43 %].

**Table 3.10** *Infrared spectroscopic data.*

Compound	Polypyridine <sup>a</sup>	Counterion <sup>a</sup>
[Pt(4'- $\beta$ Np-terpy)Cl]SbF <sub>6</sub> ( <b>1</b> )	1610(s) 1560(m) 1477(m) 1420(m) 881(w)	658(vs)
[Pt(4'- $\beta$ Np-terpy)Cl]BF <sub>4</sub> ( <b>2</b> )	1609(s) 1558(w) 1479(m) 1420(m) 879(w)	1030(vs, br)
[Pt(4'- $\beta$ Np-terpy)Cl]CF <sub>3</sub> SO <sub>3</sub> ( <b>3</b> )	1614(s) 1560(w) 1479(m) 1420(m) 883(w)	1261(vs) 1155(s) 1032(s)
Pt(4'- <i>m</i> Biph-terpy)Cl]SbF <sub>6</sub> ( <b>4</b> )	1610(s) 1560(m) 1479(m) 1416(m) 878(w)	658(vs)
[Pt(4'- <i>m</i> Biph-terpy)Cl]BF <sub>4</sub> ( <b>5</b> )	1610(s) 1560(w) 1479(m) 1416(m) 878(w)	1032(vs, br)
[Pt(4'- <i>m</i> Biph-terpy)Cl]CF <sub>3</sub> SO <sub>3</sub> ( <b>6</b> )	1610(s) 1558(w) 1479(m) 1416(m) 878(w)	1268(vs) 1155(s) 1028(s)
Pt(4'- <i>p</i> Biph-terpy)Cl]SbF <sub>6</sub> ( <b>7</b> )	1601(s) 1561(m) 1477(m) 1400(m) 885(w)	654(vs)
[Pt(4'- <i>p</i> Biph-terpy)Cl]BF <sub>4</sub> ( <b>8</b> )	1603(s) 1561(m) 1480(m) 1404(w) 888(w)	1034(vs, br)
[Pt(4'- <i>p</i> Biph-terpy)Cl]CF <sub>3</sub> SO <sub>3</sub> ( <b>9</b> )	1601(s) 1560(m) 1477(m) 1407(m) 889(w)	1252(vs) 1146(m) 1028(s)

(a) Recorded as a KBr pellet in the solid state (cm<sup>-1</sup>).

Designation: w = weak; m = medium; s = strong; vs = very strong; br = broad;

**Table 3.11** Absorption spectroscopic data recorded in fluid solution at 298 K.

Chromophore	$\lambda_{\text{abs}}$ (nm)		Assignment
	Acetonitrile	Dichloromethane	
[Pt(4'- $\beta$ Np-terpy)Cl] <sup>+</sup>	411 (14100 <sup>a</sup> )	427	MLCT [Pt(5d) $\rightarrow$ 4'- $\beta$ Np-terpy ( $\pi^*$ )]
(concentration range: 5 - 35 $\mu$ M)	394sh (10200)	405sh	MLCT [Pt(5d) $\rightarrow$ 4'- $\beta$ Np-terpy( $\pi^*$ )]
	334 (27900)	338	<sup>1</sup> ( $\pi$ - $\pi^*$ ) (4'- $\beta$ Np-terpy)
	324 (27900)	328	<sup>1</sup> ( $\pi$ - $\pi^*$ ) (4'- $\beta$ Np-terpy)
	284 (51400)	284	<sup>1</sup> ( $\pi$ - $\pi^*$ ) (4'- $\beta$ Np-terpy)
	261 (47800)	265	<sup>1</sup> ( $\pi$ - $\pi^*$ ) (4'- $\beta$ Np-terpy)
[Pt(4'- <i>m</i> Biph-terpy)Cl] <sup>+</sup>	404 (7800)	416	MLCT [Pt(5d) $\rightarrow$ 4'- <i>m</i> Biph-terpy( $\pi^*$ )]
(concentration range: 0.5 - 5 mM)	385 (6700)	396	MLCT [Pt(5d) $\rightarrow$ 4'- <i>m</i> Biph-terpy( $\pi^*$ )]
	353sh (8700)	358sh	<sup>1</sup> ( $\pi$ - $\pi^*$ ) (4'- <i>m</i> Biph-terpy)
	334 (19800)	338	<sup>1</sup> ( $\pi$ - $\pi^*$ ) (4'- <i>m</i> Biph-terpy)
	319 (21200)	323	<sup>1</sup> ( $\pi$ - $\pi^*$ ) (4'- <i>m</i> Biph-terpy)
	302 (25900)	310	<sup>1</sup> ( $\pi$ - $\pi^*$ ) (4'- <i>m</i> Biph-terpy)
	282 (37800)	285	<sup>1</sup> ( $\pi$ - $\pi^*$ ) (4'- <i>m</i> Biph-terpy)
	256 (48300)	261	<sup>1</sup> ( $\pi$ - $\pi^*$ ) (4'- <i>m</i> Biph-terpy)

(a) Molar absorptivity ( $\text{M}^{-1}\text{cm}^{-1}$ ).

sh = shoulder.

**Table 3.11** (cont.)

Chromophore	$\lambda_{\text{abs}}$ (nm)		Assignment
	Acetonitrile	Dichloromethane	
[Pt(4'- <i>p</i> Biph-terpy)Cl] <sup>+</sup>	410 (17400 <sup>a</sup> )	423	MLCT [Pt(5d) → 4'- <i>p</i> Biph-terpy( $\pi^*$ )]
(concentration range: 5 - 30 mM)	390sh (14000)	403sh	MLCT [Pt(5d) → 4'- <i>p</i> Biph-terpy( $\pi^*$ )]
	354sh (23100)	365sh	<sup>1</sup> ( $\pi$ - $\pi^*$ ) (4'- <i>p</i> Biph-terpy)
	336 (34300)	339	<sup>1</sup> ( $\pi$ - $\pi^*$ ) (4'- <i>p</i> Biph-terpy)
	322sh (26700)	325sh	<sup>1</sup> ( $\pi$ - $\pi^*$ ) (4'- <i>p</i> Biph-terpy)
	284 (58700)	287	<sup>1</sup> ( $\pi$ - $\pi^*$ ) (4'- <i>p</i> Biph-terpy)
	275 (45200)	277	<sup>1</sup> ( $\pi$ - $\pi^*$ ) (4'- <i>p</i> Biph-terpy)
	262 (36600)	266	<sup>1</sup> ( $\pi$ - $\pi^*$ ) (4'- <i>p</i> Biph-terpy)

(a) Molar absorbtivity (M<sup>-1</sup>.cm<sup>-1</sup>).  
sh = shoulder.

**Table 3.12** Solution absorption and emission spectroscopic data.

Compound	Absorption maxima (nm)	Emission maxima (nm) [77 K]	fwhm (cm <sup>-1</sup> )	$\tau$ (ns) [77 K]
[Pt(4'- $\beta$ Np-terpy)Cl] <sup>+</sup>	411, 394 <sup>MeCN</sup> 427, 405 <sup>DCM</sup>	<u>570</u> , 615sh, 670sh <sup>DCM</sup>	-	11900 <sup>DCM</sup>
		[0.1 $\mu$ M <u>545</u> , 585sh] <sup>DME, b</sup>	-	-
		[1 $\mu$ M <u>546</u> , 583, 626sh] <sup>DME, b</sup>	-	-
		[5 $\mu$ M <u>545</u> , 585, 627sh] <sup>DME, b</sup>	-	-
		[10 $\mu$ M <u>545</u> , 583, 627sh] <sup>DME, b</sup>	-	-
		[50 $\mu$ M <u>550</u> , 585, 629sh] <sup>DME, b</sup>	-	-
		[100 $\mu$ M <u>550</u> , 590, 638sh] <sup>DME, b</sup>	-	[47000] <sup>DME</sup>
		[10 $\mu$ M <u>546</u> , 583, 633sh] <sup>DME, b</sup> [100 $\mu$ M 696] <sup>DME, d</sup>	-	- [1900] <sup>DME</sup>
		<u>564</u> , 595sh <sup>BuCN, 32</sup> [ <u>542</u> , 583, 625sh] <sup>BuCN, 32</sup>	- -	- -
	[Pt(4'- $\alpha$ Np-terpy)Cl] <sup>+</sup> <sup>32, 111</sup>	406 <sup>MeCN, 32</sup> 423 <sup>DCM, 32</sup>	<u>588</u> - <u>592</u> <sup>DCM, 32, 111</sup>	
		<u>588</u> <sup>D/A, 111</sup>		2000 <sup>D/A, 111</sup>
		<u>581</u> <sup>BuCN, 32</sup>		-
		[ <u>540</u> , 587] <sup>BuCN, 32</sup>		-

Table 3.12 (cont.)

Compound	Absorption maxima (nm)	Emission maxima (nm) [77 K]	fwhm (cm <sup>-1</sup> )	$\tau$ (ns) [77 K]
[Pt(4'- <i>m</i> Biph-terpy)Cl] <sup>+</sup>	404, 385 <sup>MeCN</sup> 416, 396 <sup>DCM</sup>	<u>536</u> , 570sh, 625sh <sup>DCM, a</sup>	-	115 <sup>DCM</sup>
		[0.1 $\mu$ M <u>553</u> ] <sup>DME, a</sup>	-	-
		[1 $\mu$ M 508, <u>552</u> , 590sh] <sup>DME, a</sup>	-	-
		[5 $\mu$ M 510, <u>550</u> , 590sh] <sup>DME, a</sup>	-	-
		[10 $\mu$ M 511, <u>551</u> , 590sh] <sup>DME, a</sup>	-	-
		[20 $\mu$ M 513, <u>553</u> , 590sh] <sup>DME, a</sup>	-	-
		[30 $\mu$ M 513, <u>554</u> , 590sh] <sup>DME, a</sup>	-	[< 10000] <sup>DME</sup>
		[20 $\mu$ M 602] <sup>DME, c</sup>	[4100]	-
		[30 $\mu$ M 671] <sup>DME, c</sup>	[2330]	[1890] <sup>DME</sup>

Underlined values refer to the most intense bands within a manifold.

sh = shoulder.

(a)  $\lambda_{ex}(\max) < 440$  nm (c)  $\lambda_{ex}(\max) = 470$  nm (e)  $\lambda_{ex}(\max) = 510$  nm

(DCM) Spectrum recorded in dichloromethane solution.

(DME) Spectrum recorded in 1:5:5 (v/v) DMF/methanol/ethanol solvent mixture.

(MeCN) Spectrum recorded in acetonitrile solution.

Table 3.12 (cont.)

Compound	Absorption maxima (nm)	Emission maxima (nm) [77 K]	fwhm (cm <sup>-1</sup> )	$\tau$ (ns) [77 K]
[Pt(4'-pBiph-terpy)Cl] <sup>+</sup>	410, 390 <sup>MeCN</sup> 423, 403 <sup>DCM</sup>	564, 602sh, 650sh <sup>DCM</sup>	-	4000 <sup>DCM</sup>
		[0.1 $\mu$ M <u>545</u> , 574sh] <sup>DME, b</sup>	-	-
		[1 $\mu$ M <u>542</u> , 572, 626sh] <sup>DME, b</sup>	-	-
		[5 $\mu$ M <u>545</u> , 574, 627sh] <sup>DME, b</sup>	-	-
		[10 $\mu$ M <u>543</u> , 579, 627sh] <sup>DME, b</sup>	-	-
		[20 $\mu$ M <u>546</u> , 580, 627sh] <sup>DME, b</sup>	-	-
		[50 $\mu$ M <u>549</u> , 578, 633sh] <sup>DME, b</sup>	-	-
		[100 $\mu$ M <u>551</u> , 583, 638sh] <sup>DME, b</sup>	-	-
		[150 $\mu$ M <u>555</u> , 583, 641sh] <sup>DME, b</sup>	-	[2900] <sup>DME</sup>
		[50 $\mu$ M ~ 600] <sup>DME, c</sup>	4400	-
		[150 $\mu$ M 685] <sup>DME, e</sup>	2300	[1900] <sup>DME</sup>
		[50 $\mu$ M 680] <sup>DME, f</sup>	2500	-
	[100 $\mu$ M 688] <sup>DME, f</sup>	2400	-	
	[150 $\mu$ M 695] <sup>DME, f</sup>	2300	-	

Underlined values refer to the most intense bands within a manifold.  
sh = shoulder.

(a)  $\lambda_{ex}(\max) < 440$  nm (b)  $440 < \lambda_{ex}(\max) < 470$  nm (c)  $\lambda_{ex}(\max) = 470$  nm (d)  $490 < \lambda_{ex}(\max) < 510$  nm (e)  $\lambda_{ex}(\max) = 510$  nm (f)  $\lambda_{ex}(\max) = 520$  nm

(D/A) Spectrum recorded in a 20:1 (v/v) dichloromethane/acetonitrile solvent mixture.

(DCM) Spectrum recorded in dichloromethane solution.

(DME) Spectrum recorded in 1:5:5 (v/v) DMF/methanol/ethanol solvent mixture.

(MeCN) Spectrum recorded in acetonitrile solution.

# Biphasic decay, tail-end sampled.

**Table 3.13** Solid state absorption and emission spectroscopic data.

Compound	Colour	Absorption maxima (nm)	Emission maxima (nm) [77 K]	fwhm (cm <sup>-1</sup> ) [77 K]	$\tau$ (ns) [77 K]
[Pt(4'- $\beta$ Np-terpy)Cl]SbF <sub>6</sub> ( <b>1</b> )	orange	<u>470</u> , ca. 520, ca. 560	<u>572</u> , 615, 663, [596, 655, 723]	- -	395 <sup>#</sup> [3800]
[Pt(4'- $\beta$ Np-terpy)Cl]BF <sub>4</sub> ( <b>2</b> )	orange	<u>460</u>	<u>582</u> , 621, 670 [622, 684, 750]	- -	360 <sup>#</sup> [3900]
[Pt(4'- $\beta$ Np-terpy)Cl]CF <sub>3</sub> SO <sub>3</sub> ( <b>3</b> )	yellow	<u>460</u> , ca. 520, ca. 560	<u>578</u> , 621, 668 [612, 674, 740]	- -	390 <sup>#</sup> [4200]
[Pt(4'- $\alpha$ Np-terpy)Cl]SbF <sub>6</sub> <sup>111</sup>	orange-yellow	-	<u>656</u> [656]	3506 [1666]	192 [3000]
[Pt(4'- <i>m</i> Biph-terpy)Cl]SbF <sub>6</sub> ( <b>4</b> )	orange	443, <u>525</u>	<u>640</u> [623]	2693 [1625]	250 <sup>#</sup> [1620]
[Pt(4'- <i>m</i> Biph-terpy)Cl]SbF <sub>6</sub> .CH <sub>3</sub> CN ( <b>4a</b> )	yellow-orange	-	<u>565</u> , <u>644</u> [557, 612, 666]	- -	† [†]
[Pt(4'- <i>m</i> Biph-terpy)Cl]BF <sub>4</sub> ( <b>5</b> )	yellow	<u>443</u> , 525	545sh, 580, <u>653</u> , 715sh [543, 580, <u>621</u> , 650sh, 715sh]	- -	† [†]
[Pt(4'- <i>m</i> Biph-terpy)Cl]CF <sub>3</sub> SO <sub>3</sub> ( <b>6</b> )	orange	<u>435</u> , 500	524, 556, <u>657</u> [540, 583, <u>625</u> ]	- -	† [†]

Underlined values refer to the most intense bands within a manifold

sh = shoulder

# Biphasic decay, tail-end sampled

† Multiple emission components and lifetime determination not possible



**Table 3.13** (*cont.*)

Compound	Colour	Absorption maxima (nm)	Emission maxima (nm) [77 K]	fwhm (cm <sup>-1</sup> ) [77 K]	τ (ns) [77 K]
[Pt(4'- <i>p</i> Biph-terpy)Cl]SbF <sub>6</sub> ( <b>7</b> )	pale orange	478	<u>566</u> , 603, <i>ca.</i> 660sh <sup>a</sup> [ <u>570</u> , 620, <i>ca.</i> 670sh] <sup>a</sup>	- -	870 [6780]
			576, 612, <i>ca.</i> 670 <sup>b</sup> [576, 623, <i>ca.</i> 670] <sup>b</sup>	- -	- -
[Pt(4'- <i>p</i> Biph-terpy)Cl]BF <sub>4</sub> ( <b>8</b> )	yellow	436	<u>555</u> , 597, 647 [552sh, <u>574</u> , 623, 677]	- -	2780 <sup>#</sup> [28000] <sup>#</sup>
[Pt(4'- <i>p</i> Biph-terpy)Cl]BF <sub>4</sub> ( <b>8</b> ) <i>red form</i>	red	560	683 [586, <u>720</u> ]	2130 [1920]	- -
[Pt(4'- <i>p</i> Biph-terpy)Cl]CF <sub>3</sub> SO <sub>3</sub> ( <b>9</b> )	bright orange	<u>475</u> , 560	627 [684]	2400 [1800]	510 [1540]

Underlined values refer to the most intense bands within a manifold

sh = shoulder

<sup>a</sup> λ<sub>em</sub>(max) = 400 nm

<sup>b</sup> λ<sub>em</sub>(max) = 450 nm

<sup>#</sup> Biphasic decay, tail-end sampled

### 3.4.2 Crystal structure determination

#### 3.4.2.1 Single crystal X-ray diffraction study on [Pt(4'-*m*Biph-terpy)Cl]SbF<sub>6</sub>·CH<sub>3</sub>CN

A rectangular orange block-shaped crystal was grown by the slow evaporation of a concentrated acetonitrile solution of the complex at room temperature. Crystals were stable for at least 2 hours once removed from the mother liquor before showing visible signs of deterioration. For this reason X-ray diffraction measurements were carried out at 173 K using a Siemens SMART CCD 1K diffractometer fitted with an attachment for low temperature data collection at the Centre for Molecular Design at the University of the Witwatersrand. The program OSCAIL, which facilitates the direct use of SHELXS-97<sup>166</sup>, SHELXL-97/2<sup>167</sup> and ORTEX<sup>168</sup>, was used for structure solution (by direct methods in this case), structure refinement (on  $F^2$ ) and in labelling atoms in a three dimensional peak plot (generated by ORTEX) respectively for a paperless structure determination. Hydrogen atoms were placed in calculated positions using a riding model and refined isotropically. The following pages contain tables listing the unit cell dimensions and pertinent crystallographic data (Table 3.14), fractional atomic coordinates (Table 3.15), bond lengths (Table 3.16), bond angles (Table 3.17) and finally the anisotropic displacement parameters in Table 3.18. Lists of observed and calculated structure factors are available on request.<sup>169</sup>

Residual indices given in Table 3.14 are derived as follows:

$$R1 = \Sigma |F_o - F_c| / \Sigma F_o$$

$$wR2 = \{ \Sigma [w(F_o^2 - F_c^2)]^2 / \Sigma (wF_o^2)^2 \}^{1/2}$$

$$w = 1.0 / [ \sigma^2(F_o^2) + (0.1000 * P)^2 + 0.00 * P ]$$

$$\text{where } P = (F_o^2 + 2F_c^2) / 3$$

**Table 3.14** *Crystal data and structure refinement for [Pt(4'-mBip-terpy)Cl]SbF<sub>6</sub>·CH<sub>3</sub>CN.*

Empirical formula	C <sub>29</sub> H <sub>22</sub> ClF <sub>6</sub> N <sub>4</sub> PtSb
Colour and description	Orange block
Formula weight	892.80 g.mol <sup>-1</sup>
Temperature	173(2) K
Wavelength { $\lambda(\text{Mo} - \text{K}_\alpha)$ }	0.71069 Å
Crystal system	Triclinic
Space group	P $\bar{1}$
Unit cell dimensions	$a = 7.5949(4)$ Å $\alpha = 116.040(1)^\circ$ $b = 13.8767(7)$ Å $\beta = 97.704(1)^\circ$ $c = 15.3307(7)$ Å $\gamma = 98.386(1)^\circ$
Volume	1400.08(12) Å <sup>3</sup>
Z	2
Density (calculated)	2.118 Mg.m <sup>-3</sup>
Absorption coefficient	6.119 mm <sup>-1</sup>
F(000)	848
Crystal size	0.50 × 0.40 × 0.20 mm
$\theta$ range for data collection	1.52 to 28.28 °
Index ranges	-9 ≤ h ≤ 10; -17 ≤ k ≤ 18; -19 ≤ l ≤ 20
Reflections collected	9210
Independent reflections	6147 [R(int) = 0.0240]
Reflections observed [I > 2 $\sigma$ (I)]	5786
Refinement method	Full-matrix least-squares on F <sup>2</sup>
Data / restraints / parameters	6147 / 0 / 380
Goodness-of-fit on F <sup>2</sup>	1.086
Final R indices [I > 2 $\sigma$ (I)]	R1 = 0.0281 wR2 = 0.0629
R indices (all data)	R1 = 0.0316 wR2 = 0.0649
Largest diff. peak and hole	1.195 and -1.346 e.Å <sup>-3</sup>

**Table 3.15** Atomic coordinates ( $\times 10^4$ ) and equivalent isotropic displacement parameters ( $\text{\AA}^2 \times 10^3$ ) for  $[\text{Pt}(4\text{-}m\text{Biph-terpy})\text{Cl}]\text{SbF}_6 \cdot \text{CH}_3\text{CN}$  (4a)

$U_{\text{eq}}$  is defined as one third of the trace of the orthogonalized  $U_{ij}$  tensor.

i.e.,  $U_{\text{eq}} = 1/3 \sum_i \sum_j U_{ij} a_i^* a_j^* (a_i a_j)$

	x	y	z	$U_{\text{eq}}$
Pt	1600(1)	9260(1)	4790(1)	18(1)
Sb	7321(1)	12769(1)	917(1)	29(1)
Cl	3147(2)	10762(1)	4704(1)	29(1)
N2	317(4)	7997(3)	4864(2)	17(1)
N1	2835(5)	9641(3)	6197(3)	20(1)
N3	-26(5)	8441(3)	3401(3)	20(1)
F1	6833(5)	11230(2)	408(2)	48(1)
F2	9323(4)	12889(3)	1855(2)	45(1)
F3	5254(5)	12595(3)	-9(2)	53(1)
F4	5840(5)	12817(3)	1810(2)	57(1)
F5	8764(5)	12656(3)	0(3)	63(1)
F6	7780(7)	14293(3)	1448(3)	77(1)
N4	1269(9)	736(6)	2036(6)	80(2)
C1	4226(6)	10504(3)	6822(3)	25(1)
C2	4952(6)	10648(4)	7754(3)	31(1)
C3	4245(6)	9914(4)	8071(3)	29(1)
C4	2826(6)	9021(4)	7425(3)	27(1)
C5	2147(5)	8888(3)	6484(3)	18(1)
C6	709(5)	7942(3)	5722(3)	18(1)
C7	-160(6)	7045(3)	5795(3)	20(1)
C8	-1462(5)	6186(3)	4965(3)	18(1)

**Table 3.15** (cont.)

---

C9	-1844(5)	6298(3)	4096(3)	18(1)
C10	-942(5)	7214(3)	4060(3)	18(1)
C11	-1169(6)	7479(3)	3226(3)	21(1)
C12	-2393(6)	6833(4)	2327(3)	27(1)
C13	-2457(7)	7156(4)	1586(3)	32(1)
C14	-1293(7)	8108(4)	1761(3)	32(1)
C15	-83(6)	8745(4)	2675(3)	26(1)
C16	-2374(5)	5196(3)	5019(3)	18(1)
C17	-2279(6)	5192(3)	5936(3)	21(1)
C18	-3146(5)	4274(3)	6005(3)	20(1)
C19	-4121(6)	3342(3)	5131(3)	24(1)
C20	-4250(6)	3334(4)	4223(3)	27(1)
C21	-3381(6)	4258(3)	4162(3)	23(1)
C22	-3025(6)	4326(3)	7001(3)	22(1)
C23	-3049(7)	5291(4)	7829(4)	34(1)
C24	-2848(8)	5351(4)	8768(4)	42(1)
C25	-2594(8)	4450(5)	8898(4)	40(1)
C26	-2605(7)	3473(4)	8080(4)	36(1)
C27	-2836(6)	3405(4)	7138(4)	28(1)
C28	1536(8)	963(5)	1436(5)	46(1)
C29	1879(8)	1251(5)	661(5)	46(1)
H1	4711	11020	6616	32
H2	5942	11255	8181	40
H3	4721	10019	8720	38
H4	2323	8503	7627	35
H7	112	7003	6399	26
H9	-2727	5741	3531	23

---

**Table 3.15** (cont.)

---

H12	-3185	6174	2215	35
H13	-3300	6721	964	41
H14	-1317	8329	1255	41
H15	716	9405	2792	34
H17	-1608	5829	6527	27
H19	-4701	2707	5162	32
H20	-4932	2698	3635	35
H21	-3478	4245	3532	30
H23	-3204	5919	7753	44
H24	-2885	6015	9325	54
H25	-2413	4503	9544	52
H26	-2455	2847	8161	47
H27	-2867	2727	6579	36
H29A	758	984	143	60
H29B	2840	910	367	60
H29C	2271	2054	949	60

---

**Table 3.16** Bond lengths [ $\text{\AA}$ ] for  $[\text{Pt}(4\text{-}m\text{Biph-terpy})\text{Cl}]\text{SbF}_6 \cdot \text{CH}_3\text{CN}$  (**4a**).

Pt-N2	1.933(3)	Pt-N3	2.027(4)
Pt-N1	2.030(3)	Pt-Cl	2.3046(10)
Pt-Cl	2.3046(10)	Sb-F6	1.859(3)
Sb-F5	1.863(3)	Sb-F4	1.871(3)
Sb-F3	1.878(3)	Sb-F2	1.880(3)
Sb-F1	1.880(3)	N2-C6	1.348(5)
N2-C10	1.349(5)	N1-C1	1.350(6)
N1-C5	1.366(5)	N3-C15	1.352(5)
N3-C11	1.375(5)	N4-C28	1.129(8)
C1-C2	1.375(6)	C2-C3	1.381(7)
C3-C4	1.388(6)	C4-C5	1.386(6)
C5-C6	1.474(6)	C6-C7	1.378(6)
C7-C8	1.416(6)	C8-C9	1.405(5)
C8-C16	1.487(5)	C9-C10	1.380(5)
C10-C11	1.475(5)	C11-C12	1.376(6)
C12-C13	1.390(6)	C13-C14	1.373(7)
C14-C15	1.385(7)	C16-C21	1.395(6)
C16-C17	1.401(6)	C17-C18	1.400(5)
C18-C19	1.396(6)	C18-C22	1.486(6)
C19-C20	1.376(6)	C20-C21	1.402(6)
C22-C23	1.387(6)	C22-C27	1.406(6)
C23-C24	1.392(7)	C24-C25	1.384(7)
C25-C26	1.384(8)	C26-C27	1.389(7)
C28-C29	1.452(8)		

**Table 3.17** Bond angles [°] for [Pt(4'-mBiph-terpy)Cl]SbF<sub>6</sub>.CH<sub>3</sub>CN (**4a**).

N2-Pt-N3	80.67(13)	N2-Pt-N1	80.93(14)
N3-Pt-N1	161.57(13)	N2-Pt-C1	179.64(10)
N3-Pt-Cl	99.52(10)	N1-Pt-C1	98.87(10)
F6-Sb-F5	92.0(2)	F6-Sb-F4	90.5(2)
F5-Sb-F4	177.55(18)	F6-Sb-F3	91.23(17)
F5-Sb-F3	90.33(17)	F4-Sb-F3	89.27(16)
F6-Sb-F2	90.86(17)	F5-Sb-F2	91.58(16)
F4-Sb-F2	88.74(15)	F3-Sb-F2	177.12(15)
F6-Sb-F1	178.52(18)	F5-Sb-F1	89.49(17)
F4-Sb-F1	88.09(17)	F3-Sb-F1	89.09(15)
F2-Sb-F1	88.76(14)	C6-N2-C10	122.7(3)
C6-N2-Pt	118.5(3)	C10-N2-Pt	118.8(3)
C1-N1-C5	119.8(4)	C1-N1-Pt	127.4(3)
C5-N1-Pt	112.8(3)	C15-N3-C11	119.5(4)
C15-N3-Pt	127.2(3)	C11-N3-Pt	113.3(3)
N1-C1-C2	121.0(4)	C1-C2-C3	120.2(4)
C2-C3-C4	118.8(4)	C5-C4-C3	119.5(4)
N1-C5-C4	120.6(4)	N1-C5-C6	115.3(3)
C4-C5-C6	124.1(4)	N2-C6-C7	119.9(4)
N2-C6-C5	112.5(3)	C7-C6-C5	127.6(4)
C6-C7-C8	119.6(4)	C9-C8-C7	118.0(4)
C9-C8-C16	121.6(4)	C7-C8-C16	120.4(4)
C10-C9-C8	120.2(4)	N2-C10-C9	119.5(4)
N2-C10-C11	112.5(3)	C9-C10-C11	128.0(4)
N3-C11-C12	121.0(4)	N3-C11-C10	114.6(4)
C12-C11-C10	124.4(4)	C11-C12-C13	119.3(4)
C14-C13-C12	119.4(4)	C13-C14-C15	120.0(4)



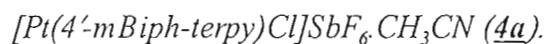
**Table 3.17** (cont.)

---

N3-C15-C14	120.8(4)	C21-C16-C17	118.3(4)
C21-C16-C8	120.9(4)	C17-C16-C8	120.8(4)
C18-C17-C16	121.7(4)	C19-C18-C17	118.5(4)
C19-C18-C22	122.2(4)	C17-C18-C22	119.3(4)
C20-C19-C18	120.7(4)	C19-C20-C21	120.4(4)
C16-C21-C20	120.4(4)	C23-C22-C27	117.9(4)
C23-C22-C18	121.1(4)	C27-C22-C18	121.0(4)
C22-C23-C24	120.8(4)	C25-C24-C23	120.6(5)
C26-C25-C24	119.5(5)	C25-C26-C27	120.0(4)
C26-C27-C22	121.1(4)	N4-C28-C29	179.8(9)

---

**Table 3.18** Anisotropic displacement parameters ( $\text{\AA}^2 \times 10^3$ ) for



The anisotropic displacement factor exponent takes the form:

$$-2\pi^2 [h^2 a^{*2} U_{11} + \dots + 2 h k a^* b^* U_{12} + \dots + 2 k l b^* c^* U_{23}]$$

where  $a^*$ ,  $b^*$  and  $c^*$  are reciprocal cell dimensions.

	$U_{11}$	$U_{22}$	$U_{33}$	$U_{23}$	$U_{13}$	$U_{12}$
Pt	21(1)	17(1)	19(1)	10(1)	6(1)	5(1)
Sb	40(1)	27(1)	19(1)	10(1)	0(1)	11(1)
Cl	30(1)	24(1)	39(1)	20(1)	14(1)	5(1)
N2	18(2)	16(2)	16(2)	7(1)	2(1)	4(1)
N1	22(2)	18(2)	18(2)	7(1)	6(1)	5(1)
N3	24(2)	22(2)	23(2)	15(2)	8(1)	8(1)
F1	62(2)	30(2)	38(2)	10(1)	-8(2)	6(2)
F2	43(2)	49(2)	34(2)	19(2)	-8(1)	5(2)
F3	64(2)	67(2)	28(2)	21(2)	-4(1)	31(2)
F4	59(2)	82(3)	27(2)	19(2)	13(2)	21(2)
F5	69(2)	89(3)	54(2)	48(2)	28(2)	22(2)
F6	104(3)	28(2)	81(3)	18(2)	-6(2)	16(2)
N4	73(4)	124(6)	106(5)	95(5)	42(4)	46(4)
C1	26(2)	20(2)	23(2)	8(2)	6(2)	0(2)
C2	27(2)	28(2)	27(2)	7(2)	1(2)	-2(2)
C3	28(2)	31(2)	20(2)	7(2)	-2(2)	3(2)
C4	31(2)	25(2)	23(2)	11(2)	2(2)	4(2)
C5	19(2)	17(2)	17(2)	7(2)	4(2)	2(2)
C6	19(2)	20(2)	16(2)	10(2)	3(2)	5(2)
C7	22(2)	23(2)	16(2)	11(2)	1(2)	5(2)
C8	18(2)	18(2)	19(2)	9(2)	4(2)	6(2)

**Table 3.18** (cont.)

---

C9	15(2)	18(2)	16(2)	7(2)	1(1)	1(2)
C10	19(2)	18(2)	17(2)	8(2)	3(2)	6(2)
C11	23(2)	24(2)	19(2)	13(2)	5(2)	9(2)
C12	35(2)	29(2)	18(2)	12(2)	3(2)	9(2)
C13	38(3)	39(3)	22(2)	17(2)	4(2)	15(2)
C14	42(3)	43(3)	25(2)	25(2)	12(2)	20(2)
C15	33(2)	34(2)	24(2)	21(2)	12(2)	16(2)
C16	18(2)	17(2)	19(2)	9(2)	2(2)	4(2)
C17	22(2)	16(2)	21(2)	7(2)	3(2)	1(2)
C18	20(2)	18(2)	23(2)	10(2)	6(2)	5(2)
C19	23(2)	17(2)	32(2)	13(2)	5(2)	0(2)
C20	23(2)	21(2)	28(2)	7(2)	1(2)	2(2)
C21	27(2)	21(2)	21(2)	11(2)	1(2)	5(2)
C22	23(2)	23(2)	23(2)	12(2)	6(2)	3(2)
C23	49(3)	25(2)	32(3)	17(2)	11(2)	7(2)
C24	63(4)	34(3)	28(3)	15(2)	12(2)	7(3)
C25	47(3)	51(3)	32(3)	30(3)	8(2)	6(3)
C26	39(3)	40(3)	48(3)	33(3)	14(2)	12(2)
C27	29(2)	26(2)	38(3)	21(2)	14(2)	11(2)
C28	35(3)	53(3)	59(4)	33(3)	11(3)	15(3)
C29	38(3)	48(3)	58(4)	30(3)	11(3)	7(3)

---

## Chapter Four

## Synthesis and photophysical properties of phenyl-bipyridyl ligand complexes of platinum(II)

### 4.1 INTRODUCTION

The underlying theme of the work presented in Chapter 3 is an investigation of the effect of changing the substituent (R) in the 4'-position of the terpyridyl ligand on the luminescence properties of the complex  $[\text{Pt}(4'\text{-R-terpy})\text{Cl}]^+$ . Of interest in this chapter is the effect on the luminescence properties of the complex brought about by modifying the terpyridyl ligand *close to the platinum centre*, rather than further away. Specifically, the *ortho*-C-deprotonated phenyl-bipyridyl ligand is employed for the following reasons. The enhanced  $\sigma$ -donor ability of the carbon donor is expected to alter the electronic structure of the complex, especially with respect to the relative energies of the metal-based and ligand centred orbitals. In fact, previous spectroscopic investigations of the excited states of the chloro(phenyl-bipyridyl)platinum(II)<sup>44</sup> complex indicate that the strong  $\sigma$ -donating power of the ligand increases the energy difference between the MLCT excited state and metal-centred d-d state compared to that of chloro(terpyridine)platinum(II).<sup>44,170,171</sup> The metal-centred d-d state is known to be susceptible to radiationless decay and by discouraging the population of this state, it may be possible to facilitate the formation of longer-lived radiative excited states.

It is thought that the metal-centred state is populated to a sufficient extent to render the chloro(terpyridine)platinum(II) complex non-emissive in fluid solution at ambient temperatures.<sup>27-29,42</sup> For this reason comparisons between the monomeric excited states of chloro(terpyridine)platinum(II) and chloro(phenyl-bipyridine)platinum(II) are limited to emission spectra recorded in a rigid glass at 77 K.<sup>28,29,31,32,42</sup> McMillin and coworkers have shown that it is possible for the (terpyridine)platinum(II) fragment to luminesce in room temperature fluid solution by replacing the fourth (chloride) ligand with  $\text{OMe}^-$ ,  $\text{OH}^-$  or  $\text{SCN}^-$ .<sup>27</sup> The 4'-phenyl substituted terpyridyl luminophore *viz.*,  $[\text{Pt}(4'\text{-Ph-terpy})\text{Cl}]^+$ , also luminesces in room temperature fluid solution<sup>31,32</sup>, but direct comparison is not possible since, to date,

there are no published reports of the excited state properties of the [Pt(4-Ph-phbipy)Cl] complex (where 4-Ph-phbipy is the *ortho*-C deprotonated form of the 4,6-diphenyl-2,2'-bipyridyl ligand).

We are interested in understanding the change in the monomeric excited state brought about by altering the nature of the organic ligand at the point at which it is bound to platinum. To this end the photophysical properties of the two complexes [Pt(4- $\beta$ Np-phbipy)Cl] and [Pt(4-*p*Biph-phbipy)Cl] are reported here, where 4- $\beta$ Np-phbipy is the anionic deprotonated form of the 4-( $\beta$ -naphthyl)-6-phenyl-2,2'-bipyridyl ligand (H4- $\beta$ Np-phbipy); and 4-*p*Biph-phbipy the anionic deprotonated form of the 4-(*para*-biphenyl)-6-phenyl-2,2'-bipyridyl ligand (H4-*p*Biph-phbipy). Ligands with these substituents in the 4-position were chosen in order to allow direct comparisons to be made between the photophysical properties of [Pt(4- $\beta$ Np-phbipy)Cl] and [Pt(4-*p*Biph-phbipy)Cl] and those of their terpyridyl counterparts, as reported in Chapter 3.

The two new luminophores emit in their solution monomeric forms both at room temperature in fluid solution and in a rigid glass at 77 K.

## 4.2 RESULTS AND DISCUSSION

### 4.2.1 [Pt(4- $\beta$ Np-phbipy)Cl] (10) and [Pt(4-*p*Biph-phbipy)Cl] (11)

{where 4- $\beta$ Np-phbipy and 4-*p*Biph-phbipy are the anionic deprotonated form of the 4-( $\beta$ -naphthyl)-6-phenyl-2,2'-bipyridyl (H4- $\beta$ Np-phbipy) and 4-(*para*-biphenyl)-6-phenyl-2,2'-bipyridyl ligand (H4-*p*Biph-phbipy) ligands respectively}

#### 4.2.1.1 Synthesis and characterisation of [Pt(4- $\beta$ Np-phbipy)Cl] (10) and [Pt(4-*p*Biph-phbipy)Cl] (11)

Approaches to the cycloplatination of phenyl-bipyridyl ligands have seen a number of diverse synthetic routes. Initial efforts involved a two-step procedure whereby lithiated ligands were generated *in situ* by the action of *n*-BuLi, before addition of a suitable platinum reagent {typically potassium tetrachloroplatinate(II)} to give the desired cycloplatinated product.<sup>172</sup>

Constable and coworkers developed a method based on organomercuriation reactions which uses mercury(II)acetate as the starting material.<sup>105</sup> In the first step of this procedure mercury(II)acetate is reacted with an equivalent of the 6-phenyl-2,2'-bipyridyl ligand (HL) before a metathesis step, using LiCl, introduces a chloride ligand and  $[\{\text{HgL}(\text{Cl})\}_n]$  is isolated as the arylmercury(II) intermediate. The yield for this step is a mere 15 %. The second step involves reacting the mercury(II) intermediate with  $[\text{Pt}(\text{MeCN})_2\text{Cl}_2]$  in acetonitrile to give the desired final product,  $[\text{Pt}(\text{L})\text{Cl}]$  in a 61 % yield (where L is the phenyl *ortho*-C deprotonated cyclometallating form of the phenyl-bipyridyl ligand HL). Chemists needing to perform such cycloplatinations have been reluctant to use this organomercuriation method because it is a two step procedure, and especially in view of the low yield for the first step. In the same paper, Constable and coworkers provide an alternative approach that achieves the cycloplatination without the necessity for the isolation of an intermediate.<sup>105</sup> The procedure involves refluxing equimolar amounts of the phenyl-bipyridyl ligand (HL) and potassium tetrachloroplatinum(II) in a 1:1 (v/v) acetonitrile/water mixture. The reaction proceeds to completion in 14 - 18 h, forming  $[\text{Pt}(\text{L})\text{Cl}]$  in yields of up to 80 % and showing no evidence of non-metallated byproducts. This method has proved popular and repeated use has resulted in slight improvements being made to the method, with Che *et al.* using a different work-up of the reaction<sup>44</sup> and Campagna and coworkers adjusting the solvent mixture by the inclusion of ethanol.<sup>107</sup> In all cases yields in excess of 80 % have consistently been obtained and therefore it is the method employed in this work.

Another convenient cycloplatination developed by Pregosin *et al.*<sup>173</sup> uses the  $\mu$ -Cl bridged diplatinum complex  $[\text{Pt}(\mu\text{-Cl})(\eta^3\text{-C}_3\text{H}_5)]_2$  as the starting material. This method allows efficient cycloplatination under mild conditions and features yields of 62 - 87 %. Unfortunately this procedure has proved unsuccessful in the cycloplatination of phenyl-bipyridyl ligands such as those described in this chapter.<sup>107</sup>

Thus in order to achieve the cycloplatination of the H4- $\beta$ Np-phbipy and H4-*p*Biph-phbipy ligands, a modification of the method of Constable *et al.* was used. Equimolar amounts of  $[\text{K}_2\text{PtCl}_4]$  and the appropriate ligand are refluxed overnight in a 1:1 (v/v) acetonitrile/water mixture. The orange precipitate is filtered off, washed on the frit with large quantities of diethyl ether, followed by smaller amounts of cold acetonitrile. The solid is then

systematically vapour-extracted into dichloromethane to remove any remaining polar residues. After removal of the dichloromethane under reduced pressure the solid is recrystallised by the slow diffusion of diethyl ether into a dimethylformamide solution of the product. Successful cycloplatination, which requires the phenyl ring to be deprotonated, is confirmed by a  $^1\text{H}$  NMR spectrum which has lost a phenyl proton resonance (that of  $\text{H}^{2''}$ ) compared to the spectrum of the free ligand. In addition, evidence for successful cycloplatination can be seen in an upfield shift of the proton resonances of the phenyl moiety ( $\text{H}^{4''} - 6''$ ), presumably due to the electropositivity of the platinum metal core. (See Table 4.1.) The chemical shifts of the protons of the outer pyridine ring ( $\text{H}^{3'} - 6'$ ) are shifted downfield, except those of  $\text{H}^{3'}$  which are distant from the platinum metal centre and are essentially unaffected by the metal coordination. This trend is consistent with observations reported in the literature<sup>105, 174</sup>, but a quantitative evaluation of the signal displacement is precluded by differences in the solvent medium. The analytically pure product is recovered from the solution as a fine orange powder in a yield of ~ 65 %. The compound is air and moisture stable with the elemental analysis for C, H and N confirming the empirical formulation as  $[\text{Pt}(\text{C}_{26}\text{H}_{17}\text{N}_2)\text{Cl}]$  and  $[\text{Pt}(\text{C}_{28}\text{H}_{19}\text{N}_2)\text{Cl}]$  for  $[\text{Pt}(4\text{-}\beta\text{Np-phbipy})\text{Cl}]$  and  $[\text{Pt}(4\text{-}p\text{Biph-phbipy})\text{Cl}]$  respectively. Peaks in the proton NMR spectra recorded in deuterated dimethylsulfoxide ( $\text{DMSO-d}_6$ ) were assigned by comparison with the spectrum of the free ligand (recorded in deuterated chloroform; see Table 4.1) and with the assistance of an absolute value correlation spectroscopy (COSY) experiment. The protons are numbered according to the scheme introduced in Chapter 2. Salient chemical shifts are recorded in Table 4.1 and a complete listing is provided in the experimental section of this chapter.

The  $\text{H}^{6'}$  and  $\text{H}^{3'}$  protons occur furthest downfield at  $\sim \delta$  8.9 and  $\sim \delta$  8.7 respectively. (In the case of  $[\text{Pt}(4\text{-}\beta\text{Np-phbipy})\text{Cl}]$  the latter signal is hidden beneath that of a proton of the naphthyl substituent.) The other two protons of the outer pyridine ring are also obscured by peaks from close-lying signals but can be distinguished by the COSY experiment at  $\delta$  8.3 ( $\text{H}^{4'}$ ) and  $\delta$  7.9 ( $\text{H}^{5'}$ ). The inequivalent protons of the central pyridine ring occur as singlets at *ca.*  $\delta$  8.55 ( $\text{H}^{3''}$ ) and  $\delta$  8.3 ( $\text{H}^{5''}$ ) and show a weak coupling with each other. The four protons of the coordinated phenyl ring occur further upfield at  $\delta$  7.8 ( $\text{H}^{3''}$ ), 7.45 ( $\text{H}^{6''}$ ), 7.1 ( $\text{H}^{5''}$ ) and 7.07 ( $\text{H}^{4''}$ ). The remaining resonances can be assigned to the group in the 4-position. A complete listing of the proton NMR resonances can be found in the experimental section of this chapter.



**Table 4.1**  $^1\text{H}$  NMR chemical shifts for related phenyl-bipyridyl complexes.<sup>a</sup>

	H <sup>3</sup>	H <sup>5</sup>	H <sup>3'</sup>	H <sup>4'</sup>	H <sup>5'</sup>	H <sup>6'</sup>	H <sup>3''</sup>	H <sup>4''</sup>	H <sup>5''</sup>	H <sup>6''</sup>
phbipy <sup>105, b</sup>	8.36	7.79	8.63	7.85	7.32	8.69	7.55	7.55	7.55	8.14
H4- $\beta$ Np-phbipy <sup>c</sup>	8.77	8.09	8.71	7.86	7.33	8.74	7.53	7.53	7.53	8.74
H4- <i>p</i> Biph-phbipy <sup>c</sup>	8.69	8.02	8.69	7.86	7.33	8.74	7.53	7.53	7.53	8.24
[Pt(phbipy)Cl] <sup>105, b</sup>	7.60	7.56	7.90	8.05	7.56	8.96	7.32	7.08	7.18	7.45
[Pt(4- $\beta$ Np-phbipy)Cl] <sup>d</sup>	8.56	8.30	8.69	8.32	7.86	8.85	7.78	7.07	7.11	7.45
[Pt(4- <i>p</i> Biph-phbipy)Cl] <sup>d</sup>	8.53	8.29	8.72	8.34	7.90	8.90	7.81	7.08	7.14	7.48

(a) Protons numbered according to Figure 2.3 in Chapter 2.

(b) Shifts measured in CD<sub>2</sub>Cl<sub>2</sub>-d<sub>2</sub> relative to TMS as internal standard, ( $\delta$ ), ppm.

(c) Shifts measured in CDCl<sub>3</sub>-d<sub>1</sub> relative to TMS as internal standard, ( $\delta$ ), ppm.

(d) Shifts measured in DMSO-d<sub>6</sub> relative to TMS as internal standard, ( $\delta$ ), ppm.

The chemical shifts of the two complexes described in this chapter compare well with one another, but as can be seen in Table 4.1, direct comparison with the reported chemical shifts of [Pt(phbipy)Cl]<sup>105</sup> is hampered by the different solvents in which the respective proton NMR spectra have been recorded.

A solid state infrared spectrum of each complex was recorded as a KBr pellet and the most prominent peaks are listed in Table 4.5 at the end of this chapter.

#### 4.2.1.2 Photophysical properties of [Pt(4- $\beta$ Np-phbipy)Cl] (**10**) and [Pt(4-*p*Biph-phbipy)Cl] (**11**)

##### *Fluid solution absorption spectroscopy*

Each complex was dissolved in acetonitrile and in dichloromethane to give yellow solutions of which the absorption spectra were studied at room temperature. The absorption spectra of [Pt(4- $\beta$ Np-phbipy)Cl] and [Pt(4-*p*Biph-phbipy)Cl] in acetonitrile are depicted in Figures 4.1 and 4.2 respectively, and a listing of the peak maxima in both acetonitrile and in dichloromethane is provided at the end of this chapter (Table 4.6). In acetonitrile there is a

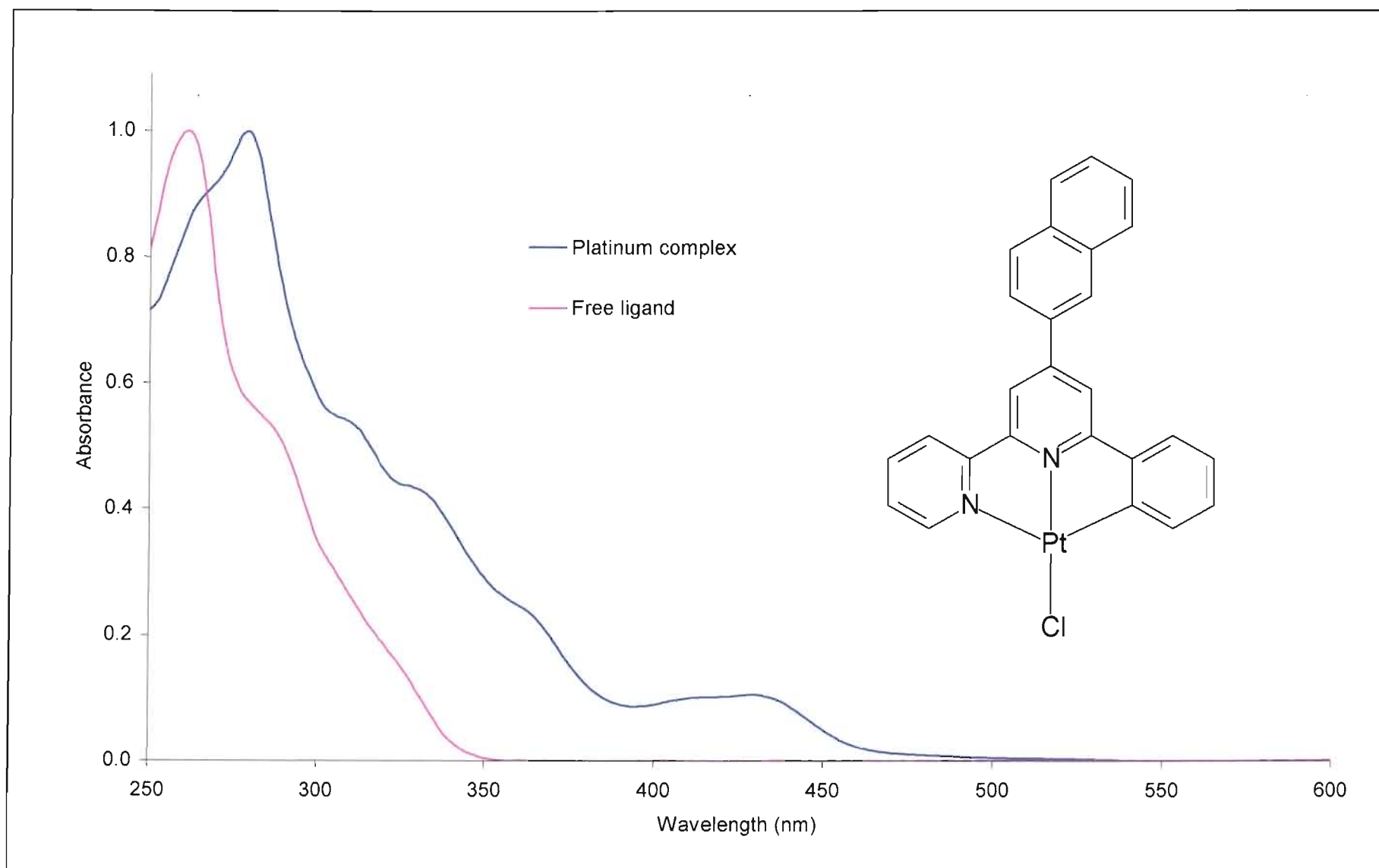


**Figure 4.1** Acetonitrile solution absorption spectra of the  $[Pt(4-\beta Np-phbipy)Cl]$  and  $4-\beta Np-phbipy$  chromophores recorded at 298 K.

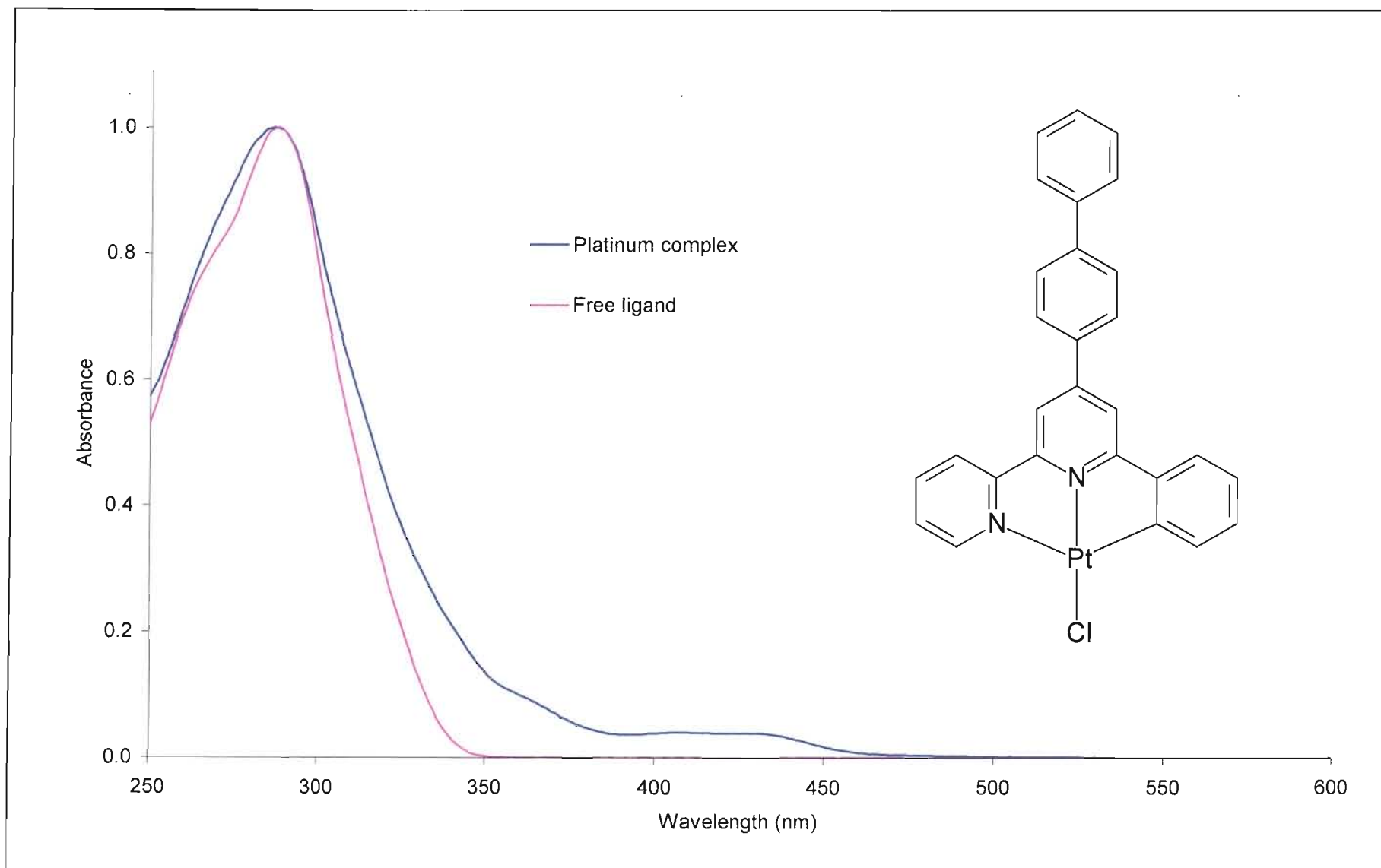


**Figure 4.2** Acetonitrile solution absorption spectra of the  $[Pt(4\text{-pBiph-phbipy})Cl]$  and 4-pBiph-phbipy chromophores recorded at 298 K.

range of intense transitions between 250 and 370 nm with a pair of broad, moderately intense absorptions at lower energy in the 400 - 445 nm range. The bands between 400 and 445 nm shift to even lower energy when dissolved in the less polar solvent, dichloromethane. The absorptions adhere to Beer's law in the 10 - 100  $\mu\text{M}$  concentration range, suggesting that aggregation is absent at the higher concentrations. This pattern is identical to the set of absorptions obtained by Che *et al.* for the closely related  $[\text{Pt}(\text{phbipy})\text{Cl}]$  chromophore<sup>28</sup> (where phbipy is the phenyl *ortho*-C deprotonated form of 6-phenyl-2,2'-bipyridine); absorption assignments therefore follow those made by Che *et al.* for this complex.<sup>28</sup> The intense transitions at higher energy are attributed to intraligand processes, most likely  $\pi$ - $\pi^*$  transitions. The lower energy of the transitions between 400 and 445 nm precludes a similar ligand centred assignment while they are too intense to be ligand field transitions. The bands are therefore tentatively assigned to MLCT transitions,  $^1[\text{d}(\text{Pt}) \rightarrow \pi^*(\text{ligand})]$ .

The basic absorption pattern which can be regarded in terms of two regions of absorptions, one ascribed to  $\pi$ - $\pi^*$  transitions and the other to MLCT transitions, is very similar to that of the related terpyridyl complex described in Chapter 3. There is very little to distinguish the higher energy structured  $\pi$ - $\pi^*$  absorbances, but the differences in the MLCT bands are more interesting. Absorption data for these lower energy bands of the  $[\text{Pt}(4'\text{-}\beta\text{Np-terpy})\text{Cl}]^+$  (**1**),  $[\text{Pt}(4'\text{-}\beta\text{Np-phbipy})\text{Cl}]$  (**10**),  $[\text{Pt}(4'\text{-}p\text{Biph-terpy})\text{Cl}]^+$  (**7**) and  $[\text{Pt}(4'\text{-}p\text{Biph-phbipy})\text{Cl}]$  (**11**) complexes; as well as those of closely related complexes reported in the literature, specifically,  $[\text{Pt}(\text{terpy})\text{Cl}]^+$ <sup>29,30</sup>,  $[\text{Pt}(\text{phbipy})\text{Cl}]$ <sup>44</sup> and  $[\text{Pt}(4'\text{-Ph-terpy})\text{Cl}]^+$ <sup>32,53</sup>, are condensed in Table 4.2.

In all cases the charge transfer nature of the bands is evident from the shift to higher energy observed in the more polar solvent, acetonitrile, as a result of the net reduction in dipole moment experienced by the MLCT excited state in this solvent.<sup>44,175</sup> Based on the limited data available it does appear that the wavelength of these bands increase as the size of the aromatic R-groups is increased. However, this trend only holds if the  $\beta$ -naphthyl and *para*-biphenyl groups are taken as the same size; as the data in Table 4.2 shows the MLCT bands for complexes of these two ligands occur at very similar energies. A clear trend is the significant reduction in absorption energy when the binding domain of the organic fragment is changed from terpyridine to phenyl-bipyridine. It appears that the strong  $\sigma$ -donor strength of the

coordinated carbon atom present in the phenyl-bipyridyl coordinated complexes is the cause of the stabilisation of the energy of the <sup>1</sup>MLCT transition. This most likely occurs because of an increase in the energy of the platinum metal-centred orbitals, thereby reducing the energy gap between the HOMO and LUMO associated with the MLCT transition. Interestingly, the low energy absorption bands of the terpyridyl complexes tend to be more intense than those of their phenyl-bipyridyl coordinated counterparts as evidenced by their respective molar absorptivities in acetonitrile. This effect is particularly pronounced for the  $\beta$ -naphthyl and *para*-biphenyl substituted luminophores and it is possible that the more intense absorptions of the terpyridyl ligands are enhanced by the presence of intraligand charge transfer transitions, which have been identified in Chapter 3.

**Table 4.2** Comparison of low energy absorption bands for a selection of complexes.

R-group	[Pt(4'-R-terpy)Cl] <sup>+</sup> <sup>a</sup>		[Pt(4-R-phbipy)Cl]	
	$\lambda_{\text{abs}}$ (max) in CH <sub>2</sub> Cl <sub>2</sub> (nm)	$\lambda_{\text{abs}}$ (max) in MeCN (nm)	$\lambda_{\text{abs}}$ (max) in CH <sub>2</sub> Cl <sub>2</sub> (nm)	$\lambda_{\text{abs}}$ (max) in MeCN (nm)
H	405 <sup>29, 30</sup> 388sh	390sh (1960 <sup>b</sup> ) <sup>29, 30</sup> 377 (2200)	43044	420 (1550 <sup>b</sup> ) <sup>44</sup>
phenyl	412 <sup>32</sup> 397sh	403 (6664) <sup>53</sup> 383 (5724)	No data	No data
$\beta$ -naphthyl	427405	411 (14100) 394 (10200)	438420	429 (4800) 411 (4700)
<i>para</i> -biphenyl	423403	410 (17400) 390 (14000)	437419	427 (2100) 407 (2100)

(a) Data from Chapter 3, unless otherwise referenced.

(b) Molar absorptivity (M<sup>-1</sup>.cm<sup>-1</sup>).

### *Solution emission spectroscopy*

The room temperature solution emission spectra of [Pt(4- $\beta$ Np-phbipy)Cl] and [Pt(4-*p*Biphphbipy)Cl] are sufficiently similar that a single discussion of the monomeric emission origin of [Pt(4- $\beta$ Np-phbipy)Cl] will suffice for both complexes. This will be followed by a discussion of the emission of both complexes in a rigid glass at 77 K. Emission data from all the measurements have been condensed in Table 4.7 at the end of this chapter.

Emission from the [Pt(4- $\beta$ Np-phbipy)Cl] luminophore was recorded both in deoxygenated acetonitrile and dichloromethane solutions, and in a rigid glassy medium. The luminescence spectrum of the neutral complex in deoxygenated dichloromethane is presented in Figure 4.3 and consists of a mildly structured band with maximum intensity at *ca.* 570 nm. (The emission maximum and profile in deoxygenated acetonitrile is practically identical.) The band is broad and asymmetric, showing a steeper increase in intensity on its high energy side while tailing off more gradually on the lower energy side. Lifetimes in dichloromethane and acetonitrile have been evaluated at 750 and 90 ns respectively {610 and 70 ns in the case of [Pt(4-*p*Biphphbipy)Cl]} and excitation matches absorption for emission from both media. The emission intensity is extremely low which is most likely due to the limited solubility of the complex in the solvents that were used.

The emission spectra in Figure 4.3 were recorded at a concentration of 20  $\mu$ M, which is slightly below the limiting solubility of [Pt(4- $\beta$ Np-phbipy)Cl] in dichloromethane at ambient temperatures. At such low intensity it becomes difficult to interpret the band profile and even distinct vibrational progressions are essentially indistinguishable leaving us to interpret the emission origin based more on the energy of the emission and relying less on the observed band shape. The limited solubility, allows us to discount the formation of excimer or MMLCT excited states which arise due to intermolecular interactions. Such interactions are unlikely at such a low concentration. In any event, the MMLCT state emits at a significantly lower energy than that observed for [Pt(4- $\beta$ Np-phbipy)Cl]. Furthermore a metal-centred d-d transition can be excluded as the emission source, given that transitions of this type give rise to emission spectra with a symmetric, *i.e.* Gaussian, band profile.<sup>108, 110, 176</sup> As noted the low intensity of the emission signal makes it difficult to describe the band profile accurately. At

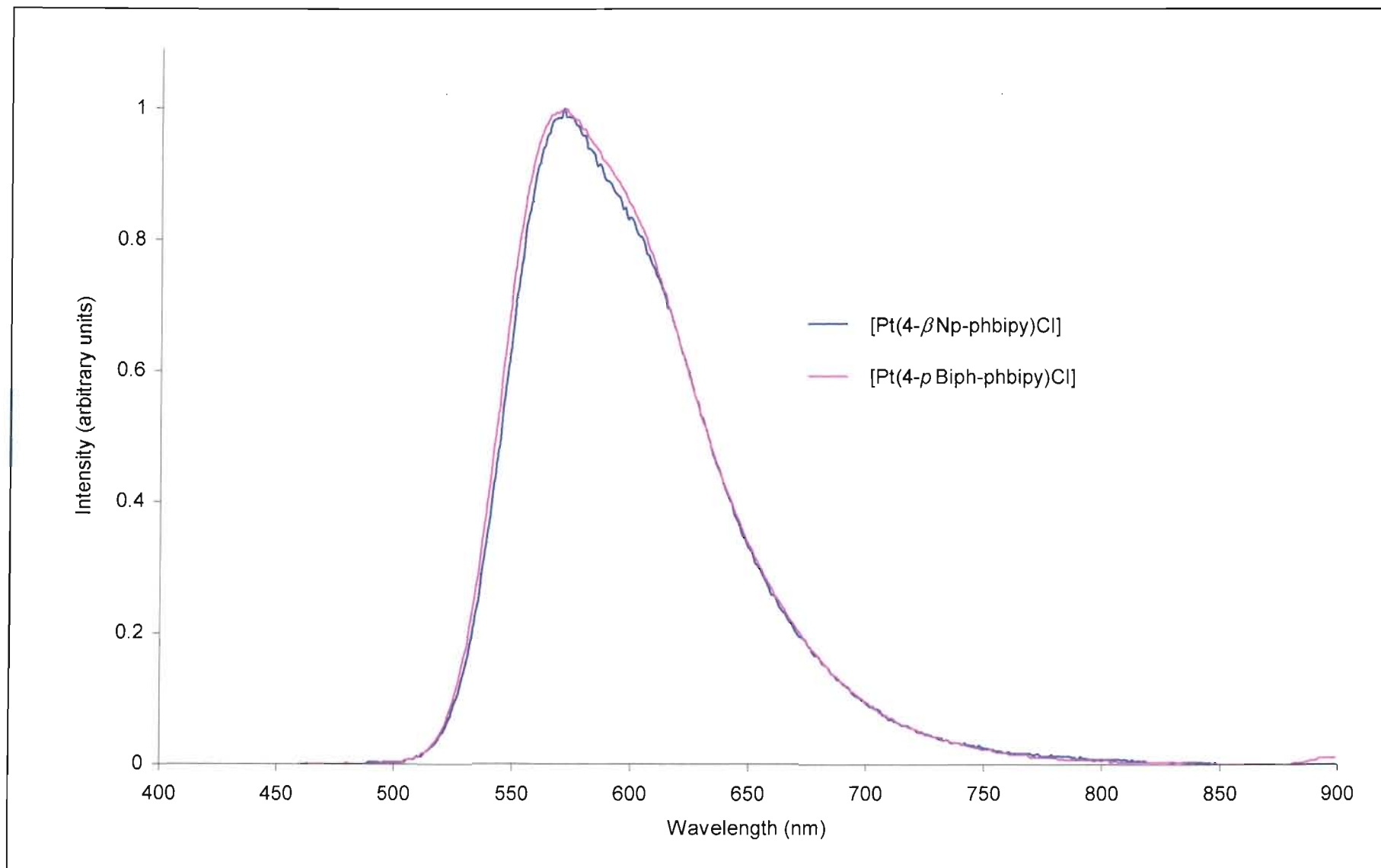


**Figure 4.3** Dichloromethane solution emission spectra of [Pt(4-βNp-phbipy)Cl] (**10**) and [Pt(4-pBiph-phbipy)Cl] (**11**) recorded at 298 K.

such a low intensity, the distinct progressions associated with the presence of ligand character in the excited state would be very poorly resolved. Nevertheless the energy of the band is too low to entertain any thoughts of a purely ligand centred emission origin. Indeed, emission from the free ligand has its highest energy emission band at 498 nm, well above the emission energy for the orthometallated complex, indicating significant metal participation in the excited state. The wavelength of the 0-0 transition is almost identical to that of the terpyridyl analogue, [Pt(4'- $\beta$ Np-terpy)Cl]X {X<sup>-</sup> = SbF<sub>6</sub><sup>-</sup> (**1**), BF<sub>4</sub><sup>-</sup> (**2**) and CF<sub>3</sub>SO<sub>3</sub><sup>-</sup> (**3**)}, measured under the same conditions, and in this case emission has been assigned to radiative relaxation from a hybrid excited state with IL, ILCT and MLCT character (see Chapter 3). The fact that the complex luminesces at all in acetonitrile can be taken to indicate that the excited state is not brought about by a pure MLCT transition, since such a process involves an increased formal oxidation state of the metal, that is expected to render the metal prone to coordination by the solvent and consequent radiationless deactivation.<sup>48</sup> However, a much reduced emission lifetime of 90 ns in acetonitrile compared to that in non-coordinating dichloromethane solution is a good indication that solvent induced exciplex quenching is likely to play a role in acetonitrile and that the excited state must have a degree of MLCT character. Moreover, the emission falls within the energy range expected of a MLCT emission. Taken together the above evidence suggests an excited state of mixed <sup>3</sup>IL and <sup>3</sup>MLCT character. Although the band does not show obvious ligand character in the form of distinct vibrational progressions, we suggest that this deficiency is a result of the extremely low intensity of the band, which blurs its profile.

Evidence for a significant ILCT character in the excited state of the related terpyridyl complexes with large fused-ring aromatic systems in the 4'-position has been invoked to explain very long emission lifetimes even at relatively low energies.<sup>31,32</sup> When the emission lifetime of [Pt(4'- $\beta$ Np-phbipy)Cl] in dichloromethane (750 ns) is compared to the 12.0  $\mu$ s recorded for the terpyridyl analogue, [Pt(4'- $\beta$ Np-terpy)Cl]<sup>+</sup>, measured under the same conditions it becomes clear that different processes are at work. It is possible that ILCT processes still contribute to the excited state of [Pt(4'- $\beta$ Np-phbipy)Cl] in solution, but to a very limited extent. The most probable explanation is that the presence of the orthometallating carbon atom near the metal centre renders the metal-ligand binding domain less susceptible to reduction, and hence for participation in ILCT processes.



The emission behaviour of [Pt(4-*p*Biph-phbipy)Cl] in room temperature fluid solution is entirely similar and there are only minor differences in emission lifetimes. The emission assignments for [Pt(4- $\beta$ Np-phbipy)Cl] and [Pt(4-*p*Biph-phbipy)Cl] are the same.

#### *Glass emission spectroscopy*

In order to minimise participation of thermally activated radiationless decay processes, and to ensure that measurement of monomer emission are made, the emission spectra of [Pt(4- $\beta$ Np-phbipy)Cl] (**10**) and [Pt(4-*p*Biph-phbipy)Cl] (**11**) have been performed in a dilute rigid glass at 77 K. It was not possible to dissolve both [Pt(4- $\beta$ Np-phbipy)Cl] and [Pt(4-*p*Biph-phbipy)Cl] in the same solvent due to differences in solubility. For this reason [Pt(4- $\beta$ Np-phbipy)Cl] was studied in rigid DME solution {where DME is a 1:5:5 (v/v) DMF/MeOH/EtOH solvent mixture} at 77 K and [Pt(4-*p*Biph-phbipy)Cl] was studied in a butyronitrile glass. In spite of the difference in solvent, emission from both complexes is very similar and their emission from a rigid glassy medium will be described together. Slight differences that do exist will be highlighted at the end of this section.

Emission from a 20  $\mu$ M solution of [Pt(4- $\beta$ Np-phbipy)Cl] (**10**) and [Pt(4-*p*Biph-phbipy)Cl] (**11**) recorded in a rigid glass at 77 K is presented in Figure 4.4. The relevant spectroscopic data are condensed in Table 4.7 at the end of this chapter. Emission is in a vibrationally structured band with maxima at 549, 591 and 642 nm {543, 585, and 635 nm for [Pt(4-*p*Biph-phbipy)Cl]} with the band at highest energy being most intense (Huang-Rhys factor:  $I_{0,1}/I_{0,0} \approx 0.65$ ). Vibrational progressions are spaced 1200 to 1300  $\text{cm}^{-1}$  apart, providing strong evidence of ligand participation in the excited state. This deduction is based on the similarity of the magnitude of the vibrational spacing with skeletal stretching modes of ligand C=C and C=N bonds. The radiative lifetime has been evaluated at nearly 23  $\mu$ s and 9.8  $\mu$ s for [Pt(4- $\beta$ Np-phbipy)Cl] and [Pt(4-*p*Biph-phbipy)Cl] respectively. The emission gives every indication of being a more explicitly structured version of the solution emission spectra recorded at ambient temperatures (*vide supra*). The emission profile and maxima observed for the three highest energy bands correspond almost exactly to spectra recorded of [Pt(4'- $\beta$ Np-terpy)Cl]<sup>+</sup> also made in a 77 K butyronitrile glass (*viz.* 542, 583, and 625sh nm) and reported in our recent publication.<sup>32</sup> Emission in this case is assigned to a configurationally mixed state with

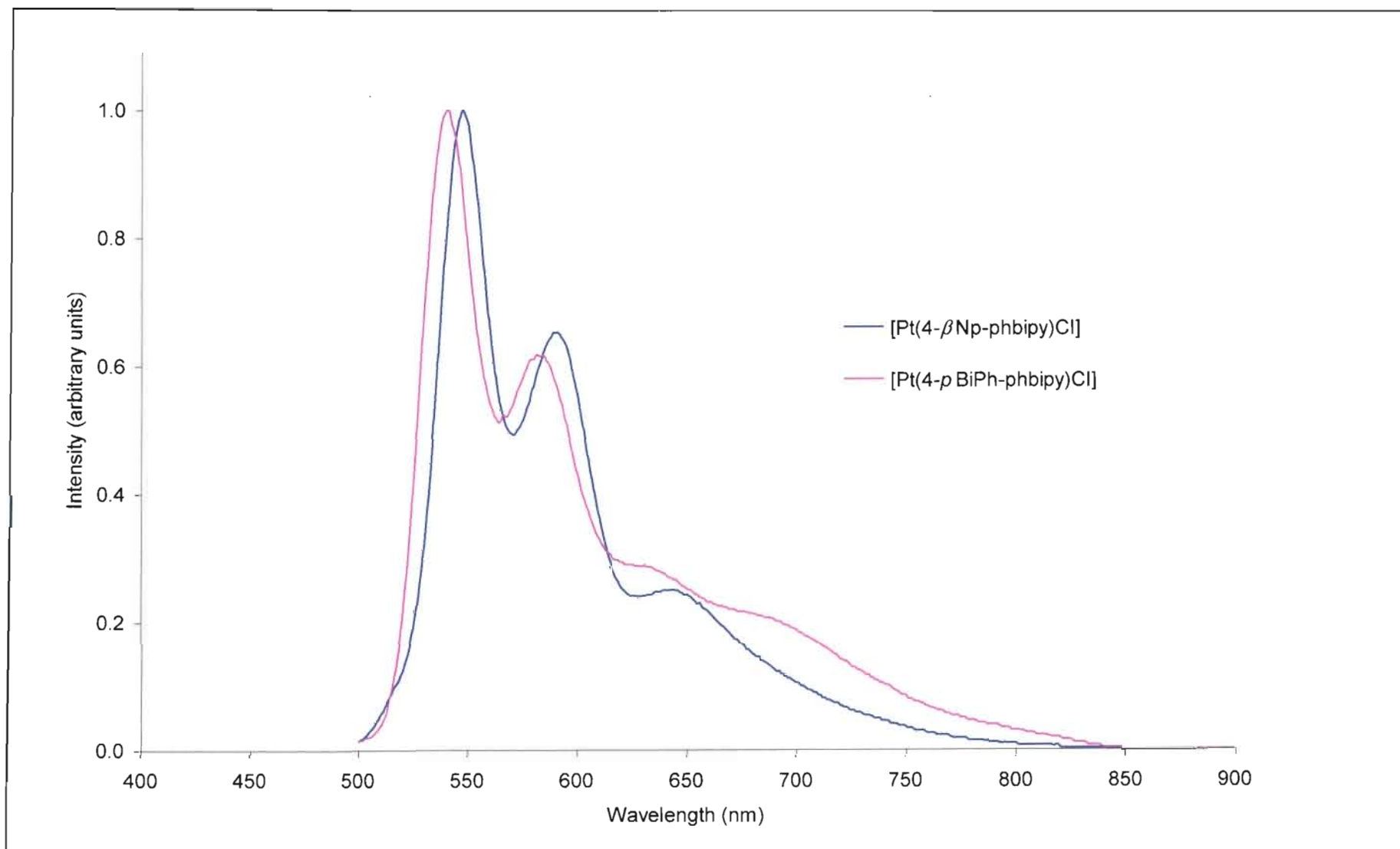


**Figure 4.4** Solution emission spectra of [Pt(4-βNp-phbipy)Cl] (**10**) and [Pt(4-pBiPh-phbipy)Cl] (**11**) recorded in glassy DME and butyronitrile solution at 77 K respectively.

<sup>3</sup>IL, <sup>3</sup>ILCT and <sup>3</sup>MLCT character. Based on this observation such an assignment is also invoked for the emission from dilute glassy medium for [Pt(4-*β*Np-phbipy)Cl] and [Pt(4-*p*Biph-phbipy)Cl]. However, in the case of [Pt(4-*p*Biph-phbipy)Cl] the ILCT character probably constitutes a smaller proportion of the excited state as reflected in the somewhat shorter emission lifetime. As in Chapter 3, this can be rationalised by the greater ease of ionising the electron-rich naphthyl group than the biphenyl moiety. Moreover, given the similarity of the room temperature solution emissions of [Pt(4-*β*Np-phbipy)Cl] and [Pt(4-*p*Biph-phbipy)Cl] it does not appear that the nature of the monomeric excited state has been significantly altered in reducing the temperature to 77 K and the discussion of the nature of the excited state applies equally to observations in a rigid glassy medium.

In addition to the monomer emission already described, emission from [Pt(4-*p*Biph-phbipy)Cl] shows an additional concentration dependent band at 695 nm. Given its low energy and greater intensity in more concentrated solution leads to an assignment of a <sup>3</sup>MMLCT excited state brought about by the overlap of platinum d<sub>2</sub>-orbitals on adjacent luminophores as the most likely emission origin. There should be little question that overlap of this nature is sterically possible for [Pt(4-*p*Biph-phbipy)Cl] in view of the MMLCT emission displayed by the red form of [Pt(4'-*p*Biph-terpy)Cl]BF<sub>4</sub> described in Chapter 3. In this case the luminophore is [Pt(4'-*p*Biph-terpy)Cl]<sup>+</sup> which is essentially identical to [Pt(4-*p*Biph-phbipy)Cl] from the point of view of its steric demands.

### 4.3 SUMMARY AND CONCLUSIONS

As an extension to the work described in Chapter 3 the two complexes [Pt(4- $\beta$ Np-phbipy)Cl] (**10**) and [Pt(4- $p$ Biph-phbipy)Cl] (**11**), containing orthometallated phenyl-bipyridyl ligands, were synthesised and their photophysical properties studied. These two complexes constitute direct analogues to the [Pt(4'- $\beta$ Np-terpy)Cl]<sup>+</sup> and [Pt(4'- $p$ Biph-terpy)Cl]<sup>+</sup> complexes described in Chapter 3 differing only in having an anionic phenyl-bipyridyl *C, N, N* binding domain, with orthometallation *via* an *ortho*-C deprotonated carbon atom of the phenyl ring. A similar change has previously been made to the unsubstituted chloro(terpyridine)platinum(II) backbone with the synthesis of [Pt(phbipy)Cl], where phbipy is the *ortho*-C deprotonated form of 6-phenyl-2,2'-bipyridine.<sup>44</sup> The monomeric luminescence of [Pt(phbipy)Cl] has been studied both in a room temperature fluid solution and in a rigid glassy medium at 77 K. Luminescence studies of the closely related 4'-phenyl substituted luminophore, [Pt(4'-Ph-terpy)Cl]<sup>+</sup>, where 4'-Ph-terpy is the 4'-phenyl-2,2':6',2''-terpyridyl ligand have also been reported.<sup>42,53,32</sup> However, to date, no similar studies have been published of emission from its phenyl-bipyridyl analogue *viz.* [Pt(4-Ph-phbipy)Cl], where 4-Ph-phbipy is the *ortho*-(2'')-C deprotonated form of 4-phenyl-6-phenyl-2,2'-bipyridine. The available luminescence data recorded at room temperature in fluid solution are summarised in Table 4.3. These will now be discussed.

We start with the photophysical properties of the unsubstituted [Pt(phbipy)Cl] luminophore in fluid solution at room temperature.<sup>44</sup> The luminophore is strongly emissive at room temperature, but the emission energy and profile are highly dependent on the nature of the solvent. The lifetime and quantum yield were also found to decrease as the polarity of the solvent was increased. The [Pt(phbipy)Cl] luminophore even shows emission in acetonitrile solution,<sup>44</sup> indicating that the excited state is not highly sensitive to solvent induced exciplex quenching.<sup>48</sup> By contrast the terpyridyl analogue, [Pt(terpy)Cl]<sup>+</sup> is non-emissive in room temperature fluid solution. Che *et al.* assign emission from [Pt(phbipy)Cl] to an excitation that is <sup>3</sup>MLCT in nature<sup>44</sup> but make no effort to explain why the emission is not quenched by solvent attack, as is normally the case when the emitting state is <sup>3</sup>MLCT.<sup>48</sup>

**Table 4.3** Comparison of room temperature fluid solution emission.<sup>a</sup>

R-group	[Pt(4'-R-terpy)Cl] <sup>+</sup>			[Pt(4-R-phbipy)Cl]			
	$\lambda_{em}(\text{max})$ in CH <sub>2</sub> Cl <sub>2</sub> (nm)	$\tau$ ( $\mu\text{s}$ )	$\lambda_{em}(\text{max})$ in MeCN (nm)	$\lambda_{em}(\text{max})$ in CH <sub>2</sub> Cl <sub>2</sub> (nm)	$\tau$ ( $\mu\text{s}$ )	$\lambda_{em}(\text{max})$ in MeCN (nm)	$\tau$ ( $\mu\text{s}$ )
H	No emission	-	No emission	56544	0.5	55044	0.2
phenyl	<u>535</u> , 570sh, 608sh <sup>32</sup>	0.09	No emission	No data		No data	
$\beta$ -naphthyl	<u>570</u> , 615sh, 670sh	11.90	No emission	<u>573</u> , 600sh	0.8	<u>570</u> , 600sh	0
<i>para</i> -biphenyl	<u>562</u> , 602sh, 650sh	4.00	No emission	<u>573</u> , 600sh	0.6	<u>568</u> , 600sh	0

Underlined values refer to the most intense bands within a manifold.  
sh = shoulder.

(a) Data from Chapter 3, unless otherwise referenced.

Referring to the 4- $\beta$ Np-phbipy and 4-*p*Biph-phbipy derivatives we note that an anionic carbon is a much stronger  $\sigma$ -donor than a pyridyl nitrogen. This property is manifested in an absorption spectrum with a prominent stabilisation of the lowest energy (MLCT) absorption band for the phenyl-bipyridyl compounds as compared to that for their terpyridyl counterparts. Similarly, the emitting state is stabilised, but only if it is also essentially MLCT in character (see Table 4.3). With this in mind we note that the emitting state of [Pt(4-*p*Biph-phbipy)Cl] (0-0 transition at 573 nm) is stabilised compared to its terpyridyl counterpart, [Pt(4'-*p*Biph-terpy)Cl]<sup>+</sup> (0-0 transition at 562 nm). A reduction in the energy of the <sup>3</sup>MLCT ( $d - \pi^*$ ) component of the emission is to be expected, given that the energy of the metal d-orbital is raised when a stronger  $\sigma$ -donor is used. In contrast, the emission energies of [Pt(4- $\beta$ Np-

phbipy)Cl] and [Pt(4'- $\beta$ Np-terpy)Cl]<sup>+</sup> are very similar. However, emission from the latter complexes also contain an ILCT contribution, with the result that the MLCT contribution is less and any stabilisation of the emitting state is dampened.

Noteworthy also is the significantly longer room temperature solution emission lifetimes of the [Pt(4'- $\beta$ Np-terpy)Cl]<sup>+</sup> and [Pt(4'-*p*Biph-terpy)Cl]<sup>+</sup> complexes compared to those of their phenyl-bipyridyl counterparts (see Table 4.3). Though we are uncertain of the precise reasons, this is presumably also related to the stronger  $\sigma$ -donor strength of the deprotonated carbon atom orthometallated to the platinum(II) centre. Strong  $\sigma$ -donation would deactivate ILCT processes from the electron-rich naphthyl and biphenyl groups to the metal. As previously noted, an enhanced ILCT component is expected to prolong the lifetime of the emitting state.<sup>32</sup> We note that deactivation of the ILCT component results in an emission for the naphthyl substituted [Pt(4'- $\beta$ Np-phbipy)Cl] complex that is very similar to that for the [Pt(4-*p*Biph-phbipy)Cl] complex. This near independence of the emission properties on the R-group for the [Pt(4-R-phbipy)Cl] phenyl-bipyridyl complexes contrasts the situation for the terpyridyl analogues where changing the R-group does have a distinct effect on the emission energy and lifetime (see Table 4.3). Moreover,  $\sigma$ -donation is likely to result in a concomitant enhancement of the MLCT transitions by increasing the electron density on the metal which is already in a low oxidation state. All things being equal it is expected that the lifetime for the emitting state of a "pure" <sup>3</sup>MLCT transition will be shorter than that of a "pure" <sup>3</sup>IL (or <sup>3</sup>ILCT) state.<sup>37, 43</sup>

Of particular interest is that the phenyl-bipyridyl complexes, [Pt(phbipy)Cl], [Pt(4'- $\beta$ Np-phbipy)Cl] and [Pt(4-*p*Biph-phbipy)Cl], emit in acetonitrile and their terpyridyl analogues do not. (See Table 4.3) This is surprising as emission by all these luminophores is expected to derive from a state that has at least partial (if not entirely) MLCT character. It is well established that MLCT emission is often quenched in coordinating solvents such as acetonitrile.<sup>27,30,37,48,177</sup> Though the degree of MLCT character is a factor, on balance it seems that the presence of the *ortho*-deprotonated phenyl-bipyridyl ligand stabilises a MLCT excited state to radiative decay. Certainly, it is not inconceivable that the strong  $\sigma$ -donor property of the deprotonated carbon ligand will result in an increase in the electron density at the metal centre that is sufficient to discourage the formation of solvent coordinated species in the

excited state, so allowing for emission in a coordinating solvent. Although discouraged, this effect may not be entirely absent, as displayed by the roughly 9-fold reduction in emission lifetimes of [Pt(4- $\beta$ Np-phbipy)Cl] and [Pt(4-*p*Biph-phbipy)Cl] in acetonitrile as compared to emission recorded in the non-coordinating solvent dichloromethane.

Emission data have been recorded for the same group of complexes but in a dilute low temperature glass. Data from these measurements are presented in Table 4.4.

**Table 4.4** Comparison of emission recorded in rigid glassy medium at 77 K.<sup>a</sup>

R-group	[Pt(4'-R-terpy)Cl] <sup>+</sup>			[Pt(4-R-phbipy)Cl]		
	$\lambda_{em}(\text{max})$	Huang-Rhys ratio	$\tau$ ( $\mu\text{s}$ )	$\lambda_{em}(\text{max})$	Huang-Rhys ratio	$\tau$ ( $\mu\text{s}$ )
H	<u>470</u> , 506, 546, 580 <sup>BuCN, 32</sup>	0.6	15.04	<u>512</u> , 544 <sup>MeCN, 44</sup>	0.65	0.2
phenyl	<u>503</u> , 540, 582 <sup>BuCN, 32</sup>	0.75	15.04	No data	-	-
$\beta$ -naphthyl	<u>545</u> , 583, 633 <sup>DME</sup>	0.75	47	<u>549</u> , 591, 642 <sup>DME</sup>	0.65	23
<i>para</i> -biphenyl	<u>543</u> , 579, 627 <sup>DME</sup>	0.8	2.9	<u>543</u> , 585, 635, 695 <sup>BuCN</sup>	0.6	9.8

Underlined values refer to the most intense bands within a manifold.

sh = shoulder.

(a) Data from Chapter 3, unless otherwise referenced.

(BuCN) Spectrum recorded in butyronitrile solution.

(MeCN) Spectrum recorded in acetonitrile solution.

(DME) Spectrum recorded in 1:5:5 (v/v) DMF/methanol/ethanol solvent mixture.

Unfortunately the available data do not allow valid comparisons to be made between the

emission properties of the terpyridyl complexes and their phenyl-bipyridyl analogues since, for solubility reasons, the measurements have not been made in the same medium (see Table 4.4). One exception is the pair of complexes  $[\text{Pt}(4'\text{-}\beta\text{Np-terpy})\text{Cl}]^+$  and  $[\text{Pt}(4\text{-}\beta\text{Np-phbipy})\text{Cl}]$  since for both of these complexes the measurements have been recorded in glassy DME. In so far as these two complexes are concerned the trends are the same as those deduced from the data in fluid solution. However, one further deduction can be made by noting that, since the glass spectra are more structured than their fluid solution counterparts, reliable measurements of Huang-Rhys ratios ( $I_{0,1}/I_{0,0}$ ) can be made. Values obtained for the ratios are 0.75 for the terpy complex and 0.65 for the phenyl-bipyridyl complex (refer to Table 4.4). A reduced Huang-Rhys ratio is generally taken to indicate a reduced IL ( $\pi\text{-}\pi^*$ ) component and an increased MLCT ( $d\text{-}\pi^*$ ) component in an emitting state. This observation is entirely consistent with the earlier conclusion that the energy of the MLCT component of the emitting state will become less when the terpyridyl ligand is replaced with a phenyl-bipyridyl ligand.

In summary the principal effects of replacing a N-donor in a terpy ligand with an anionic carbon donor to give the phenyl-bipyridyl ligand are:

- i) A reduction in the energy of the MLCT ( $d\text{-}\pi^*$ ) component of the emission. This is to be expected given that the energy of the metal  $d$ -orbital is raised when a stronger  $\sigma$ -donor is used.
- ii) A reduced likelihood of the MLCT emission being quenched in a coordinating solvent.
- iii) A decreased lifetime for the emitting state. We associate this with the increase in MLCT character in the excited state. It is well established that longer lifetimes are associated with IL (or ILCT) rather than MLCT emission.<sup>32, 37, 43</sup>

We acknowledge that the above conclusions are based on the limited data available. Moreover, the situation is often complicated by the fact that the emitting state is one of mixed character. Nevertheless the conclusions make sense and we believe them to be correct.



## 4.4 EXPERIMENTAL

### 4.4.1 Synthetic procedures

#### 4.4.1.1 [Pt(4- $\beta$ Np-phbipy)Cl] (**10**)

{where 4- $\beta$ Np-phbipy is the anionic deprotonated form of the 4-( $\beta$ -naphthyl)-6-phenyl-2,2'-bipyridine ligand (H4- $\beta$ Np-phbipy)}

A mixture of K<sub>2</sub>PtCl<sub>4</sub> (100 mg; 0.24 mmol) and 4-( $\beta$ -naphthyl)-6-phenyl-2,2'-bipyridine (H4- $\beta$ Np-phbipy) (141 mg; 0.24 mmol) was refluxed in acetonitrile/water (10 ml; 1:1) for 48 h. The orange precipitate was filtered and washed on the frit with large amounts of diethyl ether followed by smaller amounts of acetonitrile. The resulting solid was vapour extracted with dichloromethane and excess solvent removed under reduced pressure. The precipitate was recrystallised by the slow diffusion of diethyl ether into a dimethylformamide solution containing the product. The solid product was recovered and dried *in vacuo*.

[Pt(4- $\beta$ Np-phbipy)Cl] (**10**): Yield 90 mg (64 %). Molecular mass 588.0 g.mol<sup>-1</sup>. [Calc. for C<sub>26</sub>H<sub>17</sub>ClN<sub>2</sub>Pt: C, 53.11; H, 2.91; N, 4.76. Found: C, 53.02; H, 2.75; N, 4.70 %].

<sup>1</sup>H NMR for [Pt(4- $\beta$ Np-phbipy)Cl] (DMSO-d<sub>6</sub>):  $\delta$  8.85(1H, d, H<sup>6</sup>) 8.69(1H, d (signal obscured), H<sup>3</sup>) 8.68(1H, s, naphthyl H) 8.56 (1H, s, H<sup>3</sup>) 8.32(1H, t (signal obscured), H<sup>4</sup>) 8.30(1H, s, H<sup>5</sup>) 8.18(1H, d, naphthyl H) 8.09(1H, d, naphthyl H) 8.06(1H, m, naphthyl H) 8.01(1H, m, naphthyl H) 7.86(1H, dd, H<sup>5</sup>) 7.78(1H, d, H<sup>3</sup>) 7.63(2H, m, naphthyl H's) 7.45(1H, d, H<sup>6</sup>) 7.11(1H, t, H<sup>5</sup>) 7.07(1H, t, H<sup>4</sup>)

#### 4.4.1.2 [Pt(4-*p*Biph-phbipy)Cl] (**11**)

{where 4-*p*Biph-phbipy is the anionic deprotonated form of the 4-(*para*-biphenyl)-6-phenyl-2,2'-bipyridine ligand (H4-*p*Biph-phbipy)}

A mixture of K<sub>2</sub>PtCl<sub>4</sub> (100 mg; 0.24 mmol) and 4-(*para*-biphenyl)-6-phenyl-2,2'-bipyridine (H4-*p*Biph-phbipy) (147 mg; 0.24 mmol) was refluxed in acetonitrile/water (10 ml; 1:1) for 48 h. The orange precipitate was filtered and washed on the frit with large amounts of diethyl ether followed by smaller amounts of acetonitrile. The resulting solid was vapour extracted with dichloromethane and excess solvent removed under reduced pressure. The precipitate was recrystallised by the slow diffusion of diethyl ether into a dimethylformamide solution containing the product. The solid product was recovered and dried *in vacuo*.

[Pt(4-*p*Biph-phbipy)Cl] (**11**): Yield 100 mg (68 %). Molecular mass 614.0 g.mol<sup>-1</sup>. [Calc. for C<sub>28</sub>H<sub>19</sub>ClN<sub>2</sub>Pt: C, 54.77; H, 3.12; N, 4.56. Found: C, 55.04; H, 2.99; N, 4.45 %].

<sup>1</sup>H NMR for [Pt(4-*p*Biph-phbipy)Cl] (DMSO-d<sub>6</sub>): δ 8.90(1H, d, H<sup>6</sup>) 8.72(1H, d, H<sup>3</sup>) 8.53(1H, s, H<sup>3</sup>) 8.34(1H, td, H<sup>4</sup>) 8.29(1H, s, H<sup>5</sup>) 8.20(2H, d, H<sup>2''',6''</sup>) 7.90(1H, t (signal obscured), H<sup>5</sup>) 7.88(2H, d, H<sup>3''',5''</sup>) 7.81(1H, d, H<sup>3''</sup>) 7.78(2H, d, H<sup>2''',6''</sup>) 7.51(2H, t, H<sup>3''',5''</sup>) 7.48(1H, d, H<sup>6''</sup>) 7.42(1H, t, H<sup>4''</sup>) 7.14(1H, t, H<sup>5''</sup>) 7.08(1H, t, H<sup>4''</sup>)

**Table 4.5** *Infrared spectroscopic data.*

<b>Compound</b>	<b>Polypyridine<sup>a</sup></b>
[Pt(4- $\beta$ Np-phbipy)Cl] ( <b>10</b> )	738(m) 743(s) 778(s) 819(w) 1019(w) 1131(w) 1160(w) 1354(w) 1404(s) 1436(w) 1460(w) 1480(m) 1540(m) 1582(m) 1605(vs) 1612(vs)
[Pt(4- <i>p</i> Biph-phbipy)Cl] ( <b>11</b> )	730(m) 764(s) 774(m) 794(m) 1022(w) 1117(w) 1159(w) 1293(w) 1403(m) 1461(w) 1476(m) 1536(m) 1580(m) 1603(vs)

(a) Recorded as a KBr pellet in the solid state (cm<sup>-1</sup>).  
Designation: w = weak; m = medium; s = strong; vs = very strong;

**Table 4.6** Absorption spectroscopic data recorded in fluid solution at 298 K

Chromophore	$\lambda_{\text{abs}}$ (nm)		Assignment
	Acetonitrile	Dichloromethane	
[Pt(4- $\beta$ Np-phbipy)Cl] ( <b>10</b> )	429 (4800 <sup>a</sup> )	438	MLCT [Pt(5d) $\rightarrow$ 4- $\beta$ Np-phbipy( $\pi^*$ )]
(concentration range: 10 - 100 $\mu$ M)	411sh (4700)	420sh	MLCT [Pt(5d) $\rightarrow$ 4- $\beta$ Np-phbipy( $\pi^*$ )]
	361sh (11600)	365sh	<sup>1</sup> ( $\pi$ - $\pi^*$ ) (4- $\beta$ Np-phbipy)
	328sh (19400)	333sh	<sup>1</sup> ( $\pi$ - $\pi^*$ ) (4- $\beta$ Np-phbipy)
	308sh (24300)	311sh	<sup>1</sup> ( $\pi$ - $\pi^*$ ) (4- $\beta$ Np-phbipy)
	278 (45200)	281	<sup>1</sup> ( $\pi$ - $\pi^*$ ) (4- $\beta$ Np-phbipy)
	266sh (41200)	268sh	<sup>1</sup> ( $\pi$ - $\pi^*$ ) (4- $\beta$ Np-phbipy)
[Pt(4- <i>p</i> Biph-phbipy)Cl] ( <b>11</b> )	427 (2100)	437	MLCT [Pt(5d) $\rightarrow$ 4- <i>p</i> Biph-phbipy( $\pi^*$ )]
(concentration range: 10 - 100 $\mu$ M)	407sh (2100)	419sh	MLCT [Pt(5d) $\rightarrow$ 4- <i>p</i> Biph-phbipy( $\pi^*$ )]
	361sh (3800)	370sh	<sup>1</sup> ( $\pi$ - $\pi^*$ ) (4- <i>p</i> Biph-phbipy)
	286 (41800)	287	<sup>1</sup> ( $\pi$ - $\pi^*$ ) (4- <i>p</i> Biph-phbipy)

(a) Molar absorptivity ( $\text{M}^{-1}\cdot\text{cm}^{-1}$ )  
sh = shoulder

**Table 4.7** Absorption and emission spectroscopic data recorded in dilute solution.

Compound	Absorption maxima (nm)	Emission maxima (nm) [77 K]	$\tau$ (ns) [77 K]
[Pt(4- $\beta$ Np-phbipy)Cl] ( <b>10</b> )	<u>429</u> , 411 <sup>MeCN</sup> 438, 420 <sup>DCM</sup>	<u>573</u> , 600sh <sup>DCM</sup> <u>570</u> , 600sh <sup>MeCN</sup> [ <u>549</u> , 591, 642] <sup>DME</sup>	750 <sup>DCM</sup> 85 <sup>MeCN</sup> [22600] <sup>DME</sup>
[Pt(4- <i>p</i> Biph-phbipy)Cl] ( <b>11</b> )	427, 407 <sup>MeCN</sup> 437, 419 <sup>DCM</sup>	<u>573</u> , 600sh <sup>DCM</sup> <u>568</u> , 600sh <sup>MeCN</sup> [ <u>543</u> , 585, 635, 695] <sup>BuCN</sup>	610 <sup>DCM</sup> 70 <sup>MeCN</sup> [9800] <sup>BuCN</sup>

Underlined values refer to the most intense bands within a manifold.

sh = shoulder

(DCM) Spectrum recorded in dichloromethane solution

(MeCN) Spectrum recorded in acetonitrile solution

(DME) Spectrum recorded in 1:5:5 (v/v) DMF/methanol/ethanol solution

## Chapter Five

## Synthesis and photophysical properties of pyrazinyl-bipyridyl ligand complexes of platinum(II)

### 5.1 INTRODUCTION

In 1980 Crutchley and Lever were able to show that substituting bipyrazine for bipyridine in  $[\text{Ru}(\text{bipy})_3]^{2+}$  has the effect of dramatically increasing the MLCT (metal to ligand charge transfer) emission lifetime in solution at room temperature<sup>178</sup> and hence improving the utility of the complex as a photosensitizer in photoredox reactions. Ernst and Kaim have performed a similar study of the effect on the emission from ruthenium(II) polyazine complexes when pyridine is replaced by a variety of diazines.<sup>117</sup> It was found that the lifetime of the MLCT excited state is prolonged as the reduced, or partially reduced, diazine ligand in this excited state becomes more basic (*i.e.*, a stronger  $\sigma$ -donor). The authors propose that the increased basicity possibly leads to a reduced probability of radiationless deactivation *via* thermally accessible metal-centred excited states and in this way the emission lifetime is extended.<sup>117</sup> Although metal-centred d-d states are generally too high in energy to influence the radiationless deactivation processes of platinum terpyridyl complexes it was decided to try and extend the emission lifetimes of the platinum terpyridyl complexes in a similar way, by replacing one (or more) pyridine rings in the terpyridyl ligand with pyrazine rings. It is known that pyrazine is a weaker  $\sigma$ -donor and superior  $\pi$ -acceptor compared to pyridine, but it was unknown what effect such an interchange of polyazines would have on the emission of the platinum terpyridyl complexes. Initial efforts centred on the replacement of one of the two outer pyridine rings in the 4'-phenyl-terpyridyl ligand, resulting in the synthesis of the ligand 4-Ph-pzbipy {where 4-Ph-pzbipy is 4-phenyl-6-(2''-pyrazinyl)-2,2'-bipyridine} (see Chapter 2) and, in turn, the platinum coordinated complex  $[\text{Pt}(4\text{-Ph-pzbipy})\text{Cl}]\text{BF}_4$ . This complex was intended as a direct analogue of  $[\text{Pt}(4'\text{-phenyl-terpy})\text{Cl}]\text{BF}_4$  which has been described in the literature<sup>53</sup> and with which comparisons could be made. It was hoped that the same effect observed by Crutchley and Lever for  $[\text{Ru}(\text{bipy})_3]^{2+}$  of extending the lifetime of the monomeric emitting state would extend the lifetime of the emitting state of  $[\text{Pt}(4\text{-Ph-pzbipy})\text{Cl}]^+$  in

solution. In order to maximise the benefits of pyrazine ligands in our work the ligand 4-Ph-pybipz {4-Ph-pybipz is 4-phenyl-2,6-bis(2'-pyrazinyl)-pyridine} which incorporates two pyrazine rings was synthesised (see Chapter 2). Attempts to coordinate this ligand to platinum(II) are also described in this chapter.

Recent work in our laboratories involved a study of the structure and photophysical properties of complexes of the type  $[\text{Pt}\{4'-(ortho\text{-R-phenyl})-2,2':6',2''\text{-terpyridine}\}\text{Cl}]\text{X}$ , where R is either a methyl or trifluoromethyl group in the *ortho*-position of the phenyl ring and X is an anion in the outer coordination sphere of the complex.<sup>54</sup> Summerton and coworkers have shown these complexes to exhibit remarkable photophysical properties in the solid state.<sup>54</sup> The  $[\text{Pt}(4'\text{-}o\text{MePh-terpy})\text{Cl}]\text{SbF}_6$  complex is of particular interest since the cations in the solid state stack head-to-tail with a constant Pt...Pt separation of 3.368(1) Å along the stack. This is close enough for there to be significant interaction between the platinum metal centres of adjacent atoms and, accordingly, solid samples of the complex emit from a MMLCT (metal-metal to ligand charge transfer) excited state.<sup>54</sup> The significance of the R-group in the *ortho*-position of the phenyl ring is that it enforces non-planarity of the complex, because of steric interaction between the *ortho*-substituents (-CH<sub>3</sub> and -CF<sub>3</sub>) and the adjacent protons of the central pyridine ring. This idea, pioneered and utilised with great success by Summerton and coworkers, appears to encourage solid state packing by a “lock and key” mechanism; that is where the 4'-*o*RPh group twists about the interannular bond in a direction towards a “hole” in the next layer of cations.<sup>54</sup> Replacing one of the outer pyridine rings with a pyrazine ring in this system is not expected to alter the solid state packing of the complex in any way since the spatial consequences of replacing CH by N are likely to be negligible. As a result of the success of the work of Summerton *et al.*, and since a synthetic protocol had been established by the synthesis of 4-Ph-pzbipy, the ligands 4-*o*MePh-pzbipy {4-*o*MePh-pzbipy is 4-(*o*-CH<sub>3</sub>-phenyl)-6-(2''-pyrazinyl)-2,2'-bipyridine} and 4-*o*CF<sub>3</sub>Ph-pzbipy {4-*o*CF<sub>3</sub>Ph-pzbipy is 4-(*o*-CF<sub>3</sub>-phenyl)-6-(2''-pyrazinyl)-2,2'-bipyridine} have been synthesised (see Chapter 2). The synthesis and photophysical properties of salts of their corresponding complexes,  $[\text{Pt}(4'\text{-}o\text{MePh-pzbipy})\text{Cl}]^+$  and  $[\text{Pt}(4'\text{-}o\text{CF}_3\text{Ph-pzbipy})\text{Cl}]^+$  are reported in this chapter. Of particular interest are the solid state photophysical properties of these salts. To this end the three non-coordinating counterions, hexafluoroantimonate, tetrafluoroborate and triflate, have been used in the hope of improving our chances of growing single crystals suitable for X-ray diffraction experiments.



Although no single crystals have been grown, it is shown that the incorporation of a pyrazine ring has a profound effect on the solid state emission of the complexes.

We finally note that an early study of the energy levels of bipyrazine and bipyridine found that the former ligand has a more accessible  $\pi^*$ -orbital than the latter ligand<sup>179</sup> and is therefore expected to be a better  $\pi$ -acceptor. If this applies to our systems, the effect could have favourable consequences for extended metal-metal interactions in the solid state. A good  $\pi$ -acceptor would reduce the electron density on the metal centre, thereby promoting close metal-metal contacts as the intermetallic repulsions are reduced. In addition the weaker  $\sigma$ -donor strength of pyrazine compared to pyridine is likely to promote stronger Pt...Pt interactions in the solid state. Lippert and coworkers have studied a range of square-planar  $d^8$ - $d^8$  dimer complexes<sup>180</sup> and have undertaken a theoretical analysis of metal-metal bond orders using extended Hückel molecular orbital (EHMO) calculations.<sup>181 - 183</sup> This study has shown that weaker  $\sigma$ -donors increase residual  $s$ -orbital contributions on the metal, which in turn strengthens the platinum-platinum interactions in dimers of this kind.<sup>180</sup>

## **5.2 RESULTS AND DISCUSSION**

### **5.2.1 [Pt(4-Ph-pzbipy)Cl]BF<sub>4</sub> (12)**

**{where 4-Ph-pzbipy is 4-phenyl-6-(2''-pyrazinyl)-2,2'-bipyridine}**

#### **5.2.1.1 Synthesis and characterisation of [Pt(4-Ph-pzbipy)Cl]BF<sub>4</sub> (12)**

Before attempting the coordination of the pyrazinyl-bipyridyl ligand (4-Ph-pzbipy) to platinum(II) it was necessary to take into account the weaker  $\sigma$ -donor strength of pyrazine compared to that of pyridine.<sup>117</sup> As there was no precedent for the coordination of a pyrazinyl-bipyridine binding domain to platinum(II) it was decided to attempt the method developed previously in our laboratories<sup>53, 111, 184</sup> (and described in Chapter 3 of this work) for the coordination of terpyridyl ligands to platinum(II). Fortunately this approach was successful at the first attempt and was implemented throughout, although yields are noticeably reduced compared to the similar procedure using a terpyridyl ligand. (A more favourable method

would probably be one using  $[\text{Pt}(1,5\text{-COD})\text{I}_2]$  as a starting material in a facile approach to platinum coordination employed by Lowe and Vilaivan.<sup>68)</sup>

The neutral platinum(II) complex  $[\text{Pt}(\text{PhCN})_2\text{Cl}_2]$  is refluxed overnight in acetonitrile in the presence of one equivalent of silver tetrafluoroborate resulting in the precipitation of creamy white silver chloride from the colourless solution. The precipitate is filtered off, the filtrate added to an equimolar amount of the ligand 4-Ph-pzbipy and the mixture again refluxed overnight. The solid precipitates from the solution as an analytically pure and air stable yellow powder. Further precipitation is induced by removal of the solvent under reduced pressure before the precipitate is filtered and washed on the frit with copious quantities of diethyl ether followed by smaller amounts of acetonitrile. Final purification is by recrystallisation from a boiling acetonitrile solution. The yield of 48 % is less than the 75 % obtained for the analogous terpyridyl complex.<sup>53</sup>

An examination of the C, H and N content of the salt by elemental analysis is in agreement with the proposed formulation. A proton NMR spectrum was recorded in deuterated dimethylsulfoxide ( $\text{DMSO-d}_6$ ) which was interpreted with the assistance of an absolute value correlation spectroscopy (COSY) experiment and by comparison with the  $^1\text{H}$  NMR spectrum of the free ligand (see Chapter 2). A complete listing of the proton NMR signals is provided in the experimental section of this chapter. The  $\text{H}^{3''}$ ,  $\text{H}^{5''}$  and  $\text{H}^{6''}$  protons of the pyrazine ring are the most deshielded and hence occur furthest downfield at  $\delta$  9.92, 8.76 and 9.10 respectively. The inclusion of a pyrazine ring introduces asymmetry in the luminophore compared to the terpyridyl case and as a result the protons of the central pyridine ring are no longer equivalent and occur as separate finely split doublets at  $\delta$  9.02 and  $\delta$  8.92. Of the protons on the outer pyridine ring  $\text{H}^{3'}$  and  $\text{H}^{6'}$  are most deshielded and produce a signal furthest downfield at  $\delta$  8.70 and  $\delta$  8.66 respectively. The resonance of  $\text{H}^{4'}$  is at  $\delta$  8.44 and that of  $\text{H}^{5'}$  at  $\delta$  7.82. Remaining resonances can be assigned to the protons of the phenyl ring.

An IR spectrum of the salt was recorded in the solid state from a KBr pellet and the salient peaks are tabulated at the end of this chapter (Table 5.7).

Attempts to grow single crystals by slow cooling and slow evaporation of an acetonitrile solution of the complexes were unsuccessful, as were attempts to grow crystals by the slow diffusion of diethyl ether into an acetonitrile solution of the complex.

### 5.2.1.2 Photophysical properties of [Pt(4-Ph-pzbipy)Cl]BF<sub>4</sub> (**12**)

#### *Fluid solution absorption spectroscopy*

Absorption spectra of the [Pt(4-Ph-pzbipy)Cl]<sup>+</sup> chromophore were recorded at room temperature in deoxygenated acetonitrile and dichloromethane. The spectrum in acetonitrile is presented in Figure 5.1 and the pertinent data from both media are summarised in Table 5.8 at the end of this chapter.

The absorption profile can be considered as consisting of two regions. In acetonitrile the first region, at wavelengths shorter than 370 nm, consists of a pair of intense absorptions at 262 and 284 nm, and in the second of a vibrationally structured band between 300 and 350 nm. The intense absorptions at high energy correspond to the most prominent bands of the free ligand. The vibrational spacing of the structured band between 300 and 350 nm is ~ 1200 - 1600 cm<sup>-1</sup>. At lower energy there is a moderately intense structured band with its maximum intensity at 404 nm and a shoulder at 384 nm. These latter bands experience a marked shift to lower energy in the less polar dichloromethane.

This absorption behaviour and the absorption energies are practically identical to those of the closely related terpyridyl analogue, [Pt(4'-phenyl-terpy)Cl]<sup>+</sup>.<sup>32, 42, 53</sup> Assignment of the absorption origin therefore follows that made by the authors of this preceding work. Bands at high energy (between 370 and 250 nm) are assigned to transitions localized to the ligand, in particular the bands between 280 and 250 nm are assigned to <sup>1</sup>(π - π\*) absorptions. The less intense bands at lower energy (at wavelengths longer than 375 nm) are assigned to spin-allowed metal-to-ligand charge transfer transitions. Both Campagna *et al.*<sup>42</sup> and Field, McMillin and coworkers<sup>53</sup> base their assignments on measurements made on the [Pt(terpy)Cl]<sup>+</sup> luminophore.<sup>27-29</sup> The higher energy bands are assigned partly by comparison with spectra recorded of the free ligand. A vibrational spacing in the 300 - 350 nm region, of between 1200

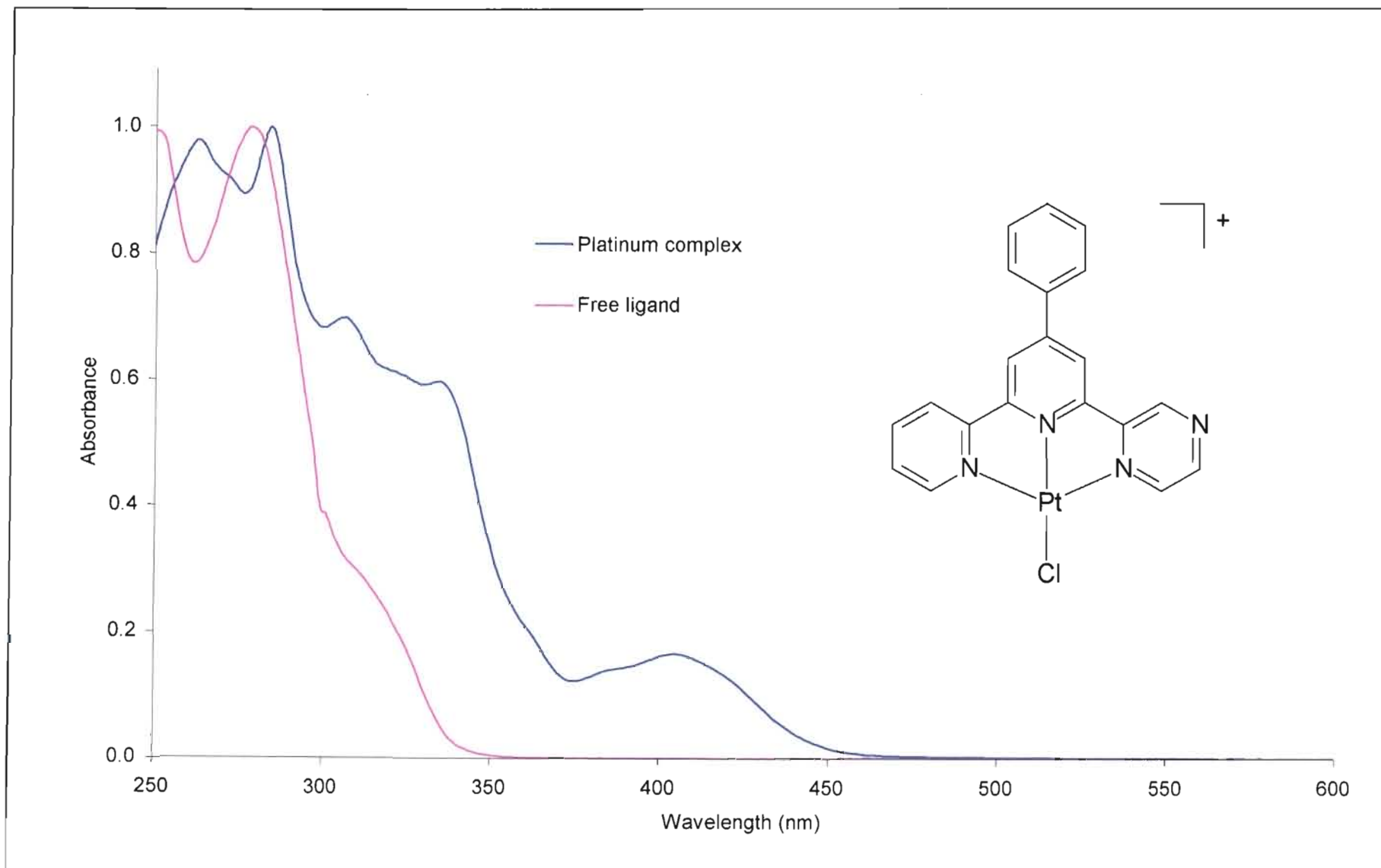


**Figure 5.1** Acetonitrile solution absorption spectra of the  $[Pt(4-Ph-pzbipy)Cl]^+$  and 4-Ph-pzbipy chromophores recorded at 298 K.

and  $1600\text{ cm}^{-1}$ , is indicative of vibrational stretches associated with the conjugated heterocyclic ligand. The charge transfer transitions at lower energy were assigned based on the energy and intensity of the bands and by comparison with the absorption regime of the free ligand. The free 4'-phenyl-terpyridyl ligand, and indeed the ligand 4-Ph-pzbipy, lack absorbances in the visible spectrum at which the MLCT bands occur, indicating an obvious metal involvement in the absorption origin. The energy of the absorptions fall comfortably into the manifold of charge transfer and certain ligand field (LF) bands. The LF and ligand-to-metal charge transfer (LMCT) transitions can be excluded based on the intensity of the absorptions. In any event, LMCT transitions are unlikely, as this would involve the reduction of the metal centre, already in a stable low oxidation state. In conclusion we assign the low energy transitions as MLCT transitions. Campagna and coworkers point out that low energy transitions of this type are a feature of platinum(II) - polypyridine complexes.<sup>42</sup>

The relative energies of the terpyridyl and pyrazinyl-bipyridyl complexes in acetonitrile and in dichloromethane have been summarised in Table 5.1.

**Table 5.1** Comparison of MLCT absorption energies for  $[\text{Pt}(4'\text{-Ph-terpy})\text{Cl}]^+$  and  $[\text{Pt}(4\text{-Ph-pzbipy})\text{Cl}]^+$  recorded in room temperature fluid solution.

Complex	Solvent	
	Acetonitrile	Dichloromethane
$[\text{Pt}(4'\text{-Ph-terpy})\text{Cl}]^{+ 32}$	402 (5200 <sup>a</sup> ), 380sh	412, 397sh
$[\text{Pt}(4\text{-Ph-pzbipy})\text{Cl}]^+$	404 (5700a), 384sh	417, 392sh

(a) Molar absorptivity ( $\text{M}^{-1}\cdot\text{cm}^{-1}$ ).  
sh = shoulder.

The MLCT absorption energies of the terpyridyl and phenyl-bipyrazinyl are essentially the same in both acetonitrile and in dichloromethane. No significant stabilisation in energy due to the presence of the pyrazine ring is observed. Possible reasons for this are discussed in the conclusions section of this chapter (*vide infra*).

### *Fluid solution emission spectroscopy*

Emission spectra of the  $[\text{Pt}(4\text{-Ph-pzbipy})\text{Cl}]^+$  luminophore were recorded in deoxygenated acetonitrile and dichloromethane solutions at room temperature. Although non-emissive in deoxygenated acetonitrile, emission in a  $20\ \mu\text{M}$  dichloromethane solution is observed, in particular in a band that peaks in intensity at 550 nm and that has a shoulder at *ca.* 580 nm. (See Figure 5.2) The emission lifetime has been measured at 96 ns in this medium. An excitation spectrum was recorded that shows a low energy band centred at 420 nm. This band corresponds to the lowest energy absorption band recorded in the same medium and confirms that emission is from a single species.

The concentration of the solution was intentionally kept relatively low ( $20\ \mu\text{M}$ ) in order to ensure emission from an essentially monomeric species. (In any event, the limiting solubility of  $[\text{Pt}(4\text{-Ph-pzbipy})\text{Cl}]^+$  in dichloromethane is below  $50\ \mu\text{M}$ .) The structure shown in the emission profile (albeit poorly resolved) suggests ligand centred character in the emitting state, although the vibrational spacing of  $1100\ \text{cm}^{-1}$  is somewhat less than values of  $1200 - 1400\ \text{cm}^{-1}$  that one would typically expect of a ligand centred emission. In addition an excited state with strong ligand character (either in the form of  $\pi\text{-}\pi^*$  or ILCT transitions) normally emits with a much longer-lived excited state. Moreover, the energy of the band is too low for a purely ligand centred emission since organic, aromatic ligands of this nature emit at higher energies. The most likely emission source reduces to a state with strong MLCT character. The marked solvent sensitivity of emission from  $[\text{Pt}(4\text{-Ph-pzbipy})\text{Cl}]^+$  is further evidence for a MLCT state since an excitation of this type is known to be susceptible to solvent induced exciplex quenching in the presence of a Lewis base.<sup>48</sup> Also typical of a charge transfer state is the lowest energy absorption band that occurs at higher energies when dissolved in a more polar solvent (404 nm in acetonitrile and 417 nm in dichloromethane). It is likely that the excited state is configurationally mixed, given the observations made in a rigid glassy medium (*vide infra*) and that  $\pi\text{-}\pi^*$  transitions also play a role, but is clear that any such contribution is overshadowed by the strong MLCT character of the excited state.

These observations are consistent with deductions made by Field, McMillin *et al.* in their study of emission from the closely related terpyridyl analogue,  $[\text{Pt}(4'\text{-Ph-terpy})\text{Cl}]^+$ .<sup>32</sup> The latter

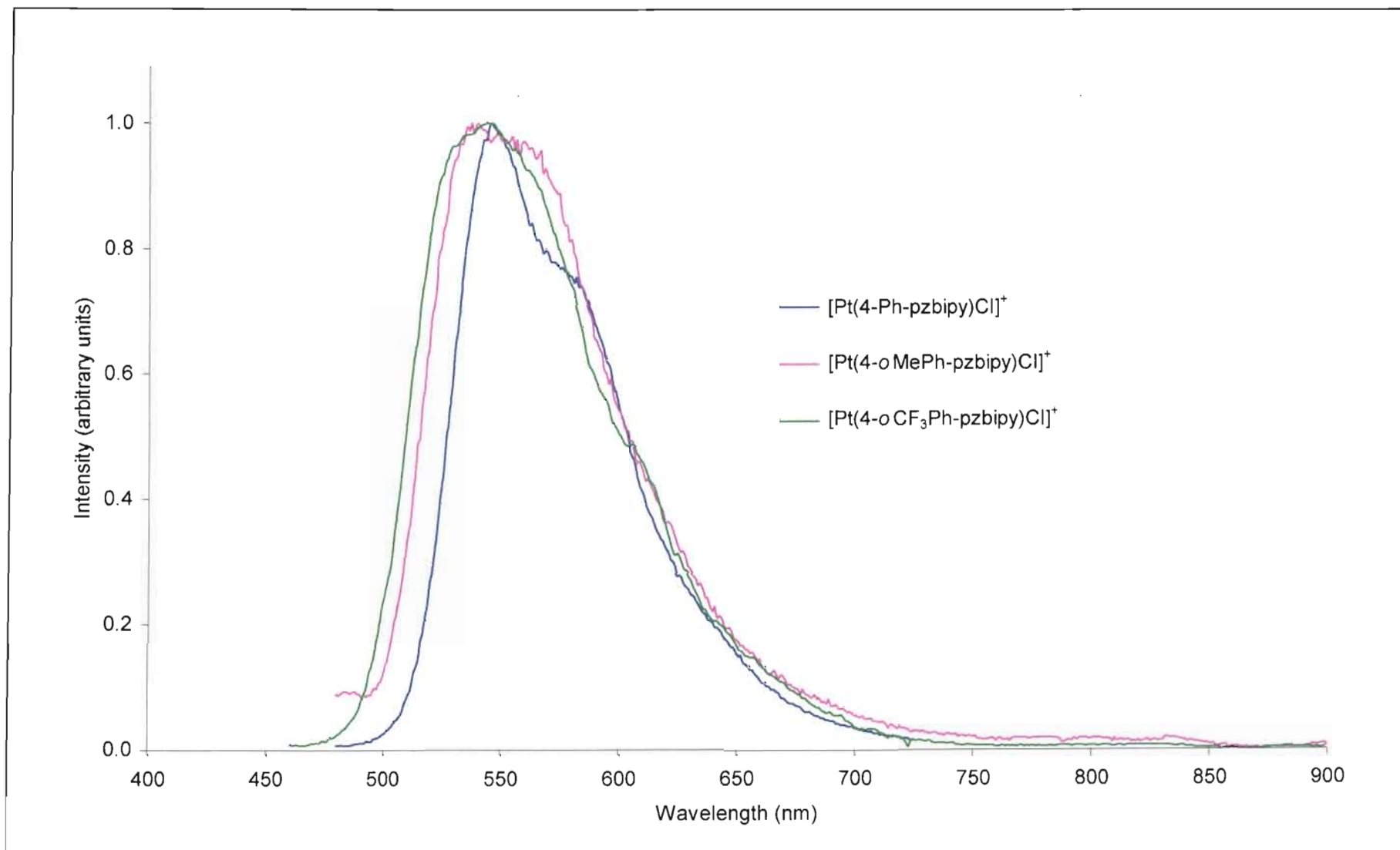


**Figure 5.2** Dichloromethane solution emission spectra of the  $[Pt(4-R-pzbipy)Cl]^+$  luminophores recorded at 298 K. ( $R = Ph, oMePh, oCF_3Ph$ )

luminophore emits in a weakly structured band in acetonitrile, the emission being sensitive to the presence of a coordinating solvent and as a result the excited state assignment agrees with that made here for  $[\text{Pt}(4\text{-Ph-pzbipy})\text{Cl}]^+$ , *viz.* an excited state with dominant MLCT character. However, emission is at a slightly higher energy (0-0 transition at 535 nm) and the lifetime (at 85 ns) is a little shorter than that for the pyrazinyl-bipyridyl derivative. The slight reduction in energy brought about by exchanging terpyridine for pyrazinyl-bipyridine indicates a narrowing of the HOMO-LUMO energy gap. We suggest that this is due to a stabilisation of the ligand centred  $\pi^*$ -LUMO brought about by the better  $\pi$ -acceptor ability of pyrazinyl-bipyridyl ligand compared to the terpyridyl ligand.<sup>117, 179</sup>

#### *Glass emission spectroscopy*

Emission was also recorded in a rigid glassy medium. The glassy solution of choice consisted of a 1:5:5 (v/v) DMF/EtOH/MeOH (DME) solvent mixture due to the favourable solubility of the complex above that in butyronitrile. Emission is in a vibrationally structured band (progressions 1200 - 1400  $\text{cm}^{-1}$ ) with a 0-0 transition at 516 nm, a subsequent band peaking at 556 nm and a lower intensity shoulder at 592 nm (see Figure 5.3). The lifetime of this emission is *ca.* 15  $\mu\text{s}$ .

The same deductions are made as for emission from deoxygenated dichloromethane solution at ambient temperatures. Since we are again investigating emission from the monomer we expect our conclusions for emission from the rigid glass to be no different to those made for emission in dichloromethane solution. The enhanced structure and the slight shift to higher energies are attributed to the change in temperature. It may be possible that the admixture of states making up the excited state is slightly altered and now has a more enhanced ligand centred character. We base this statement on the vibrational spacing which corresponds with ligand stretching frequencies and also the significantly longer-lived excited state, both factors indicative of a ligand centred contribution to the excited state.

For comparison purposes the glass emission exhibited by the terpyridyl analogue,  $[\text{Pt}(4'\text{-Ph-terpy})\text{Cl}]^+$  which has been studied by various authors<sup>32, 42, 53</sup> is now described. Michalec *et al.* report an emission spectrum recorded in a low temperature glass that shows progressions



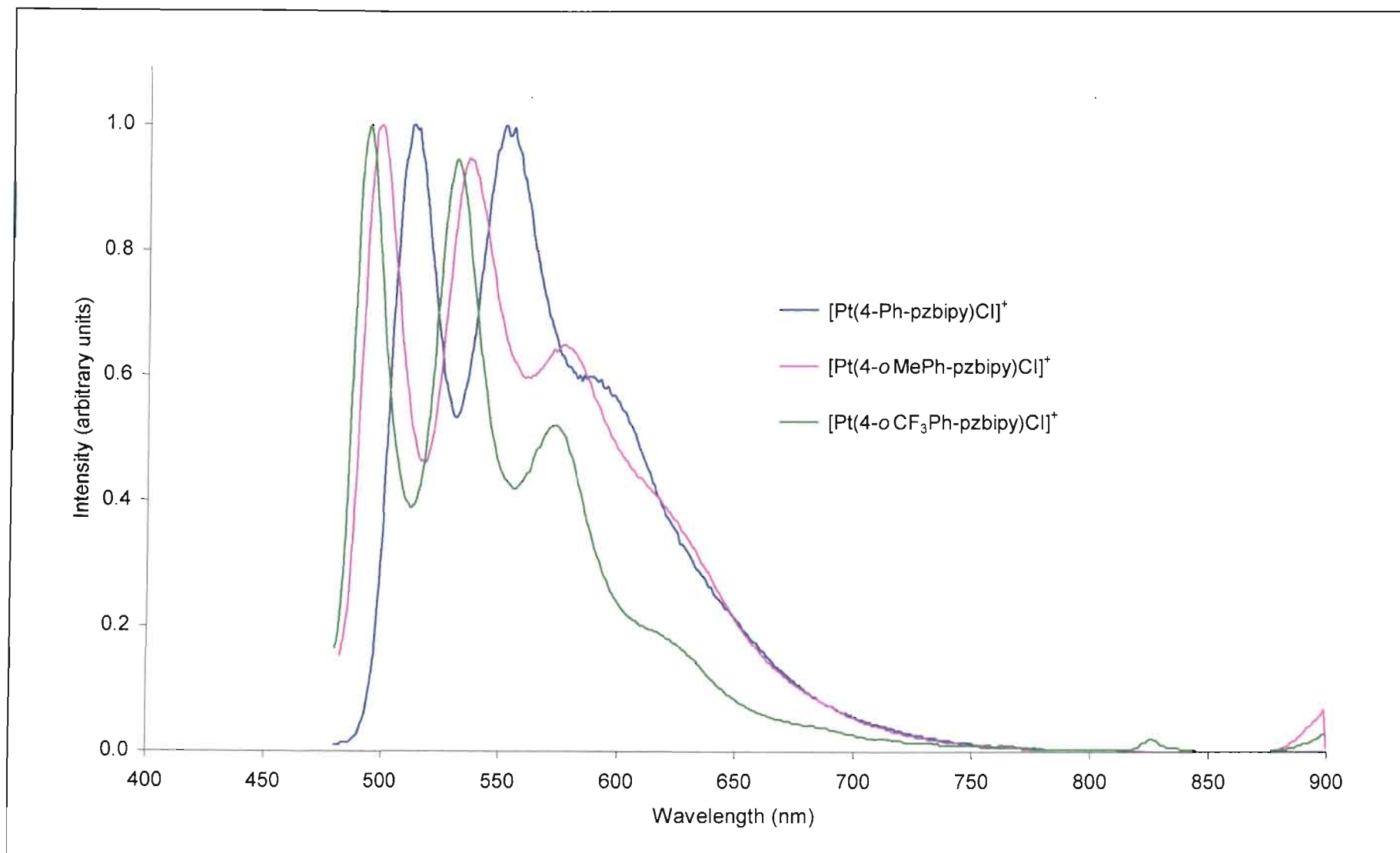


**Figure 5.3** Solution emission spectra of the  $[Pt(4-R-pzbipy)Cl]^+$  luminophores recorded in a 20  $\mu M$  DME rigid glass at 77 K. ( $R = Ph, oMePh, oCF_3Ph$ )

occurring at 503, 540 and 582 nm, with the most intense band at highest energy.<sup>32</sup> Campagna and coworkers report an emission lifetime of 15  $\mu\text{s}$  for  $[\text{Pt}(4'\text{-Ph-terpy})\text{Cl}]^+$  but in a different rigid glassy medium {viz. 4:1 (v/v) methanol/ethanol mixture (M/E)} at 77 K.<sup>42</sup> (A complete description of the photophysical properties of  $[\text{Pt}(4'\text{-Ph-terpy})\text{Cl}]^+$  recorded to date is provided in section 1.2.1.1 of chapter 1.) The authors argue for an excited state that is largely MLCT in character but do not discount a contribution from a ligand based  $\pi\text{-}\pi^*$  excitation. They note, for example, that a purely ligand-based emission would have a lifetime longer than the 15  $\mu\text{s}$  actually recorded. The similarities in the glass emission spectra recorded for  $[\text{Pt}(4'\text{-Ph-terpy})\text{Cl}]^+$  and  $[\text{Pt}(4\text{-Ph-pzbipy})\text{Cl}]^+$  suggests that in both cases the emission is from an excited state that is largely  $^3\text{MLCT}$  but probably also contains some  $^3\text{IL}$  ( $\pi\text{-}\pi^*$ ) character. As for the fluid solution emission displayed by these two complexes, emission by the pyrazinyl-bipyridyl derivative occurs at slightly lower energies, presumably for the same reason: the pyrazinyl-bipyridine is a better  $\pi$ -acceptor than the terpy ligand.<sup>117, 179</sup> It is interesting to note that the glass emission for both  $[\text{Pt}(4'\text{-Ph-terpy})\text{Cl}]^+$  and  $[\text{Pt}(4\text{-Ph-pzbipy})\text{Cl}]^+$  occurs at a higher energy and is more structured than that observed in a fluid solution such as dichloromethane.

### **5.2.2 [Pt(4-Ph-pybipz)Cl]SbF<sub>6</sub> (13)**

**{where 4-Ph-pybipz is 4-phenyl-2,6-bis(2'-pyrazinyl)-pyridine}**

#### **5.2.2.1 Synthesis and characterisation of [Pt(4-Ph-pybipz)Cl]SbF<sub>6</sub> (13)**

Attempts to synthesise the dipyrazinyl platinum complex,  $[\text{Pt}(4\text{-Ph-pybipz})\text{Cl}]\text{SbF}_6$  (**13**), by the method used previously in this chapter for the coordination of the pyrazinyl-bipyridine ligands 4-Ph-pzbipy, 4-*o*MePh-pzbipy and 4-*o*CF<sub>3</sub>Ph-pzbipy proved fruitless. The neutral platinum complex  $[\text{Pt}(\text{PhCN})_2\text{Cl}_2]$  was used as starting material for the coordination of ligand 4-Ph-pybipz to platinum(II). What was noticeable in the coordination reactions of the three pyrazinyl-bipyridines was the conspicuously lower yields compared to the similar reaction with terpyridyl ligands. This effect is presumably due to the weaker  $\sigma$ -donor strength of pyrazine relative to pyridine, making it more difficult for the pyrazine to displace the existing ligands on the platinum. In the case of ligand 4-Ph-pybipz this phenomenon would be even more pronounced as two pyrazine rings have to coordinate to the central metal atom; possibly

the ligand is unable to coordinate at all, at least under the conditions employed here. In support of such a conclusion, a proton NMR spectrum shows evidence of uncoordinated ligand recovered from the reaction mixture. Clearly a different synthetic method is required with a platinum starting material in which the metal atom bears ligands that are more easily displaced by the weakly  $\sigma$ -donating ligands. Such a procedure is available in the work performed by Lowe and Vilaivan whereby  $[\text{Pt}(1,5\text{-COD})\text{I}_2]$  (1,5-COD is 1,5-cyclooctadiene) is utilised to provide facile coordination.<sup>68</sup> Cummings and coworkers have recently shown that it is also possible to achieve tridentate coordination of a weakly  $\sigma$ -donating ligand to platinum by the use of  $[\text{Pt}(\text{DMSO})\text{Cl}_2]$  (where DMSO is dimethylsulfoxide) as a starting material.<sup>50</sup> Unfortunately neither of these procedures were attempted with ligand 4-Ph-pybipz due to time constraints.

### **5.2.3 $[\text{Pt}(4\text{-}o\text{MePh-pzbipy})\text{Cl}]\text{X}$ [ $\text{X}^- = \text{SbF}_6^-$ (**14**), $\text{BF}_4^-$ (**15**), $\text{CF}_3\text{SO}_3^-$ (**16**)]**

**{where 4-*o*MePh-pzbipy is 4-(*o*-CH<sub>3</sub>-phenyl)-6-(2'-pyrazinyl)-2,2'-bipyridine}**

#### **5.2.3.1 Synthesis and characterisation of $[\text{Pt}(4\text{-}o\text{MePh-pzbipy})\text{Cl}]\text{X}$ [ $\text{X}^- = \text{SbF}_6^-$ (**14**), $\text{BF}_4^-$ (**15**), $\text{CF}_3\text{SO}_3^-$ (**16**)]**

The procedure followed in the synthesis of the three complex salts  $[\text{Pt}(4\text{-}o\text{MePh-pzbipy})\text{Cl}]\text{X}$  [ $\text{X}^- = \text{SbF}_6^-$  (**14**),  $\text{BF}_4^-$  (**15**),  $\text{CF}_3\text{SO}_3^-$  (**16**)] is identical to that employed in making the 4'-phenyl substituted complexes described in section 5.2.1.1. The hexafluoroantimonate (**14**), tetrafluoroborate (**15**) and triflate (**16**) salts were obtained as maroon, deep red and orange red solids respectively. Each salt was then recrystallised from a boiling acetonitrile solution that was allowed to cool slowly to room temperature. Attempts were made to grow single crystals by slowly cooling an acetonitrile solution of each complex and also by allowing an acetonitrile solution of the complexes to evaporate over a period of days. These methods did not yield single crystals of sufficient quality for X-ray diffraction studies. Neither did efforts to grow crystals by the slow diffusion of ether into an acetonitrile solution of the complex.

The empirical formulation of each of the three complexes as  $[\text{Pt}(\text{C}_{21}\text{H}_{16}\text{N}_4)\text{Cl}]\text{X}$  [ $\text{X}^- = \text{SbF}_6^-$  (**14**),  $\text{BF}_4^-$  (**15**),  $\text{CF}_3\text{SO}_3^-$  (**16**)] is confirmed by the elemental analysis for C, H and N (see the

experimental section, *viz.* section 5.4). A proton NMR spectrum of [Pt(4-*o*MePh-pzbipy)Cl]SbF<sub>6</sub> was recorded in DMSO-d<sub>6</sub> at room temperature. The spectra of the tetrafluoroborate and triflate salts are identical and need not be discussed separately. The spectra show a similar pattern of resonances as seen for [Pt(4-Ph-pzbipy)Cl]BF<sub>4</sub> (discussed in section 5.2.1.1) and the assignment of the peaks is again aided by COSY experiments and by comparison with assignments made for the free ligand. The signals occurring furthest downfield can be ascribed to the pyrazinyl proton resonances H<sup>3''</sup>, H<sup>5''</sup> and H<sup>6''</sup> at δ 9.89, 8.83 and 9.11 respectively. The inequality of the protons on the central pyridyl ring is borne out by separate signals from H<sup>3</sup> and H<sup>5</sup> at δ 8.85 and δ 8.79. Further upfield on the outer pyridyl ring, H<sup>3'</sup>, H<sup>4'</sup>, H<sup>5'</sup> and H<sup>6'</sup> produce signals at δ 8.71, 8.48, 7.85 and 8.76 respectively. The methyl protons in the *ortho*-position of the phenyl ring cause a prominent singlet far upfield at δ 2.45. Remaining peaks can be assigned to the protons of the phenyl ring. Again, a complete listing of the proton NMR resonances can be found in the experimental section (section 5.4) of this chapter.

An IR spectrum was recorded of each salt as a KBr pellet and the most prominent peaks are summarised in Table 5.7 at the end of this chapter. The spectra of the three salts are identical with the exception of prominent bands associated with stretches localised to each of the three counterions.

### 5.2.3.2 Photophysical properties of [Pt(4-*o*MePh-pzbipy)Cl]X [X<sup>-</sup> = SbF<sub>6</sub><sup>-</sup> (**14**), BF<sub>4</sub><sup>-</sup> (**15**), CF<sub>3</sub>SO<sub>3</sub><sup>-</sup> (**16**)]

#### *Fluid solution absorption spectroscopy*

The absorption spectra of [Pt(4-*o*MePh-pzbipy)Cl]SbF<sub>6</sub> (**14**), [Pt(4-*o*MePh-pzbipy)Cl]BF<sub>4</sub> (**15**) and [Pt(4-*o*MePh-pzbipy)Cl]CF<sub>3</sub>SO<sub>3</sub> (**16**) were recorded in acetonitrile and dichloromethane at room temperature. The absorptions of the three salts are unaffected by the nature of the counterion and therefore the absorption behaviour of the hexafluoroantimonate salt will form the basis of this discussion. The absorption characteristics are compiled in Table 5.8 at the end of this chapter and a spectrum of [Pt(4-*o*MePh-pzbipy)Cl]SbF<sub>6</sub> is reproduced in Figure 5.4.

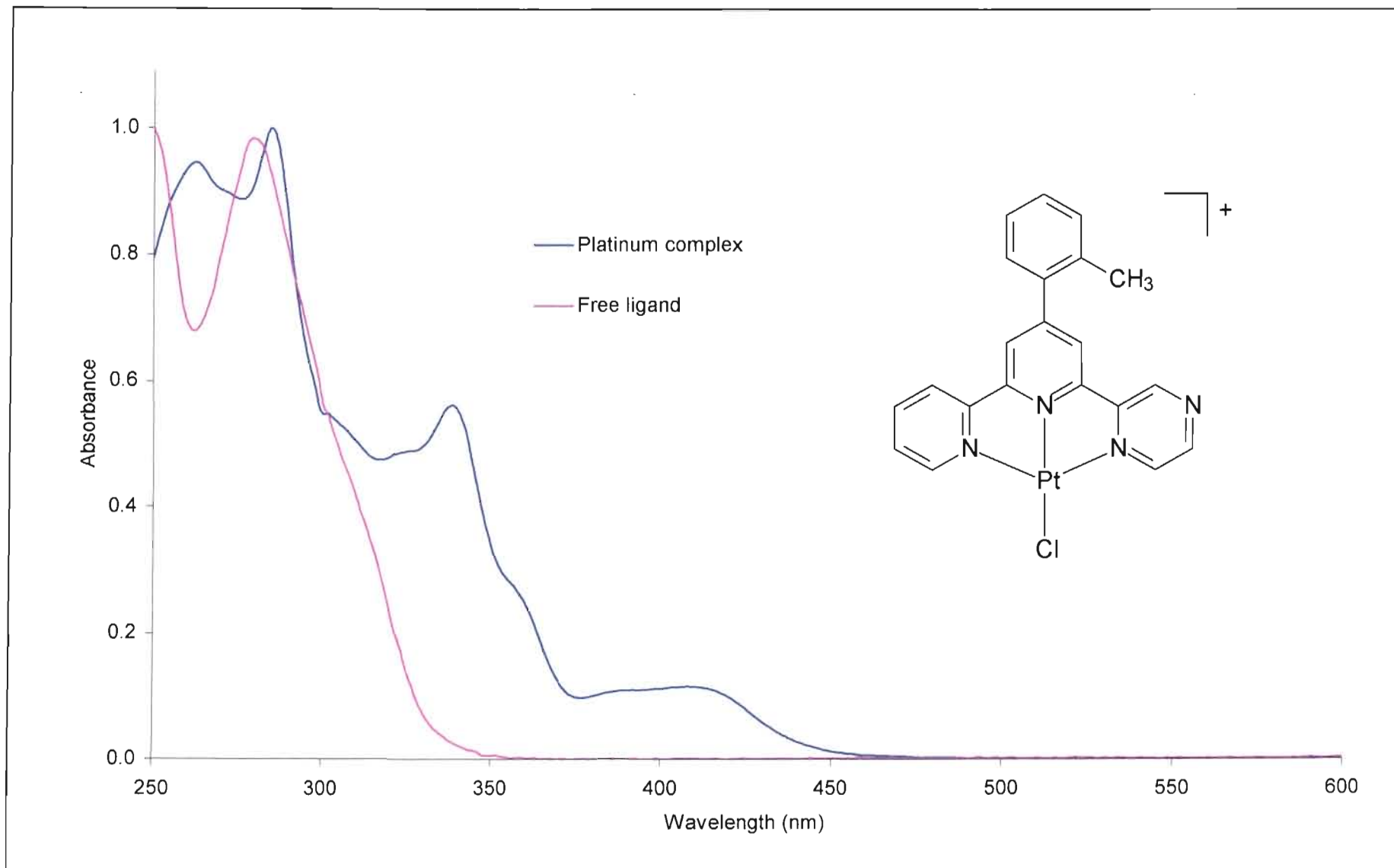


**Figure 5.4** Acetonitrile solution absorption spectra of the  $[Pt(4\text{-}o\text{MePh-pzbipy})Cl]^+$  and 4-*o*MePh-pzbipy chromophores recorded at 298 K.

At high energy the spectrum shows two intense absorptions at 262 and 285 nm. Between 290 and 375 nm there is a vibrationally structured band with a vibrational spacing of *ca.* 1200 - 1500 cm<sup>-1</sup>. Above 375 nm there is a broad, moderately intense band with a maximum at approximately 408 nm. A similar absorption regime is produced from a dichloromethane solution with the bands, in particular those above 375 nm, shifted to lower energy.

As expected, this absorption behaviour is almost identical to that of the analogous luminophore without a substituent in the *ortho*-phenyl position, *viz.*, [Pt(4-Ph-pzbipy)Cl]BF<sub>4</sub>. Assignment of the absorption bands is therefore no different. The intense high energy peak at 285 nm and the vibrationally structured band in the 290 - 375 nm region are assigned to <sup>1</sup>( $\pi$ - $\pi^*$ ) transitions localised to the conjugated ligand. The broad, low energy band above 375 nm is assigned to charge transfer transitions and in particular MLCT transitions.

The energies of these MLCT absorptions in both acetonitrile and in dichloromethane are compared with those of the terpyridyl complexes which have been synthesised previously (see Table 5.2). In addition the MLCT absorption energies for complexes without a methyl substituent in the *ortho*-position of the phenyl ring are also included in this table.

**Table 5.2** Comparison of MLCT absorption energies recorded in room temperature fluid solution.

R-group	[Pt(4'-R-terpy)Cl] <sup>+</sup>		[Pt(4-R-pzbipy)Cl] <sup>+</sup>	
	Solvent		Solvent	
	Acetonitrile	CH <sub>2</sub> Cl <sub>2</sub>	Acetonitrile	CH <sub>2</sub> Cl <sub>2</sub>
phenyl	402 (5200 <sup>a</sup> )	412	404 (5700 <sup>a</sup> )	417
	380sh <sup>32</sup>	397sh <sup>32</sup>	384sh	392sh
<i>ortho</i> -CH <sub>3</sub> -phenyl	399 (4500 <sup>a</sup> )	no data	408 (3600 <sup>a</sup> )	426
	380 <sup>54</sup>	reported <sup>54</sup>	387sh	395sh

(a) Molar absorptivity (M<sup>-1</sup>.cm<sup>-1</sup>).  
sh = shoulder.

The MLCT absorption bands of  $[\text{Pt}(4\text{-}o\text{MePh-pzbipy})\text{Cl}]^+$  occur at 408 nm while those of  $[\text{Pt}(4'\text{-}o\text{MePh-terpy})\text{Cl}]^+$  is recorded at 399 nm.<sup>54</sup> Thus changing the metal-ligand binding domain from terpyridyl to pyrazinyl-bipyridyl has the effect of stabilising the absorption energy of the chromophore, an effect not observed when there is no methyl substituent on the phenyl ring (see Table 5.2). Presumably the effect of the more strongly  $\pi$ -accepting pyrazinyl-bipyridyl ligand is more pronounced for the methyl substituted complexes. Why this should be the case is unclear, but the effect may be related to the non-planarity of the ligand when the terminal phenyl ring is *ortho*-methyl substituted. We note that when the group in the 4-position is phenyl, more extensive electron delocalisation can be achieved. This extensive delocalisation may dilute any stabilisation associated with the presence of a more strongly  $\pi$ -accepting pyrazine ring.

#### *Fluid solution emission spectroscopy*

Room temperature solution spectra of all three complexes  $[\text{Pt}(4\text{-}o\text{MePh-pzbipy})\text{Cl}]\text{SbF}_6$ ,  $[\text{Pt}(4\text{-}o\text{MePh-pzbipy})\text{Cl}]\text{BF}_4$  and  $[\text{Pt}(4\text{-}o\text{MePh-pzbipy})\text{Cl}]\text{CF}_3\text{SO}_3$  were recorded in deoxygenated acetonitrile and dichloromethane. Complexes with a coordinated pyrazine ring are less soluble in the two solvents used here than their pyridine ring coordinated analogues. This effect is especially pronounced in the less polar dichloromethane. No emission was detected from the acetonitrile solution and the low solubility would have contributed to the difficulty in observing emission. In addition, the existence of a close-lying thermally activated excited states are known to lead to efficient radiationless decay *via* molecular distortion. In particular, metal-centred d-d excited states are susceptible to distortions<sup>35</sup> capable of such deactivation.<sup>36</sup> Alternatively the existence of a MLCT excited state could increase the oxidation state of the platinum centre and encourage solvent coordination at the metal, thereby deactivating the excited state.<sup>48</sup>

Emission of  $[\text{Pt}(4\text{-}o\text{MePh-pzbipy})\text{Cl}]^+$  was however recorded in deoxygenated dichloromethane (Figure 5.2) for the triflate salt as a band with  $\lambda_{\text{em}}(\text{max})$  at 543 nm. (Emission from the other two complexes,  $[\text{Pt}(4\text{-}o\text{MePh-pzbipy})\text{Cl}]\text{BF}_4$ , and  $[\text{Pt}(4\text{-}o\text{MePh-pzbipy})\text{Cl}]\text{CF}_3\text{SO}_3$  is identical and does not require separate descriptions.) This emission has a lifetime of 20 ns.

As expected, the emission features of  $[\text{Pt}(4\text{-}o\text{MePh-pzbipy})\text{Cl}]^+$  (including emission profile and energy) are very similar to that of  $[\text{Pt}(4\text{-Ph-pzbipy})\text{Cl}]^+$  although the weak vibrational structure observed in the emission spectrum of  $[\text{Pt}(4\text{-Ph-pzbipy})\text{Cl}]^+$  is absent from the emission profile of  $[\text{Pt}(4\text{-}o\text{MePh-pzbipy})\text{Cl}]^+$ . Based on these similarities, assignment of the excited state parallels that made in the previous section for  $[\text{Pt}(4\text{-Ph-pzbipy})\text{Cl}]^+$  and emission of  $[\text{Pt}(4\text{-}o\text{MePh-pzbipy})\text{Cl}]^+$  in deoxygenated dichloromethane solution is assigned to a configurationally mixed state consisting of  ${}^3\text{IL}(\pi\text{-}\pi^*)$  and  ${}^3\text{MLCT}$  transitions. Consistent with the presence of a MLCT contribution is that emission quenching takes place in acetonitrile, which is a coordinating solvent.<sup>48</sup> The emission lifetime of 20 ns recorded for  $[\text{Pt}(4\text{-}o\text{MePh-pzbipy})\text{Cl}]^+$  is far shorter than that of 100 ns measured for  $[\text{Pt}(4\text{-Ph-pzbipy})\text{Cl}]^+$ . Exactly why is uncertain, but the out-of-plane twisting of *o*MePh group in  $[\text{Pt}(4\text{-}o\text{MePh-pzbipy})\text{Cl}]^+$  will render the cation distinctly non-planar<sup>54</sup>, with the result that the contribution of the  $\pi\text{-}\pi^*$  component to the emitting state will be reduced. It is well established that reduction of the  $\pi\text{-}\pi^*$  component in an excited state reduces its lifetime.<sup>42, 43</sup>

#### *Glass emission spectroscopy*

Emission from  $[\text{Pt}(4\text{-}o\text{MePh-pzbipy})\text{Cl}]^+$  was also recorded as a 20  $\mu\text{M}$  DME solution at 77 K. Emission is reproduced in Figure 5.3 and consists of a highly structured band with 0-0 transition at 501 nm. Additional progressions occur to lower energy at 539, 580 and 620 (sh) nm, spaced approximately 1400  $\text{cm}^{-1}$  apart. As was the case in fluid solution, the emission profile and energy is very similar to that of  $[\text{Pt}(4\text{-Ph-pzbipy})\text{Cl}]^+$ . The emission has a lifetime of almost 11  $\mu\text{s}$ , which is somewhat shorter-lived than that of  $[\text{Pt}(4\text{-Ph-pzbipy})\text{Cl}]^+$  which is *ca.* 15  $\mu\text{s}$ .

Emission in such a highly structured band with vibrational progressions spaced 1400  $\text{cm}^{-1}$  apart is an immediate indication of a strong ligand centred character to the excited state. The vibrational spacing is characteristic of ligand stretching frequencies associated with C=C and C=N bonds. In addition the high energy of the 0-0 transition provides further justification for strong ligand character to the emitting state. Strong ligand centred character is moderated somewhat by an emission lifetime which Campagna and coworkers regard as significantly shorter than that of a “pure” ligand centred emitter.<sup>42, 43</sup> The most obvious reason for a reduced



radiative rate constant is coordination to platinum and hence it is possible that the excited state also incorporates metal character. Thus an excited state of mixed orbital parentage, made up of strong ligand character and also metal centred transition, is assigned to the monomeric emission in rigid glassy medium. Such an excited state coincides with the assignment made for the emitting state in room temperature dichloromethane solution and with that made for the emission from dilute glassy solution of  $[\text{Pt}(4\text{-Ph-pzbipy})\text{Cl}]^+$  (*vide supra*). The reasons for the shorter emission lifetime are the same as those proposed for the reduced emission lifetime in room temperature fluid solution.

#### *Solid state absorption and emission spectroscopy*

Solid state absorption and emission spectra of  $[\text{Pt}(4\text{-}o\text{MePh-pzbipy})\text{Cl}]\text{SbF}_6$  (**14**),  $[\text{Pt}(4\text{-}o\text{MePh-pzbipy})\text{Cl}]\text{BF}_4$  (**15**) and  $[\text{Pt}(4\text{-}o\text{MePh-pzbipy})\text{Cl}]\text{CF}_3\text{SO}_3$  (**16**) have been recorded. The complexes are maroon, deep red and orange red respectively. All three spectra share essential features and the solid state photophysical properties of the hexafluoroantimonate salt (**14**) will be discussed as representative of the photophysical properties of the other two salts.

As already noted, significant changes in the electronic structure of the isolated cation are not expected when the *ortho*-substituent of the 4-phenyl ring is changed from H to  $\text{CH}_3$ ; nor are significant changes observed. However, as previous work in our laboratories has shown, choosing the *ortho*-substituent can and usually does have a marked effect on the solid state structure of the salt.<sup>54</sup> Of particular interest here is whether  $[\text{Pt}(4\text{-}o\text{MePh-pzbipy})\text{Cl}]\text{SbF}_6$  has the same crystal structure and exhibits the same emission behaviour as its terpyridyl analogue  $[\text{Pt}(4'\text{-}o\text{MePh-terpy})\text{Cl}]\text{SbF}_6$ . The latter provides a rare example of a compound with a uniform chain structure that exhibits  $^3\text{MMLCT}$  emission and with an emission maximum that shifts markedly to the red on cooling.<sup>54</sup>

A solid state absorption spectrum of  $[\text{Pt}(4\text{-}o\text{MePh-pzbipy})\text{Cl}]\text{SbF}_6$  was recorded at room temperature and shows a prominent broad peak with maximum absorbance at roughly 575 nm  $\{[\text{Pt}(4\text{-}o\text{MePh-pzbipy})\text{Cl}]\text{BF}_4$  and  $[\text{Pt}(4\text{-}o\text{MePh-pzbipy})\text{Cl}]\text{CF}_3\text{SO}_3$  absorb at 550 and 540 nm respectively}. This is a significantly lower energy than the lowest energy band in the

absorption spectrum of  $[\text{Pt}(4\text{-}o\text{MePh-pzbipy})\text{Cl}]^+$  recorded in dilute solution with maximum at 408 nm. (Indeed the absorption is extraordinarily low and no reports of an absorption of lower energy from a similar platinum-polypyridyl complex could be found in the literature.) The latter absorption was assigned to charge transfer transitions localised to the monomer. Such a significant shift to lower energy indicates processes more than mere stabilisation brought about by a change of phase to the solid state. The low energy absorption in the solid state is most likely brought about by absorption from low energy molecular orbitals produced by aggregation.

Emission of  $[\text{Pt}(4\text{-}o\text{MePh-pzbipy})\text{Cl}]\text{SbF}_6$  (**14**) is depicted in Figure 5.5, and at room temperature consists of a narrow (fwhm  $\approx 1730\text{ cm}^{-1}$ ) structureless and asymmetric band with  $\lambda_{\text{em}}(\text{max})$  at 674 nm. At ambient temperature the emission lifetime is 80 ns. Reducing the temperature to 80 K results in a shift of the band maximum to 723 nm and a further reduction in the width of the band to a fwhm of *ca.*  $1200\text{ cm}^{-1}$ . The emission lifetime increases to 1.3  $\mu\text{s}$ . Emission behaviour of this type is typical of emission from a  $^3\text{MMLCT}$  excited state. In particular the red shift in emission energy as temperature is reduced is characteristic of emission from luminophores stacked with significant overlap of platinum  $d_{z^2}$ -orbitals on adjacent luminophores and where a temperature reduction typically leads to a systematic reduction in the Pt...Pt spacing.<sup>41, 44, 47, 53, 54</sup> Moreover a X-ray crystal structure exists of the terpyridyl analogue of  $[\text{Pt}(4\text{-}o\text{MePh-pzbipy})\text{Cl}]\text{SbF}_6$ , *viz.*  $[\text{Pt}(4'\text{-}o\text{MePh-terpy})\text{Cl}]\text{SbF}_6$  which indicates packing of luminophores in a stack which allows for significant overlap of metal orbitals on adjacent luminophores.<sup>54, 111</sup> The steric demands of  $[\text{Pt}(4\text{-}o\text{MePh-pzbipy})\text{Cl}]\text{SbF}_6$  should be identical and hence the solid state packing architecture should also be very similar. The terpy complex also emits with distinctive MMLCT emission behaviour, showing a red shift from 616 nm at room temperature to 673 nm at 80 K. The lower energy of emission from  $[\text{Pt}(4\text{-}o\text{MePh-pzbipy})\text{Cl}]\text{SbF}_6$  is attributed to the better  $\pi$ -acceptor and weaker  $\sigma$ -donor abilities of pyrazine. The stronger  $\pi$ -accepting strength is expected to lower the energy of the LUMO, which in the case of a MMLCT excitation is a  $\pi^*$ -orbital, thereby reducing the energy of the emission. The weaker  $\sigma$ -donating strength of pyrazine compared to pyridine is expected to function slightly differently. Lippert *et al.* have shown that intermetallic interactions between  $d^8$ - $d^8$  systems of this type are strengthened by the use of weaker  $\sigma$ -donating ligands

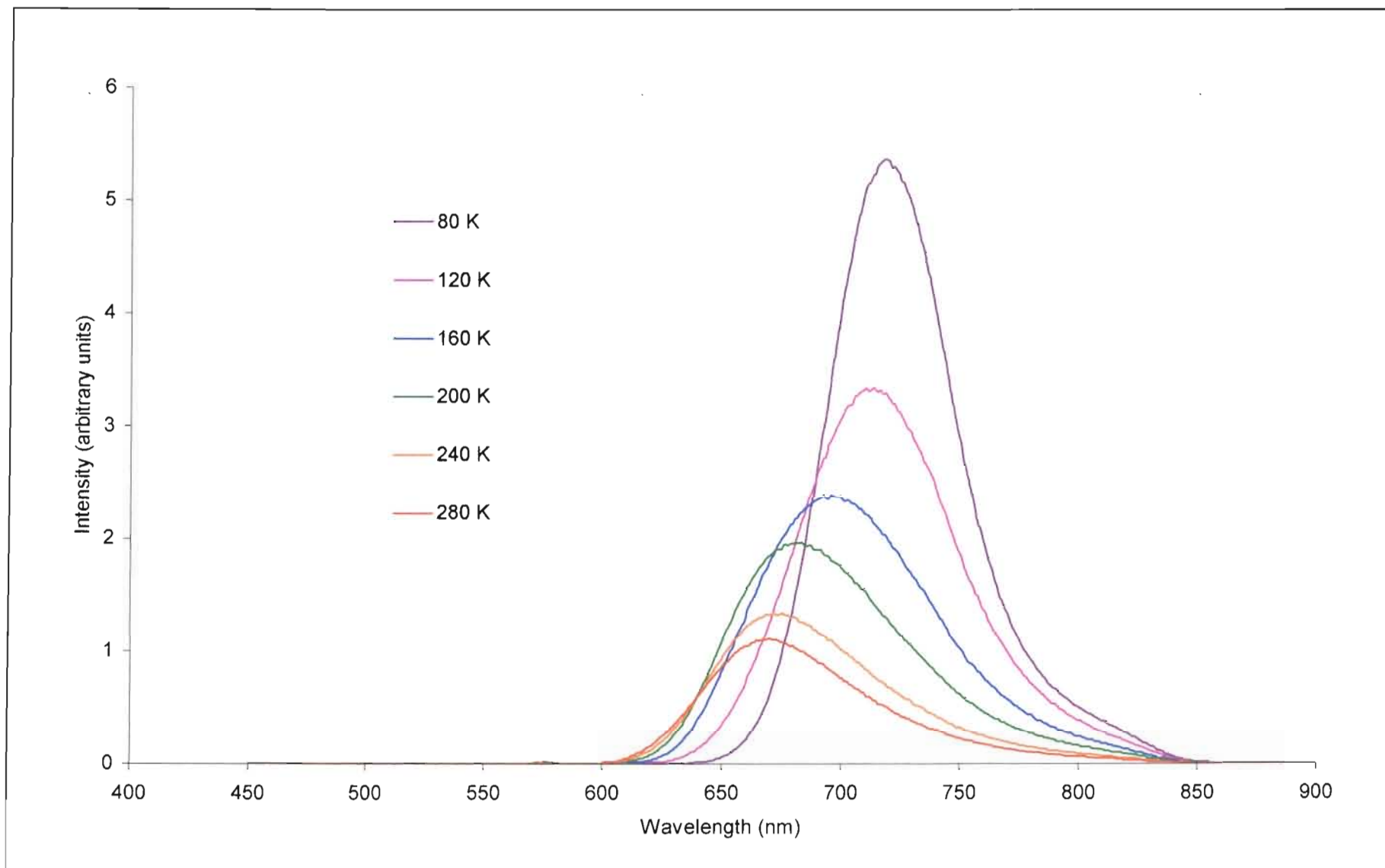


**Figure 5.5** Solid state emission spectra of  $[Pt(4\text{-oMePh-pzbipy})Cl]SbF_6$

surrounding the square-planar metal centre.<sup>180</sup> Improved intermetallic interactions would have the effect of reducing the HOMO-LUMO gap of a MMLCT state even further, thereby lowering the emission energy.

As mentioned before [Pt(4-*o*MePh-pzbipy)Cl]BF<sub>4</sub> and [Pt(4-*o*MePh-pzbipy)Cl]CF<sub>3</sub>SO<sub>3</sub> display essentially identical emission features and despite the obvious differences in the positions of the peak maxima, the essential features of the two salts [Pt(4-*o*MePh-pzbipy)Cl]BF<sub>4</sub> and [Pt(4-*o*MePh-pzbipy)Cl]CF<sub>3</sub>SO<sub>3</sub> are still consistent with the discussion of the emission origin for [Pt(4-*o*MePh-pzbipy)Cl]SbF<sub>6</sub>.

#### **5.2.4 [Pt(4-*o*CF<sub>3</sub>Ph-pzbipy)Cl]X [X<sup>-</sup> = SbF<sub>6</sub><sup>-</sup> (17), BF<sub>4</sub><sup>-</sup> (18), CF<sub>3</sub>SO<sub>3</sub><sup>-</sup> (19)]**

**{where 4-*o*CF<sub>3</sub>Ph-pzbipy is 4-(*o*-CF<sub>3</sub>-phenyl)-6-(2''-pyrazinyl)-2,2'-bipyridine}**

##### **5.2.4.1 Synthesis and characterisation of [Pt(4-*o*CF<sub>3</sub>Ph-pzbipy)Cl]X [X<sup>-</sup> = SbF<sub>6</sub><sup>-</sup> (17), BF<sub>4</sub><sup>-</sup> (18), CF<sub>3</sub>SO<sub>3</sub><sup>-</sup> (19)]**

The synthetic approach to the synthesis of the three salts [Pt(4-*o*CF<sub>3</sub>Ph-pzbipy)Cl]SbF<sub>6</sub> (17), [Pt(4-*o*CF<sub>3</sub>Ph-pzbipy)Cl]BF<sub>4</sub> (18) and [Pt(4-*o*CF<sub>3</sub>Ph-pzbipy)Cl]CF<sub>3</sub>SO<sub>3</sub> (19) is identical to the method used to synthesize the related complexes, derived from the [Pt(4-Ph-pzbipy)Cl]<sup>+</sup> and [Pt(4-*o*MePh-pzbipy)Cl]<sup>+</sup> cations, which is described in sections 5.2.1.1 and 5.2.3.1 of this chapter. The hexafluoroantimonate salt was isolated in two forms; as small, dark red crystalline needles and in an orange powdery form. It seems to be possible to crystallise each form selectively by the slow diffusion of diethyl ether into acetonitrile, with the red form crystallising from slightly more dilute solutions. The red form is thus constructed by less rapid precipitation suggesting that it forms in a thermodynamically more stable arrangement. The tetrafluoroborate salt on the other hand was only isolated as an orange powder while the triflate salt is red.

In all cases elemental analysis for C, H and N agreed with the proposed formulation of the salt. Proton NMR spectra were recorded in DMSO-*d*<sub>6</sub>, and interpretation was facilitated by comparison with the spectra of the free ligand and by performing a COSY experiment. The

protons of the pyrazine ring can be found at  $\delta$  9.84 ( $H^3$ ),  $\delta$  8.90 ( $H^5$ ) and  $\delta$  9.15 ( $H^6$ ). Singlets due to the  $H^3$  and  $H^5$  protons of the central pyridine ring occur at  $\delta$  8.81 and  $\delta$  8.88 respectively. Signals from the protons of the outer pyridine ring are obscured by near-lying peaks and their positions were determined by the COSY experiment and are at  $\delta$  8.85, 7.94, 8.48, and 8.65 for  $H^6$ ,  $H^5$ ,  $H^4$  and  $H^3$  respectively. An infrared spectrum was recorded for each of the complexes  $[Pt(4\text{-}oCF_3Ph\text{-}pz\text{bipy})Cl]SbF_6$ ,  $[Pt(4\text{-}oCF_3Ph\text{-}pz\text{bipy})Cl]BF_4$  and  $[Pt(4\text{-}oCF_3Ph\text{-}pz\text{bipy})Cl]CF_3SO_3$  as KBr pellets. The spectra for the complexes are essentially the same save for prominent peaks associated with the respective counterions. A list of the most prominent peaks is provided in Table 5.7 at the end of this chapter.

#### 5.2.4.2 Photophysical properties of $[Pt(4\text{-}oCF_3Ph\text{-}pz\text{bipy})Cl]X$ [ $X^- = SbF_6^-$ (17), $BF_4^-$ (18), $CF_3SO_3^-$ (19)]

##### *Fluid solution absorption spectroscopy*

UV/vis absorption spectra of both complexes were recorded at room temperature in acetonitrile and in dichloromethane. The absorbances in acetonitrile obey Beer's law indicating dissolution into monomeric ions. (The concentration dependence was not examined in dichloromethane.) Figure 5.6 will form the basis of this discussion and shows the spectrum of the tetrafluoroborate salt,  $[Pt(4\text{-}oCF_3Ph\text{-}pz\text{bipy})Cl]BF_4$ , in acetonitrile, which is no different from the absorption spectra of the other two salts of the same chromophore. Absorption data for these chromophores are condensed in Table 5.8 at the end of this chapter.

The absorption spectrum of the  $[Pt(4\text{-}oCF_3Ph\text{-}pz\text{bipy})Cl]^+$  chromophore consists of intense bands at high energy (wavelengths below 300 nm) with a pair of poorly resolved and moderately intense bands at 407 and 390 nm. Between these two sets of absorbances there is a vibrationally structured band with spacings of 1200 - 1400  $cm^{-1}$ . The magnitude of the spacing corresponds with the C=C and C=N stretching frequencies suggesting that the absorption bands have their origin in a ligand-centred transition, probably  $\pi\text{-}\pi^*$  transitions. By comparing the spectrum with that of the free ligand and considering the intensity and energy of the bands at wavelengths below 300 nm, we conclude that these absorptions also originate in electronic transitions localised to the ligand. The bands at 407 and 390 nm have

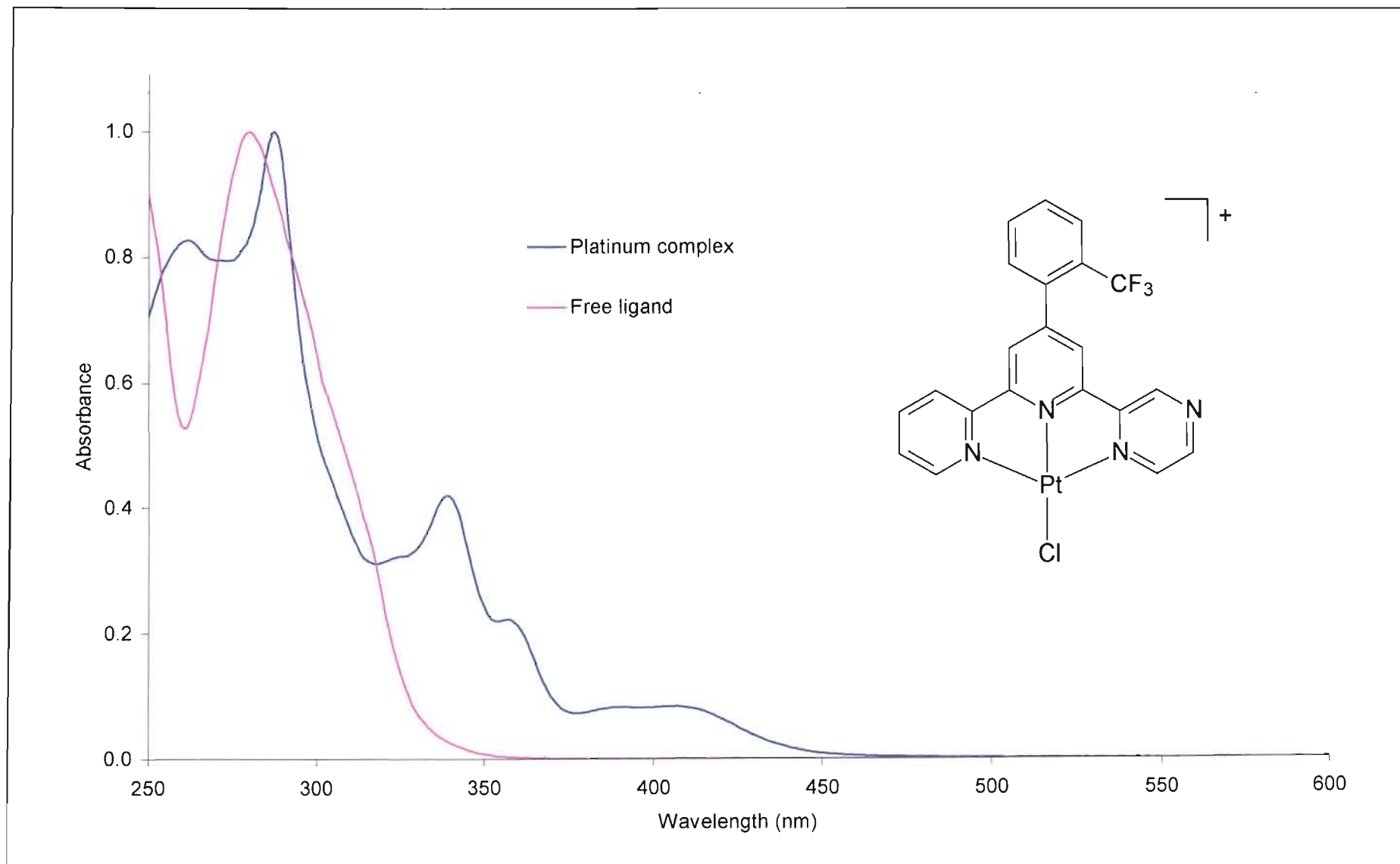


**Figure 5.6** Acetonitrile solution absorption spectra of the  $[Pt(4\text{-}oCF_3Ph\text{-}pzbipy)Cl]^+$  and  $4\text{-}oCF_3Ph\text{-}pzbipy$  chromophores recorded at 298 K.

no counterpart in the absorption regime of the free ligand and are therefore unlikely to have a ligand-centred origin. Their molar absorptivities ( $\epsilon$  3100 M<sup>-1</sup>.cm<sup>-1</sup>) also discount such an assignment. The positions and intensities of the bands, as well as the fact that they show a marked shift to lower energy in a less polar solvent, indicate that these low energy peaks have their origin in a charge transfer transition, most likely a MLCT transition. The absorption behaviour of the [Pt(4-*o*CF<sub>3</sub>Ph-pzbipy)Cl]<sup>+</sup> chromophore is typical of the absorptions of related platinum(II)-polypyridine compounds, including the [Pt(4-Ph-pzbipy)Cl]<sup>+</sup> and [Pt(4-*o*MePh-pzbipy)Cl]<sup>+</sup> chromophores described earlier in this chapter. Accordingly, the assignment of the absorption bands correspond.

As was observed for the [Pt(4-*o*MePh-pzbipy)Cl]<sup>+</sup> chromophore, the absorption energy is slightly reduced when the metal ligand binding domain is pyrazinyl-bipyridine as opposed to terpyridine. The MLCT absorption energy of [Pt(4'-*o*CF<sub>3</sub>Ph-terpy)Cl]<sup>+</sup> {where 4'-*o*CF<sub>3</sub>Ph-terpy denotes 4'-(*ortho*-CF<sub>3</sub>-phenyl)-2,2':6',2''-terpyridine} is 396 nm while that of [Pt(4-*o*CF<sub>3</sub>Ph-pzbipy)Cl]<sup>+</sup> absorbs at 407 nm. This reduction in energy is again associated with the stronger  $\pi$ -accepting strength of pyrazine as opposed to pyridine which would result in a reduction in the  $\pi^*$ -LUMO.

#### *Fluid solution emission spectroscopy*

Attempts were made to record the room temperature luminescence of the [Pt(4-*o*CF<sub>3</sub>Ph-pzbipy)Cl]<sup>+</sup> luminophore in deoxygenated acetonitrile and dichloromethane. As for the [Pt(4-*o*MePh-pzbipy)Cl]<sup>+</sup> complex, no emission was detected from a solution of the former solvent, presumably due to solvent induced exciplex quenching. In fact, emission from room temperature acetonitrile solutions of luminophores incorporating a pyrazine fragment is consistently absent. Emission in dichloromethane is in a band almost identical to that of [Pt(4-*o*MePh-pzbipy)Cl]<sup>+</sup>, consisting of a band with maximum intensity at *ca.* 545 nm (Figure 5.2). The same assignment for the emitting state is therefore made for the excited state of [Pt(4-*o*MePh-pzbipy)Cl]<sup>+</sup> in fluid solution at room temperature, namely that the emitting state consists of a largely ligand centred state perturbed by metal centred transitions.

### *Glass emission spectroscopy*

Emission in a 20  $\mu\text{M}$  rigid glassy DME solution at 77 K (Figure 5.3) is also essentially identical to that of  $[\text{Pt}(4\text{-Ph-pzbipy})\text{Cl}]^+$  and  $[\text{Pt}(4\text{-}o\text{MePh-pzbipy})\text{Cl}]^+$  recorded under that same conditions, with energies only very slightly higher in the case of  $[\text{Pt}(4\text{-}o\text{CF}_3\text{Ph-pzbipy})\text{Cl}]^+$ . Again, the discussion provided for the  $[\text{Pt}(4\text{-}o\text{MePh-pzbipy})\text{Cl}]^+$  luminophore applies and hence the emission assignment is the same, namely one of mixed orbital parentage with strong  $\pi\text{-}\pi^*$  (pzbipy) and some  $^3\text{MLCT}$  character.

### *Solid state emission spectroscopy*

As mentioned previously the hexafluoroantimonate salt,  $[\text{Pt}(4\text{-}o\text{CF}_3\text{Ph-pzbipy})\text{Cl}]\text{SbF}_6$ , exists in a red and in an orange morph. The tetrafluoroborate  $\{[\text{Pt}(4\text{-}o\text{CF}_3\text{Ph-pzbipy})\text{Cl}]\text{BF}_4\}$  salt is orange and the triflate salt  $\{[\text{Pt}(4\text{-}o\text{CF}_3\text{Ph-pzbipy})\text{Cl}]\text{CF}_3\text{SO}_3\}$  is red. Solid state absorption and emission data are collected in Table 5.10 at the end of this chapter.

The solid state and emission properties of salts incorporating the  $[\text{Pt}(4\text{-}o\text{CF}_3\text{Ph-pzbipy})\text{Cl}]^+$  luminophore have been recorded for all three salts,  $[\text{Pt}(4\text{-}o\text{CF}_3\text{Ph-pzbipy})\text{Cl}]\text{SbF}_6$ ,  $[\text{Pt}(4\text{-}o\text{CF}_3\text{Ph-pzbipy})\text{Cl}]\text{BF}_4$  and  $[\text{Pt}(4\text{-}o\text{CF}_3\text{Ph-pzbipy})\text{Cl}]\text{CF}_3\text{SO}_3$ . A single discussion will suffice for the photophysical properties of each of the red complexes {the red form of  $[\text{Pt}(4\text{-}o\text{CF}_3\text{Ph-pzbipy})\text{Cl}]\text{SbF}_6$  and  $[\text{Pt}(4\text{-}o\text{CF}_3\text{Ph-pzbipy})\text{Cl}]\text{CF}_3\text{SO}_3$ } and again in the case of the two orange complexes {the orange form of  $[\text{Pt}(4\text{-}o\text{CF}_3\text{Ph-pzbipy})\text{Cl}]\text{SbF}_6$  and  $[\text{Pt}(4\text{-}o\text{CF}_3\text{Ph-pzbipy})\text{Cl}]\text{BF}_4$ }. The red complexes will be discussed first, based in particular on the emission observed for the hexafluoroantimonate salt.

A solid state absorption spectrum has been recorded for  $[\text{Pt}(4\text{-}o\text{CF}_3\text{Ph-pzbipy})\text{Cl}]\text{SbF}_6$ , the transition of lowest energy appearing as a broad absorption band centred at 540 nm. The features of the absorption band are similar to those of the red salts of the  $[\text{Pt}(4\text{-}o\text{MePh-pzbipy})\text{Cl}]^+$  described in section 5.2.3 and hence the same band assignments apply.

Emission from  $[\text{Pt}(4\text{-}o\text{CF}_3\text{Ph-pzbipy})\text{Cl}]\text{SbF}_6$  is depicted in Figure 5.7 and at 298 K consists of a narrow (fwhm  $\approx 2070\text{ cm}^{-1}$ ), markedly asymmetric band with  $\lambda_{\text{em}}(\text{max})$  at 661 nm. An



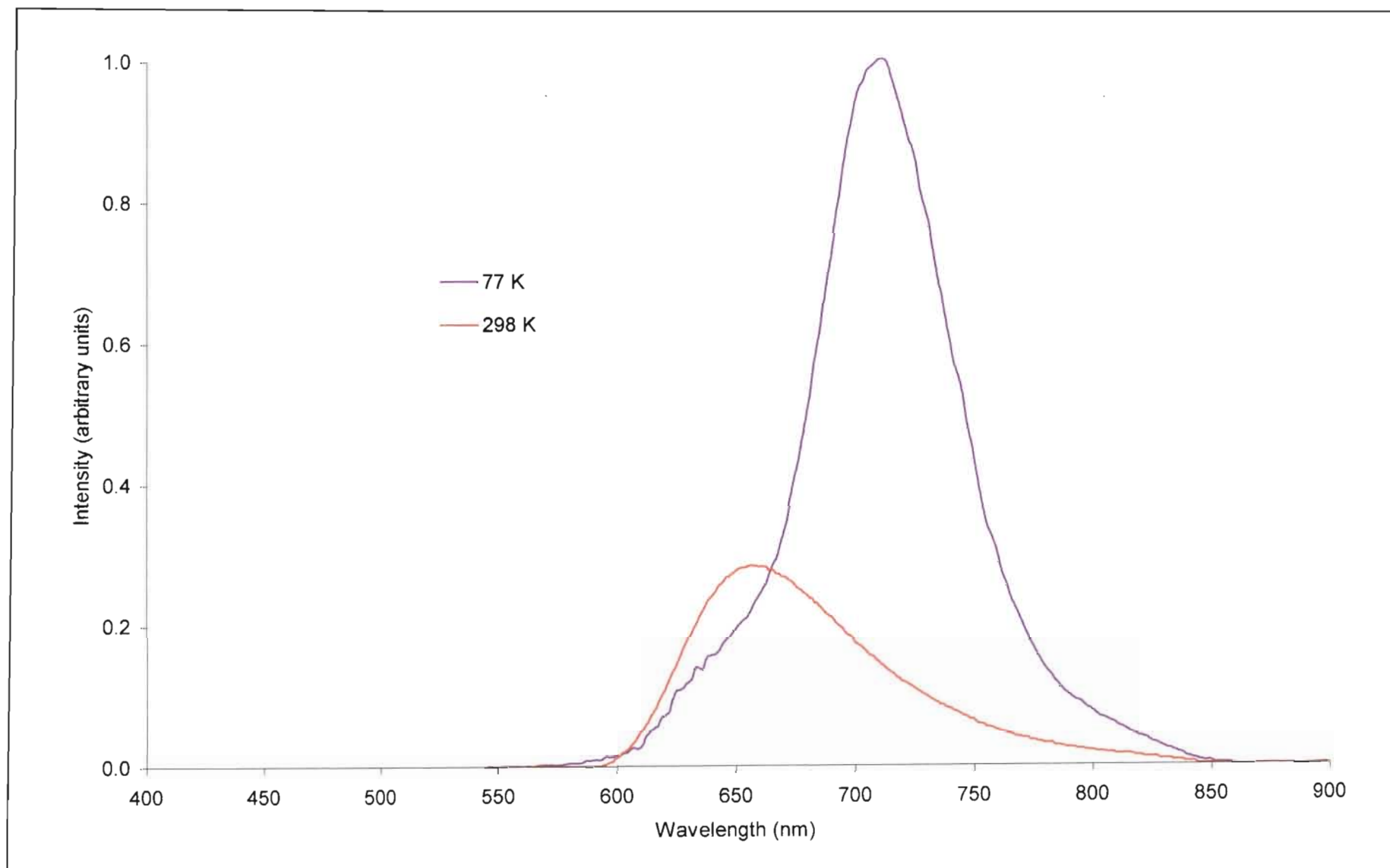


**Figure 5.7** Solid state emission spectra of the red form of  $[Pt(4-oCF_3Ph-pzbipy)Cl]SbF_6$ .

emission lifetime of 125 ns has been recorded at this temperature. Reducing the temperature results in a large increase in intensity and a shift to lower energies ( $\lambda_{em}(max) = 714$  at 77 K), and is accompanied by a further narrowing of the band to a fwhm of  $1300\text{ cm}^{-1}$ . At 77 K the emission lifetime is  $1.9\ \mu\text{s}$ . (In comparison the triflate salt,  $[\text{Pt}(4\text{-}o\text{CF}_3\text{Ph-pzbipy})\text{Cl}]\text{CF}_3\text{SO}_3$ , shows a shift from 658 to 709 nm as the temperature is reduced from 298 to 77 K.) Excitation spectra have been recorded and match bands in the solid state absorption spectra. Emission behaviour of this type is very similar to that displayed by all the methyl-substituted complexes,  $[\text{Pt}(4\text{-}o\text{MePh-pzbipy})\text{Cl}]\text{SbF}_6$ ,  $[\text{Pt}(4\text{-}o\text{MePh-pzbipy})\text{Cl}]\text{BF}_4$  and  $[\text{Pt}(4\text{-}o\text{MePh-pzbipy})\text{Cl}]\text{CF}_3\text{SO}_3$  (described in section 5.2.3) and attributed to  $^3\text{MMLCT}$  emission. By analogy the same assignment is made here for emission from the red hexafluoroantimonate and triflate salts of  $[\text{Pt}(4\text{-}o\text{CF}_3\text{Ph-pzbipy})\text{Cl}]^+$ .

The final two complexes under investigation are the orange hexafluoroantimonate and the tetrafluoroborate salts of  $[\text{Pt}(4\text{-}o\text{CF}_3\text{Ph-pzbipy})\text{Cl}]^+$ . Solid state absorption spectra of these complexes show prominent absorption bands at lowest energy centred at *ca.* 525 and 538 nm respectively. As in the case of the red form of complexes containing this luminophore, absorption is assigned to aggregated species in the solid state, based in large part on the large energy stabilisation observed in the solid state compared to the monomer absorption recorded in fluid solution at room temperature.

Solid state emission and excitation spectra of the orange form of  $[\text{Pt}(4\text{-}o\text{CF}_3\text{Ph-pzbipy})\text{Cl}]\text{SbF}_6$  and  $[\text{Pt}(4\text{-}o\text{CF}_3\text{Ph-pzbipy})\text{Cl}]\text{BF}_4$  salts have also been recorded. The basic features of emission from these two salts correspond closely enough to warrant a single discussion. The room temperature emission of the orange form of  $[\text{Pt}(4\text{-}o\text{CF}_3\text{Ph-pzbipy})\text{Cl}]\text{SbF}_6$  emits with  $\lambda_{em}(max)$  at 626 nm and is only slightly red shifted to 632 nm at 77 K (see Figure 5.8). In the case of  $[\text{Pt}(4\text{-}o\text{CF}_3\text{Ph-pzbipy})\text{Cl}]\text{BF}_4$  the maxima are 658 and 648 nm at 298 K and at 77 K respectively. The similarity lies in the very slight emission shifts for both salts on altering the temperature from ambient temperatures to 77 K. Band widths for both complexes decrease from a fwhm of just over  $2000\text{ cm}^{-1}$  at ambient temperature to values of 1615 and  $1710\text{ cm}^{-1}$  at 77 K for the orange form of  $[\text{Pt}(4\text{-}o\text{CF}_3\text{Ph-pzbipy})\text{Cl}]\text{SbF}_6$  and  $[\text{Pt}(4\text{-}o\text{CF}_3\text{Ph-pzbipy})\text{Cl}]\text{BF}_4$  respectively. Emission lifetimes at room temperature for the two complexes were measured at 810 ns {orange form of  $[\text{Pt}(4\text{-}o\text{CF}_3\text{Ph-pzbipy})\text{Cl}]\text{SbF}_6$ } and 480 ns { $[\text{Pt}(4\text{-}o\text{CF}_3\text{Ph-pzbipy})\text{Cl}]\text{BF}_4$ }.

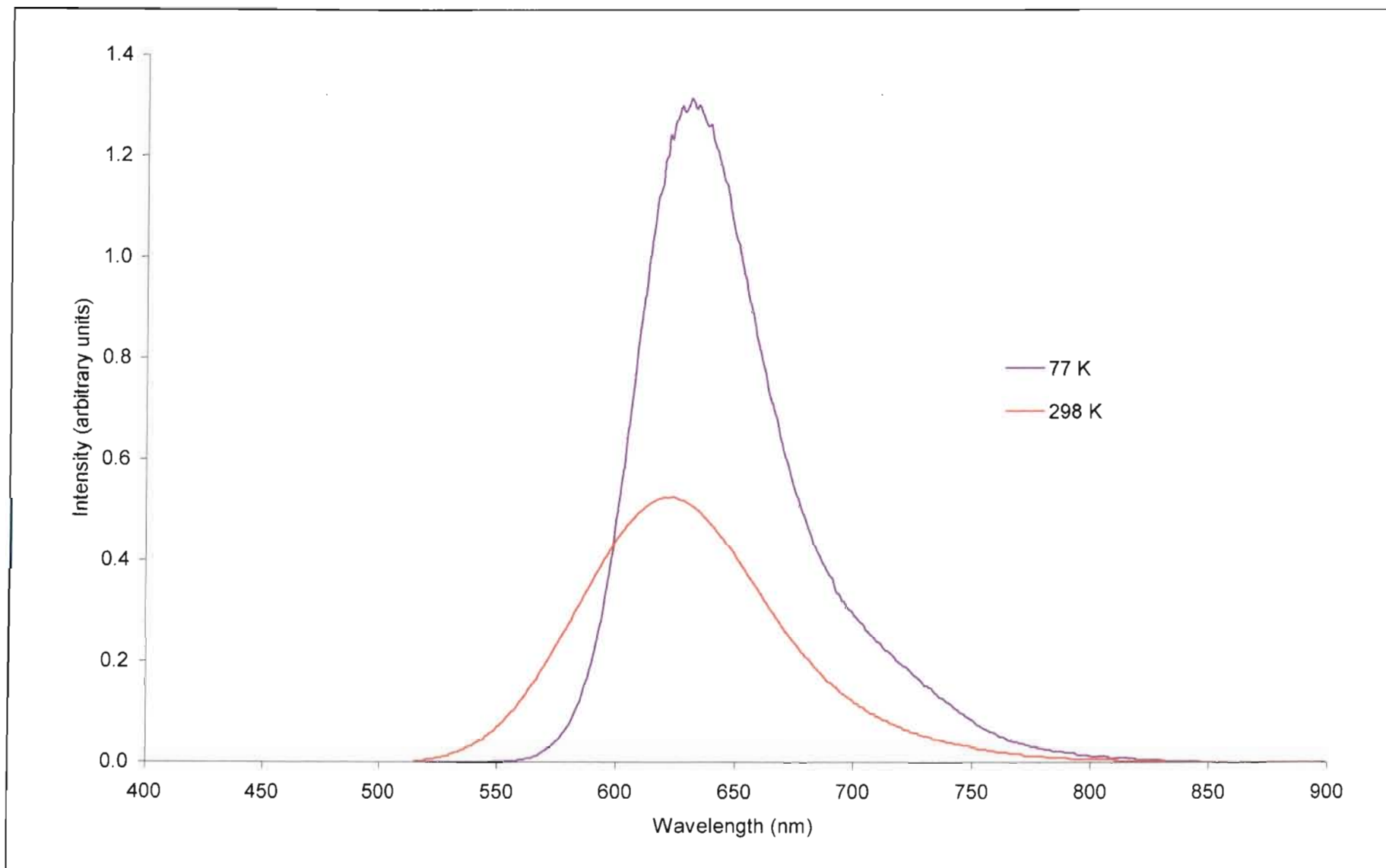


**Figure 5.8** Solid state emission spectra of the orange form of  $[Pt(4-oCF_3Ph-pzbipy)Cl]SbF_6$ .

pzbipy)Cl]BF<sub>4</sub>}. These values increase to well over 2 μs when the temperature is 77 K. In both cases excitation maxima match the lowest energy bands recorded in the absorption spectra.

Three features set the emission behaviour of the orange complexes apart from that of the red salts of the [Pt(4-*o*CF<sub>3</sub>Ph-pzbipy)Cl]<sup>+</sup> luminophore. First is the small shift in emission maxima accompanying an alteration in temperature. Secondly the emission lifetimes are consistently longer for the orange complexes compared to the red and, thirdly, the bands are broader for the orange complexes. Taken together this implies a different emission origin for the orange salts that will now be discussed.

Field, Summerton and coworkers report emission from terpyridyl ligand complexes analogous to those presented here in which the aromatic ligand is 4'-(*ortho*-CF<sub>3</sub>-phenyl)-2,2':6',2''-terpyridine.<sup>54</sup> This terpyridyl ligand has been coordinated to platinum, with the analogous hexafluoroantimonate and the tetrafluoroborate complexes having been prepared *viz.* [Pt(4'-*o*CF<sub>3</sub>Ph-terpy)Cl]SbF<sub>6</sub> and [Pt(4'-*o*CF<sub>3</sub>Ph-terpy)Cl]BF<sub>4</sub> {where 4'-*o*CF<sub>3</sub>Ph-terpy denotes 4'-(*ortho*-CF<sub>3</sub>-phenyl)-2,2':6',2''-terpyridine}. Both these salts have been isolated in an orange form and emit in broad bands (fwhm > 2400 cm<sup>-1</sup>) which show essentially no energy shifts (from 589 and 571 nm respectively) as the temperature is lowered. Emission lifetimes are longer than 300 ns at ambient temperatures and longer than 2.5 μs at 77 K. In both cases the authors favour an assignment of emission from an excimeric excited state brought about by the interaction of the organic portions of adjacent molecules in the excited state. In the case of [Pt(4'-*o*CF<sub>3</sub>Ph-terpy)Cl]SbF<sub>6</sub> the assignment is aided by a X-ray crystal structure corroborating the presence of the close intermolecular contacts on which the emission assignment is based. The authors note that the assignment of the emitting state as excimeric in origin is consistent with the relatively long lifetimes and broadness of the bands.<sup>54</sup>

Given the similarities to the emission properties of the pzbipy salts the emission by [Pt(4-*o*CF<sub>3</sub>Ph-pzbipy)Cl]SbF<sub>6</sub> (**17**) and [Pt(4-*o*CF<sub>3</sub>Ph-pzbipy)Cl]BF<sub>4</sub> (**18**) is assigned to excimer emission as well. Note that both the orange pyrazinyl-bipyridyl complexes luminesce at lower energies than their respective terpyridyl counterparts. This fits the trend observed for complexes in this chapter where terpyridyl ligand complexes are compared to complexes

which bind platinum *via* a pyrazinyl-bipyridyl unit and which have emitting states where the LUMO is essentially localised to the ligand *i.e.*, mostly  $\pi^*$  in nature. In every case emission from the pyrazinyl-bipyridyl ligand complex occurs at a lower energy. As in previous cases this stabilisation in emission energy is attributed to the better  $\pi$ -acceptor ability of pyrazine compared to pyridine which reduces the energy of the LUMO hence resulting in a reduced emission energy.

### 5.3 SUMMARY AND CONCLUSIONS

The first complex described in this chapter *viz.*, [Pt(4-Ph-pzbipy)Cl]BF<sub>4</sub> (**12**) incorporates the 4-Ph-pzbipy ligand. This ligand was designed as a direct analogue to the 4'-phenyl-2,2':6',2''-terpyridine (4'-Ph-terpy) ligand, the only difference being the replacement of one of the outer pyridine rings of the terpyridyl moiety with a pyrazine ring. We wished to establish what effect this would have on the photophysical properties of the complex. Emission from the monomeric excited state has been recorded in room temperature fluid solution, the data being shown in Table 5.3. Also shown in Table 5.3 are the salient fluid solution room temperature luminescence data from the previously studied chloro-platinum(II) terpyridyl complexes as well as fluid solution data for the other pyrazinyl complexes studied here. Luminescence data obtained in rigid glassy solutions for the same set of complexes are collected in Table 5.4. Trends and assignments in both media are the same and a single discussion will suffice.

It has previously been shown that replacing bipyridine with bipyrazine in the [Ru(bipy)<sub>3</sub>]<sup>2+</sup> system has the effect of significantly prolonging the emission of the emitting state in solution.<sup>117, 178</sup> No definite reason for this observation has been provided but the authors speculate that the longer emission lifetime is related to a reduced probability of radiationless deactivation *via* metal-centred d-d states in the pyrazine substituted systems. If this is indeed the reason for the elongation of the lifetime, the same effect would be absent when pyridine is replaced with pyrazine in the platinum-polyazine systems studied here. This is because metal-centred states are generally too high in energy to influence the non-radiative processes of the platinum-polyazines. Certainly the work presented here supports this notion since the substitution of pyrazine for pyridine had no effect on the emission lifetime of [Pt(4'-Ph-terpy)Cl]<sup>+</sup> compared to that of [Pt(4-Ph-pzbipy)Cl]<sup>+</sup> (see Table 5.3 and Table 5.4).

An interesting comparison is that of the emission energies and lifetimes for [Pt(4-Ph-pzbipy)Cl]<sup>+</sup> and [Pt(4-*o*MePh-pzbipy)Cl]<sup>+</sup>. In both the room temperature fluid solution and in the low temperature glass, monomeric emission from the latter complex is at a slightly higher energy, but with a shorter emission lifetime. This trend contradicts the energy gap law which predicts that for a homologous series of complexes, those complexes in the series which emit at the lowest energy will have the highest non-radiative rate constant,<sup>57</sup> *i.e.* these

complexes will have the shortest emission lifetimes. This observation is regarded as strong evidence that the excited states of  $[\text{Pt}(4\text{-Ph-pzbipy})\text{Cl}]^+$  and  $[\text{Pt}(4\text{-}o\text{MePh-pzbipy})\text{Cl}]^+$  are not composed of the same admixture of contributing states making up the emitting state. This is not surprising, since  $[\text{Pt}(4\text{-Ph-pzbipy})\text{Cl}]^+$  is likely to have a stronger  $\pi\text{-}\pi^*$  component to its excited state. This is because this complex lacks an *ortho*-substituted phenyl ring and is therefore likely to adopt a more planar configuration with a greater  $\pi$ -electron delocalisation. A consequence of the greater  $\pi$ -electron delocalisation is that the  $\pi(\text{HOMO})\text{-}\pi^*(\text{LUMO})$  gap will be reduced. This accounts for the lower energy of the emission exhibited by  $[\text{Pt}(4\text{-Ph-pzbipy})\text{Cl}]^+$  as compared to  $[\text{Pt}(4\text{-}o\text{MePh-pzbipy})\text{Cl}]^+$  and  $[\text{Pt}(4\text{-}o\text{CF}_3\text{Ph-pzbipy})\text{Cl}]^+$ . This result is consistent with observations made in Chapter 3 where the monomeric emission from the  $[\text{Pt}(4'\text{-}\beta\text{Np-terpy})\text{Cl}]^+$  luminophore, which is more likely to be nearly planar, occurs at a higher energy than that from the related non-planar  $[\text{Pt}(4'\text{-}\alpha\text{Np-terpy})\text{Cl}]^+$  luminophore.

**Table 5.3** Summary of emission data recorded in dichloromethane solution at 298 K.

Compound	Emission maximum of 0-0 transition (nm)	$\tau$ ( $\mu\text{s}$ )	Emission assignment
$[\text{Pt}(4'\text{-Ph-terpy})\text{Cl}]^{+ 32}$	535	0.09	IL/MLCT
$[\text{Pt}(4\text{-Ph-pzbipy})\text{Cl}]^+$	550	0.10	IL/MLCT
$[\text{Pt}(4'\text{-}o\text{MePh-terpy})\text{Cl}]^{+ 54}$	solubility problems, no data available	-	-
$[\text{Pt}(4\text{-}o\text{MePh-pzbipy})\text{Cl}]^+$	543	0.02	IL/MLCT
$[\text{Pt}(4'\text{-}o\text{CF}_3\text{Ph-terpy})\text{Cl}]^{+ 54}$	solubility problems, no data available	-	-
$[\text{Pt}(4\text{-}o\text{CF}_3\text{Ph-pzbipy})\text{Cl}]^+$	545	not measured	IL/MLCT

**Table 5.4** Summary of emission data recorded in a rigid glass at 77 K.

Compound	Emission maximum of 0-0 transition (nm)	Huang-Rhys ratio	$\tau$ ( $\mu$ s)	Emission Assignment
[Pt(4'-Ph-terpy)Cl] <sup>+</sup> <sup>32</sup>	503 <sup>BuCN</sup> <sup>32</sup>	0.75	15.0 <sup>M/E</sup> <sup>42</sup>	IL/MLCT <sup>32</sup>
[Pt(4-Ph-pzbipy)Cl] <sup>+</sup>	516 <sup>DME</sup>	1.00	15.2 <sup>DME</sup>	IL/MLCT
[Pt(4'-oMePh-terpy)Cl] <sup>+</sup> <sup>54</sup>	477 <sup>DME</sup>	0.79	not reported	IL <sup>54</sup>
[Pt(4-oMePh-pzbipy)Cl] <sup>+</sup>	501 <sup>DME</sup>	0.95	10.8 <sup>DME</sup>	IL/MLCT
[Pt(4'-oCF <sub>3</sub> Ph-terpy)Cl] <sup>+</sup> <sup>54</sup>	not reported	-	-	-
[Pt(4-oCF <sub>3</sub> Ph-pzbipy)Cl] <sup>+</sup>	495 <sup>DME</sup>	0.95	not measured	IL/MLCT

(BuCN) Spectrum recorded in butyronitrile solution.

(M/E) Spectrum recorded in 4:1 (v/v) methanol/ethanol solution.

(DME) Spectrum recorded in 1:5:5 (v/v) DMF/methanol/ethanol solution.

Hence, the most obvious reason for the significantly reduced emission lifetime of [Pt(4-oMePh-pzbipy)Cl]<sup>+</sup> compared to that of [Pt(4-Ph-pzbipy)Cl]<sup>+</sup> is a reduced  $\pi$ - $\pi^*$  component in the emitting state relative to the MLCT part. This not only results in a shorter-lived luminescence, but the emission band (in room temperature solution) is completely devoid of vibrational structure. A reduced IL component in the emitting state can be rationalised by a twist in the interannular band between the terpyridyl and phenyl ring systems as a result of the steric hindrance between the *ortho*-substituent of the phenyl ring and the protons of the central pyridine ring. Since the two aromatic moieties are now no longer nearly coplanar, electron delocalisation between the aromatic moieties is significantly reduced and hence the IL contribution to the excited state is smaller.

Emission in the glass provides additional information since, not only is the vibrational structure more pronounced at 77 K but, in the case of [Pt(4'-oMePh-terpy)Cl]<sup>+</sup>, it is possible to observe a monomeric emission spectrum in dilute solution. Huang-Rhys ratios are



significant since these values are regarded as a measure of the Franck-Condon factor for the respective excited states.<sup>21</sup> Since ligand  $\pi$ -bond orders are significantly smaller in IL states than in MLCT states, this would result in ligand-based excited state distortions which are larger for IL transitions than for MLCT transitions.<sup>21</sup> As a result the Franck-Condon factor (and hence the Huang-Rhys ratio) is larger as the ligand character of the emission is increased. An analysis of the Huang-Rhys factors as measured in a rigid glass at 77 K for each of the complexes (see Table 5.4) suggests that the IL character for the pyrazinyl-bipyridyl complexes are larger than those of their terpyridyl analogues. No doubt this is related to the superior  $\pi$ -accepting abilities of pyrazine over pyridine as measured by the respective reduction potentials.<sup>179</sup>

### *Emission in the solid state*

The solid state emission studies in this chapter have to a large extent been motivated by the success achieved by Summerton and coworkers in bringing about close packing in the solid state by the use of an *ortho*-substituted phenyl ring in the 4'-position of the chloro(terpyridyl)platinum(II) system.<sup>54</sup> Given the nominal steric changes brought about by exchanging CH for N and the success of the *ortho*-substituent on the phenyl ring, in conjunction with the nature of the counterion, in imposing a particular solid state packing arrangement, it was hoped that it would be possible to synthesise isomorphous compounds which have the same excited state, but different emission properties in the solid state. This aim appears to have been achieved. In particular, compare the emission from the two related complexes, [Pt(4-*o*MePh-pzbipy)Cl]SbF<sub>6</sub> (**14**) and [Pt(4'-*o*MePh-terpy)Cl]SbF<sub>6</sub> which has been described in the literature<sup>54</sup> (see Table 5.5).

The only difference between the complexes is in the binding domain where platinum in [Pt(4-*o*MePh-pzbipy)Cl]SbF<sub>6</sub> is coordinated *via* a pyrazinyl-bipyridyl binding domain while [Pt(4'-*o*MePh-terpy)Cl]SbF<sub>6</sub> has a terpyridyl coordinated platinum centre. Judging by the emission from each of the complexes there is strong evidence that the two compounds have an isomorphous packing arrangement in the solid state. In particular, both emit from a MMLCT excited state. This type of emission is brought about by a specific solid state arrangement, necessitating close Pt...Pt contacts. Since both complexes emit from this type of excited state

it is likely that the salts are isomorphous. This complex in particular embodies success in achieving our objective of modifying the emission properties of the salt without changing the solid state packing arrangement.

**Table 5.5** Emission comparison between  $[Pt(4\text{-}o\text{MePh-pzbipy})Cl]SbF_6$  and  $[Pt(4'\text{-}o\text{MePh-terpy})Cl]SbF_6$ .

Compound	Emission maximum (nm) [77 K]	$\tau$ (ns) [77 K]	Emission Assignment
$[Pt(4\text{-}o\text{MePh-pzbipy})Cl]SbF_6$	674 [723]	80 [1320]	MMLCT
$[Pt(4'\text{-}o\text{MePh-terpy})Cl]SbF_6$ <sup>54</sup>	616 [673]	155 [1680]	MMLCT

What sets the emission properties of the two complexes apart is the prominent stabilisation (of *ca.* 1030  $\text{cm}^{-1}$  at 77 K) of the emission energy for  $[Pt(4\text{-}o\text{MePh-pzbipy})Cl]SbF_6$ . As before for all the complexes coordinated *via* a single pyrazine ring, the stabilisation is attributed to a lower energy  $\pi^*$ -LUMO due to the superior  $\pi$ -accepting ability of this six-membered azine ring above that of pyridine. In addition Mealli *et al.* have performed EHMO (Extended Hückel Molecular orbital) calculations which show that  $d^8$ - $d^8$  interactions of the type necessary for MMLCT emission are stabilised by weakly  $\sigma$ -donating ligands.<sup>180</sup> In conjunction these factors result in emission from  $[Pt(4\text{-}o\text{MePh-pzbipy})Cl]SbF_6$  that is stabilised to such an extent that this extraordinary salt luminesces at wavelengths approaching the infrared at 77 K. In addition, its solid state absorption maximum at 575 nm is exceptionally low for this type of platinum-polypyridyl compound.

It is also interesting to note that the lower energy excited state of  $[Pt(4\text{-}o\text{MePh-pzbipy})Cl]SbF_6$  which emits with a  $\lambda_{em}(\text{max})$  at 723 nm at 77 K has a somewhat shorter emission lifetime of 1320 ns compared to  $[Pt(4'\text{-}o\text{MePh-terpy})Cl]SbF_6$  which emits at 673 nm with a lifetime of 1680 ns at the same temperature. This result is consistent with the energy gap law for radiationless decay which applies to complexes which emit from an excited state with the same

origin.<sup>57</sup> Certainly that is the case here since both complexes emit from a MMLCT excited state.

Polymorphism such as that shown by  $[\text{Pt}(4\text{-}o\text{CF}_3\text{Ph-pzbipy})\text{Cl}]\text{SbF}_6$ , which exists in a red and in an orange form, is not unusual for square-planar platinum(II) complexes and a number of platinum(II) polypyridyl complexes have been reported which also show polymorphic behaviour.<sup>29, 46, 53, 157, 162, 164</sup> Of importance here are the two complexes  $[\text{Pt}(4'\text{-Ph-terpy})\text{Cl}]\text{BF}_4$ <sup>53</sup> and  $[\text{Pt}(\text{bipy})\text{Cl}_2]$ <sup>164</sup> (where bipy is 2,2'-bipyridine). Both complexes exist in two forms of which one is red. Not only do the red forms of both complexes show a MMLCT emission, but significantly in both cases X-ray crystal structures have been able to confirm the existence of extended metal-metal interactions. This result provides impetus to our assessment that the red form of  $[\text{Pt}(4\text{-}o\text{CF}_3\text{Ph-pzbipy})\text{Cl}]\text{SbF}_6$  also exists with extended intermolecular Pt...Pt interactions. It is noteworthy that the proton NMR spectrum (recorded on a solution of the crystals in DMSO- $d_6$ ) and elemental analysis of both red and orange forms do not indicate any evidence of solvent included in the lattice. This means that the packing architecture of neither form is governed by the need to accommodate a solvent molecule in the crystal lattice. As noted above, the crystal form is determined by the concentration of the solution from which it precipitates; in particular the likely stacked structure for the red form is a consequence of a relatively slow crystallisation process from a more dilute solution. It also follows that the red form is the more stable one, a conclusion corroborated by the findings of Gray, Marsh *et al.* in their investigation of factors influencing linear chain formation.<sup>157</sup> In the absence of a X-ray crystal structure it is not clear what determines the packing arrangement in the orange form of  $[\text{Pt}(4\text{-}o\text{CF}_3\text{Ph-pzbipy})\text{Cl}]\text{SbF}_6$ , but the emission displayed by these complexes make it clear what value X-ray crystal structures have in providing conclusive assignment of excited states.

Summarising, the solid state emission exhibited by the complexes in this work, that is by  $[\text{Pt}(4\text{-}o\text{MePh-pzbipy})\text{Cl}]\text{X}$  [ $\text{X}^- = \text{SbF}_6^-$  (**14**),  $\text{BF}_4^-$  (**15**),  $\text{CF}_3\text{SO}_3^-$  (**16**)],  $[\text{Pt}(4\text{-}o\text{CF}_3\text{Ph-pzbipy})\text{Cl}]\text{X}$  [ $\text{X}^- = \text{SbF}_6^-$  (**14**),  $\text{BF}_4^-$  (**15**),  $\text{CF}_3\text{SO}_3^-$  (**16**)] takes two forms. The complexes emit either from a MMLCT or an excimeric excited state and in every case the pyrazinyl complexes have shown emission at a significantly reduced energy.

### *Final comments*

The most significant and consistent effect observed when one of the outer pyridine rings of the terpyridine in the platinum coordinated complexes reported here is a reduction in energy of the emitting state. As the data in Tables 5.3, 5.4 and 5.5 show, there is a consistent shift to the red in the emission maximum when an outer pyridine ring is replaced by a pyrazine ring. We propose that this is due to the superior  $\pi$ -accepting capability of pyrazine<sup>117</sup> compared to that of pyridine which results in a reduction in the energy of the  $\pi^*$ -LUMO and hence in the energy of the emitting state.

However, this picture is not complete in the sense that in this work no attempt has been made as yet to provide a quantitative measure of the stabilisation. In this regard we note that the  $\pi$ -accepting strength of pyrazine compared to pyridine has been evaluated by measuring the reduction potentials of free bipyrazine compared to bipyridine as well as for the tris-coordinated ruthenium(II) complexes,  $[\text{Ru}(\text{bipy})_3]^{2+}$  and  $[\text{Ru}(\text{bipz})_3]^{2+}$  (where bipy is 2,2'-bipyridine and bipz is 2,2'-bipyrazine).<sup>178, 179</sup> In every case the pyrazine compound is more readily reduced by *ca.* 0.5 eV (*ca.* 4000  $\text{cm}^{-1}$ ).<sup>117, 179</sup> In spite of this large stabilisation neither the MLCT absorption nor the emission exhibited by the ruthenium(II) complexes reflect a similar stabilisation. The MLCT absorption band of  $[\text{Ru}(\text{bipz})_3]^{2+}$  {with  $\lambda_{\text{abs}}(\text{max})$  at 443 nm} occurs at higher energy than that of the related  $[\text{Ru}(\text{bipy})_3]^{2+}$  {with  $\lambda_{\text{abs}}(\text{max})$  at 452 nm}, which represents a destabilisation of *ca.* 500  $\text{cm}^{-1}$ .<sup>178, 179</sup> Crutchley and Lever rationalise this observation by proposing that the stabilisation of the  $\pi$ -accepting orbitals when pyridine is replaced by pyrazine is accompanied by a concomitant stabilisation of the metal donor orbitals by roughly the same energy, leading to no observable energy change in the MLCT absorption bands.<sup>179</sup> The authors propose that the metal orbitals are stabilised by the weaker  $\sigma$ -donor strength of pyrazine which allow the metal ion to have a higher effective nuclear charge.<sup>179</sup> This effect extends to the emission by the two complexes with  $[\text{Ru}(\text{bipz})_3]^{2+}$  and  $[\text{Ru}(\text{bipy})_3]^{2+}$  emitting with peak intensity at 603 and 610 nm respectively, which represents an energy difference of  $\sim 190 \text{ cm}^{-1}$ . Thus, in contrast to our observations of platinum(II) polypyridyl complexes, the emission of the pyrazine coordinated complex is very slightly *blue*-shifted. Crutchley and Lever (and others after them<sup>117</sup>) point out that the superior  $\pi$ -accepting strength of pyrazine over pyridine is not fully utilised due to the weaker  $\sigma$ -donating power of pyrazine compared to pyridine.<sup>179</sup>

In trying to quantify the stabilisation of pyrazinyl-bipyridyl complexes over terpyridyl complexes by an analysis of emission energies in our study we have selected complexes based on a number of criteria. These were i) that the complexes were directly analogous, differing only in the nature of one of the outer azine rings coordinating the platinum centre ii) that there is evidence that the emissions have the same origin and show evidence for a similar solid state packing and finally iii) it is still prudent to compare only emissions at the lowest temperatures since it has been established that it is the emission at these temperatures that are most representative of the true emission of complexes in question.<sup>47</sup>

Only emission from four complexes qualify for comparison based on these criteria. These complexes and their stabilisation measured in the emission energy compared to the similar terpyridyl complexes are condensed in Table 5.6.

Emission in these cases has been assigned to a variety of excited states. Those in a dilute glass have been assigned to emission with mixed IL/MLCT orbital parentage. That from solid [Pt(4-*o*MePh-pzbipy)Cl]SbF<sub>6</sub> is assigned to a MMLCT excited state, while the solid emission from [Pt(4-*o*CF<sub>3</sub>Ph-pzbipy)Cl]SbF<sub>6</sub> is assigned to an excimeric excited state (*vide supra*). In spite of these differences in emission origin from a rather limited selection of compounds, it is possible to draw meaningful conclusions from these data. Noticeable is the emission stabilisation of *ca.* 1000 cm<sup>-1</sup> for complexes which have an *ortho*-substituted phenyl ring. In the case of emission from [Pt(4-Ph-pzbipy)Cl]<sup>+</sup> in dilute glassy medium the stabilisation is evaluated at roughly half this value. (It may be significant to comment that emission in a dilute room temperature dichloromethane solution, not included in Table 5.6, is similarly stabilised by ~ 500 cm<sup>-1</sup>.)

We first need to address the issue that our complexes exhibit emission that shows a consistent stabilisation while the tris-coordinated ruthenium(II) complexes show only a very small change to higher energies. Two effects may be coming into play. The first is the difference in the metal centre. Any stabilisation of platinum donor orbitals due to a reduction in the effective nuclear charge of the metal centre due to the weaker  $\sigma$ -donor strength of a pyrazine nitrogen, would be smaller than that for a second-row transition metal, *e.g.* ruthenium. A smaller stabilisation of the metal donor orbitals would result in a smaller HOMO-LUMO energy gap

for the MLCT transition. This can be seen by absorption bands for the pyrazinyl-bipyridyl complexes presented in this work which are slightly red-shifted compared to their terpyridyl analogues, while a replacement of pyridine for pyrazine in the ruthenium(II) trisbipyridyl complexes results in a slight shift to the *blue*.

**Table 5.6** Evaluation of emission stabilisation at 77 K due to the presence of pyrazine.

Compound	$\lambda_{em}(\text{max})$ (nm)	Energy ( $\text{cm}^{-1}$ )	Difference ( $\text{cm}^{-1}$ )
[Pt(4'-Ph-terpy)Cl] <sup>+</sup> in DME solution <sup>32</sup>	503	19880	
[Pt(4-Ph-pzbipy)Cl] <sup>+</sup> in DME solution	516	19379	501
[Pt(4'- <i>o</i> MePh-terpy)Cl] <sup>+</sup> in DME solution <sup>54</sup>	477	20964	
[Pt(4- <i>o</i> MePh-pzbipy)Cl] <sup>+</sup> in DME solution	501	19960	1004
[Pt(4'- <i>o</i> MePh-terpy)Cl]SbF <sub>6</sub> ; red solid <sup>54</sup>	673	14858	
[Pt(4- <i>o</i> MePh-pzbipy)Cl]SbF <sub>6</sub> ; red solid	723	13831	1027
[Pt(4'- <i>o</i> CF <sub>3</sub> Ph-terpy)Cl]SbF <sub>6</sub> ; orange solid <sup>54</sup>	589	16977	
[Pt(4- <i>o</i> CF <sub>3</sub> Ph-pzbipy)Cl]SbF <sub>6</sub> ; orange solid	633	15797	1180

Secondly, in the case of the pyrazinyl-bipyridyl ligand complexes presented in our work the pyrazine ligand is used in conjunction with pyridine ligands which have a stronger  $\sigma$ -donating strength than does pyrazine. This could have the effect that in our systems the better  $\pi$ -accepting strength of pyrazine can be more effectively employed to remove electron density from a metal centre that has its electron density enhanced by the stronger  $\sigma$ -donor ability of the pyridines.

Note that in the case of [Pt(4-Ph-pzbipy)Cl]<sup>+</sup>, where the complex is without an *ortho*-substituent on the phenyl ring the stabilisation due to pyrazine is  $\sim 500 \text{ cm}^{-1}$ , whereas for complexes with an *ortho*-substituted phenyl ring this stabilisation compared to the terpyridyl

analogues is  $\sim 1000 \text{ cm}^{-1}$ . As mentioned before the configurationally mixed excited states which give rise to the emission of these complexes differ in their excited state make-ups, with the  $[\text{Pt}(4\text{-Ph-pzbipy})\text{Cl}]^+$  luminophore showing evidence for a stronger ligand centred component to its configurationally mixed excited state. Results presented here suggest that any stabilisation of the excited state brought about by the presence of pyrazine is diluted by prominent  $\pi\text{-}\pi^*$  character in excited states of mixed orbital parentage. The greater stabilisation by pyrazine of excited states with less MLCT character is sensible since the pyrazine ring particularly influences the energy of MLCT transitions (as opposed to IL transitions which constitute the remainder of the excited state) by its interactions and proximity to the metal centre.

## 5.4 EXPERIMENTAL

### 5.4.1 Synthetic procedures

#### 5.4.1.1 [Pt(4-Ph-pzbipy)Cl]BF<sub>4</sub> (**12**)

{where 4-Ph-pzbipy is 4-phenyl-6-(2''-pyrazinyl)-2,2'-bipyridine}

Silver tetrafluoroborate was dissolved in acetonitrile (5 ml) and added to a suspension of [Pt(PhCN)<sub>2</sub>Cl<sub>2</sub>] (100 mg, 0.21 mmol) in acetonitrile (10 ml). The mixture was refluxed overnight under an inert atmosphere before the resultant precipitate of AgCl was removed by filtration. An approximately equimolar amount of solid 4-phenyl-6-(2''-pyrazinyl)-2,2'-bipyridine (4-Ph-pzbipy) (62 mg, 0.20 mmol) was added and the mixture refluxed for an additional 24 hrs. Once reflux was complete the mixture was filtered hot and the solvent partially removed under reduced pressure resulting in the precipitation of [Pt(4-Ph-pzbipy)Cl]BF<sub>4</sub>. The product was washed on the frit with copious amounts of diethyl ether and then smaller amounts of acetonitrile. The resulting powder was recrystallised from hot acetonitrile.

[Pt(4-Ph-pzbipy)Cl]BF<sub>4</sub> (**12**): Yield 60 mg (48 %). Molecular mass 627.7 g.mol<sup>-1</sup>. [Calc. for C<sub>20</sub>H<sub>14</sub>BClF<sub>4</sub>N<sub>4</sub>Pt: C, 38.27; H, 2.25; N, 8.93. Found: C, 38.62; H, 2.17; N, 8.50 %].

<sup>1</sup>H NMR for [Pt(4-Ph-pzbipy)Cl]BF<sub>4</sub> (DMSO-d<sub>6</sub>): δ 9.92(1H, d, H<sup>3''</sup>) 9.10(1H, d, H<sup>6''</sup>) 9.02(1H, s, H<sup>5</sup>) 8.92(1H, s, H<sup>3</sup>) 8.76(1H, d, H<sup>5''</sup>) 8.70(1H, m, H<sup>3'</sup>) 8.66(1H, m, H<sup>6'</sup>) 8.44(1H, td, H<sup>4'</sup>) 8.06 - 8.18(2H, m, H<sup>2''',6''</sup>) 7.82(1H, qd, H<sup>5'</sup>) 7.64 - 7.73(3H, m, H<sup>3'',4'',5''</sup>)



5.4.1.2 [Pt(4-*o*MePh-pzbipy)Cl]X [ $X^- = \text{SbF}_6^-$  (**14**),  $\text{BF}_4^-$  (**15**),  $\text{CF}_3\text{SO}_3^-$  (**16**)]  
{where 4-*o*MePh-pzbipy is 4-(*o*-CH<sub>3</sub>-phenyl)-6-(2''-pyrazinyl)-2,2'-bipyridine}

The appropriate silver salt AgX (73 mg for  $X^- = \text{SbF}_6^-$ ; 41 mg for  $X^- = \text{BF}_4^-$ ; 54 mg for  $X^- = \text{CF}_3\text{SO}_3^-$ ; 0.21 mmol), depending on the complex to be made, was dissolved in acetonitrile (5 ml) and added to a suspension of [Pt(PhCN)<sub>2</sub>Cl<sub>2</sub>] (100 mg, 0.21 mmol) in acetonitrile (10 ml). The mixture was refluxed overnight under an inert atmosphere before the resultant precipitate of AgCl was removed by filtration. An approximately equimolar amount of solid 4-(*ortho*-CH<sub>3</sub>-phenyl)-6-(2''-pyrazinyl)-2,2'-bipyridine (4-*o*MePh-pzbipy) (65 mg, 0.20 mmol) was added and the mixture refluxed for an additional 24 hrs. Once reflux was complete the mixture was filtered hot and the solvent partially removed under reduced pressure resulting in the precipitation of [Pt(4-*o*MePh-pzbipy)Cl]X. The product was washed on the frit with copious amounts of diethyl ether and then smaller amounts of acetonitrile. The resulting powder was recrystallised from hot acetonitrile.

[Pt(4-*o*MePh-pzbipy)Cl]SbF<sub>6</sub> (**14**): Yield 79 mg (50 %). Molecular mass 790.7 g.mol<sup>-1</sup>. [Calc. for C<sub>21</sub>H<sub>16</sub>ClF<sub>6</sub>N<sub>4</sub>PtSb: C, 31.90; H, 2.04; N, 7.09. Found: C, 31.81; H, 1.84; N, 7.04 %]. <sup>1</sup>H NMR for [Pt(4-*o*MePh-pzbipy)Cl]SbF<sub>6</sub> (DMSO-*d*<sub>6</sub>): δ 9.89(1H, d, H<sup>3''</sup>) 9.11(1H, d, H<sup>6''</sup>) 8.85(1H, s, H<sup>5</sup>) 8.83(1H, d, H<sup>5''</sup>) 8.79(1H, s, H<sup>3</sup>) 8.76(1H, m, H<sup>6</sup>) 8.71(1H, m, H<sup>3'</sup>) 7.86(1H, m, H<sup>5'</sup>) 7.40 - 7.90(4H, m, phenyl H's) 2.45(3H, s, CH<sub>3</sub>)

[Pt(4-*o*MePh-pzbipy)Cl]BF<sub>4</sub> (**15**): Yield 65 mg (51 %). Molecular mass 641.7 g.mol<sup>-1</sup>. [Calc. for C<sub>21</sub>H<sub>16</sub>BClF<sub>4</sub>N<sub>4</sub>Pt: C, 39.31; H, 2.51; N, 8.73. Found: C, 38.91; H, 2.41; N, 8.48 %].

[Pt(4-*o*MePh-pzbipy)Cl]CF<sub>3</sub>SO<sub>3</sub> (**16**): Yield 63 mg (45 %). Molecular mass 703.98 g.mol<sup>-1</sup>. [Calc. for C<sub>22</sub>H<sub>16</sub>ClF<sub>3</sub>N<sub>4</sub>O<sub>3</sub>PtS: C, 37.54; H, 2.29; N, 7.96. Found: C, 37.75; H, 1.80; N, 7.91 %].

**5.4.1.3 [Pt(4-*o*-CF<sub>3</sub>Ph-pzbipy)Cl]X [X<sup>-</sup> = SbF<sub>6</sub><sup>-</sup> (**17**), BF<sub>4</sub><sup>-</sup> (**18**), CF<sub>3</sub>SO<sub>3</sub><sup>-</sup> (**19**)**  
{where 4-*o*-CF<sub>3</sub>Ph-pzbipy is 4-(*o*-CF<sub>3</sub>-phenyl)-6-(2''-pyrazinyl)-2,2'-bipyridine}

The appropriate silver salt AgX (73 mg for X<sup>-</sup> = SbF<sub>6</sub><sup>-</sup>; 41 mg for X<sup>-</sup> = BF<sub>4</sub><sup>-</sup>; 54 mg for X<sup>-</sup> = CF<sub>3</sub>SO<sub>3</sub><sup>-</sup>; 0.21 mmol), depending on the complex to be made, was dissolved in acetonitrile (5 ml) and added to a suspension of [Pt(PhCN)<sub>2</sub>Cl<sub>2</sub>] (100 mg, 0.21 mmol) in acetonitrile (10 ml). The mixture was refluxed overnight under an inert atmosphere before the resultant precipitate of AgCl was removed by filtration. An approximately equimolar amount of solid 4-(*ortho*-CF<sub>3</sub>-phenyl)-6-(2''-pyrazinyl)-2,2'-bipyridine (4-*o*-CF<sub>3</sub>Ph-pzbipy) (76 mg, 0.20 mmol) was added and the mixture refluxed for an additional 24 hrs. Once reflux was complete the mixture was filtered hot and the solvent partially removed under reduced pressure resulting in the precipitation of [Pt(4-*o*-CF<sub>3</sub>Ph-pzbipy)Cl]X. The product was washed on the frit with copious amounts of diethyl ether and then smaller amounts of acetonitrile. The resulting powder was recrystallised from hot acetonitrile.

[Pt(4-*o*-CF<sub>3</sub>Ph-pzbipy)Cl]SbF<sub>6</sub> (**17**): Yield 95 mg (56 %). Molecular mass 844.62 g.mol<sup>-1</sup>. [Calc. for C<sub>21</sub>H<sub>13</sub>ClF<sub>9</sub>N<sub>4</sub>PtSb: C, 29.86; H, 1.55; N, 6.63. Found: C, 29.94; H, 1.37; N, 6.54 %].

<sup>1</sup>H NMR for [Pt(4-*o*-CF<sub>3</sub>Ph-pzbipy)Cl]SbF<sub>6</sub> (DMSO-*d*<sub>6</sub>): δ 9.84(1H, s, H<sup>3''</sup>) 9.15(1H, d, H<sup>6''</sup>) 8.90(1H, d, H<sup>5''</sup>) 8.88(1H, s, H<sup>5</sup>) 8.85(1H, d, H<sup>6</sup>) 8.81(1H, s, H<sup>3</sup>) 8.65(1H, d, H<sup>3'</sup>) 8.48(1H, t, H<sup>4'</sup>) 8.06(1H, d, H<sup>3'''</sup>) 7.96(1H, t, H<sup>5'''</sup>) 7.94(1H, t, H<sup>5'</sup>) 7.87(1H, t, H<sup>4'''</sup>) 7.69(1H, d, H<sup>6'''</sup>)

[Pt(4-*o*-CF<sub>3</sub>Ph-pzbipy)Cl]BF<sub>4</sub> (**18**): Yield 71 mg (51 %). Molecular mass 695.7 g.mol<sup>-1</sup>. [Calc. for C<sub>21</sub>H<sub>13</sub>BClF<sub>7</sub>N<sub>4</sub>Pt: C, 36.26; H, 1.88; N, 8.05. Found: C, 36.11; H, 1.55; N, 8.00 %].

[Pt(4-*o*-CF<sub>3</sub>Ph-pzbipy)Cl]CF<sub>3</sub>SO<sub>3</sub> (**19**): Yield 82 mg (54 %). Molecular mass 757.9 g.mol<sup>-1</sup>. [Calc. for C<sub>22</sub>H<sub>13</sub>ClF<sub>6</sub>N<sub>4</sub>O<sub>3</sub>PtS: C, 34.86; H, 1.73; N, 7.39. Found: C, 34.77; H, 1.65; N, 7.37 %].

**Table 5.7** *Infrared spectroscopic data*

Compound	Polypyridine <sup>a</sup>	Counterion <sup>a</sup>
[Pt(4-Ph-pzbipy)Cl]BF <sub>4</sub> ( <b>12</b> )	1610(s) 1560(w) 1474(m) 1418(m) 889(w) 791(s)	1053(vs, br)
Pt(4- <i>o</i> MePh-pzbipy)Cl]SbF <sub>6</sub> ( <b>14</b> )	1610(s) 1560(w) 1473(m) 1420(m) 889(w) 768(s)	662(vs)
[Pt(4- <i>o</i> MePh-pzbipy)Cl]BF <sub>4</sub> ( <b>15</b> )	1613(s) 1558(w) 1471(m) 1417(m) 863(w) 767(s)	1052(vs, br)
[Pt(4- <i>o</i> MePh-pzbipy)Cl]CF <sub>3</sub> SO <sub>3</sub> ( <b>16</b> )	1612(s) 1559(w) 1468(m) 1418(m) 885(w) 766(s)	1271(vs) 1144(m) 1032(s)
Pt(4- <i>o</i> CF <sub>3</sub> Ph-pzbipy)Cl]SbF <sub>6</sub> ( <b>17</b> )	1612(m) 1560(w) 1472(m) 1420(m) 1317(s) 889(w) 777(s)	658(vs)
Pt(4- <i>o</i> CF <sub>3</sub> Ph-pzbipy)Cl]BF <sub>4</sub> ( <b>18</b> )	1618(m) 1560(w) 1472(m) 1420(m) 1319(s) 883(w) 777(s)	1051(vs, br)
Pt(4- <i>o</i> CF <sub>3</sub> Ph-pzbipy)Cl]CF <sub>3</sub> SO <sub>3</sub> ( <b>19</b> )	1618(m) 1560(w) 1469(m) 1420(m) 1317(s) 881(w) 780(s)	1268(vs) 1174(s) 1030(s)

(a) Recorded as a KBr pellet in the solid state (cm<sup>-1</sup>).

Designation: w = weak; m = medium; s = strong; vs = very strong; br = broad;

**Table 5.8** Absorption spectroscopic data recorded in fluid solution at 298 K.

Chromophore	$\lambda_{\text{abs}}$ (nm)		Assignment
	Acetonitrile	Dichloromethane	
[Pt(4-Ph-pzbipy)Cl] <sup>+</sup>	404 (5700 <sup>a</sup> )	417	MLCT [Pt(5d) → 4-Ph-pzbipy( $\pi^*$ )]
concentration range: 1 - 10 $\mu\text{M}$	384sh (4800)	392sh	MLCT [Pt(5d) → 4-Ph-pzbipy( $\pi^*$ )]
	334 (19900)	341	<sup>1</sup> ( $\pi$ - $\pi^*$ ) (4-Ph-pzbipy)
	321sh (20600)	330sh	<sup>1</sup> ( $\pi$ - $\pi^*$ ) (4-Ph-pzbipy)
	306 (23600)	314	<sup>1</sup> ( $\pi$ - $\pi^*$ ) (4-Ph-pzbipy)
	284 (33900)	287	<sup>1</sup> ( $\pi$ - $\pi^*$ ) (4-Ph-pzbipy)
	262 (33400)	267	<sup>1</sup> ( $\pi$ - $\pi^*$ ) (4-Ph-pzbipy)
[Pt(4- <i>o</i> MePh-pzbipy)Cl] <sup>+</sup>	408 (3600)	426	MLCT [Pt(5d) → 4- <i>o</i> MePh-pzbipy( $\pi^*$ )]
concentration range: 5 - 30 $\mu\text{M}$	387sh (3300)	395sh	MLCT [Pt(5d) → 4- <i>o</i> MePh-pzbipy( $\pi^*$ )]
	356sh (8000)	363sh	<sup>1</sup> ( $\pi$ - $\pi^*$ ) (4- <i>o</i> MePh-pzbipy)
	338 (16600)	344	<sup>1</sup> ( $\pi$ - $\pi^*$ ) (4- <i>o</i> MePh-pzbipy)
	325sh (14800)	330sh	<sup>1</sup> ( $\pi$ - $\pi^*$ ) (4- <i>o</i> MePh-pzbipy)
	308sh (16500)	316sh	<sup>1</sup> ( $\pi$ - $\pi^*$ ) (4- <i>o</i> MePh-pzbipy)
	285 (30100)	285	<sup>1</sup> ( $\pi$ - $\pi^*$ ) (4- <i>o</i> MePh-pzbipy)
	262 (28400)	262	<sup>1</sup> ( $\pi$ - $\pi^*$ ) (4- <i>o</i> MePh-pzbipy)

**Table 5.8** (cont.)

Chromophore	$\lambda_{\text{abs}}$ (nm)		Assignment
	Acetonitrile	Dichloromethane	
[Pt(4- <i>o</i> CF <sub>3</sub> Ph-pzbipy)Cl] <sup>+</sup>	407 (3100 <sup>a</sup> )	418	MLCT [Pt(5d) → 4- <i>o</i> CF <sub>3</sub> Ph-pzbipy( $\pi^*$ )]
concentration range: 2 - 20 $\mu$ M	390sh (3100)	397sh	MLCT [Pt(5d) → 4- <i>o</i> CF <sub>3</sub> Ph-pzbipy( $\pi^*$ )]
	357 (8200)	364sh	<sup>1</sup> ( $\pi$ - $\pi^*$ ) (4- <i>o</i> CF <sub>3</sub> Ph-pzbipy)
	339 (15300)	344	<sup>1</sup> ( $\pi$ - $\pi^*$ ) (4- <i>o</i> CF <sub>3</sub> Ph-pzbipy)
	325sh (11700)	329	<sup>1</sup> ( $\pi$ - $\pi^*$ ) (4- <i>o</i> CF <sub>3</sub> Ph-pzbipy)
	287 (36600)	287	<sup>1</sup> ( $\pi$ - $\pi^*$ ) (4- <i>o</i> CF <sub>3</sub> Ph-pzbipy)
	262 (30200)	265	<sup>1</sup> ( $\pi$ - $\pi^*$ ) (4- <i>o</i> CF <sub>3</sub> Ph-pzbipy)

(a) Molar absorbtivity (M<sup>-1</sup>.cm<sup>-1</sup>).  
sh = shoulder.

**Table 5.9** Absorption and emission spectroscopic data recorded in solution.

Compound	Absorption maxima (nm)	Emission maxima (nm) [77 K]	$\tau$ (ns) [77 K]
[Pt(4-Ph-pzbipy)Cl] <sup>+</sup>	384, 404 <sup>MeCN</sup> 392, 417 <sup>DCM</sup>	<u>550</u> , 580sh <sup>DCM</sup> [ <u>516</u> , 556, 592] <sup>DME</sup>	96 <sup>DCM</sup> [15190] <sup>DME</sup>
[Pt(4'-Ph-terpy)Cl] <sup>+</sup> <sup>32, 42, 53</sup>	380sh, 402 <sup>MeCN, 32</sup> 397sh, 412 <sup>DCM, 32</sup>	<u>535</u> , 570sh, 608sh <sup>DCM, 32</sup> [ <u>515</u> ] <sup>M/E, 42</sup> [ <u>503</u> , 540, 582] <sup>BuCN, 32</sup>	85 <sup>DCM, 32</sup> [15000] <sup>M/E, 42</sup>
[Pt(4- <i>o</i> MePh-pzbipy)Cl] <sup>+</sup>	387, 408 <sup>MeCN</sup> 392, 417 <sup>DCM</sup>	543 <sup>DCM</sup> [ <u>501</u> , 539, 580, 620sh] <sup>DME</sup>	20 <sup>DCM</sup> [10800] <sup>DME</sup>
[Pt(4'- <i>o</i> MePh-terpy)Cl] <sup>+</sup> <sup>54, 111</sup>	380, 399 <sup>MeCN 54</sup>	Non-emissive at ambient temperatures <sup>MeCN 54, 111</sup> Solubility problems in DCM <sup>54, 111</sup> [477, 513, 555] <sup>DME 54, 111</sup>	not measured not measured
[Pt(4- <i>o</i> CF <sub>3</sub> Ph-pzbipy)Cl] <sup>+</sup>	390, 407 <sup>MeCN</sup> 397, 418 <sup>DCM</sup>	545 <sup>DCM</sup> [ <u>495</u> , 533, 576, 620sh] <sup>DME</sup>	not measured not measured
[Pt(4'- <i>o</i> CF <sub>3</sub> Ph-terpy)Cl] <sup>+</sup> <sup>54, 111</sup>	381, 396 <sup>MeCN 54</sup>	Non-emissive at ambient temperatures <sup>MeCN 54, 111</sup> Solubility problems in DCM <sup>54, 111</sup>	-

Underlined values refer to the most intense bands within a manifold.

sh = shoulder.

(DCM) Spectrum recorded in dichloromethane solution.

(DME) Spectrum recorded in 1:5:5 (v/v) DMF/methanol/ethanol solution.

(M/E) Spectrum recorded in 4:1 (v/v) methanol/ethanol solution.

(MeCN) Spectrum recorded in acetonitrile solution.

**Table 5.10** *Solid state absorption and emission spectroscopic data.*

Compound	Colour	Absorption maxima (nm)	Emission maxima (nm) [77 K]	fwhm (cm <sup>-1</sup> )	$\tau$ (ns) [77 K]
[Pt(4- <i>o</i> MePh-pzbipy)Cl]SbF <sub>6</sub> ( <b>14</b> )	maroon	575	674 [723]	1730 [1205]	80 [1320]
[Pt(4'- <i>o</i> MePh-terpy)Cl]SbF <sub>6</sub> ( <b>14a</b> ) <sup>54, 111</sup>	red	not measured	616 <sup>54, 111</sup> [673] <sup>54, 111</sup>	1635 [1119]	155 [1680]
[Pt(4- <i>o</i> MePh-pzbipy)Cl]BF <sub>4</sub> ( <b>15</b> )	dark orange	550	688 [739]	2200 [1280]	130 [1360]
[Pt(4'- <i>o</i> MePh-terpy)Cl]BF <sub>4</sub> ( <b>15a</b> ) <sup>54, 111</sup>	light orange	not measured	564 <sup>54, 111</sup> [566] <sup>54, 111</sup>	2508 [2109]	348 [2880]
[Pt(4- <i>o</i> MePh-pzbipy)Cl]CF <sub>3</sub> SO <sub>3</sub> ( <b>16</b> )	deep red	543	665 [726]	2120 [1270]	230 [1440]

**Table 5.10** (*cont.*)

Compound	Colour	Absorption maxima (nm)	Emission maxima (nm) [77 K]	fwhm (cm <sup>-1</sup> )	Solid $\tau$ (ns) [77 K]
[Pt(4- <i>o</i> CF <sub>3</sub> Ph-pzbipy)Cl]SbF <sub>6</sub> ( <b>17</b> ) <i>red form</i>	deep red	540	661 [714]	2070 [1300]	125 [1930]
[Pt(4- <i>o</i> CF <sub>3</sub> Ph-pzbipy)Cl]SbF <sub>6</sub> ( <b>17</b> ) <i>orange form</i>	orange	525	626 [632]	2380 [1615]	810 [2810]
[Pt(4'- <i>o</i> CF <sub>3</sub> Ph-terpy)Cl]SbF <sub>6</sub> ( <b>17a</b> ) <sup>54, 111</sup>	orange	not measured	589 <sup>54, 111</sup> [589] <sup>54, 111</sup>	2735 [2596]	325 <sup>54, 111</sup> [2620] <sup>54, 111</sup>
[Pt(4- <i>o</i> CF <sub>3</sub> Ph-pzbipy)Cl]BF <sub>4</sub> ( <b>18</b> )	orange	538	658 [648]	2200 [1710]	480 [2460]
[Pt(4'- <i>o</i> CF <sub>3</sub> Ph-terpy)Cl]BF <sub>4</sub> ( <b>18a</b> ) <sup>54, 111</sup>	orange	not measured	571 <sup>54, 111</sup> [571] <sup>54, 111</sup>	3100 [2450]	not measured
[Pt(4- <i>o</i> CF <sub>3</sub> Ph-pzbipy)Cl]CF <sub>3</sub> SO <sub>3</sub> ( <b>19</b> )	deep red	560	658 [709]	2200 [1410]	90 [1810]



# Appendices

## APPENDIX A

### General experimental details

#### A.1 EXPERIMENTAL TECHNIQUES

Synthesis of the ligands described in this work took place in reaction vessels open to the atmosphere. All platinum coordinations and cycloplatinations were performed under an inert nitrogen atmosphere using standard Schlenk techniques. Solvents were distilled and dried prior to use. In particular, great care was taken in the purification of acetonitrile by literature methods.<sup>185</sup>

#### A.2 INSTRUMENTATION

Mass spectra were recorded using a Hewlett-Packard HP 5988A gas chromatographic mass spectrometer.

<sup>1</sup>H and <sup>13</sup>C NMR spectra were recorded at ambient temperatures using a Gemini 200 MHz spectrometer. Chemical shifts are reported in ppm (parts per million) relative to an internal standard of tetramethylsilane (TMS) which is assigned a shift of 0 ppm.

Elemental analyses for carbon, hydrogen and nitrogen were performed in the School of Chemical and Physical Sciences at the University of Natal (Pietermaritzburg) using a Perkin Elmer 2400 CHN Elemental Analyzer.

Infrared spectra were recorded on a Shimadzu Fourier Transform IR 4300 spectrometer.

UV/vis absorption spectra were recorded at 298 K using a Shimadzu UV-2101PC spectrometer. Solid state spectra were recorded by making up the sample as a Nujol® mull. This mixture was held in place between two NaCl windows and inserted into the UV/vis absorption spectrometer, taking care to exclude air bubbles.

The fluorometer was a SLM-Aminco SPF-500C. All solution samples were prepared using spectroscopic grade solvents and thoroughly deoxygenated using three freeze, pump, thaw cycles. Measurements of microcrystalline solid state samples were made with the sample housed in a quartz tube. Data recorded at 77 K was measured in an EPR tube cooled in a quartz finger dewar that was filled with liquid nitrogen. Variable temperature emission measurements were made using an Oxford Instruments (model DN 1704) liquid-nitrogen cooled cryostat. Temperature control was with an Oxford Instruments Temperature Controller.

Lifetime measurements were made using a VSL-337ND-S nitrogen dye laser manufactured by Laser Science, Inc. Emission decay was monitored by a Hamamatsu R928 phototube powered by a Pacific Instruments (model 277) high voltage supply. Decay was captured on a Tektronix TDS 520 digitizing oscilloscope interfaced to a personal computer with TEKDIG software, supplied by Tektronix. A fit of the recorded software to mono-exponential decay curves was performed by the user written BASIC program PER.EXE.<sup>186</sup>

## APPENDIX B

### Sources of Chemicals

#### B.1 COMMERCIALY AVAILABLE CHEMICALS

Other than for solvents and where otherwise stated, chemicals were used as supplied.

<b>Chemical</b>		<b>Source</b>
acetophenone	distilled	Riedel de Haen
2-acetylpyridine		Aldrich Chemical Company Inc.
acetylpyrazine		Aldrich Chemical Company Inc.
AgBF <sub>4</sub>		Fluka AG
AgCF <sub>3</sub> SO <sub>3</sub>		Fluka AG
AgSbF <sub>6</sub>		Fluka AG
ammonium acetate	dried over P <sub>2</sub> O <sub>5</sub>	SAARchem
benzaldehyde	distilled	Aldrich Chemical Company Inc.
K <sub>2</sub> [PtCl <sub>4</sub> ]		Strem Chemicals
<i>β</i> -naphthaldehyde		Aldrich Chemical Company Inc.
<i>m</i> -bromobiphenyl		Aldrich Chemical Company Inc.
<i>p</i> -biphenylcarboxaldehyde		Aldrich Chemical Company Inc.
[Pt(PhCN) <sub>2</sub> Cl <sub>2</sub> ]		Strem Chemicals
2-tolualdehyde	distilled	Aldrich Chemical Company Inc.
<i>α,α,α</i> -trifluoromethyltolualdehyde	distilled	Aldrich Chemical Company Inc.

## B.2 CHEMICALS PREPARED BY LITERATURE METHODS

The ligand precursor *N*-{1-pyrazinyl-1-oxo-2-ethyl}pyridinium iodide was prepared by adaptation of the method published by Kröhnke.<sup>131</sup>

The two enones, [1-(2'-pyridyl)-3-(2''-R-phenyl)-prop-2-en-1-one (R = CH<sub>3</sub>, CF<sub>3</sub>)] were synthesised in the method established by Summerton.<sup>111</sup>

Conversion of *m*-bromobiphenyl to the precursor of ligand L2, *m*-biphenylcarboxaldehyde, was accomplished by the method of Beuhler, Smith, Glenn and Nayak.<sup>145</sup>



## REFERENCES

1. Balzani, V.; Carassitti, V.; *"Photochemistry of Coordination Compounds"*, Academic Press, London, (1970).
2. Constable, E.C.; *Adv. Inorg. Chem. Radiochem.*, 30 (1986) 69.
3. Constable, E.C.; *J. Chem. Soc., Chem. Commun.*, (1997) 1073.
4. Constable, E.C.; Harverson, P.; *Inorg. Chim. Acta*, 252 (1996) 9.
5. Amadelli, R.; Argazzi, R.; Bignozzi, C.A.; Scandola, F.; *J. Am. Chem. Soc.*, 112 (1990) 7099.
6. Jennette, K.W.; Gill, J.T.; Sadownick, J.A.; Lippard, S.J.; *J. Am. Chem. Soc.*, 98 (1976) 6159.
7. Brothers, H.M., II; Kostić, N.M.; *Biochemistry*, 29 (1990) 7468.
8. Brothers, H.M., II; Kostić, N.M.; *Inorg. Chem.*, 27 (1988) 1761.
9. Appleton, T.G.; Pesch, F.J.; Wienken, M.; Menzer, S.; Lippert, B.; *Inorg. Chem.*, 31 (1992) 4410.
10. Ratilla, E.M.A.; Scott, B.K.; Moxness, M.S.; Kostić, N.M.; *Inorg. Chem.*, 29 (1990) 918.
11. Bonser, A.M.; Moe, O.A.; *J. Chem. Edu.*, 73 (1996) 794.
12. Gouille, V.; Harriman, A.; Lehn, J.-M.; *J. Chem. Soc., Chem. Commun.*, (1993) 1034.
13. Belser, P.; Baak, M.; Dux, R.; De Cola, L.; Balzani, V.; *Angew. Chem., Int. Ed. Engl.*, 34 (1995) 595.
14. Harriman, A.; Ziessel, R.; *J. Chem. Soc., Chem. Commun.*, (1996) 1707.
15. Lecompte, J.P.; Kirsch-De Mesmaeker, A.; Orellana, G.; *J. Phys. Chem.*, 98 (1994) 5382.
16. Klimant, I.; Wolfbeis, O.S.; *Anal. Chem.*, 67 (1995) 3160.
17. Xu, W.Y.; Kneas, K.A.; Demas, J.N.; DeGraff, B.A.; *Anal. Chem.*, 68 (1996) 2605.
18. Fabbrizzi, L.; Licchelli, M.; Pallavicini, P.; Perotti, A.; Taglietti, A.; Sacchi, D.; *Chem. Eur. J.*, 2 (1996) 75.
19. Di Marco, G.; Lanza, M.; Pieruccini, M.; Campagna, S.; *Adv. Mater.*, 8 (1996) 576.

20. Smith, D.C.; Miskowski, V.M.; Mason, W.R.; Gray, H.B.; *J. Am. Chem. Soc.*, 112 (1990) 3759.
21. Miskowski, V.M.; Houlding V.H.; *Inorg. Chem.*, 30 (1991) 4446.
22. Shin, Y.K.; Brunschwig, Creutz, C.; Sutin, N.; *J. Phys. Chem.*, 100 (1996) 8157.
23. Metcalfe, R.A.; Dodsworth, E.S.; Fielder, S.S.; Stufkens, D.J.; Lever, A.B.P.; Pietro, W.J.; *Inorg. Chem.*, 35 (1996) 7741.
24. Lippard, S.J.; *Acc. Chem. Res.*, 11 (1978) 211.
25. Howe-Grant, M.; Lippard, S.J.; *Biochemistry*, 18 (1979) 5762.
26. Ratilla, E.M.A.; Brothers, H.M., II; Kostić, N.M.; *J. Am. Chem. Soc.*, 109 (1987) 4592.
27. Aldridge, T.K.; Stacy, E.M.; McMillin, D.R.; *Inorg. Chem.*, 33 (1994) 722.
28. Yip, H.-K.; Cheng, L.-K.; Cheung, K.-K.; Che, C.-M.; *J. Chem. Soc., Dalton Trans.*, (1993) 2933.
29. Bailey, J.A.; Hill, M.G.; Marsh, R.E.; Miskowski, V.M.; Schaefer, W.P.; Gray, H.B.; *Inorg. Chem.*, 34 (1995) 4591.
30. Crites, D.K.; Cunningham, C.T.; McMillin, D.R.; *Inorg. Chim. Acta*, 273 (1998) 346.
31. Michalec, J.F.; Bejune, S.A.; McMillin, D.R.; *Inorg. Chem.*, 39 (2000) 2708.
32. Michalec, J.F.; Bejune, S.A.; Cuttell, D.G.; Summerton, G.C.; Gertenbach, J.A.; Field, J.S.; Haines, R.J.; McMillin, D.R.; *Inorg. Chem.*, 40 (2001) 2193.
33. Watts, R.J.; Crosby, G.A.; Sansregret, J.L.; *Inorg. Chem.*, 7 (1972) 1474.
34. Indelli, M.T.; Bignozzi, C.A.; Marioni, A.; Scandola, F.; *J. Am. Chem. Soc.*, 110 (1988) 7381.
35. Ballhausen, C.J.; Bjerrum, N.; Dingle, R.; Eriks, K.; Hare, C.R.; *Inorg. Chem.*, 4 (1965) 514.
36. Andrews, L.J.; *J. Phys. Chem.*, 83 (1979) 3203.
37. Maestri, M.; Deuschel-Cornioley, C.; von Zelewsky, A.; *Coord. Chem. Rev.*, 111 (1991) 117.
38. Thummel, R.P.; Jahng, Y.; *J. Org. Chem.*, 50 (1985) 3635.
39. Maestri, M.; Sandrini, D.; Balzani, V.; von Zelewsky, A.; Deuschel-Cornioley, C.; Jolliet, P.; *Helv. Chim. Acta*, 71 (1988) 1053.



40. Bailey, J.A.; Miskowski, V.M.; Gray, H.B.; *Inorg. Chem.*, 32 (1993) 369.
41. Houlding, V.H.; Miskowski, V.M.; *Coord. Chem. Rev.*, 111 (1991) 145.
42. Arena, G.; Calogero, G.; Campagna, S.; Monsú Scolaro, L.; Ricevuto, V.; Romeo, R.; *Inorg. Chem.*, 37 (1998) 2763.
43. Chassot, L.; von Zelewsky, A.; Sandrini, D.; Maestri, M.; Balzani, V.; *J. Am. Chem. Soc.*, 108 (1986) 6084.
44. Cheung, T.-C.; Cheung, K.-K.; Peng, S.-M.; Che, C.-M.; *J. Chem. Soc., Dalton Trans.*, (1996) 1645.
45. Gliemann, G.; Yersin, H.; *Structure and Bonding* 62, (1985) 87.
46. Connick, W.B.; Henling, L.M.; Marsh, R.E.; Gray, H.B.; *Inorg. Chem.*, 35 (1996) 6261.
47. Büchner, R.; Field, J.S.; Haines, R.J.; Cunningham, C.T.; McMillin, D.R.; *Inorg. Chem.*, 36 (1997) 3952.
48. Crites Tears, D.K.; McMillin, D.R.; *Coord. Chem. Rev.*, 211 (2001) 195.
49. Gutmann, V.; *Chimia*, 31 (1977) 1.
50. Hobert, S.E.; Carney, J.T.; Cummings, S.D.; *Inorg. Chim. Acta*, 318 (2001) 89.
51. Arena, G.; Monsú Scolaro, L.; Pasternack, R.F.; Romeo, R.; *Inorg. Chem.*, 34 (1995) 2994.
52. Lai, S.-W.; Chan, M.C.-W.; Cheung, K.-K.; Che, C.-M.; *Inorg. Chem.*, 38 (1999) 4262.
53. Büchner, R.; Cunningham, C.T.; Field, J.S.; Haines, R.J.; McMillin, D.R.; Summerton, G.C.; *J. Chem. Soc., Dalton Trans.*, (1999) 711.
54. Field, J.S.; Haines, R.J.; McMillin, D.R.; Summerton, G.C.; *J. Chem. Soc., Dalton Trans.*, (2002) 1369.
55. Vlcek, A.A.; Dodsworth, E.S.; Pietro, W.J.; Lever, A.B.P.; *Inorg. Chem.*, 34 (1995) 1906.
56. Hunter, C.A.; Sanders, J.K.M.; *J. Am. Chem. Soc.*, 112 (1990) 5525.
57. Englman, R.; Jortner, J.; *Mol. Phys.*, 18 (1970) 145.
58. Jortner, J.; Rice, S.A.; Hochstrasser, R.M.; *Adv. Photochem.*, 7 (1969) 149.
59. Caspar, J.V.; Meyer, T.J.; *J. Am. Chem. Soc.*, 105 (1983) 5583.

60. Hill, M.G.; Bailey, J.A.; Miskowski, V.M.; Gray, H.B.; *Inorg. Chem.*, 35 (1996) 4585.
61. Miskowski, V.M.; Houlding, V.H.; *Inorg. Chem.*, 28 (1989) 1529.
62. Romeo, R.; Arena, G.; Monsú Scolaro, L.; Pasternack, R.F.; *Nuovo Cimento della Soceita Italiana di Fisica D*, 16 (1994) 1523.
63. Morgan, G.T.; Burstall, F.H.; *J. Chem. Soc.*, (1934) 1498.
64. Chan, C.-W.; Lai, T.F.; Che, C.-M.; Peng, S.M.; *J. Am. Chem. Soc.*, 115 (1993) 11245.
65. Akiba, M.; Sasaki, Y.; *Inorg. Chem. Commun.*, 1 (1998) 61.
66. Roszak, A.W.; Clement, O.; Buncel, E.; *Acta Cryst. C*, 52 (1996) 1645.
67. Bailey, J.A.; Catalano, V.J.; Gray, H.B.; *Acta Cryst. C*, 49 (1993) 1598.
68. Lowe, G.; Vilaivan, T.; *J. Chem. Res., Synop.*, (1996) 386.
69. Chernega, A.; Droz, A.-S.; Prout, K.; Vilaivan, T.; Weaver, G.W.; Lowe, G.; *J. Chem. Res., Synop.*, (1996) 402.
70. Lowe, G.; Droz, A.-S.; Vilaivan, T.; Weaver, G.W.; Park, J.J.; Pratt, J.M.; Tweedale, L.; Kelland, L.R.; *J. Med. Chem.*, 42 (1999) 3167.
71. Bonse, S.; Richards, J.M.; Ross, S.A.; Lowe, G.; Krauth-Siegel, R.L.; *J. Med. Chem.*, 43 (2000) 4812.
72. Annibale, G.; Marangoni, G.; Pitteri, B.; Visentin, F.; Bobbo, T.; *Transition Met. Chem.*, 25 (2000) 485.
73. Cusumano, M.; Di Pietro, M.L.; Giannetto, A.; Romano, F.; *Inorg. Chem.*, 39 (2000) 50.
74. McCoubrey, A.; Latham, H.C.; Cook, P.R.; Rodger, A.; Lowe, G.; *FEBS Lett.*, 380 (1996) 73.
75. Lowe, G.; Vilaivan, T.; *J. Chem. Soc., Perkin Trans. 1*, (1996) 1499.
76. Ratilla, E.M.A.; Kostić, N.M.; *J. Am. Chem. Soc.*, 110 (1988) 4427.
77. Cosar, S.; Janik, M.B.L.; Flock, M.; Freisinger, E.; Farkas, E.; Lippert, B.; *J. Chem. Soc., Dalton Trans.*, (1999) 2329.
78. Lowe, G.; Droz, A.-S.; Vilaivan, T.; Weaver, G.W.; Tweedale, L.; Pratt, J.M.; Rock, P.; Yardley, V.; Croft, S.L.; *J. Med. Chem.*, 42 (1999) 999.
79. Carr, C.A.; Richards, J.M.; Ross, S.A.; Lowe, G.; *J. Chem. Res., Synop.*, (2000) 566.

80. Wong, K.-Y.; Lee, W.W.-S.; *J. Photochem. Photobiol. A*, 102 (1997) 231.
81. Peyratout, C.S.; Aldridge, T.K.; Crites, D.K.; McMillin, D.R.; *Inorg. Chem.*, 34 (1995) 4484.
82. Annibale, G.; Bergamini, P.; Bertolasi, V.; Cattabriga, M.; Lazzaro, A.; Marchi, A.; Vertuani, G.; *J. Chem. Soc., Dalton Trans.*, (1999) 3877.
83. Howe-Grant, M.; Lippard, S.J.; *Inorg. Synth.*, 20 (1980) 101.
84. McFayden, W.D.; Wakelin, L.P.G.; Roos, I.A.G.; Hillcoat, B.L.; *Biochem. J.*, 242 (1987) 177.
85. Cheng, C.-C.; Lu, Y.-L.; *J. Chem. Soc., Chem. Commun.*, (1998) 253.
86. McFadyen, W.D.; Wakelin, L.P.G.; Roos, I.A.G.; Hillcoat, B.L.; *Biochem. J.*, 238 (1986) 757.
87. Tanaka, K.; Shigemori, K.; Shionoya, M.; *J. Chem. Soc., Chem. Commun.*, (1999) 2475.
88. Juranić, N.; Likić, V.; Kostić, N.M.; Macura, S.; *Inorg. Chem.*, 34 (1995) 938.
89. Huang, W.; Li, C.; Wang, J.; Zhu, L.; *Spec. Lett.*, 31 (1998) 1793.
90. Cheng, C.-C.; Pai, C.-H.; *J. Inorg. Biochem.*, 71 (1998) 109.
91. Brownlee, R.T.C.; McFayden, W.D.; O'Connor, M.J.; Rook, T.J.; Roos, I.A.G.; Wakelin, L.P.G.; *Magn. Reson. Chem.*, 25 (1987) 492.
92. Wakelin, L.P.G.; McFadyen, W.D.; Walpole, A.; Roos, I.A.G.; *Biochem. J.*, 222 (1984) 203.
93. Tzeng, B.-C.; Fu, W.-F.; Che, C.-M.; Chao, H.-Y.; Cheung, K.-K.; Peng, S.-M.; *J. Chem. Soc., Dalton Trans.*, (1999) 1017.
94. Yam, V.W.-W.; Tang, R.P.-L.; Wong, K.M.-C.; Ko, C.-C.; Cheung, K.-K.; *Inorg. Chem.*, 40 (2001) 571.
95. Yip, H.-K.; Che, C.-M.; Zhou, Z.-Y.; Mak, T.C.W.; *J. Chem. Soc., Chem. Commun.*, (1992) 1369.
96. Roothan, C.C.J.; *Rev. Mod. Phys.*, 23 (1951) 69.
97. Pople, J.A.; Nesbet, R.K.; *J. Chem. Phys.*, 22 (1954) 571.
98. McWeeny, R.; Dierksen, G.; *J. Chem. Phys.*, 49 (1968) 4852.
99. Bevilacqua, J.M.; Eisenberg, R.; *Inorg. Chem.*, 33 (1994) 2913.
100. Cummings, S.D.; Eisenberg, R.; *Inorg. Chem.*, 34 (1995) 2007.

101. Bevilacqua, J.M.; Zuleta, J.A.; Eisenberg, R.; *Inorg. Chem.*, 32 (1993) 3689.
102. Zuleta, J.A.; Burberry, M.S.; Eisenberg, R.; *Coord. Chem. Rev.*, 97 (1990) 47.
103. Vogler, A.; Kunkely, H.; *J. Am. Chem. Soc.*, 103 (1981) 1559.
104. Paw, W.; Lachicotte, R.J.; Eisenberg, R.; *Inorg. Chem.*, 37 (1998) 4139.
105. Constable, E.C.; Henney, R.P.G.; Leese, T.A.; Tocher, D.A.; *J. Chem. Soc., Dalton Trans.*, (1990) 443.
106. Constable, E.C.; Henney, R.P.G.; Leese, T.A.; Tocher, D.A.; *J. Chem. Soc., Chem. Commun.*, (1990) 513.
107. Neve, F.; Crispini, A.; Campagna, S.; *Inorg. Chem.*, 36 (1997) 6150.
108. Crosby, G.A.; *Acc. Chem. Res.*, 8 (1975) 231.
109. Tse, M.-C.; Cheung, K.-K.; Chan, M.C.-W.; Che, C.-M.; *J. Chem. Soc., Chem. Commun.*, (1998) 2295.
110. Miskowski, V.M.; Houlding, V.H.; Che, C.-M.; Wang, Y.; *Inorg. Chem.*, 32 (1993) 2518.
111. Summerton, G.C.; *Ph.D. Thesis, University of Natal, Pietermaritzburg, RSA*, (1997).
112. Yam, V.W.-W.; Wong, K.M.-C.; Zhu, N.; *J. Am. Chem. Soc.*, 124 (2002) 6506.
113. Kato, M.; Omura, A.; Toshikawa, A.; Kishi, S.; Sugimoto, Y.; *Angew. Chem., Int. Ed. Engl.*, 41 (2002) 3183.
114. Buss, C.E.; Mann, K.R.; *J. Am. Chem. Soc.*, 124 (2002) 1031.
115. Hecker, C.R.; Gushurst, A.K.I.; McMillin, D.R.; *Inorg. Chem.*, 30 (1991) 538.
116. Stone, M.L.; Crosby, G.A.; *Chem. Phys. Lett.*, 79 (1981) 169.
117. Ernst, S.D.; Kaim, W.; *Inorg. Chem.*, 28 (1989) 1520.
118. Morgan, G.T.; Burstall, F.H.; *J. Chem. Soc.*, (1934) 965.
119. Cargill Thompson, A.M.W.; *Coord. Chem. Rev.*, 160 (1997) 1.
120. Hollins, C.; *"Synthesis of Nitrogen Ring Compounds"*, Van Nostrand, London, (1924) 227.
121. Tschitschibabin, A.E.; *J. Prakt. Chem.* 2, 107 (1924) 122.
122. Frank, R.L.; Riener, E.F.; *J. Am. Chem. Soc.*, 72 (1950) 4182.
123. Burstall, F.H.; *J. Chem. Soc.*, (1938) 1662.

124. Kauffman, T.; König, J.; Woltermann, A.; *Chem. Berichte*, 109 (1976) 3864.
125. Uenishi, J.; Tanaka, T.; Wakabayashi, S.; Oae, S.; Tsukube, H.; *Tetrahedron Lett.*, 31 (1990) 4625.
126. Potts, K.T.; Cipullo, M.J.; Ralli, P.; Theodoridis, G.; *J. Org. Chem.*, 47 (1982) 3027.
127. Jeffrey, J.C.; Maher, J.P.; Otter, C.A.; Thornton, P.; Ward, M.D.; *J. Chem. Soc., Dalton Trans.*, (1995) 819.
128. Potts, K.T.; Keshavarz-K., M.; Tham, F.S.; Abruña, H.D.; Arana, C.; *Inorg. Chem.*, 32 (1993) 4450.
129. Potts, K.T.; Usifer, D.A.; Guadalupe, A.; Abruña, H.D.; *J. Am. Chem. Soc.*, 109 (1987) 3961.
130. Jameson, D.L.; Guise, L.E.; *Tetrahedron Lett.*, 32 (1991) 1999.
131. Kröhnke, F.; *Synthesis*, (1976) 1.
132. Otto, S.; Bertoncin, F.; Engberts, J.B.F.N.; *J. Am. Chem. Soc.*, 118 (1996) 7702.
133. Anastas, P.T.; Warner, J.C.; *"Green Chemistry, Theory and Practice"*, Oxford University Press, (1998).
134. Tanaka, K.; Toda, F.; *Chem. Rev.*, 100 (2000) 1025.
135. Cave, G.W.V.; Raston, C.L.; *J. Chem. Soc., Chem. Commun.*, (2000) 2199.
136. Mannich, C.; Koch, W.; Borowsky, F.; *Ber. Dtsch. Chem. Ges. B*, 70 (1937) 355.
137. Constable, E.C.; Ward, M.D.; *J. Chem. Soc., Dalton Trans.*, (1990) 1405.
138. Constable, E.C.; Lewis, J.; Liptrot, M.C.; Raithby, P.R.; *Inorg. Chim. Acta*, 178 (1990) 47.
139. Constable, E.C.; Neuberger, M.; Smith, D.R.; Zehnder, M.; *Inorg. Chim. Acta*, 275-276 (1998) 359.
140. Owlsey, D.C.; Nelke, J.M.; Bloomfield, J.J.; *J. Org. Chem.*, 38 (1973) 901.
141. Constable, E.C.; Smith, D.R.; *Supramolecular Chemistry*, 4 (1994) 5.
142. Alcock, N.W.; Barker, P.R.; Haider, J.M.; Hannon, M.J.; Painting, C.L.; Pikramenou, Z.; Plummer, E.A.; Rissanen, K.; Saarenketo, P.; *J. Chem. Soc., Dalton Trans.*, (2000) 1447.
143. Constable, E.C.; Cargill Thompson, A.M.W.; *New J. Chem.*, 20 (1996) 65.

144. Drew, M.G.B.; Iveson, P.B.; Hudson, M.J.; Liljenzin, J.O.; Spjuth, L.; Cordier, P.-Y.; Enarsson, A.; Hill, C.; Madic, C.; *J. Chem. Soc., Dalton Trans.*, (2000) 821.
145. Beuhler, C.A.; Smith, H.A.; Glenn, D.M.; Nayak, K.V.; *J. Org. Chem.*, 23 (1958) 1432.
146. Mureinik, R.J.; Bidani, M.; *Inorg. Nucl. Chem. Lett.*, 13 (1977) 625.
147. Based on lifetime measurements conducted by J.F. Michalec and C.T. Cunningham at Purdue University, West Lafayette, Indiana, USA.
148. Baghurst, D.R.; Cooper, S.R.; Greene, D.L.; Mingos, D.M.P.; Reynolds, S.M.; *Polyhedron*, 9 (1990) 893.
149. Annibale, G.; Brandolisio, M.; Pitteri, B.; *Polyhedron*, 14 (1995) 451.
150. Fanizzi, F.P.; Intini, F.P.; Maresca, L.; Natile, G.; *J. Chem. Soc., Dalton Trans.*, (1990) 199.
151. Nakamoto, K.; *J. Phys. Chem.*, 64 (1960) 1420.
152. Fink, D.W.; Ohnesorge, W.E.; *J. Phys. Chem.*, 74 (1970) 72.
153. Bessel, C.A.; See, R.F.; Jameson, D.L.; Churchill, M.R.; Takeuchi, K.J.; *J. Chem. Soc., Dalton Trans.*, (1992) 3223.
154. Storrier, G.D.; Colbran, S.B.; Craig, D.C.; *J. Chem. Soc., Dalton Trans.*, (1997) 3011.
155. Constable, E.C.; Cargill Thompson, A.M.W.; Tocher, D.A.; Daniels, M.A.M.; *New J. Chem.*, 16 (1992) 855.
156. Constable, E.C.; Housecroft, C.E.; Neuberger, M.; Phillips, D.; Raithby, P.R.; Schofield, E.; Sparr, E.; Tocher, D.A.; Zehnder, M.; Zimmerman, Y.; *J. Chem. Soc., Dalton Trans.*, (2000) 2219.
157. Connick, W.B.; Marsh, R.E.; Schaefer, W.P.; Gray, H.B.; *Inorg. Chem.*, 36 (1997) 913.
158. Kato, M.; Sasano, K.; Kosuge, C.; Yamazaki, M.; Yano, S.; Kimura, M.; *Inorg. Chem.*, 35 (1996) 116.
159. Kato, M.; Kosuge, C.; Morii, K.; Ahn, J.S.; Kitagawa, H.; Mitani, T.; Matsushita, M.; Kato, T.; Yano, S.; Kimura, M.; *Inorg. Chem.*, 38 (1999) 1638.
160. March, J.; *"Advanced Organic Chemistry"*, John Wiley & Sons, New York, (1992).

161. Achar, S.; Catalano, V.J.; *Polyhedron*, 16 (1997) 1555.
162. Gillard, R.D.; Sengul, A.; Oldroyd, A.; *Transition Met. Chem.*, 26 (2001) 339.
163. Herber, R.H.; Croft, M.; Coyer, M.J.; Bilash, B.; Sahiner, A.; *Inorg. Chem.*, 33 (1994) 2422.
164. Osborn, R.S.; Rogers, D.; *J. Chem. Soc., Dalton Trans.*, (1974) 1002.
165. Lewis, G.N.; Kasha, M.; *J. Am. Chem. Soc.*, 66 (1944) 2100.
166. Sheldrick, G.M.; *Acta Cryst. A*, 46 (1990) 467.
167. Sheldrick, G.M.; Schneider, T.R.; "*SHELXL: High-Resolution Refinement*", *Methods in Enzymology*, 277 (1997) 319.
168. McArdle, P.; *J. Appl. Cryst.*, 28 (1995) 65.
169. Field, J.S.; School of chemical and physical sciences, University of Natal, Private Bag X01, Scottsville, 3209.
170. Maestri, M.; Sandrini, D.; Balzani, V.; von Zelewsky, A.; Jolliet, P.; *Helv. Chim. Acta*, 71 (1988) 134.
171. Maestri, M.; Balzani, V.; Deuschel-Cornioley, C.; von Zelewsky, A.; *Adv. Photochem.*, 17 (1992) 1.
172. Deuschel-Cornioley, C.; Ward, T.; von Zelwesky, A.; *Helv. Chim. Acta*, 71 (1988) 130.
173. Pregosin, P.S.; Wombacher, F.; Albinati, A.; Lianza, F.; *J. Organomet. Chem.*, 418 (1991) 249.
174. Jahng, Y.; Park, J.G.; *Inorg. Chim. Acta*, 267 (1998) 265.
175. Gidney, P.M.; Gillard, R.D.; Heaton, B.T.; *J. Chem. Soc., Dalton Trans.*, (1973) 132.
176. Crosby, G.A.; *J. Chem. Edu.*, 60 (1983) 791.
177. Horvath, A.; Stevenson, K.L.; *Coord. Chem. Rev.*, 153 (1996) 57.
178. Crutchley, R.J.; Lever, A.B.P.; *J. Am. Chem. Soc.*, 102 (1980) 7128.
179. Crutchley, R.J.; Lever, A.B.P.; *Inorg. Chem.*, 21 (1982) 2276.
180. Mealli, C.; Pichierri, F.; Randaccio, L.; Zangrando, E.; Krumm, M.; Holtenrich, D.; Lippert, B.; *Inorg. Chem.*, 34 (1995) 3418.
181. Hoffmann, R.; Lipscomb, W.N.; *J. Chem. Phys.*, 36 (1962) 2179.
182. Hoffmann, R.; Lipscomb, W.N.; *J. Chem. Phys.*, 37 (1962) 3489.

183. Hoffmann, R.; *J. Chem. Phys.*, 39 (1963) 1397.
184. Büchner, R.; *Ph.D. Thesis, University of Natal, Pietermaritzburg, RSA, (1996)*.
185. Carlsen, L.; Egsgaard, H.; Andersen, J.R.; *Anal. Chem.*, 51 (1979) 1593.
186. Personal communication with Prof. D.R. McMillin, Department of Chemistry, Purdue University, West Lafayette, Indiana, USA.